

UCSF

UC San Francisco Electronic Theses and Dissertations

Title

The novel long noncoding RNA Pnky regulates neurogenesis and neural stem cell maintenance in vivo

Permalink

<https://escholarship.org/uc/item/2c0846rw>

Author

Andersen, Rebecca Ellen

Publication Date

2019

Peer reviewed|Thesis/dissertation

The novel long noncoding RNA Pnky regulates neurogenesis and neural stem cell maintenance in vivo

by
Rebecca Andersen

DISSERTATION

Submitted in partial satisfaction of the requirements for degree of
DOCTOR OF PHILOSOPHY

in

Developmental and Stem Cell Biology

in the

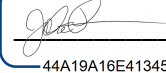
GRADUATE DIVISION

of the

UNIVERSITY OF CALIFORNIA, SAN FRANCISCO

Approved:

DocuSigned by:



44A19A16E413450...

John Rubenstein

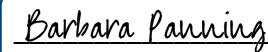
Chair

DocuSigned by:



DocuSigned by: 428...

Daniel Lim



DocuSigned by: 417...

Barbara Panning



A670FC1AD0F64CD...

Arturo Alvarez-Buylla

Committee Members

Copyright 2019
by
Rebecca E. Andersen

Dedication

This dissertation is dedicated to my family and friends, whose continuous support was essential to the success of this project.

Acknowledgements

I would like to thank my mentor, Dan Lim, who not only supported this project but was also instrumental in guiding my growth as a scientist. Dan has always allowed me the space to follow my project in the directions that I found most appealing, which provided me with an enormous opportunity for my personal scientific development. He is also a skilled writer, and I have learned a great deal about scientific storytelling from working on manuscripts with him. As I continue pursuing a career in academic science, these lessons will undoubtedly shape my future endeavors.

I am also grateful to my thesis committee members — John Rubenstein, Barbara Panning, and Arturo Alvarez-Buylla — for their invaluable guidance throughout my time at UCSF. Their insightful comments and suggestions always helped me to view my project in new ways and to consider possibilities that I might have otherwise overlooked. Their curiosity and scientific rigor have served as exemplary models, and I will strive to follow their lead.

This project also relied on support from members of the Lim Lab as well as all of the labs in Pod D of the Regeneration Medicine Building at UCSF. In particular, Alex Ramos began the long noncoding RNA projects in the Lim Lab, and was an essential part of the start of this project. Sung Hong was also extremely helpful in completing the later stages of this project.

Finally, I would like to thank my family and friends, who have been incredibly supportive throughout this entire process. I am very grateful for their constant encouragement and their patience whenever I had to run to lab to take care of “just one more thing”.

Contributions

All of the work presented here was designed and executed under the supervision of Dr. Daniel Lim. This project was supported in part by National Science Foundation Graduate Research Fellowship Grant Number 1144247 and National Institutes of Health Grant Number 1F31NS098562 to R.E.A.

Chapter 1 of this dissertation was published as: Andersen, R.E., and Lim, D.A. (2018). Forging our understanding of lncRNAs in the brain. *Cell Tissue Res.* 371, 55–71.

Chapter 2 was published as: Ramos, A.D., Andersen, R.E., Liu, S.J., Nowakowski, T.J., Hong, S.J., Gertz, C.C., Salinas, R.D., Zarabi, H., Kriegstein, A.R., and Lim, D.A. (2015). The long noncoding RNA Pnky regulates neuronal differentiation of embryonic and postnatal neural stem cells. *Cell Stem Cell* 16, 439–447.

Chapter 3 has been modified from its published form, which is available as: Andersen, R.E., Hong, S.J., Lim, J.J., Cui, M., Harpur, B.A., Hwang, E., Delgado, R.N., Ramos, A.D., Liu, S.J., Blencowe, B.J., et al. (2019). The Long Noncoding RNA Pnky Is a Trans-acting Regulator of Cortical Development In Vivo. *Dev. Cell* 49, 632–642.e7.

The novel long noncoding RNA *Pnky* regulates neurogenesis and neural stem cell maintenance *in vivo*

Rebecca E. Andersen

Abstract

While it is now appreciated that certain long noncoding RNAs (lncRNAs) have important functions in cell biology, relatively few have been shown to regulate development *in vivo*, particularly with genetic strategies that establish *cis* versus *trans* mechanisms. We have identified *Pinky* (*Pnky*) as a lncRNA that regulates neurogenesis in the embryonic and postnatal mouse brain. *Pnky* is a nuclear-enriched lncRNA that is divergent to the neighboring proneural transcription factor *Pou3f2*. In postnatal neural stem cells (NSCs) from the ventricular-subventricular zone (V-SVZ), *Pnky* knockdown promotes neuronal lineage commitment and expands the transit amplifying cell population, increasing neuron production several-fold. In the embryonic cortex, *Pnky* knockdown increases neuronal differentiation and depletes the NSC population prematurely. Furthermore, genetic deletion of *Pnky* results in the aberrant production of neuronal masses along the postnatal V-SVZ. In the developing cortex, *Pnky* regulates the production of projection neurons from NSCs in a cell-autonomous manner, and loss of *Pnky* alters postnatal cortical lamination. Surprisingly, *Pou3f2* expression is not disrupted by deletion of the entire *Pnky* gene. Moreover, expression of *Pnky* from a bacterial artificial chromosome (BAC) transgene rescues the differential gene expression and increased neurogenesis of *Pnky*-knockout NSCs, as well as the developmental phenotypes of *Pnky*-deletion *in vivo*. Thus, despite being transcribed divergently from a key developmental transcription factor, the lncRNA *Pnky* regulates neural development in *trans*.

Table of Contents

Chapter 1: Introduction	1
Summary	1
Background	1
Overlapping, antisense lncRNAs	4
<i>BACE1-AS</i>	4
<i>BDNF-AS</i>	6
<i>Evf2</i>	7
<i>Dlx1as</i>	10
<i>KCNA2-AS</i>	12
<i>Ube3a-ATS</i>	14
Non-overlapping lncRNAs	15
<i>Six3OS</i>	15
<i>Pnky</i>	17
<i>Gomafu</i>	20
Concluding Remarks	23
Figures and Tables	26
Chapter 2: The long noncoding RNA <i>Pnky</i> regulates neuronal differentiation of embryonic and postnatal neural stem cells	30
Summary	30
Introduction	30
Results	32
Discussion	38

Figures and Tables	41
Experimental Procedures.....	66
Chapter 3: The long noncoding RNA <i>Pnky</i> is a <i>trans</i>-acting regulator of cortical development <i>in vivo</i>	77
Summary.....	77
Introduction.....	77
Results	79
Generation of a conditional <i>Pnky</i> deletion allele	79
<i>Pnky</i> regulates development of the mouse neocortex	81
<i>Pnky</i> functions in <i>trans</i> to regulate cortical development.....	84
Discussion.....	87
Figures and Tables	91
Experimental Procedures.....	113
Chapter 4: Loss of <i>Pnky</i> disrupts neurogenesis and long-term neural stem cell abundance in the ventricular-subventricular zone	127
Summary.....	127
Introduction.....	127
Results	129
Discussion.....	132
Figures and Tables	135
Experimental Procedures.....	140
Chapter 5: Conclusions and Future Directions	145
References.....	149

List of Figures

Chapter 1

Figure 1.1: Examples of possible genomic configurations of lncRNAs.....	26
Figure 1.2: The genomic configurations of <i>Evf2</i> and <i>Dlx1as</i> , and the genetic mouse lines created to disrupt their transcription	27
Figure 1.3: The lncRNA <i>Pnky</i> is transcribed in a diverging manner from its nearest neighboring gene, <i>Pou3f2</i> (<i>Bm2</i>).....	28

Chapter 2

Figure 2.1: The lncRNA <i>Pinky</i> is expressed in SVZ-NSCs and regulates neuronal differentiation	41
Figure 2.2: <i>Pinky</i> knockdown leads to an expansion of neurogenic transit amplifying progenitors	42
Figure 2.3: <i>Pinky</i> is expressed in the developing mouse and human cortex and regulates the differentiation of mouse cortical progenitors <i>in vivo</i>	43
Figure 2.4: <i>Pinky</i> interacts with PTBP1 and regulates RNA expression and splicing.....	45
Figure 2.S1: Characterization of the long noncoding RNA <i>Pnky</i> and <i>Pnky</i> -KD cultures	46
Figure 2.S2: Analysis of time-lapse imaging of V-SVZ cultures.....	48
Figure 2.S3: <i>Pnky</i> is evolutionarily conserved and expressed in the developing mouse and human cortex	50
Figure 2.S4: Characterization of the interaction of <i>Pnky</i> and PTBP1	52

Chapter 3

Figure 3.1: Generation of a conditional deletion allele for the lncRNA <i>Pnky</i>	91
Figure 3.2: <i>Pnky</i> regulates cortical neurogenesis <i>in vivo</i>	92

Figure 3.3: <i>Pnky</i> functions cell-autonomously in the developing cortex	93
Figure 3.4: BAC transgenic expression of <i>Pnky</i> rescues loss of the endogenous gene.....	94
Figure 3.5: Loss of <i>Pnky</i> leads to persistent defects in the postnatal cortex	96
Figure 3.S1: Conditional deletion of <i>Pnky</i> in cultured cells and <i>in vivo</i>	97
Figure 3.S2: Loss of <i>Pnky</i> disrupts cortical development	99
Figure 3.S3: <i>Pnky</i> deletion from a small cohort of cells in the developing cortex.....	100
Figure 3.S4: Loss of <i>Pnky</i> is rescued by transgenic expression from a BAC	101

Chapter 4

Figure 4.1: Loss of <i>Pnky</i> results in the aberrant formation of neuroblast nodules	135
Figure 4.2: <i>Pnky</i> regulates progression through the V-SVZ neurogenic lineage	136

List of Tables

Chapter 1

Table 1.1: Summary of the neural lncRNAs discussed here, grouped by configuration..... 29

Chapter 2

Table 2.1: Differential expression of genes regulated by *Pnky* and PTBP1 54

Table 2.2: Gene ontology terms for *Pnky* and PTBP1 co-regulated genes 62

Table 2.3: Differential exon usage for genes regulated by *Pnky* and PTBP1 65

Chapter 3

Table 3.1: *Pnky* knockout *in vivo* alters transcript abundance 103

Table 3.2: *Pnky* knockout *in vivo* alters transcript splicing 106

Table 3.3: BAC^{*Pnky*} rescues transcript abundance changes in *Pnky*-KO cNSCs 107

Table 3.4: Altered splicing in *Pnky*-KO cNSCs overlaps PTBP1-regulated events 109

Chapter 4

Table 4.1: Deletion of *Pnky* results in intraventricular neuroblast nodules 137

Table 4.2: Mouse and human *Pnky* RNA physically interact with multiple proteins..... 138

Table 4.3: *Pnky*-interacting proteins are associated with RNA processing..... 139

Chapter 1: Introduction

Summary

During both development and adulthood, the human brain expresses many thousands of long noncoding RNAs (lncRNAs), and aberrant lncRNA expression has been associated with a wide range of neurological diseases. Although the biological significance of most lncRNAs remains to be discovered, it is now clear that certain lncRNAs carry out important functions in neurodevelopment, neural cell function, and perhaps even diseases of the human brain. Given the relatively inclusive definition of lncRNAs — transcripts longer than 200 nucleotides with essentially no protein coding potential — this class of noncoding transcript is both large and very diverse. Furthermore, emerging data indicate that lncRNA genes can act via multiple, non-mutually exclusive molecular mechanisms, and specific functions are difficult to predict from lncRNA expression or sequence alone. Thus, the different experimental approaches used to explore the role of a lncRNA might each shed light upon distinct facets of its overall molecular mechanism, and combining multiple approaches may be necessary to fully illuminate the function of any particular lncRNA. To understand how lncRNAs affect brain development and neurological disease, *in vivo* studies of lncRNA function are required. Thus, this introduction focuses on a small set of neural lncRNAs that have been experimentally manipulated in mice. Together, these examples illustrate how studies of individual lncRNAs using multiple experimental approaches can help reveal the richness and complexity of lncRNA function in both neurodevelopment and diseases of the brain.

Background

The human genome produces tens of thousands of long noncoding RNAs (lncRNAs) — transcripts of greater than 200 nucleotides that lack evident protein coding potential (Djebali et

al., 2012) — and it is now clear that certain lncRNAs can regulate important biological processes including those that underlie human disease (Batista and Chang, 2013; Briggs et al., 2015; Lee, 2012; Mercer and Mattick, 2013; Rinn and Chang, 2012). The developing and adult central nervous system (CNS) express a tremendous diversity of lncRNAs, many of which are brain-specific (Derrien et al., 2012; Mercer et al., 2008). Aberrant lncRNA expression has been associated with some of the most devastating neurological diseases including glioma (Ramos et al., 2016), schizophrenia (Barry et al., 2014), Alzheimer's disease (Faghihi et al., 2008), developmental delay (Talkowski et al., 2012), and autism (Ziats and Rennert, 2013). Though lncRNAs comprise an extensive class of noncoding transcripts, our general understanding of lncRNA function is still in its relative infancy. Nevertheless, the study of individual lncRNAs in the context of neural development and disease has provided fascinating and fundamentally important insights into the biological roles of this aspect of the noncoding genome.

Like protein coding messenger RNAs (mRNAs), lncRNAs are transcribed from the genome by RNA Polymerase II, and many are also 5' capped, spliced, and polyadenylated (Quinn and Chang, 2015). lncRNA genes can have various genomic orientations (**Figure 1.1**), with some overlapping protein-coding genes in the sense or antisense direction, others located between protein coding genes (intergenic), and a subset transcribed divergently from a neighboring gene through a shared promoter. While the genomic structure of lncRNAs can be sub-classified further (Mattick and Rinn, 2015), the aforementioned basic differences in lncRNA gene location and orientation can provide some insight into potential mechanisms through which they might function.

The currently known molecular mechanisms of lncRNA genes are very diverse, including the production of functional RNA transcripts (Rinn and Chang, 2012), *cis* regulation of neighboring genes through lncRNA promoter activity and/or transcriptional elongation (Engreitz et al., 2016; Kornienko et al., 2013; Li et al., 2013; Ørom et al., 2010), and enhancer-like activity of lncRNA loci (Fulco et al., 2016; Paralkar et al., 2016; Yin et al., 2015). Furthermore, recent

evidence indicates that certain transcripts currently annotated as lncRNAs can encode functional micropeptides (Anderson et al., 2015; Andrews and Rothnagel, 2014; Nelson et al., 2016). Of note, these functions are not mutually exclusive, and any particular lncRNA gene might have multiple molecular roles. Thus, the use of different experimental approaches, such as knockdown of the lncRNA transcript versus genetic disruption of the lncRNA gene, may reveal different aspects of lncRNA function (Bassett et al., 2014) and could produce different phenotypes.

The expression of many lncRNAs is highly dynamic during CNS development and neural stem cell (NSC) differentiation (Mercer et al., 2010; Ramos et al., 2013), and in some cases can be regulated by neuronal activity (Barry et al., 2014; Lipovich et al., 2012). Furthermore, lncRNAs exhibit a high degree of cell-type specificity, even surpassing that of protein coding genes (Cabili et al., 2011; Liu et al., 2016; Mercer et al., 2008; Ramos et al., 2013). For instance, some lncRNAs are abundantly expressed in specific cell types, such as radial glia in the developing human brain (Liu et al., 2016). Large-scale screens reveal that essential lncRNA function appears to be surprisingly cell-type specific, even for lncRNAs that are expressed across a wide range of cell types (Liu et al., 2016; Zhu et al., 2016). Therefore, experimental manipulations of lncRNAs through both large-scale screens and more in-depth individual analyses are key to advancing our understanding of the roles of lncRNAs in neural development and disease.

A growing number of lncRNAs has been found to regulate important biological functions in different neural cell types, and several recent reviews provide an excellent survey of such lncRNAs (Aprea and Calegari, 2015; Briggs et al., 2015; Clark and Blackshaw, 2014; Hart and Goff, 2016; Ramos et al., 2016). This chapter focuses on a smaller subset of lncRNAs that have been experimentally manipulated *in vivo* in mice (**Table 1.1**). By discussing specific details of the experimental methods used to manipulate each of these lncRNAs, I hope to illustrate how

studies of individual lncRNAs using multiple approaches can help reveal important insights regarding lncRNA function in both CNS development and diseases of the brain.

Overlapping, antisense lncRNAs

Numerous lncRNA genes overlap coding genes in an antisense direction (**Figure 1.1a**). While some antisense lncRNAs seem to function primarily *in cis* — local to and dependent upon their site of transcription (Guil and Esteller, 2012) — others appear to act *in trans*, independent from their site of transcription. Below, six antisense lncRNAs are reviewed on a case-by-case basis with particular focus on the methods used to manipulate lncRNA expression. Despite these genes being classified together as antisense lncRNAs, the current data suggest that they function via distinct mechanisms.

BACE1-AS: potential disease significance through the stabilization of *BACE1* mRNA

The lncRNA *BACE1-AS* is transcribed antisense to β -site APP cleaving enzyme 1 (*BACE1*), a protease that plays a role in Alzheimer's disease (AD) (Vassar, 2001; Vassar et al., 1999) and is also required for multiple aspects of normal CNS function (Laird et al., 2005; Willem et al., 2006). In the human SH-SY5Y neuroblastoma cell line, *BACE1-AS* is detected in both the nucleus and cytoplasm (Faghihi et al., 2008). *BACE1-AS* knockdown (KD) with small interfering RNA (siRNA) decreases *BACE1* mRNA and protein (Faghihi et al., 2008). Conversely, *BACE1-AS* overexpression (OE) increases *BACE1* levels. Consistent with these results in human cell lines, continuous *Bace1-AS* siRNA infusion into the third ventricle of mice for 2 weeks reduces *Bace1* mRNA and protein in the cortex, striatum, and hippocampus. Thus, *BACE1-AS* is a lncRNA that positively regulates its antisense partner, *BACE1*.

Both of the *BACE1-AS* splice variants contain sequences complementary to *BACE1* exons (Faghihi et al., 2008), which raises the possibility that the *BACE1-AS* lncRNA physically interacts with *BACE1* mRNA. Consistent with this, the overlapping regions of the lncRNA and

mRNA transcripts resist degradation in RNase protection assays, suggesting that they form an RNA duplex. Furthermore, KD of *BACE1-AS* reduces *BACE1* mRNA half-life, while OE of *BACE1-AS* increases the half-life of the mRNA. Together, these data support a model in which *BACE1-AS* forms a duplex with *BACE1* mRNA to increase its stability, leading to increased protein production (Faghihi et al., 2008).

BACE1 is a protease that cleaves amyloid precursor protein (APP), and aberrant cleavage is associated with AD (Vassar, 2001; Vassar et al., 1999). The pathogenic APP cleavage products exhibit an intriguing functional relationship with *BACE1-AS* expression. In HEK-SW cells that harbor an AD-linked mutation (Su et al., 2003), KD of *BACE1-AS* decreases the APP cleavage products amyloid β ($A\beta$) 1-40 and $A\beta$ 1-42 (Faghihi et al., 2008), suggesting that *BACE1-AS* normally promotes APP cleavage. Interestingly, cultured cells treated with $A\beta$ 1-42 protein upregulate *BACE1-AS* expression (Faghihi et al., 2008; Tamagno et al., 2006). Collectively, these results suggest a positive feedback mechanism in which $A\beta$ 1-42 induces elevated *BACE1-AS* expression, which increases *BACE1* levels and thereby further promotes production of $A\beta$ 1-42.

The expression levels of *BACE1-AS* also suggests a role for this lncRNA in AD. In patients with AD, *BACE1-AS* expression averaged across multiple brain regions is 2-fold higher as compared to controls (Faghihi et al., 2008), which is an increase larger than that observed for *BACE1*. Additionally, transgenic APP-tg19959 mice, which have elevated levels of $A\beta$ 1-42 and are considered an AD model (Oltersdorf et al., 1990), also exhibit increased expression of *Bace1-AS* and *Bace1* (Faghihi et al., 2008). From a translational standpoint, it will be very interesting to understand the effects of *Bace1-AS* KD on *Bace1* expression and $A\beta$ 1-42 biogenesis in this transgenic mouse model, as this could further implicate *BACE1-AS* in the regulation of these aspects of AD pathology.

BDNF-AS: a regulator of the growth factor BDNF

BDNF-AS is a lncRNA transcribed antisense to brain-derived neurotrophic factor (BDNF) (Liu et al., 2005), a secreted neurotrophic polypeptide that regulates neuronal differentiation, maturation, and survival (Chapleau et al., 2009; Hasbi et al., 2009; Yoshimura et al., 2009). Knockdown of *BDNF-AS* through siRNA in several human and mouse cell lines induces the upregulation of *BDNF* (Lipovich et al., 2012; Modarresi et al., 2012). Consistent with the role of BDNF in promoting neuronal differentiation (Binder and Scharfman, 2004), this resultant increase in BDNF upon KD of *Bdnf-AS* enhances neuronal outgrowth in mouse hippocampal neurosphere cultures (Modarresi et al., 2012). Moreover, in the mouse brain, *Bdnf-AS* KD achieved via intraventricular infusion of antisense oligonucleotides (ASOs) also increases BDNF and correlates with an increase in cell proliferation in the hippocampal dentate gyrus (Modarresi et al., 2012), a region of adult neurogenesis (Gonçalves et al., 2016). Thus, *BDNF-AS* appears to be a negative regulator of *BDNF* in multiple cell lines as well as in the adult mouse brain.

BDNF-AS splice variants all have exonic complementarity with *BDNF* mRNA (Modarresi et al., 2012), indicating the potential for lncRNA-mRNA duplex formation, as is observed with *BACE1-AS* and *BACE1* transcripts (Faghihi et al., 2008). However, in HEK293T cells, *BDNF-AS* KD does not alter the half-life of *BDNF* mRNA (Modarresi et al., 2012), indicating that the increase in *BDNF* transcript levels observed with *BDNF-AS* KD does not relate to a change in *BDNF* transcript stability.

Certain lncRNA transcripts interact with chromatin modifying proteins and can influence the chemical and/or structural state of chromatin at specific loci (Mercer and Mattick, 2013; Rinn and Chang, 2012). In HEK293T cells, *BDNF-AS* KD decreases the levels of histone 3 lysine 27 trimethylation (H3K27me3) — a histone modification associated with transcriptional repression (Aranda et al., 2015) — at the *BDNF* locus (Modarresi et al., 2012). This change is accompanied by a decrease in the enrichment of the H3K27-methyltransferase enhancer of zeste homolog 2 (EZH2) (Viré et al., 2005). While these data suggest a role for *BDNF-AS* in

regulating the chromatin state at the *BDNF* locus, whether *BDNF-AS* interacts with EZH2 or other chromatin modifying complexes has not been reported. It is also possible that the observed chromatin state changes at the *BDNF* locus simply reflect increased local transcriptional activity that results from increased levels of BDNF, which can promote transcription of its own gene via autoregulatory feedback (Bambah-Mukku et al., 2014). Precisely how *BDNF-AS* functions remains to be fully elucidated, but results from the siRNA- and ASO-mediated lncRNA KD experiments suggest that the *BDNF-AS* transcript itself negatively regulates the transcription and/or chromatin state of its antisense partner.

Evf2: neighboring gene regulation both *in cis* and *in trans*

With its transcriptional start site (TSS) located within the *Dlx5/6* bigene cluster, the lncRNA *Evf2* is transcribed antisense to *Dlx6* and contains the entire *Dlx6* gene within a large intron (**Figure 1.2a**) (Feng et al., 2006). *Evf2* also contains the ultraconserved *Dlx5/6* intergenic enhancer *ei* (Feng et al., 2006). In the developing mouse brain, *Evf2* transcript is localized to the nucleus, and its pattern of expression overlaps that of *Dlx5/6* and *Dlx1/2* in the medial and lateral ganglionic eminences (MGE and LGE, respectively) (Feng et al., 2006; Porteus et al., 1994). Given that the *Dlx* family of transcription factors plays critical roles in GABAergic interneuron production (Anderson et al., 1997a; Cobos et al., 2005; Pleasure et al., 2000), it has been of great interest to determine whether this lncRNA modulates the expression and/or function of the *Dlx* genes. This section describes how our understanding of *Evf2* has evolved over time with the use of different experimental approaches.

In early experiments performed in cell culture, *Evf2* was found to exhibit activity as a DLX2 transcriptional coactivator (Feng et al., 2006). *Dlx1/2* is genetically required for the expression of the *Dlx5/6* bigene cluster (Anderson et al., 1997a, 1997b; Zerucha et al., 2000), and transient transfection of *Dlx2* expression plasmids can activate reporter constructs containing *Dlx5/6* enhancers, which are known targets of DLX2 (Zerucha et al., 2000; Zhou et

al., 2004). When co-transfected with *Dlx2* into the C17 and MN9D mouse neural cell lines, *Evf2* increases *Dlx2*-dependent activation of these transcriptional reporters (Feng et al., 2006). Furthermore, immunoprecipitation of DLX proteins from cultured cells and rat branchial arches (Kohtz and Fishell, 2004) enriches for *Evf2* transcripts (Feng et al., 2006), indicating that DLX2 and *Evf2* physically interact *in vivo*. Taken together, these results suggested that *Evf2* transcripts can directly augment the ability of DLX2 protein to activate its downstream targets.

This initial understanding of *Evf2* as a transcriptional co-activator was developed primarily from studies of *Evf2* expressed from plasmids in cultured cells. To study the role of *Evf2* transcribed from its endogenous genomic locus, genetic targeting was used to deplete this lncRNA in mice. To avoid removal of genomic DNA that could disrupt the known local transcriptional enhancers, a triple polyadenylation (polyA) signal was inserted into *Evf2* exon 1 (*Evf2*^{TS}) to terminate lncRNA transcription before the ei enhancer (Bond et al., 2009) (**Figure 1.2b**). This genetic strategy ablated full-length *Evf2* transcripts in homozygous *Evf2*^{TS/TS} mice.

In the MGE of *Evf2*^{TS/TS} mice, the binding of DLX transcription factors at the *Dlx5/6* enhancers is reduced (Bond et al., 2009). Surprisingly, however, the reduction of DLX at these enhancers correlates with increased levels of *Dlx5* and *Dlx6*. While it possible that the insertion of polyA signals at this particular location disrupts uncharacterized DNA regulatory elements, siRNA-mediated *Evf2* KD *in vivo* also increases *Dlx5* expression in the MGE, suggesting that loss of the *Evf2* transcript itself underlies the observed transcriptional changes. Moreover, *Evf2* introduced *in trans* through electroporation can partially reverse the elevated levels of *Dlx5* in *Evf2*^{TS/TS} mice. These *in vivo* genetic studies suggest that *Evf2* transcripts normally inhibit *Dlx5* expression *in trans*.

In contrast, *Evf2* appears to regulate the expression of *Dlx6* *in cis*. *Evf2* expressed *in trans* via plasmid electroporation does not reduce *Dlx6* expression (Bond et al., 2009), suggesting that the increased levels of *Dlx6* in *Evf2*^{TS/TS} mice may result from a disruption of *cis* regulatory mechanisms and thus cannot be rescued *in trans*. This apparent *cis* regulation of

Dlx6 — but not *Dlx5* — may relate to the genomic structure of this locus. Given that *Dlx6* exists within an intron of *Evf2* (**Figure 1.2a**), active *Evf2* transcription might normally inhibit *Dlx6* expression from the same chromosome via transcriptional interference, wherein transcription along one DNA strand blocks transcription from the opposite strand (Cech and Steitz, 2014; Shearwin et al., 2005). Thus, early termination of *Evf2* elongation in the *Evf2*^{TS/TS} mice could alleviate transcriptional interference of *Dlx6*. Taken together, results from the *Evf2*^{TS/TS} mice indicate that *Evf2* can regulate the *Dlx5/6* bigene cluster via both *cis* and *trans* mechanisms.

DNA methylation and methyl CpG binding protein 2 (MECP2) have been investigated as mechanistic players underlying *Evf2* function. MECP2 is a DNA methyl-binding protein associated with transcriptional repression (Nan et al., 1998) and is found at the *Dlx5/6* locus (Horike et al., 2004). *Mecp2*-null mice exhibit increased *Dlx5/6* expression (Berghoff et al., 2013), suggesting that *Mecp2* normally represses this locus. In the MGE of *Evf2*^{TS/TS} mice, MECP2 enrichment at *Dlx5/6* enhancers is decreased (Bond et al., 2009), correlating with the increased transcriptional activity. These data suggest that *Evf2* is required for the localization of MECP2 at *Dlx5/6* regulatory regions.

Interestingly, *Evf2*^{TS/TS} mice have increased levels of DNA methylation at the *Dlx5/6* enhancers, and transgenic *Evf2* expression reduces this excess methylation (Berghoff et al., 2013). Thus, while *Evf2* is necessary for the enrichment of MECP2 at the *Dlx5/6* enhancers, *Evf2* also appears to inhibit DNA methylation of these enhancers in *trans*. Based on these and previous results (Anderson et al., 1997a, 1997b; Bond et al., 2009; Zerucha et al., 2000), the authors propose that *Evf2* inhibits DNA methylation at *Dlx5/6* regulatory regions, facilitating antagonistic interactions between MECP2 and DLX proteins (Berghoff et al., 2013). How the proposed interactions enable differential control of *Dlx5* and *Dlx6* remains to be demonstrated.

Moreover, *Evf2* also appears to mediate interactions between DLX1 and the SWI/SNF-related chromatin remodeler brahma-related gene 1 (BRG1) (Cajigas et al., 2015; Wang et al., 1996). DLX1 and BRG1 physically interact and co-localize at the *Dlx5/6* ei enhancer (Cajigas et

al., 2015). Furthermore, *Evf2* can directly interact with BRG1, and loss of *Evf2* reduces BRG1 levels at the *Dlx5/6* enhancers. While *Evf2* inhibits BRG1 ATPase activity in assays using recombinant proteins (Cajigas et al., 2015), the functional consequences of *Evf2*-BRG1 interactions *in vivo* remain to be tested. However, considering the previous work, one possibility is that *Evf2* promotes interactions between BRG1 and DLX1/2, which serve to activate the *Dlx5/6* locus and counteract repression by MECP2.

Given that the *Dlx* genes play crucial roles in the production of forebrain GABAergic interneurons (Anderson et al., 1997a; Cobos et al., 2005; Pleasure et al., 2000), disruption of *Evf2* might be expected to influence this developmental process. Indeed, loss of *Evf2* results in a 45-60% reduction of GAD1+ GABAergic interneurons in the hippocampus of early postnatal *Evf2*^{TS/TS} mice (Bond et al., 2009). This phenotype correlates with a 30% reduction in *Gad1* expression in the mutant embryonic MGE, which can be partially restored by electroporation of *Evf2*. Surprisingly, the number of GAD1-expressing cells returns to normal in the adult *Evf2*^{TS/TS} hippocampus (Bond et al., 2009). However, impaired synaptic inhibition in the hippocampus persists throughout adulthood, demonstrating that the disruption of a neural lncRNA can lead to long-lasting changes in CNS function.

Dlx1as: a role in interneuron production

Similar to *Dlx5/6*, the *Dlx1/2* bigene cluster also contains a lncRNA gene, *Dlx1as* (Dinger et al., 2008; Jeong et al., 2008; Kraus et al., 2013; Liu et al., 1997; McGuinness et al., 1996). Transcribed antisense to *Dlx1*, *Dlx1as* overlaps the majority of the *Dlx1* gene (**Figure 1.2c**). However, unlike the *Evf2-Dlx6* configuration, *Dlx1as* is not transcribed through the TSS of its coding gene partner *Dlx1*. To genetically disrupt *Dlx1as* expression in mice, four polyA signals were inserted between exons 1 and 2 (*Dlx1as*^{4xPA}) (Kraus et al., 2013) (**Figure 1.2d**), promoting the termination of *Dlx1as* transcription before its overlap with *Dlx1*. However, despite the

multiple polyA signals, *Dlx1as* expression is not completely ablated: in homozygous *Dlx1as*^{4xPA/4xPA} mice, *Dlx1as* is expressed at ~30% of wild-type levels.

Dlx1as is normally expressed in the embryonic ganglionic eminences (GEs) (Liu et al., 1997) in a pattern similar to that of *Dlx1/2* (Porteus et al., 1994). In the GEs of *Dlx1as*^{4xPA/4xPA} embryos, *Dlx1* transcript levels are moderately (~40%) increased (Kraus et al., 2013), suggesting that *Dlx1as* normally represses *Dlx1* expression. Although postnatal *Dlx1as*^{4xPA/4xPA} mice have a 2-fold increase in the number of *Dlx1*+ cells in the hippocampus, the number of interneurons as assessed by *Gad67* and *Somatostatin* expression was not altered in the mutant mice (Kraus et al., 2013). Given that overexpression of *Dlx1* alone does not alter the number of GABAergic interneurons in the mouse brain (Hitoshi et al., 1991), it is perhaps not surprising that *Dlx1as*^{4xPA/4xPA} mice do not exhibit obvious changes in this population of neurons. Whether the development of other neuronal (and glial) cell types is affected by *Dlx1as* genetic disruption remains to be reported.

Dlx1as is also expressed in the neurogenic lineage of the postnatal mouse ventricular-subventricular zone (V-SVZ) (Dinger et al., 2008; Ramos et al., 2013). In cultured V-SVZ neural stem cells, KD of *Dlx1as* with short hairpin RNA (shRNA) decreases the expression of *Dlx1*, *Dlx2* and *Dlx5* during differentiation (Ramos et al., 2013). These transcriptional changes correlate with a substantial decrease in the production of young neurons.

The contrasting effects upon gene expression in the embryonic brain of *Dlx1as*^{4xPA/4xPA} mice and V-SVZ cell cultures with *Dlx1as* KD could reflect potential cell type-specific functions of *Dlx1as*. In a recent genome-scale survey, lncRNA loci were found to have exquisitely cell type-specific functions for cell growth and proliferation (Liu et al., 2017). Alternatively, the differences observed may relate to the approaches used to reduce *Dlx1as* levels. In *Dlx1as*^{4xPA/4xPA} mice, transcriptional elongation of *Dlx1as* is abrogated, whereas with *Dlx1as* KD, transcript levels are depleted without a direct effect upon transcription at the locus. Since *Dlx1as* overlaps *Dlx1* (**Figure 1.2c**), transcription of this lncRNA could potentially reduce expression of

Dlx1 through transcriptional interference (Shearwin et al., 2005). Such repression *in cis* could be relieved by the transcriptional termination in *Dlx1as*^{4xPA/4xPA} mice, but not by shRNA-mediated *Dlx1as* KD in V-SVZ NSCs. Additional approaches such as *Dlx1as* OE and attempted transgenic rescue of *Dlx1as*^{4xPA/4xPA} may be helpful in addressing these and other possibilities.

The mechanism by which *Dlx1as* regulates *Dlx1* expression is still unclear, but given that *Evf2* can regulate its neighboring coding genes via both *cis* and *trans* mechanisms (Bond et al., 2009), it may be important to address both possibilities for *Dlx1as* as well. Since *Dlx1/2* are required for the expression of *Evf2* (Anderson et al., 1997b; Zerucha et al., 2000), *Dlx1as* may indirectly affect *Evf2* expression through regulating *Dlx1*. Interestingly, genetic deletion of *Dlx5* or *Dlx6* decreases *Dlx1as* expression in the developing branchial arches (Jeong et al., 2008). Given that *Evf2* regulates the expression of both *Dlx5* and *Dlx6* (Bond et al., 2009), *Evf2* may also indirectly regulate *Dlx1as*, adding an additional layer to the much studied cross-talk between the *Dlx1/2* and *Dlx5/6* bigene clusters (Anderson et al., 1997a; Liu et al., 1997; McGuinness et al., 1996; Zerucha et al., 2000).

KCNA2-AS: implications for neuropathic pain

KCNA2-AS is an antisense lncRNA that overlaps most of the *KCNA2* gene, which encodes a voltage-gated potassium channel (Zhao et al., 2013). Decreased expression of *KCNA2* correlates with neuropathic pain (Ishikawa et al., 1999; Kim et al., 2002), which can arise from damage to peripheral nerves (Campbell and Meyer, 2006). While *KCNA2-AS* has not been studied in the context of the CNS, its role in the peripheral nervous system (PNS) highlights how a lncRNA might serve as a therapeutic target for an important neurological condition.

KCNA2-AS and *KCNA2* are both expressed in the dorsal root ganglia (DRG) of rat, mouse, monkey, and human (Zhao et al., 2013). In the rat DRG, *Kcna2-AS* positive neurons generally express low levels of *Kcna2*. Peripheral nerve injury caused by lumbar spinal nerve

ligation (SNL) increases *Kcna2-AS* expression in neurons of the ipsilateral DRG, and these cells with elevated levels of *Kcna2-AS* exhibit decreased expression of *Kcna2* (Zhao et al., 2013). These dynamic, reciprocal changes in *Kcna2-AS* and *Kcna2* levels suggest a model in which expression of the *Kcna2-AS* lncRNA normally represses the expression of its antisense gene partner, *Kcna2*.

The transcription factor myeloid zinc finger 1 (MZF1) (Luo et al., 2009) binds to the *Kcna2-AS* promoter, and upon SNL, MZF1 levels increase and become further enriched at the *Kcna2-AS* promoter (Zhao et al., 2013). Moreover, MZF1 OE in cultured rat DRG neurons increases *Kcna2-AS*, while decreasing *Kcna2* levels. Taken together, these data support a model in which peripheral nerve injury increases the expression of MZF1, which directly upregulates *Kcna2-AS* expression, thereby decreasing the expression of *Kcna2*. Consistent with this model, *Kcna2-AS* OE is sufficient to decrease *Kcna2*, however the mechanism by which this lncRNA can down-regulate its antisense coding gene partner *in trans* has not been reported.

In vivo, OE of *Kcna2-AS* in the rat DRG also decreases levels of *Kcna2*, resulting in altered voltage-gated potassium current density and resting membrane potentials (Zhao et al., 2013). These electrophysiological changes correspond to behavioral abnormalities associated with neuropathic pain, such as mechanical and cold hypersensitivity. Thus, increased levels of *Kcna2-AS* transcript appear to drive neuropathic pain via suppression of *Kcna2* expression. Supporting this notion, KD of *Kcna2-AS* prior to SNL blocks the downregulation of *Kcna2* normally observed after peripheral nerve injury. Importantly, *Kcna2-AS* KD also attenuates the neuropathic pain symptoms of mechanical, cold, and thermal hypersensitivity. These data raise the intriguing possibility that KD of *Kcna2-AS* can ameliorate — or perhaps even prevent — neuropathic pain symptoms that arise from injury to the peripheral nerves.

Ube3a-ATS: a role in imprinting with relevance to Angelman syndrome

Some of the earliest-studied lncRNAs are involved in the regulation of gene dosage (Mohammad et al., 2009). The classic example is the lncRNA *XIST*, which is required for X-chromosome inactivation in female cells (Brown et al., 1992; Engreitz et al., 2013; Penny et al., 1996; Plath et al., 2002). Other lncRNAs play a role in imprinting, a process by which autosomal genes are expressed from a single allele in a parent of origin-specific manner (Bartolomei and Ferguson-Smith, 2011). For instance, the lncRNA *Air* interacts with the histone methyltransferase G9a to enable imprinting of its neighboring genes in the mouse placenta (Nagano et al., 2008). Similarly, *Kcnq1ot1* interacts with G9a as well as Polycomb repressive complex 2 (PRC2) to mediate imprinting (Pandey et al., 2008; Terranova et al., 2008). Investigating how lncRNAs regulate imprinting may be useful for understanding diseases caused by abnormal gene dosage, and could potentially lead to strategies for the reactivation of silenced alleles for therapeutic purposes.

Ube3a-ATS is a nuclear, neural-expressed antisense lncRNA that is involved in the repression of paternal *Ube3a* (Meng et al., 2012), which is imprinted specifically in neurons (Rougeulle et al., 1997; Vu and Hoffman, 1997; Yamasaki et al., 2003). *Ube3a-ATS* is part of an extremely long transcript that extends over 1000 kb through multiple genes including the 3' end of *Ube3a*. The relationship between *Ube3a-ATS* and *Ube3a* is of particular interest because of its implications for Angelman syndrome, a disorder characterized by neurological symptoms including seizures and intellectual disability. Angelman syndrome is caused by mutations in the maternal *UBE3A* allele, which results in complete loss of functional UBE3A protein in neurons due to silencing of the intact paternal copy (Albrecht et al., 1997; Kishino et al., 1997; Matsuura et al., 1997). Therefore, a potential therapeutic strategy is to reduce levels of *UBE3A-ATS*, thus relieving silencing of the normal paternal *UBE3A* (Meng et al., 2013, 2015).

In a mouse model of Angelman syndrome, genetic and pharmacological reduction of *Ube3a-ATS* expression has shown therapeutic promise. Premature termination of *Ube3a-ATS*

via the insertion of a triple polyA cassette relieves silencing of the paternal *Ube3a* allele, rescuing neurological deficits associated with Angelman syndrome (Meng et al., 2013). Moreover, a single intraventricular administration of ASOs targeting *Ube3a-ATS* reduces levels of this lncRNA in the brain, partially de-repressing paternal *Ube3a* for 4 months (Meng et al., 2015). This ASO treatment even ameliorates certain Angelman syndrome-associated phenotypes, such as aberrant contextual fear behavior. Given the sustained lncRNA KD achieved with a single intraventricular injection of ASOs, the targeting of neural lncRNAs with ASOs may be clinically feasible, at least for those that are expressed in non-dividing neurons.

Non-overlapping lncRNAs

Non-overlapping lncRNAs can vary greatly in terms of their distance from their nearest neighboring gene, with some only a few bases apart and others separated by megabases (Cabili et al., 2011) (**Figure 1.1b**). A subset of lncRNAs can carry out enhancer-like roles (Ørom et al., 2010), and the act of transcription of some lncRNAs appears to facilitate the expression of their close gene neighbors (Engreitz et al., 2016). However, even in these cases where non-overlapping lncRNAs have roles *in cis*, it is still possible that the lncRNA transcript itself has additional functions, and work from mouse ES cells suggests that many lncRNAs function *in trans* (Guttman et al., 2011).

Six3OS: a mediator of retinal progenitor cell differentiation

The lncRNA *Six3OS* (originally *Rncr1*) is transcribed divergently from *Six3*, a transcription factor that is critical for eye development (Zhu et al., 2002). *Six3OS* is largely co-expressed with its coding gene partner in cells of the developing mouse retina (Alfano et al., 2005; Blackshaw et al., 2004; Geng et al., 2007; Rapicavoli et al., 2011). *In situ* hybridization (ISH) reveals *Six3OS* transcripts in both the nucleus and cytoplasm of embryonic retinal progenitor cells (RPCs) (Rapicavoli et al., 2011).

There are multiple isoforms of *Six3OS*, and OE of the most abundant isoform in perinatal RPCs via *in vivo* plasmid electroporation indicates a functional relationship between this lncRNA and *Six3*. RPCs are multipotent, giving rise to rod cells, bipolar cells, amacrine cells, and Müller glia (Cepko, 2014). *Six3OS* OE in RPCs has a relatively modest effect, reducing the proportion of syntaxin (*syn*)-expressing amacrine cells (Rapicavoli et al., 2011). In contrast, as previously reported (Zhu et al., 2002), *Six3* OE in RPCs produces a much broader range of phenotypes, affecting the rod bipolar cells and rod photoreceptors, in addition to increasing the proportion of *syn*⁺ amacrine cells (Rapicavoli et al., 2011). Interestingly, when *Six3OS* is co-electroporated with *Six3*, these *Six3*-induced phenotypes are not observed. These results indicate that, at least in the context of overexpression, *Six3OS* can counteract the effects of *Six3*.

Interestingly, shRNA-mediated KD of *Six3* and *Six3OS* generates results that would not have been predicted by the phenotypes of their OE (Rapicavoli et al., 2011). Despite the opposing effects of *Six3OS* and *Six3* in the context of overexpression, *Six3OS* KD produces phenotypes similar to those observed with *Six3* KD. Furthermore, combined KD of *Six3OS* and *Six3* reveals complex functional relationships between this lncRNA and its coding gene neighbor. For example, some retinal cell populations that are not affected by KD of either *Six3OS* or *Six3* alone are altered upon their combined KD (Rapicavoli et al., 2011). Surprisingly, in other cell populations in which the single KDs result in similar phenotypes, the combined KD actually rescues these effects. These complex, non-additive phenotypes suggest an epistatic association between these two genes and demonstrate the elaborate relationship that a lncRNA can share with its neighbor.

How *Six3OS* functionally interacts with *Six3* is still not clear. Genetic deletion of *Six3* does not alter expression of *Six3OS* (Geng et al., 2007), indicating that neither an intact *Six3* locus nor SIX3 protein are required for expression of the *Six3OS* lncRNA. Given that neither KD nor OE of *Six3OS* transcript affects SIX3 protein abundance (Rapicavoli et al., 2011), it appears that *Six3OS* can modulate the function of *Six3* without changing the levels of SIX3 protein. It

remains to be tested whether the *Six3OS* locus itself can regulate *Six3* expression *in cis*, potentially via enhancer-like activity (Groff et al., 2016).

While *Six3OS* was not found to directly interact with SIX3 protein, both RNA immunoprecipitation and protein microarray analyses indicate that *Six3OS* binds to the EYA family of proteins as well as EZH2 (Rapicavoli et al., 2011). EYA family proteins are important transcriptional co-regulators in retinal development (Bonini et al., 1993; Pignoni et al., 1997) and can interact directly with proteins of the SIX family (Jemc and Rebay, 2007). However, it remains to be determined how the *Six3OS* interactions with EYA and EZH2 might influence cell fate outcomes.

Six3OS is also expressed in V-SVZ NSCs and is downregulated during neuronal differentiation (Ramos et al., 2013). In V-SVZ cultures, shRNA-mediated KD of *Six3OS* results in 2-fold fewer neuroblasts and 3-fold fewer oligodendrocyte lineage cells, accompanied by a corresponding increase in the proportion of glial fibrillary acidic protein (GFAP)-expressing glial cells. Thus, similar to the studies from the retina (Rapicavoli et al., 2011), these results suggest that *Six3OS* can regulate cell fate decisions in neural precursor cells of the CNS.

Pnky: a regulator of neurogenesis from postnatal and embryonic neural stem cells

The intergenic lncRNA *Pnky* neighbors the gene *Brn2* (*Pou3f2*) (Ramos et al., 2013, 2015), which encodes a transcription factor with key roles in neocortical development (Sugitani et al., 2002) and direct neuronal reprogramming (Vierbuchen et al., 2010). *Pnky* and *Brn2* are separated by 2.2 kb and are transcribed in divergent directions, and therefore do not share any overlapping regions (Ramos et al., 2015).

Pnky is neural-specific, and is enriched in the nucleus of V-SVZ NSCs (Ramos et al., 2013, 2015). Throughout postnatal and adult life, mouse V-SVZ NSCs give rise to transit amplifying cells that divide two to three times before generating neuroblasts (Doetsch et al., 1999; Lim and Alvarez-Buylla, 2014). These neuroblasts migrate through the rostral migratory

stream to the olfactory bulb where they differentiate into interneurons (Lim and Alvarez-Buylla, 2014). Over this course of V-SVZ neuronal differentiation, levels of *Pnky* transcript decrease (Ramos et al., 2013, 2015).

In V-SVZ NSC cultures, shRNA-mediated KD of *Pnky* increases neuroblast production 3-4 fold, indicating that *Pnky* influences V-SVZ neurogenesis (Ramos et al., 2015). Time-lapse microscopy analysis of individual V-SVZ NSCs reveals that *Pnky* regulates multiple aspects of V-SVZ neurogenesis. Firstly, *Pnky* KD increases neurogenic commitment by ~50% (Ramos et al., 2015). Furthermore, with *Pnky* KD, the transit amplifying population undergoes additional rounds of cell division. Combined, these effects greatly increase the number of neuroblasts produced from this population of postnatal NSCs.

Pnky also regulates neurogenesis from embryonic NSCs (Ramos et al., 2015). The cortical ventricular zone — where embryonic NSCs are located — is enriched for *Pnky* transcripts in both the mouse and human. *Pnky* KD in mouse embryonic ventricular zone cells via *in utero* electroporation of shRNA constructs promotes neurogenic differentiation *in vivo*, increasing the proportion of SATB2+ young neurons while decreasing the SOX2+ NSC population. Thus, reducing *Pnky* transcript levels in NSCs from both the embryonic and postnatal brain promotes neuronal differentiation.

This increase in neurogenesis observed with *Pnky* KD suggests a role for *Pnky* that is distinct from several other lncRNAs known to have neurodevelopmental function. For instance, KD of lncRNAs *megamind* (Lin et al., 2014), *RMST* (Ng et al., 2012, 2013), *Six3OS* (Ramos et al., 2013; Rapicavoli et al., 2011) and *Dlx1as* (Ramos et al., 2013) can all decrease neurogenesis, suggesting that these other lncRNAs are required to positively regulate neuronal differentiation. Similarly, genetic deletion of *Linc-Brn1b* appears to decrease the proliferation of embryonic cortical intermediate progenitors, reducing upper layer neurogenesis (Sauvageau et al., 2013). As noted above, mice lacking *Evf2* have defective interneuron production (Bond et al., 2009). Thus, unlike the aforementioned lncRNAs that appear to potentiate neuronal

production, *Pnky* appears to restrain neurogenesis from NSCs, perhaps serving to control their long-term self-renewal and/or rate of neuronal production.

While *Pnky* is relatively close to its neighbor *Brn2*, both genes appear to have their own promoters: each TSS region has a separate conserved CpG island that exhibits dynamic chromatin state changes characteristic of gene promoters (Ramos et al., 2013), including the H3K4me3 modification associated with transcriptional activity as well as the repression-associated H3K27me3 (Venkatesh and Workman, 2015) (**Figure 1.3**). Furthermore, while *Pnky* expression decreases during neurogenesis, *Brn2* transcript levels increase in transit amplifying cells (Ramos et al., 2013), suggesting that these gene neighbors are not always co-expressed.

Given that some lncRNAs can regulate the expression of gene neighbors *in cis*, one possibility is that *Pnky* regulates *Brn2* expression. However, KD of *Pnky* in V-SVZ cultures does not significantly alter expression of *Brn2* or any of the other genes within a 5 MB window, suggesting that the *Pnky* transcript does not regulate gene expression *in cis*, at least in this experimental context (Ramos et al., 2015). Whether the act of *Pnky* transcription (and/or the *Pnky* locus itself) can regulate expression of *Brn2* or other neighboring genes remains to be shown.

Pnky transcripts are located in multiple foci throughout the nucleus of neural cells (Ramos et al., 2015). The presence of *Pnky* transcripts in more than two spatially disparate locations indicates that this lncRNA can localize in regions of the nucleus that are far from the two *Pnky* loci, suggesting that this lncRNA has *trans* roles. Many lncRNAs with *trans* function regulate gene expression through interaction with specific proteins (Yang et al., 2015). Biotinylated-*Pnky* pulldown as well as RNA immunoprecipitation analysis reveal that polypyrimidine tract binding protein 1 (PTBP1) (Keppetipola et al., 2012) interacts with *Pnky* in cultured V-SVZ NSCs (Ramos et al., 2015). Interestingly, the lncRNAs *megamind* (Lin et al., 2014), *MEG3* (Zhang et al., 2017), and *XIST* (Maenner et al., 2010) also interact with PTBP1, but the potential significance of these other lncRNA-PTBP1 interactions has not been reported.

PTBP1 is localized in the nucleus of NSCs and appears to function as a repressor of neuronal differentiation. In the embryonic brain, genetic deletion of *Ptbp1* results in precocious neuronal differentiation (Shibasaki et al., 2013), and KD of PTBP1 alone in fibroblasts leads to direct neuronal trans-differentiation (Xue et al., 2013). In V-SVZ NSC cultures, PTBP1 KD increases the size of neurogenic colonies, which is a phenotype similar to that of *Pnky* KD (Ramos et al., 2015). The individual KDs of either PTBP1 or *Pnky* produce gene expression changes as well as mRNA splicing changes that are highly similar, suggesting that this splicing factor and lncRNA regulate a common set of transcripts in NSCs. Furthermore, double KD of PTBP1 and *Pnky* does not have a synergistic or additive effect upon transcriptional changes observed with the single KDs, suggesting that *Pnky* and PTBP1 function in the same molecular pathway. Taken together, these data indicate that *Pnky* and PTBP1 physically and genetically interact and regulate proper splicing and gene expression in V-SVZ NSCs.

Gomafu: from retinal development to schizophrenia

Gomafu (also known as *MIAT* or *Rncr2*) was identified as a lncRNA that is dynamically expressed during retinal development (along with *Six3OS*, see above) (Blackshaw et al., 2004). *Gomafu* is intergenic, located 20 kb away from its nearest protein coding neighbor (Blackshaw et al., 2004), and is expressed widely in the developing nervous system, localizing to multiple foci within the nucleus (Sone et al., 2007).

In the developing mouse retina, *Gomafu* is expressed in a large proportion of the progenitor cells, with its expression decreasing postnatally and becoming undetectable by adulthood (Rapicavoli et al., 2010). *In vivo* electroporation experiments indicate developmental roles for *Gomafu* in RPCs (Rapicavoli et al., 2010). While OE of *Gomafu* does not produce any overt phenotype, shRNA-mediated KD of this lncRNA increases the production of Müller glia and amacrine cells, suggesting that *Gomafu* normally represses these neural cell fates.

Given that the *Gomafu* lncRNA is normally found in the nucleus, the mis-localization of *Gomafu* transcripts to the cytoplasm might be expected to have a dominant-negative effect via the sequestration of its nuclear binding partners in the cytoplasmic compartment (Miyazaki et al., 2007; Zhang et al., 2004). Indeed, *Gomafu* transcripts fused to IRES-GFP sequences localize in the cytoplasm, and OE of this *Gomafu*-IRES-GFP construct in the developing retina causes phenotypes similar to those observed with *Gomafu* KD (Rapicavoli et al., 2010). As OE of *Gomafu* alone does not have an observable phenotype, the effect of *Gomafu*-IRES-GFP OE has been attributed to this mis-localization of *Gomafu* sequences. Transfection of *Gomafu*-IRES-GFP fusion constructs also enabled the dissection of distinct functional domains of *Gomafu*. For instance, when fused to IRES-GFP, OE of the 5' end increases the proportion of amacrine cells while the 3' end increases the Müller glial cell population (Rapicavoli et al., 2010). Thus, distinct regions of the *Gomafu* transcript appear to regulate different aspects of RPC fate determination, perhaps through interactions with unique binding partners.

Since lncRNAs exhibit relatively low evolutionary conservation at the primary sequence level (Johnsson et al., 2014; Ulitsky, 2016), any regions of conservation may provide insights into lncRNA function. *Gomafu* orthologs identified in mouse, human, chicken, and xenopus all contain multiple consensus recognition sites for the splicing factor quaking (QKI) (Rapicavoli et al., 2010). Furthermore, *Gomafu* physically interacts with QKI (Barry et al., 2014) and other splicing factors including serine/arginine-rich splicing factor 1 (SRSF1) (Barry et al., 2014) and splicing factor 1 (SF1) (Tsuiji et al., 2011).

Since QKI has been implicated in schizophrenia (Aberg et al., 2006b, 2006a), an interaction between *GOMAFU* and QKI could be relevant for this disorder. Interestingly, KD of *GOMAFU* in human iPSC-derived neurons increases the levels of the *DISC1* and *ERBB4* splice variants that have been associated with schizophrenia (Barry et al., 2014; Morikawa and Manabe, 2010), while *GOMAFU* OE in these cells has the opposite effect (Barry et al., 2014). In schizophrenia patient samples, *GOMAFU* levels are reduced, further suggesting a connection

between *GOMAFU* dysregulation and aberrant RNA splicing in schizophrenia (Barry et al., 2014). Additionally, *GOMAFU* expression is regulated by neuronal activity, becoming significantly decreased with depolarization (Barry et al., 2014). Thus, while *GOMAFU* downregulation may be important for splicing changes in the context of normal neuronal activity, its constitutive downregulation could be relevant to the neuropathology underlying schizophrenia.

Gomafu has also been implicated in anxiety-related behaviors in mice (Spadaro et al., 2015). Upon fear conditioning, *Gomafu* is significantly downregulated in the medial prefrontal cortex. Moreover, *Gomafu* KD through ASO infusion into the prefrontal cortex enhances freezing behavior during fear conditioning. This *in vivo* KD also increases behaviors related to anxiety, such as stereotypic grooming and avoidance of an open field. In primary cortical neuron cultures, KD of *Gomafu* upregulates *Crybb1* (Spadaro et al., 2015), a chaperone protein that has been associated with schizophrenia (Gill et al., 1996; Takahashi et al., 2003). Interestingly, in these cultures *Gomafu* physically interacts with the PRC1 complex member BMI1 (Haupt et al., 1991; Meng et al., 2010), and KD of *Gomafu* reduces BMI1 occupancy at the *Crybb1* promoter (Spadaro et al., 2015). Therefore, *Gomafu* may directly regulate *Crybb1* expression through a physical interaction with the repressor BMI1. Taken together, these results demonstrate that *Gomafu* can modulate neuronal function and potentially impact neuropsychiatric disorders through multiple molecular mechanisms.

Recently, a *Gomafu* knockout mouse has been reported (Ip et al., 2016). Surprisingly, loss of *Gomafu* did not result in any overt developmental phenotypes in the hippocampus, despite the high level of *Gomafu* expression reported in hippocampal CA1 neurons (Sone et al., 2007). This could reflect different requirements for *Gomafu* in different cell types, or developmental compensation by parallel genetic pathways. Alternatively, this could be due to differences resulting from constitutive deletion of the entire locus as opposed to acute knockdown of the transcript. Nevertheless, these mice did present moderate behavioral

abnormalities, including a hyperactivity phenotype that could be exacerbated by treatment with the psychostimulant methamphetamine (Ip et al., 2016). Given that these mice exhibit behavioral defects without any obvious developmental aberrations, it is possible that a relatively subtle effect on neurodevelopment and/or change in neuronal function underlies the behavioral abnormalities. These considerations may be particularly important for the study of complex neuropsychiatric diseases that are difficult to fully model in mice.

Concluding Remarks

From this survey of the data regarding the function of a small set of neural lncRNAs, it is apparent that this class of noncoding transcripts is extremely diverse in terms of biological roles and molecular mechanisms. This diversity, while intriguing, presents a challenge for determining the function of lncRNAs, as it is currently difficult to predict whether a particular lncRNA has important cellular function, much less how that lncRNA might operate at the level of molecular mechanism. Further complicating these issues, it appears that certain lncRNAs — despite being expressed in many different cell types — have biological functions that are exquisitely cell type-specific (Liu et al., 2017). Thus, manipulating lncRNA expression can lead to complex phenotypes that vary with the cell type being analyzed and the timing of the lncRNA perturbation. Using a combination of different, complementary strategies may therefore prove especially important for revealing the functions of lncRNAs.

Given the extraordinary diversity of lncRNA structure and function, it can be useful to sub-set this class of noncoding transcripts based on certain aspects of their genomic structure. Many antisense lncRNAs affect the expression of their partner genes transcribed from the opposite strand. However, despite this functional similarity, the mechanisms by which such regulation is achieved can be quite distinct. For example, *Evf2* regulates the expression of its gene neighbors *Dlx5* and *Dlx6* via both *cis* and *trans* mechanisms (Bond et al., 2009), while *BACE1-AS* transcripts interact directly with the *BACE1* mRNA, influencing mRNA stability

(Faghihi et al., 2008). Thus, while it might be reasonable to hypothesize that antisense lncRNAs regulate their partner genes, it is currently not possible to predict how they might do so.

Non-overlapping lncRNAs are perhaps even more challenging to decipher, particularly when they do not include any known genomic regulatory elements. Even when they are close to another gene, lncRNAs may not have any regulatory relationship with that neighbor. Given the many different possibilities, determining the molecular mechanism through which an intergenic lncRNA functions can be quite difficult. Therefore, an initial genetic characterization of whether the lncRNA acts *in cis* or *in trans* (or both) may provide a crucial foundation for developing any mechanistic understanding of how the lncRNA functions.

This chapter focused on a small set of lncRNAs in order to provide a more in-depth discussion of their neural functions. However, there are several other lncRNAs that also have important roles in the nervous system. For instance, *Taurine Upregulated Gene 1 (Tug1)* is required for proper photoreceptor differentiation (Young et al., 2005) and interacts with the PRC2 complex to repress p53-dependent cell cycle regulation (Khalil et al., 2009). *LncOL1* also interacts with components of the PRC2 complex to promote oligodendrocyte maturation and is required for proper myelination as well as remyelination following injury (He et al., 2017). Notch signaling in the developing human cortex is mediated by *LncND*, which sequesters the microRNA *miR-143-3p* to regulate the expression of Notch receptors (Rani et al., 2016). *RMST* influences the differentiation of human embryonic stem cells into dopaminergic neurons through interacting with SOX2 and enabling its binding to specific target promoters (Ng et al., 2012, 2013). *Cyrano* and *megamind* (also known as *TUNA*) are required for proper neural development in zebrafish, and their loss can be rescued by their human or mouse orthologs (Ulitsky et al., 2011). Moreover, *megamind* expression is altered in Huntington's disease, with *megamind* levels exhibiting a negative correlation with disease grade (Lin et al., 2014). Additionally, a set of knockout mice for 18 intergenic lncRNAs has been reported (Sauvageau et al., 2013). This set includes *Linc-Brn1b*, which is expressed in the neural progenitors of the VZ

and SVZ in the developing embryonic cortex. *Linc-Brn1b* appears to positively regulate the expression of its neighboring gene *Brn1*, a neurogenic transcription factor, and loss of *Linc-Brn1b* reduces the proliferation of intermediate progenitors and decreases the production of upper layer neurons (Sauvageau et al., 2013). While this set of knockout mice is further analyzed, additional lncRNAs with neural functions may be identified.

As the lncRNA field continues to mature, additional approaches will be used to manipulate lncRNA expression. For some lncRNAs, a conditional knockout allele will allow targeting of a particular subset of cells with precise control over the timing of deletion. For example, given that *Pnky* appears to function *in trans* and does not overlap known genes or enhancers (Ramos et al., 2015), this lncRNA may be suitable for conditional knockout methods. For other lncRNAs, this traditional genetic approach may not be possible due to their complex genomic configurations, such as overlapping important coding genes and/or enhancers. In these cases, perhaps CRISPR interference-based approaches can be used to affect the expression of the lncRNA while avoiding any alterations to the underlying DNA (Liu et al., 2017). Methods that specifically target the lncRNA transcript, such as KD through shRNA or ASOs, may assist in distinguishing the function of the transcript from potential regulatory roles of the locus itself. BAC transgenics could also be used to assess lncRNA overexpression or to attempt to rescue loss of the endogenous lncRNA. Combining multiple complementary approaches will provide important insights into how lncRNAs carry out their roles. Moving forward, a precise understanding of the intricate molecular mechanisms through which lncRNAs function will be essential for revealing how specific lncRNAs can play important roles in neural development and disease.

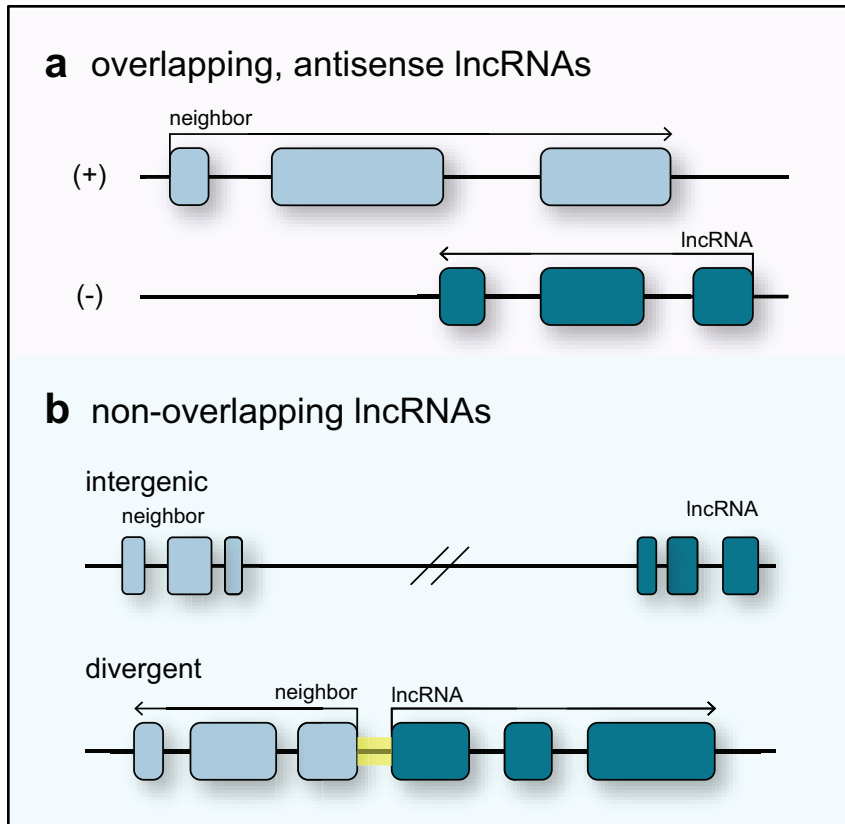


Figure 1.1: Examples of possible genomic configurations of lncRNAs.

a, Antisense lncRNAs overlap other genes in the antisense direction, but lncRNAs can also overlap other genes in the sense direction. The overlapping regions may include exons, resulting in mature transcripts that share identical regions or have sequence complementarity, depending on the direction of overlap. **b**, Non-overlapping lncRNAs can vary with respect to the distance to the nearest neighboring gene. Intergenic lncRNAs (lincRNAs) do not overlap known genes or regulatory elements, and may be transcribed in either direction relative to their nearest neighbors. A subset of intergenic lncRNAs known as divergent lncRNAs can share promoters (indicated in yellow) with their closely neighboring genes, and are transcribed in the opposite direction.

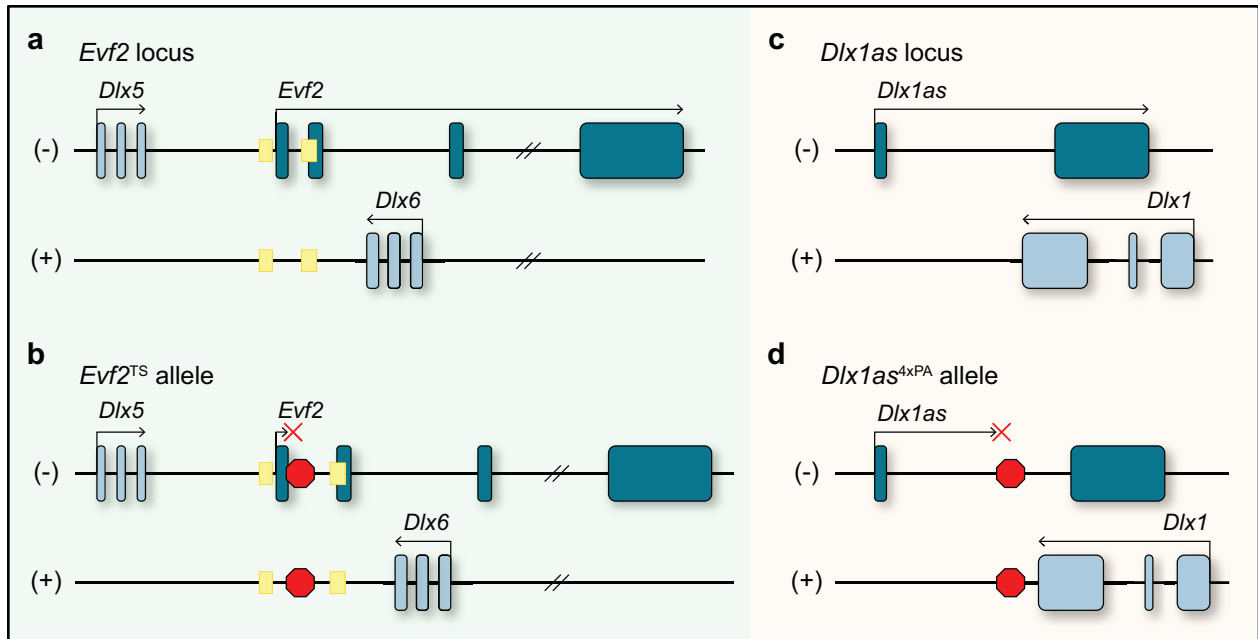


Figure 1.2: The genomic configurations of *Evf2* and *Dlx1as*, and the genetic mouse lines created to disrupt their transcription.

a, The lncRNA *Evf2* exists within the *Dlx5/6* bigene cluster. The ei and eii enhancer elements are shown in yellow. *Evf2* overlaps the ei enhancer element and contains the entire *Dlx6* gene within an intron. *Evf2* is transcribed from the same strand as *Dlx5* and the opposite strand from *Dlx6*. **b**, The *Evf2^{TS}* allele includes a 3x polyA transcriptional stop (red) in the first exon of *Evf2* to terminate transcription before the ei enhancer element. **c**, *Dlx1as* is transcribed antisense to *Dlx1* and contains exonic sequences that overlap with *Dlx1* exons. **d**, The *Dlx1as^{4xPA}* allele includes a 4x polyA transcriptional stop (red) inserted before the second exon to terminate transcription before overlap with *Dlx1*.

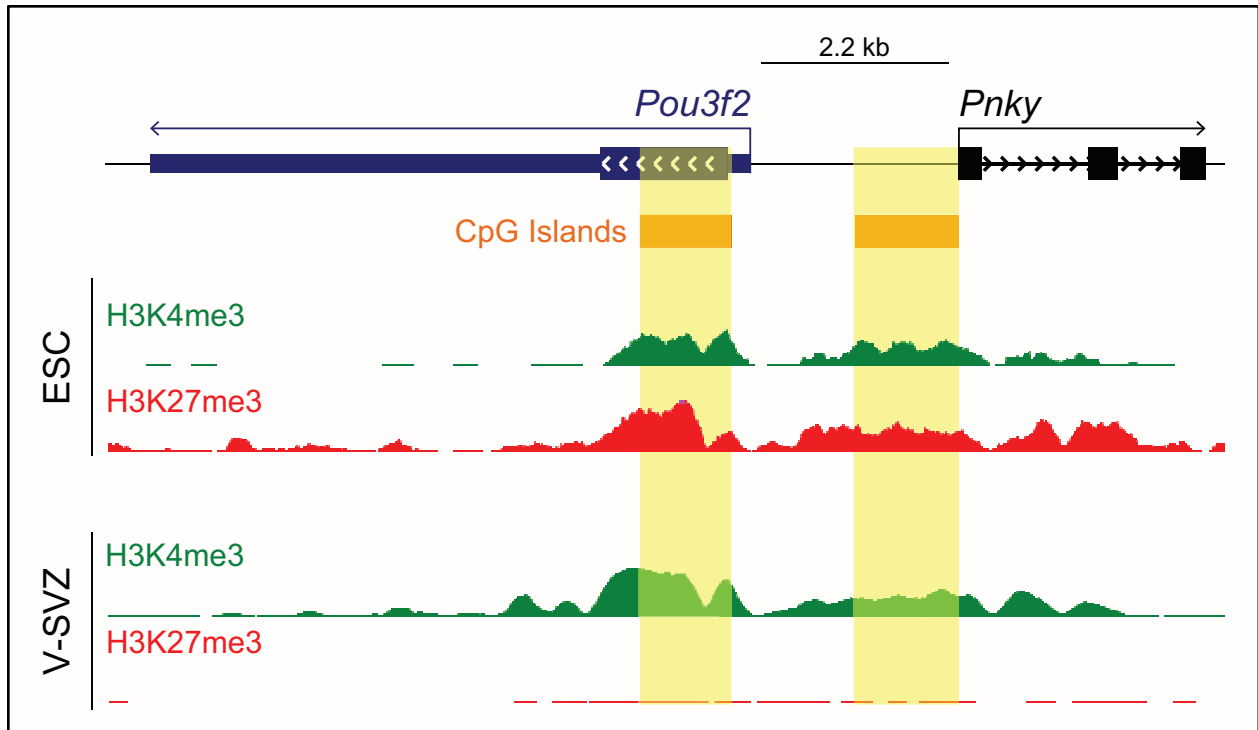


Figure 1.3: The lncRNA *Pnky* is transcribed in a diverging manner from its nearest neighboring gene, *Pou3f2* (*Brn2*).

While *Pnky* and *Pou3f2* are relatively close, they appear to have independent promoters as indicated by separate conserved CpG islands that exhibit dynamic chromatin modifications. In embryonic stem cells (ESC), these promoters are enriched with both the H3K4me3 modification, which correlates with active transcription, and the repression-associated H3K27me3. In V-SVZ NSCs only H3K4me3 is enriched, demonstrating cell type-specific chromatin modifications at these regions.

Table 1.1: Summary of the neural lncRNAs discussed here, grouped by configuration.

Antisense (AS) lncRNAs overlap with other genes in an AS direction, while non-overlapping lncRNAs do not overlap any known genes or regulatory elements. Abbreviations: knockdown (KD), short interfering RNA (siRNA), antisense oligonucleotide (ASO), polyadenylation (polyA), overexpression (OE), medial ganglionic eminence (MGE), dorsal root ganglia (DRG), knockout (KO), short hairpin RNA (shRNA), ganglionic eminences (GEs), ventricular-subventricular zone (V-SVZ), induced pluripotent stem cell (iPSC).

lncRNA	Configuration	Manipulations <i>in vivo</i>	Phenotypes	Proposed Mechanism	Disease	References
Overlapping, antisense	BACE1-AS	AS to <i>BACE1</i> , with complementarity to <i>BACE1</i> exons in its mature transcript	KD in mouse brain through siRNA infusion into third ventricle	siRNA KD in human cells reduces <i>BACE1</i> and decreases APP cleavage products. siRNA infusion into mouse brain decreases <i>BACE1</i>	Forms an RNA duplex with <i>BACE1</i> mRNA, increasing its stability	Faghihi et al. 2008
	BDNF-AS	AS to <i>BDNF</i> , with complementarity to <i>BDNF</i> exons in its mature transcript	KD in mouse brain through ASO infusion into third ventricle	KD in human/mouse cells induces upregulation of <i>BDNF</i> . <i>In vivo</i> , siRNA infusion increases <i>BDNF</i> and enhances hippocampal neurogenesis	Regulates levels of repression-associated H3K27me3 at <i>BDNF</i> promoter, possibly through mediating EZH2 interactions at this locus	Liu et al. 2005 Modarresi et al. 2012 Lipovich et al. 2012
	Evf2	AS to <i>Dlx6</i> , containing entire <i>Dlx6</i> gene within an intron and overlapping the ultraconserved <i>Dlx5/6</i> enhancer <i>ei</i> (Fig. 2a)	<i>Evf2</i> ^{TS} mouse model: triple polyA insertion (Fig. 2b). siRNA KD and OE in embryonic mouse MGE	<i>Evf2</i> ^{TS/TS} mouse MGE exhibits increased <i>Dlx5/6</i> and decreased <i>Gad1</i> . Reduced interneurons in early postnatal hippocampus, resulting in impaired synaptic inhibition	Facilitates physical interactions between <i>DLX1</i> and <i>BRG1</i> . Mediates binding of <i>MECP2</i> and <i>BRG1</i> to the <i>Dlx5/6</i> enhancers	Feng et al. 2006 Bond et al. 2009 Berghoff et al. 2013 Cajigas et al. 2015
	Dlx1as	AS to <i>Dlx1</i> , overlapping the majority of <i>Dlx1</i> gene but not its TSS (Fig. 2c)	<i>Dlx1as</i> ^{6PA} mouse model: 4x polyA insertion (Fig. 2d)	<i>Dlx1as</i> ^{6PA/6PA} mouse GEs have increased <i>Dlx1</i> and <i>Mash1</i> , leading to increased <i>Dlx1</i> + cells in hippocampus. KD in mouse V-SVZ cultures reduces neuroblast production	Negatively regulates levels of <i>Dlx1</i>	Kraus et al. 2013 Ramos et al. 2013
	KCNA2-AS	AS to <i>KCNA2</i> , overlapping almost the entire <i>KCNA2</i> gene including its TSS	KD and OE in rat DRG	OE in the rat DRG results in behavioral changes associated with neuropathic pain. KD in the DRG prior to peripheral nerve injury attenuates these symptoms	Negatively regulates levels of <i>Kcna2</i>	Zhao et al. 2013
Ube3a-ATS	AS to <i>Ube3a</i> , overlapping its 3' end	<i>Ube3a-ATS</i> ^{TOP} mouse model: triple polyA insertion. KD through ASO injection into mouse lateral ventricle	Loss of <i>Ube3a-ATS</i> relieves silencing of paternal <i>Ube3a</i> , ameliorating symptoms associated with Angelman syndrome such as aberrant contextual fear behavior	In neurons, regulates paternal imprinting of its antisense gene <i>Ube3a</i> , possibly through transcriptional interference	Meng et al. 2012 Meng et al. 2013 Meng et al. 2015	
Non-overlapping	Six3OS	transcribed divergently from <i>Six3</i>	KD and OE in perinatal mouse retina	Regulates production of multiple populations within developing mouse retina. KD in mouse V-SVZ cultures reduces production of neuroblast and oligodendrocyte lineage cells	Physically interacts with the EYA family and EZH2	Rapicavoli et al. 2011 Ramos et al. 2013
	Pnky	transcribed in the opposite direction from <i>Bm2</i> from a separate promoter (Fig. 3)	KD in embryonic mouse brain through <i>in utero</i> electroporation of shRNA constructs	KD increases neuroblast production from mouse cortex. KD promotes neurogenic differentiation	Physically interacts with the splicing regulator PTPB1	Ramos et al. 2013 Ramos et al. 2015
	Gomafu	transcribed convergently toward <i>1700028D13Rik</i>	<i>Gomafu</i> null mouse model: KO of the entire gene. KD and OE in perinatal mouse retina. KD through ASO infusion in the mouse prefrontal cortex	Regulates production of multiple populations within developing mouse retina. In human iPSC-derived neurons, affects splicing of schizophrenia-associated genes. KD results in anxiety behaviors in mice. KO mice exhibit hyperactivity	Physically interacts with the splicing factors <i>QKI</i> , <i>SRSF1</i> , and <i>SF1</i> . Also physically interacts with the <i>PRC1</i> complex member <i>BMI1</i>	Blackshaw et al. 2004 Rapicavoli et al. 2010 Barry et al. 2014 Spadaro et al. 2015 Ip et al. 2016

Chapter 2: The long noncoding RNA *Pnky* regulates neuronal differentiation of embryonic and postnatal neural stem cells

Summary

While thousands of long noncoding RNAs (lncRNAs) have been identified, few lncRNAs that control neural stem cell (NSC) behavior are known. Here, we identify *Pinky* (*Pnky*) as a neural-specific lncRNA that regulates neurogenesis from NSCs in the embryonic and postnatal brain. In postnatal NSCs, *Pnky* knockdown potentiates neuronal lineage commitment and expands the transit amplifying cell population, increasing neuron production several-fold. *Pnky* is evolutionarily conserved and expressed in NSCs of the developing human brain. In the embryonic mouse cortex, *Pnky* knockdown increases neuronal differentiation and depletes the NSC population. *Pnky* interacts with the splicing regulator PTBP1, and PTBP1 knockdown also enhances neurogenesis. In NSCs, *Pnky* and PTBP1 regulate the expression and alternative splicing of a core set of transcripts that relates to the cellular phenotype. These data thus unveil *Pnky* as a conserved lncRNA that interacts with a key RNA processing factor and regulates a critical stage of neurogenesis from embryonic and postnatal NSC populations.

Introduction

Neural stem cells (NSCs) exist in both the embryonic and postnatal mammalian brain. In the embryonic cortical ventricular zone (VZ) and adult ventricular-subventricular zone (V-SVZ), NSCs are glial cells that can both self-renew and differentiate to yield intermediate progenitors that divide once or more before producing migratory young neurons (Kriegstein and Alvarez-Buylla, 2009). The production of proper numbers of neuronal progenitors from NSCs is a key aspect of brain development, and defects at this stage of the neurogenic lineage may underlie a number of human developmental disorders (Lui et al., 2011).

The mammalian genome encodes many thousands of lncRNAs – transcripts >200 nucleotides long that have no evidence of protein coding potential – and emerging data indicate that lncRNAs can have critical biological functions (Batista and Chang, 2013; Lee, 2012; Mercer and Mattick, 2013; Rinn and Chang, 2012). Although transcription factors, microRNAs, and signaling pathways that control the transition between NSCs and neurogenic progenitors have been studied intensively (Ihrie and Álvarez-Buylla, 2011; Kriegstein and Alvarez-Buylla, 2009; Lui et al., 2011), lncRNAs that regulate this critical, early stage of neurogenesis have not been identified.

In this chapter we describe the unique developmental function of a neural-specific lncRNA we have named *Pinky* (*Pnky*) and provide insights into its molecular function. We have previously shown that knockdown of lncRNAs *Dlx1as* and *Six3os* in V-SVZ NSCs results in decreased neurogenesis (Ramos et al., 2013). Similarly, loss-of-function studies of different lncRNAs in ESC-derived NSCs (Lin et al., 2014; Ng et al., 2013), zebrafish brain (Ulitsky et al., 2011), and mouse central nervous system (Bond et al., 2009; Rapicavoli et al., 2011; Sauvageau et al., 2013) all demonstrate a loss of neuronal populations. In contrast, postnatal V-SVZ NSCs with *Pnky*-knockdown (*Pnky*-KD) generated 3-4 fold more neurons. To understand this phenotype, we used time-lapse microscopy to study lineage commitment and cell proliferation at the single-cell level. We cloned the human *PNKY* transcript and discovered its expression in the VZ of the embryonic human brain, and we demonstrated a role for *Pnky* in the development of the embryonic mouse cortex *in vivo*. Using mass spectrometry, we found that *Pnky* bound to PTBP1, an RNA-splicing factor that is a potent regulator of neural development (Keppetipola et al., 2012), direct cell reprogramming (Xue et al., 2013), and brain tumor growth (Ferrarese et al., 2014). Further analysis indicated that *Pnky* and PTBP1 modulate the expression and alternative splicing of an overlapping set of transcripts, and double-knockdown epistasis experiments suggested that *Pnky* and *Ptbp1* function in the same pathway. Overall,

our work demonstrates that an evolutionarily conserved lncRNA can regulate neurogenesis from NSCs in both the embryonic and postnatal brain.

Results

Throughout adult life, V-SVZ NSCs give rise to transit amplifying (TA) cells, which generate neuroblasts (NB) that migrate to the olfactory bulb where they differentiate into interneurons (Doetsch et al., 1999; Lois and Alvarez-Buylla, 1994; Luskin, 1998; Peretto et al., 1997). *Pnky* (previously called *Inc-pou3f2*) is a lncRNA that we initially identified as being expressed in the adult V-SVZ (Ramos et al., 2013). RACE cloning followed by Sanger sequencing demonstrated *Pnky* to be an 825 nucleotide (nt) polyadenylated RNA encoded from three exons (**Figure 2.1A**). Analysis with the Coding Potential Calculator (CPC) (Kong et al., 2007), PhyloCSF (Lin et al., 2011), and the Coding-Potential Assessment Tool (CPAT) (Wang et al., 2013) indicated that the *Pnky* transcript has no protein-coding potential (**Figure 2.S1A**). Analysis of available RNA-seq datasets indicated that *Pnky* is specifically expressed in neural tissues and lineages but is not expressed in the dentate gyrus, which contains another population of adult NSCs (**Figure 2.1B**). Furthermore, like many key developmental genes, the promoter of *Pnky* was “bivalent” with both histone 3 lysine 27-trimethylation (H3K27me3) and histone 3 lysine 4-trimethylation (H3K4me3) in embryonic stem cells (ESCs), coherent with its repressed but “poised” transcriptional state (**Figure 2.1A**). In contrast, in ESC-derived NSCs (ESC-NSCs) and V-SVZ NSCs, the *Pnky* promoter was monovalent with H3K4me3, consistent with its active transcription (**Figures 2.1A and 2.S1B**).

Nuclear fractionation of V-SVZ NSC cultures followed by RT-qPCR analysis demonstrated *Pnky* to be enriched in the nucleus as compared to coding mRNAs, which were enriched in cell lysates containing cytoplasm (**Figure 2.1C**). Consistent with the nuclear fractionation studies, *in situ* hybridization (ISH) for *Pnky* demonstrated predominantly nuclear localization of the transcript (**Figures 2.1D and 2.S1C**).

ISH of adult mouse brain tissue revealed prominent expression of *Pnky* in the V-SVZ (**Figure 2.1E**). To investigate whether *Pnky* expression is dynamic within the neurogenic lineage, we analyzed gene expression of V-SVZ cells acutely isolated from the brain through fluorescent activated cell sorting (FACS) (Ramos et al., 2013). Briefly, activated neural stem cells (NSCs) express both glial fibrillary acidic protein (GFAP) and the epidermal growth factor receptor (EGFR). Transit amplifying cells are GFAP- but retain EGFR expression, and neuroblasts express cell surface marker CD24 (Pastrana et al., 2009). *Pnky* expression was highest in NSCs, and decreased by 5.6-fold ($p=0.0003$, Student's t-test) in migratory neuroblasts (**Figure 2.1F**). Thus, *Pnky* is normally downregulated during lineage progression *in vivo*.

To investigate the role of *Pnky* in neurogenesis, we first used V-SVZ NSC monolayer cultures that recapitulate key features of neuronal differentiation as well as glial cell production (**Figure 2.1G**). *Pnky* was expressed in cultured NSCs in self-renewal conditions. Upon differentiation, *Pnky* remained expressed in GFAP+ astrocytes, but was down regulated in TUJ1+ neuronal cells (**Figure 2.S1D**), similar to the pattern of expression seen *in vivo*. After lentiviral transduction with control (shCtrl-GFP) or *Pnky* (sh*Pnky*-1-GFP and sh*Pnky*-2-GFP) knockdown constructs, GFP+ NSCs were isolated through FACS and cultured. *Pnky* knockdown was efficient in both self-renewing NSCs and after their differentiation (**Figures 2.S1E and 2.S1F**). Cells in these purified cultures uniformly expressed SOX2, a neural stem cell marker (**Figure 2.S1G**). Flow cytometric analysis of these infected cells indicated that the majority (66.0%) were also positive for both GFAP and NESTIN (**Figure 2.S1H**), markers of V-SVZ NSCs. Therefore, the majority of cells transduced with *Pnky*-KD or control vectors were GFAP+, NESTIN+, SOX2+ V-SVZ NSCs.

Pnky-KD NSCs incorporated the thymidine analog 5-ethynyl-2'-deoxyuridine (EdU) at the same rate as control NSCs, suggesting that proliferation in self-renewal conditions was not affected (**Figures 2.1H and 2.S1I**). However, *Pnky*-KD NSCs generated 3-fold more TUJ1+

neuroblasts after 7 days (7d) of differentiation (**Figures 2.1I** and **2.1J**). To further analyze the effect of *Pnky*-KD in the NSC population, we used a molecular-genetic method of targeting knockdown to V-SVZ NSCs (Doetsch et al., 1999; Park et al., 2014). We derived NSC cultures from G-TVA mice, which express the chicken retroviral receptor TVA from the GFAP promoter. For viral transduction of these cultures, we used shRNA lentiviruses pseudotyped with chicken viral EnvA protein, which restricts infection to the GFAP+ cells (**Figure 2.S1J**). In G-TVA NSCs, *Pnky*-KD did not affect NSC proliferation in self-renewal conditions (**Figure 2.S1K**). However, after differentiation, G-TVA NSC cultures produced a 3.56-fold more neuroblasts as compared to control (**Figure 2.S1L**). Thus, *Pnky*-KD targeted to the GFAP+ NSC population in V-SVZ cultures also resulted in increased neuronal production during differentiation.

V-SVZ transit amplifying cells express DLX2 and normally divide several times before giving rise to neuroblasts (Doetsch et al., 2002; Ponti et al., 2013). With *Pnky*-KD, there were 1.8 to 3.2 fold more EdU+, DLX2+ cells at 2d of differentiation, suggesting that *Pnky* plays a role at the transit amplifying stage of neuronal differentiation (**Figures 2.1K** and **2.S1M**).

To further investigate how *Pnky*-KD increases neuronal production, we plated NSCs infected with *Pnky*-KD or control vector with large numbers of uninfected NSCs (ratio of infected GFP+ NSCs to uninfected NSCs was approximately 1:5000, **Figure 2.2A**). After 4d of differentiation, these cultures produced well-isolated clusters of GFP+ cells (**Figure 2.2B**). With *Pnky* knockdown, the proportion of GFP+ cell clusters containing TUJ1+, GFP+ cells was increased (**Figure 2.2C**). Furthermore, these clusters also contained greater numbers of TUJ1+, GFP+ neuroblasts (**Figure 2.2D**). These data suggested that the increased neurogenesis resulted from both a shift towards neuronal lineage commitment and an increase in cell amplification within the neurogenic lineage.

To more directly observe the clonal behavior of individual NSCs with *Pnky*-KD, we used time-lapse microscopy to image GFP+ cells every 15 min for 3d (**Figure 2.2E**). We followed the fate of 316 GFP+ *Pnky*-KD NSCs and 531 GFP+ control NSCs. After differentiation, we could

identify both TUJ1+ neurogenic clones (**Figure 2.S2A**) and GFAP+ glial clones (**Figures 2.S2B** and **2.S2C**). Clones arising from NSCs with *Pnky*-KD were 48% more likely to be neurogenic (**Figure 2.2F**). Thus, *Pnky*-KD increased the likelihood that NSCs produced neurogenic progenitors.

Neurogenic clones with *Pnky*-KD contained 2.74 fold more neuroblasts than control (**Figure 2.S2D**). This increase in neurogenesis was in part related to an increase in progenitor cell divisions before differentiation into neuroblasts: while control progenitors divided 3.93 (SD=4.68, n=44) times and gave rise to 2.05 (SD=1.42) generations of daughter cells, *Pnky*-KD resulted in 8.94 (SD=7.64, n=33) divisions and 3.45 (SD=1.41) generations (**Figures 2.2G** and **2.2H**). The average cell cycle length was not affected by *Pnky*-KD (19.4 hours vs. 19.1 hours, p=0.89) (**Figure 2.S2E**), suggesting that the increased number of divisions related to the maintenance of a proliferative cell state and not an accelerated cell cycle. Time-lapse imaging also enabled direct observation of cell death, and the number of GFP+ neurogenic progeny (neuroblasts) that underwent cell death was reduced 57% by *Pnky*-KD (**Figure 2.2I**). Thus, *Pnky*-KD promoted neuronal lineage commitment from postnatal V-SVZ NSCs, increased the number of divisions of neurogenic progenitors, and reduced cell death (**Figures 2.2J** and **2.S2F**).

To investigate whether *Pnky* also regulates neurogenesis from other NSC populations, we next examined the embryonic brain. *Pnky* transcripts were detected in embryonic mouse brain tissue by RNA-seq (**Figure 2.1B**), and ISH revealed its expression in the cortical VZ – where embryonic NSCs reside – at embryonic day 14.5 (E14.5) and E16.5 (**Figures 2.3A**, **2.S3A**, and **2.S3B**). *Pnky* has two regions of high conservation among vertebrates (**Figures 2.3B** and **2.S3C**), and using strand-specific RNA-seq of gestational week 16 (GW16) human cortical samples, we detected a non-coding transcript divergent to *POU3F2* that included the conserved sequences. RACE cloning identified human *PINKY* (*PNKY*) as a polyadenylated 1592 nt transcript containing the two conserved elements and expressed from a conserved

promoter region (**Figure 2.3B**). As in the developing mouse brain, ISH of GW14.5 human cortex demonstrated *PNKY* expression in the VZ, with decreased levels in the subventricular zone and intermediate zone (SVZ/IZ), where young neurons begin to differentiate (**Figures 2.3C and 2.3D**).

To investigate the role of *Pnky* in the mouse embryonic VZ, we electroporated *Pnky*-KD (sh*Pnky*-2-GFP) or control (shCtrl-GFP) construct into VZ cells at E13.5 (**Figure 2.3D**). Two days later, we analyzed GFP+ cells in the VZ, SVZ/IZ, and cortical plate (CP) (**Figure 2.3E**). With *Pnky* knockdown, there was a 35% decrease in the proportion of GFP+ cells in the VZ and a 26% increase in GFP+ cells in the SVZ/IZ (**Figure 2.3F**). We did not detect apoptotic GFP+ cells as assessed by cleaved caspase-3 staining (not shown). At this time point in cortical development, SOX2+ NSCs in the VZ produce proliferative TBR2+ progenitor cells in the SVZ/IZ that differentiate into SATB2+ young neurons. With *Pnky* knockdown, the proportion of SOX2+, GFP+ cells was reduced (**Figure 2.3G**). While *Pnky* knockdown did not affect the proportion of TBR2+, GFP+ TA cells or their proliferation (**Figures 2.3E-J**), the proportion of SATB2+, GFP+ young neurons was increased (**Figure 2.3H**). These data indicate that *Pnky* regulates the production of young neurons from embryonic brain NSCs *in vivo* (**Figure 2.3K**).

Many lncRNAs regulate gene expression through interactions with specific protein partners. To identify *Pnky*-interacting proteins, we incubated biotinylated *Pnky* (S) or antisense *Pnky* (AS) control RNA with V-SVZ NSC nuclear extract and used mass spectrometry to identify proteins that bound to the transcripts (**Figures 2.4A and 2.4B**). Polypyrimidine tract-binding protein 1 (PTBP1) was identified as a binding partner of *Pnky*, and this interaction was confirmed by Western blot analysis (**Figure 2.4A**). While both *Pnky* and control RNA nonspecifically bound other RNA binding proteins including HNRNPK and ELAVL1 (**Figures 2.4A and 2.4C**), only *Pnky* RNA enriched for PTBP1, suggesting that the interaction between *Pnky* and PTBP1 is specific (**Figure 2.4A**). Furthermore, RNA immunoprecipitation with PTBP1 antibodies enriched for *Pnky* transcript but not U1 or beta-actin mRNA (**Figure 2.4B**).

PTBP1 is expressed in NSCs and functions as a repressor of neuronal differentiation. In the embryonic brain, loss of *Ptbp1* results in precocious neuronal differentiation (Shibasaki et al., 2013), and in fibroblasts, *Ptbp1* knockdown leads to direct neuronal trans-differentiation (Xue et al., 2013). PTBP1 was detected in the nucleus of V-SVZ NSCs (**Figure 2.S4D**), and *Ptbp1* knockdown resulted in larger neuronal colonies (**Figure 2.4C**), similar to the phenotype observed with *Pnky*-KD (**Figure 2.2D**).

In NSCs, PTBP1 negatively regulates the expression of *Ptbp2*, which is required for the generation of neuronal precursors (Boutz et al., 2007; Licatalosi et al., 2012). Using a PTBP2-specific antibody (Polydorides et al., 2000), we found the *Pnky* transcript did not specifically bind PTBP2 (**Figure 2.S4E**). During neurogenesis, *Ptbp1* is normally down-regulated, and *Ptbp2* is increased (Keppetipola et al., 2012). Therefore we next characterized the relationship between *Ptbp1*, *Ptbp2*, and *Pnky* expression. Upon *Ptbp1* knockdown in V-SVZ NSCs, *Ptbp2* transcripts were upregulated, as expected (**Figure 2.S4F**). *Ptbp1* knockdown did not decrease *Pnky* expression (**Figure 2.S4F**). *Pnky*-KD had no effect on *Ptbp1* expression and caused a small reduction (25%) in *Ptbp2* (**Figure 2.S4G**). Thus, the increase in neuronal differentiation observed with *Pnky*-KD does not appear to relate to changes in *Ptbp1* or *Ptbp2* expression.

PTBP1 regulates mRNA transcript levels and pre-mRNA splicing during neuronal differentiation (Keppetipola et al., 2012; Yap et al., 2012; Zheng et al., 2012). To determine whether *Pnky* and PTBP1 regulate a common set of transcripts, we performed RNA-seq of V-SVZ NSCs with either *Pnky* knockdown or *Ptbp1* knockdown. The overlap of differentially expressed genes was highly significant (**Figure 2.4D** and **Table 2.1**, 815 genes, $P = 3.8 \times 10^{-152}$) and enriched for Gene Ontology terms (Huang et al., 2009) related to cell-cell adhesion, synaptogenesis and neurogenesis (**Table 2.2**). Furthermore, using DEX-seq (Anders et al., 2012) to analyze differential exon usage, we found that *Pnky* knockdown and *Ptbp1* knockdown also resulted in a common set of splice variants (**Figure 2.4E** and **Table 2.3**, 101 exons, $P = 1.3 \times 10^{-52}$). Thus, these data demonstrate that *Pnky* and its associated protein PTBP1 regulate

an overlapping set of transcripts that underlies their role in regulating neurogenesis from V-SVZ NSCs.

To further assess whether *Pnky* and *Ptbp1* function in the same pathway, we performed an epistasis experiment. The lack of synergistic or additive effects upon combined loss of an lncRNA and coding gene pair suggests that they function in the same molecular pathway (Dimitrova et al., 2014). Therefore, we used FACS to isolate NSCs with double knockdown of *Pnky* and *Ptbp1* as well as NSCs with each single knockdown (**Figures 2.S4H-I**). We then analyzed the expression of several genes (*Ntsr2*, *Igfbp5*, *Scrg1*, and *Ppp1r3c*) that had been commonly upregulated by both *Pnky*-KD and PTBP1 knockdown in RNA-seq experiments (**Figure 2.4D**). As expected, *Ntsr2*, *Igfbp5*, *Scrg1*, and *Ppp1r3c* all had increased expression in the cells with single-knockdown as compared to control (**Figures 2.4F-H and 2.S4J**). Importantly, the combined knockdown of *Pnky* and *Ptbp1* did not further enhance this gene expression (**Figures 2.4F-H and 2.S4J**). These data indicate a genetic interaction between *Pnky* and *Ptbp1* and suggest that they function in the same pathway to regulate gene expression in NSCs.

Discussion

Taken together, our data indicate that *Pnky* is a conserved, neural-specific, nuclear lncRNA that interacts with PTBP1 and regulates the production of neurons from NSCs. While other lncRNAs have been found to function in central nervous system development – with lncRNA loss-of-function resulting in decreased neurogenesis (Bond et al., 2009; Chalei et al., 2014; Lin et al., 2014; Ng et al., 2013; Rapicavoli et al., 2011; Sauvageau et al., 2013; Ulitsky et al., 2011) – *Pnky* knockdown increased the production of neurons, suggesting a distinct developmental role for this lncRNA in controlling neurogenesis from NSCs. Our data are consistent with a model in which *Pnky* serves to “restrain” neuronal commitment, regulating the

production of young neurons from NSCs in the developing embryonic cortex as well as those in the postnatal V-SVZ.

In the developing cortex, we found that *Pnky*-KD resulted in an increase in young neurons and decreased the NSC population in the VZ. This did not appear to involve a change in the proliferation of the transit amplifying cells of this embryonic lineage. In V-SVZ NSCs from the postnatal brain, *Pnky*-KD also promoted neuronal differentiation, and we additionally observed greater numbers of divisions of the neurogenic progenitor cells. Thus, the phenotypes of *Pnky*-KD in these two very different NSC populations are largely similar in that neuronal differentiation is increased. Interestingly, *Pnky* does not appear to regulate all NSC populations, as we did not detect *Pnky* transcripts in the dentate gyrus, which harbors another population adult NSCs.

Our studies indicated that *Pnky* interacts with PTBP1, which is a key regulator of neural development (Shibasaki et al., 2013). PTBP1 is also a powerful mediator of cell reprogramming (Xue et al., 2013), and its depletion from fibroblasts can lead to direct trans-differentiation into neurons. Moreover, PTBP1 is a potent driver of brain tumor growth and invasiveness (Ferrarese et al., 2014). During neuronal differentiation, PTBP1 is normally downregulated, and there is an increase in PTBP2. We did not find evidence for a specific interaction between *Pnky* and PTPB2 or other nuclear RNA-binding proteins such as HNRNPK and ELAVL1. These data suggest that *Pnky* and PTPB1 – a splicing factor with critical functions in both normal development and brain tumors – are part of a specific ribonucleoprotein complex in NSCs.

Given this physical interaction between *Pnky* and PTBP1, we worked towards understanding whether this lncRNA and protein partner function together. First, we found that both *Pnky* and PTPB1 knockdown in V-SVZ NSCs promoted neurogenesis. Furthermore, *Pnky*-KD promoted neuronal differentiation in the developing cortex, and mice with *Ptbp1* loss-of-function also exhibit precocious cortical neurogenesis. Thus, *Pnky*-KD and loss of PTBP1 produce similar phenotypic results. Second, we found that *Pnky*-KD and PTBP1-knockdown

produced gene expression changes as well as splicing changes that were highly similar, indicating that *Pnky* and PTPB1 regulate a common set of transcripts related to neuronal differentiation. Third, our epistasis experiment indicated that *Pnky* and PTBP1 double knockdown does not produce changes greater than single knockdowns. Thus, the physical interaction between *Pnky* and PTBP1 along with the evidence for their genetic interaction is consistent with a model in which they function together in a common molecular pathway. Whether the physical interaction between *Pnky* and PTPB1 is required for their regulation of neuronal differentiation remains to be tested directly. Future work may reveal an interplay between lncRNAs and PTBP1 in different biological contexts, including cancer and direct cell reprogramming.

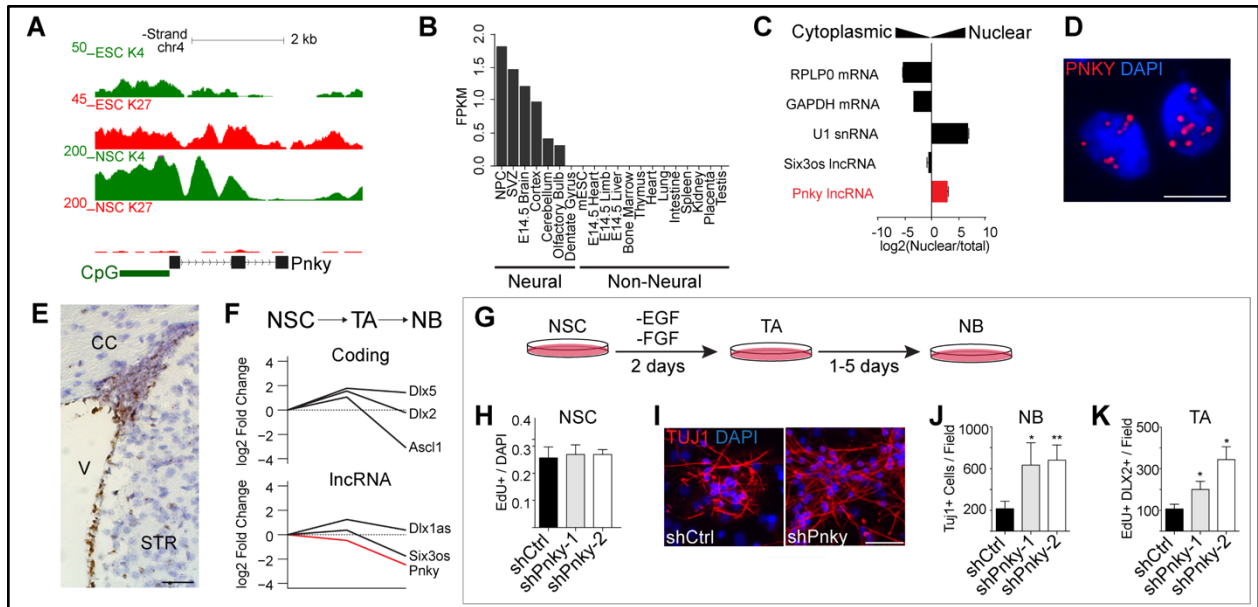


Figure 2.1: The lncRNA *Pinky* is expressed in SVZ-NSCs and regulates neuronal differentiation.

A, UCSC genome browser view of the *Pnky* locus. Also shown are ChIP-seq tracks for H3K4me3 and H3K27me3 in ESCs and V-SVZ NSCs. **B**, Fragments per kilobase per million mapped reads (FPKM) values for *Pnky* in indicated tissues. **C**, Subcellular fractionation followed by RT-qPCR for indicated lncRNAs and mRNAs. Error bars are propagated standard deviation from technical triplicate wells. **D**, Branched-DNA *in situ* hybridization for *Pnky* in V-SVZ NSC cultures. Nuclei are counter-stained with 4',6-diamidino-2-phenylindole (DAPI). Scale bar = 10 μ m. **E**, Branched-DNA *in situ* hybridization for *Pnky* in adult mouse coronal tissue section. *Pnky* stains brown, and nuclei are counter-stained with hematoxylin. V = ventricle, CC = corpus collosum, STR = striatum. Scale bar = 50 μ m. **F**, Results of microarray expression analysis from FACS-isolated neural stem cells (NSC), transit amplifying cells (TA), and neuroblasts (NB). Value in NSCs set to 0. **G**, Schematic of V-SVZ NSC culture system. **H**, Quantification of EdU labeling counted from GFP+ cultures of V-SVZ NSCs infected with control or *Pnky*-KD constructs. **I**, Immunocytochemistry for TUJ1 (red) after 7d of differentiation in control or *Pnky*-KD GFP+ cultures. Nuclei are counter-stained with DAPI (blue). Scale bar = 50 μ m. **J**, Quantification of TUJ1+ NBs produced after 7d differentiation. **K**, Quantification of the number of TA cells, defined as being co-labeled with DLX2 and EdU, after 2d of differentiation. Error bars for (H), (J), and (K) are standard deviation from triplicate wells, * $p < 0.05$, ** $p < 0.01$, Student's t-test. See also Figure 2.S1.

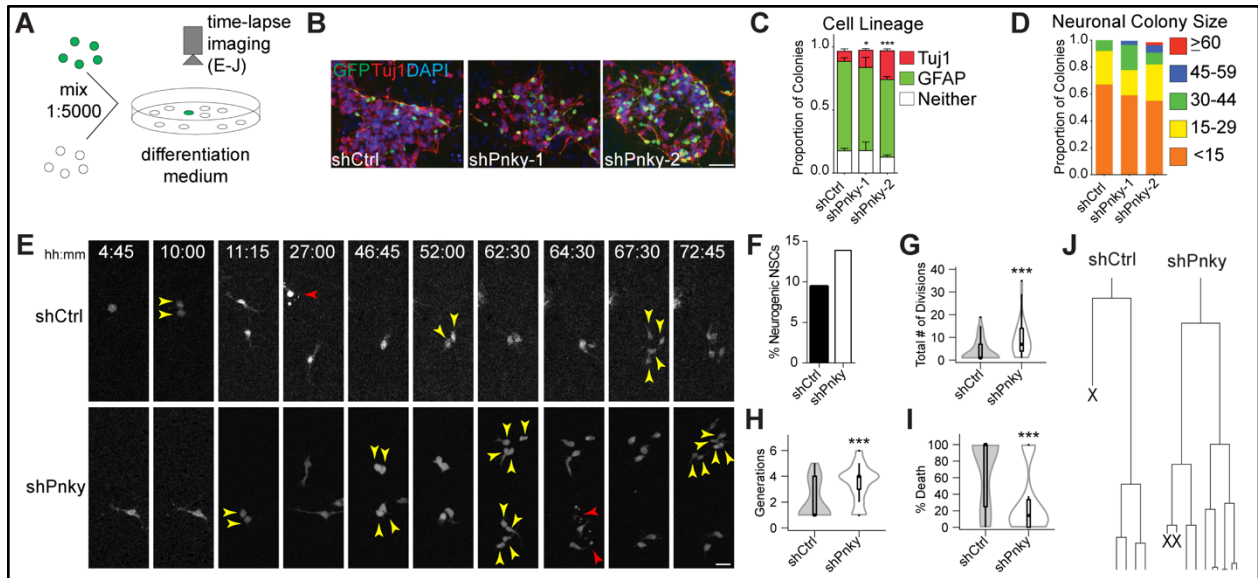


Figure 2.2: *Pinky* knockdown leads to an expansion of neurogenic transit amplifying progenitors.

A, Schematic of experimental design. **B**, Representative images of isolated colonies after 4d differentiation. Immunocytochemistry for TUJ1 (red) and GFP (green). Nuclei are counterstained with DAPI (blue). Scale bar = 50 μ m. **C**, Quantification of the fate of isolated GFP+ colonies. Error bars are standard deviation from triplicate experiments. **D**, Quantification of the number of TUJ1+ neuroblasts found in individual neurogenic colonies. **E**, Representative frames from time-lapse video of control (top) or *Pnky*-KD (bottom) single cells. Time in differentiation medium is indicated. Yellow arrows indicate daughter cells resulting from a recent division, red arrows indicate cell death. Scale bar = 25 μ m. **F**, Bar graph representing the percentage of initial tracked progenitors that gave rise to neuroblasts. N= 531 GFP+ shCtrl NSCs and 316 GFP+ sh*Pnky* NSCs. **G**, Violin plots overlaying box-and-whisker plots of total number of divisions undergone by a single initial neurogenic progenitor and all of its daughter cells. N = 44 shCtrl and 33 sh*Pnky* progenitors. **H**, Violin plots overlaying box-and-whisker plots of the number of generations per initial neurogenic progenitor for shCtrl and sh*Pnky*. N = 44 shCtrl and 33 sh*Pnky* progenitors. **I**, Violin plots overlaying box-and-whisker plots of % of progeny per single neurogenic progenitor that underwent cell death. N = 44 shCtrl and 33 sh*Pnky* progenitors. **J**, Tree diagram for the frames shown in (E) and corresponding time-lapse movies. X indicates that the cell underwent cell death. * $p < 0.05$ *** $p < 0.001$, Student's t-test. See also Figure 2.S2.

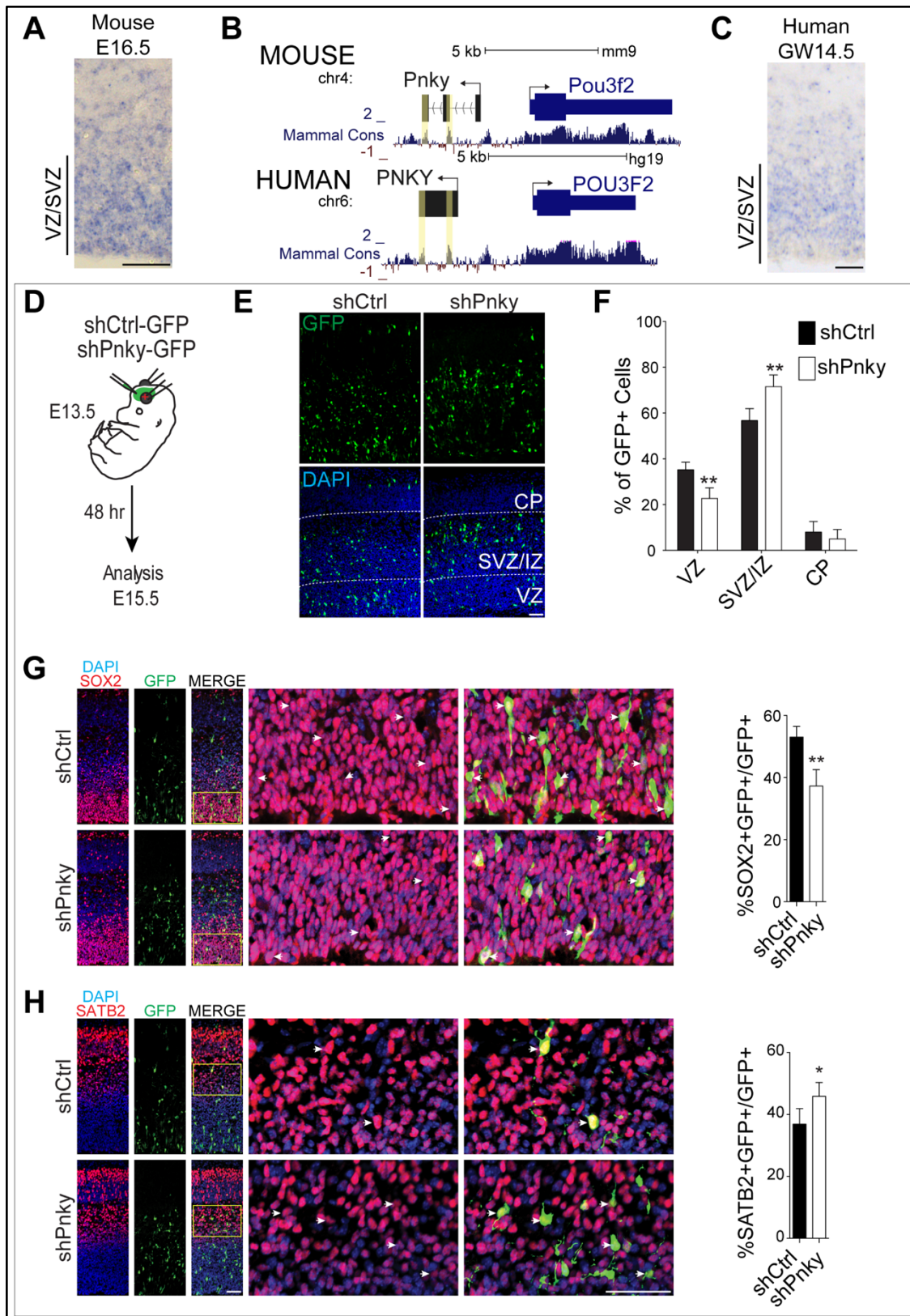


Figure 2.3: *Pinky* is expressed in the developing mouse and human cortex and regulates the differentiation of mouse cortical progenitors *in vivo*.

A, *In situ* hybridization for *Pnky* in embryonic day 16.5 (E16.5) mouse brain. **B**, Genome browser track demonstrating that the mouse *Pnky* transcript has two regions of high conservation, determined by PhyloP score (yellow boxes). Human *PNKY* genomic region is shown below with conservation indicated. For clarity, the mouse –strand is shown left to right. **C**, *In situ* hybridization for *PNKY* in gestational week 14.5 (GW14.5) human brain. **D**, Schematic of *in utero* electroporation of mouse embryonic brain. **E**, Cortical sections at E15.5, 2d after electroporation with shCtrl (left) or sh*Pnky* (right). Immunostained for GFP (top) and with DAPI counterstain (bottom). VZ = ventricular zone, SVZ/IZ = subventricular zone/intermediate zone, CP = cortical plate. **F**, Quantification of GFP+ cell distribution in indicated zones as a percentage of total GFP+ cells. **G**, Left: Cortical sections at E15.5, 2d after electroporation with shCtrl or sh*Pnky*. Immunostained for GFP (green) and SOX2 (red), with DAPI nuclear counterstain (blue). Yellow box indicates region expanded in the subsequent panels. Arrowheads indicate co-labeled cells. Right: quantification of SOX2+, GFP+ cells as a percentage of total GFP+ cells. **H**, Left: Cortical sections immunostained for GFP (green) and SATB2 (red), with DAPI nuclear counterstain (blue). Yellow box indicates region expanded in the subsequent panels. Right: Quantification of SATB2+, GFP+ cells as a percentage of total GFP+ cells. All error bars are standard deviation, n=4 brains of each condition from 3 separate surgeries. *p<0.05, **p<0.01. All scale bars = 50 μ m. See also Figure 2.S3.

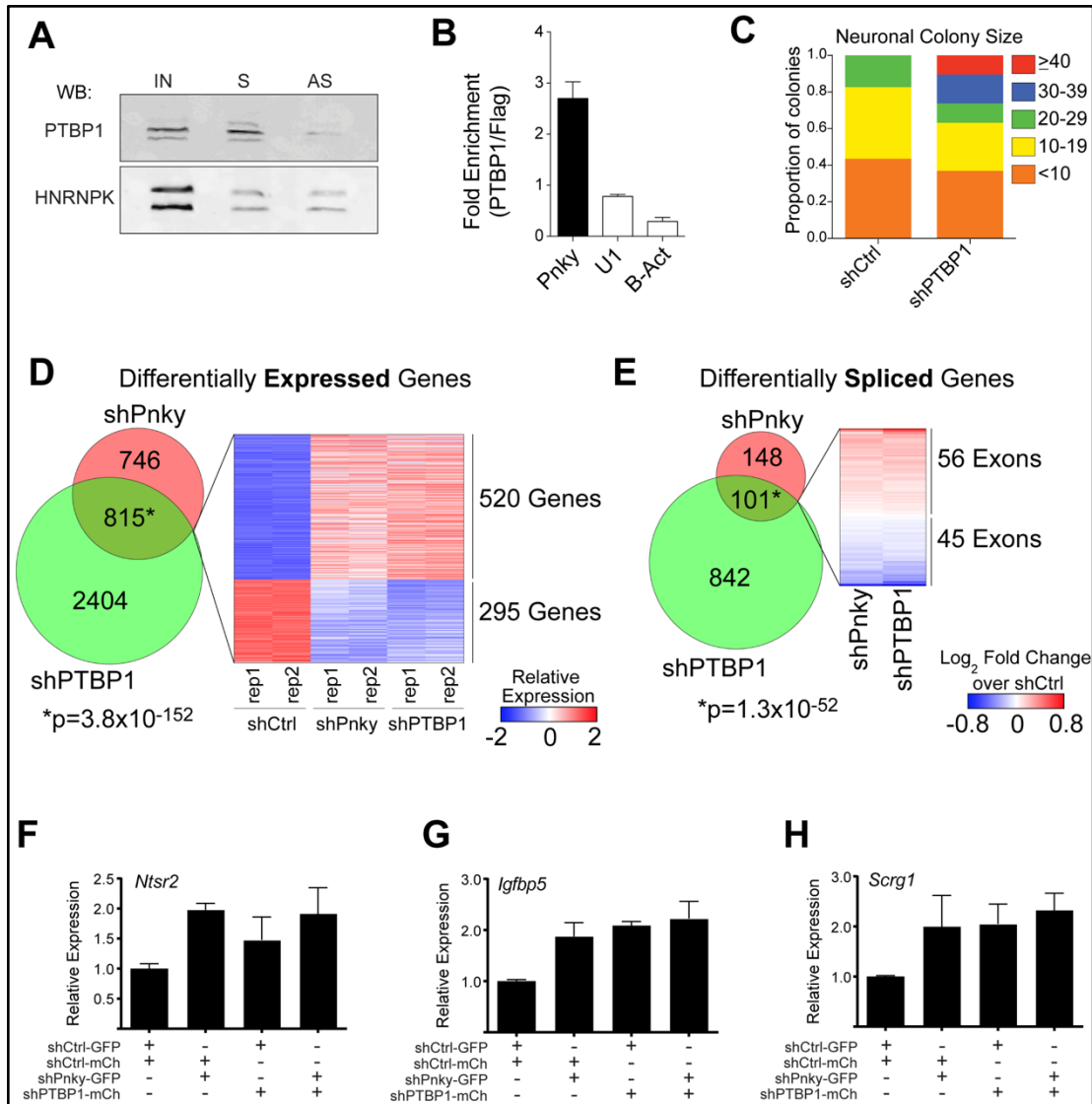


Figure 2.4: *Pinky* interacts with PTBP1 and regulates RNA expression and splicing.

A, Immunoblot for PTBP1 or HNRNPK following RNA-pulldown experiment with biotin-labeled sense (S) or anti-sense (AS) *Pnky* RNA incubated with V-SVZ NSC nuclear extract. IN = input V-SVZ nuclear extract. **B**, RT-qPCR detection for indicated RNA recovered by PTBP1-specific antibody normalized to control FLAG antibody. Error bars are propagated standard deviation from technical triplicates. **C**, Quantification of number of TUJ1+ neuroblasts found in individual neurogenic colonies with *Ptbp1*-knockdown or control. **D**, Venn Diagram demonstrating the overlap between genes differentially expressed (FDR < 0.05) upon *Ptbp1* or *Pnky* knockdown. Heatmap representation of the differential expression of the overlapping gene set in shCtrl, sh*Pnky*, and sh*Ptbp1* biological duplicate cultures. **E**, Venn Diagram demonstrating the overlap between exons showing differential usage (FDR < 0.01) upon *Ptbp1* or *Pnky* knockdown. Heatmap representation of the differential usage of the overlapping gene set in sh*Pnky* and sh*Ptbp1* cultures compared to control. **F-H**, RT-qPCR detection of expression of indicated genes normalized to *Gapdh*. Expression in each condition is shown relative to control (shCtrl-GFP, shCtrl-mCherry). Error bars are 95% confidence intervals from 3 separate cultures. See also Figure 2.S4 and Tables 2.1-2.3.

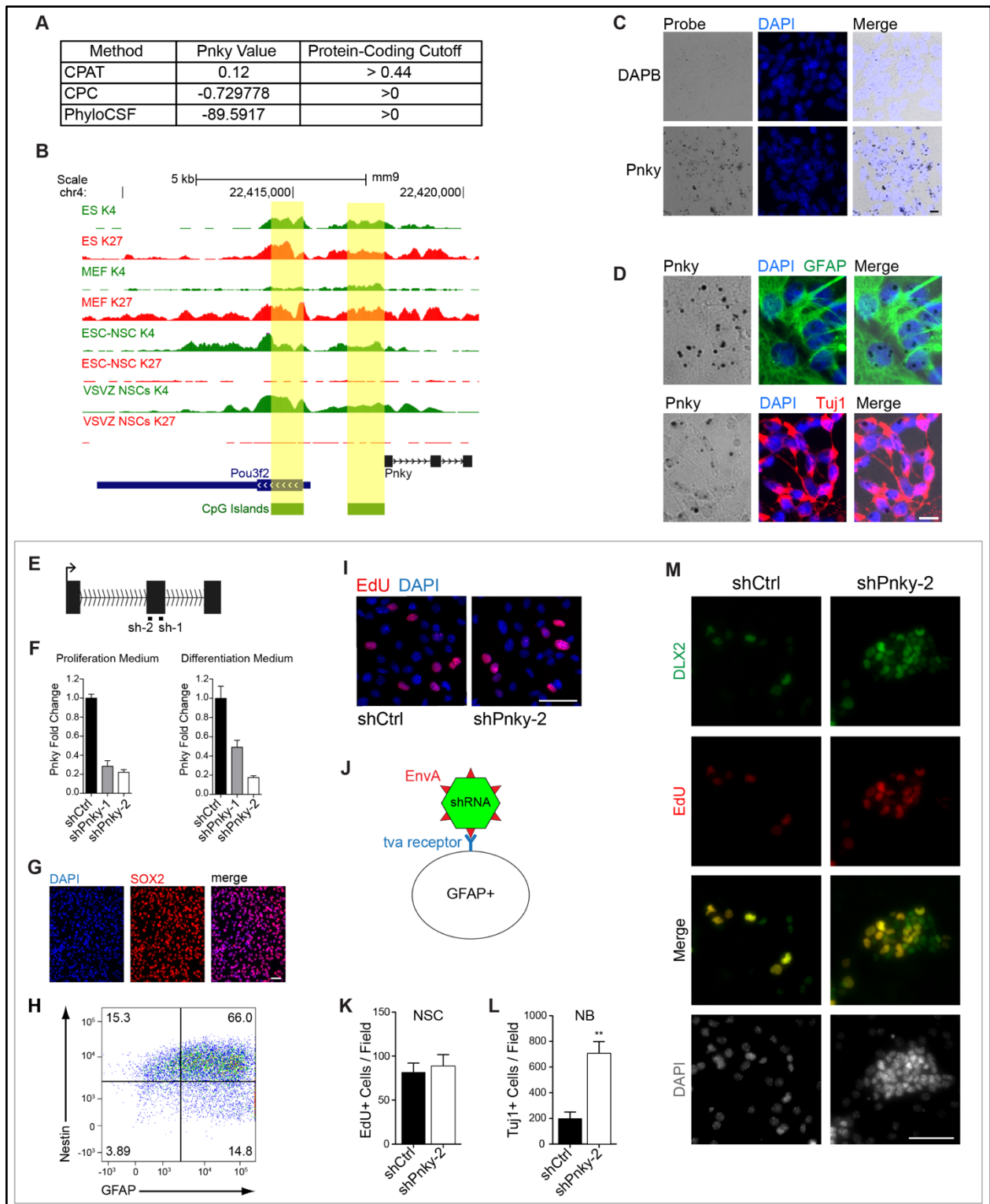


Figure 2.S1: Characterization of the long noncoding RNA *Pnky* and *Pnky*-KD cultures.
A, Table of protein-coding scores derived from CPAT, CPC, and PhyloCSF, and the cut-off for determining that a transcript is likely to encode a protein. **B**, Genome browser view of the *Brn2* and *Pnky* loci with H3K4me3 and H3K27me3 ChIP-seq tracks for embryonic stem cells (ES),

mouse embryonic fibroblasts (MEF), ESC-derived neural stem cells (ESC-NSCs), and V-SVZ NSCs. Yellow boxes indicate promoter regions defined by CpG islands. **C**, *In situ* hybridization using branched DNA probes targeting *Pnky* and negative control bacterial transcript DAPB in V-SVZ-NSC cultures. Nuclei are counter-stained with DAPI. Scale bar = 10 μ m. **D**, *In situ* hybridization using branched DNA probes targeting *Pnky* in V-SVZ-NSC cultures after 4 days of differentiation, immunostained with GFAP (green) or Tuj1 (red). Nuclei are counter-stained with DAPI (blue). Scale bar = 20 μ m. **E**, Schematic of *Pnky* RNA and the regions targeted by sh*Pnky*-1 and sh*Pnky*-2. **F**, *Pnky* knockdown efficiency in purified cultures in proliferation medium (left) or differentiation medium (right). Fold change was calculated with the delta-delta Ct method, normalized to shCtrl and *Rplp0* housekeeping gene. Error bars are standard deviation propagated by least-squares method from technical triplicate. **G**, V-SVZ NSC cultures in proliferation conditions immunostained with SOX2 (red). Nuclei are counter-stained with DAPI (blue). Scale bar = 50 μ m. **H**, FACS plot of GFAP and NESTIN expression in GFP+ cells from V-SVZ cultures infected with control lentivirus. **I**, Purified cultures of V-SVZ-NSCs infected with shCtrl (left) or sh*Pnky*-2 (right) labeled with EdU for 1h and stained for incorporated EdU with Click-iT chemistry. Nuclei are counterstained with DAPI (blue). Scale bar = 50 μ m. **J**, Schematic depicting targeting of shRNA constructs to NSCs with the TVA-EnvA system. **K**, Quantification of EdU labeling counted from purified cultures of GTVA V-SVZ NSCs infected with control or *Pnky*-knockdown constructs. **L**, Quantification of Tuj1+ NBs produced from purified cultures of GTVA V-SVZ NSCs after 4d differentiation. **M**, Purified cultures immunostained with DLX2 (green) and stained for EdU (red) after 3h of labeling in differentiation medium. Nuclei are counterstained with DAPI. Scale bar = 50 μ m.

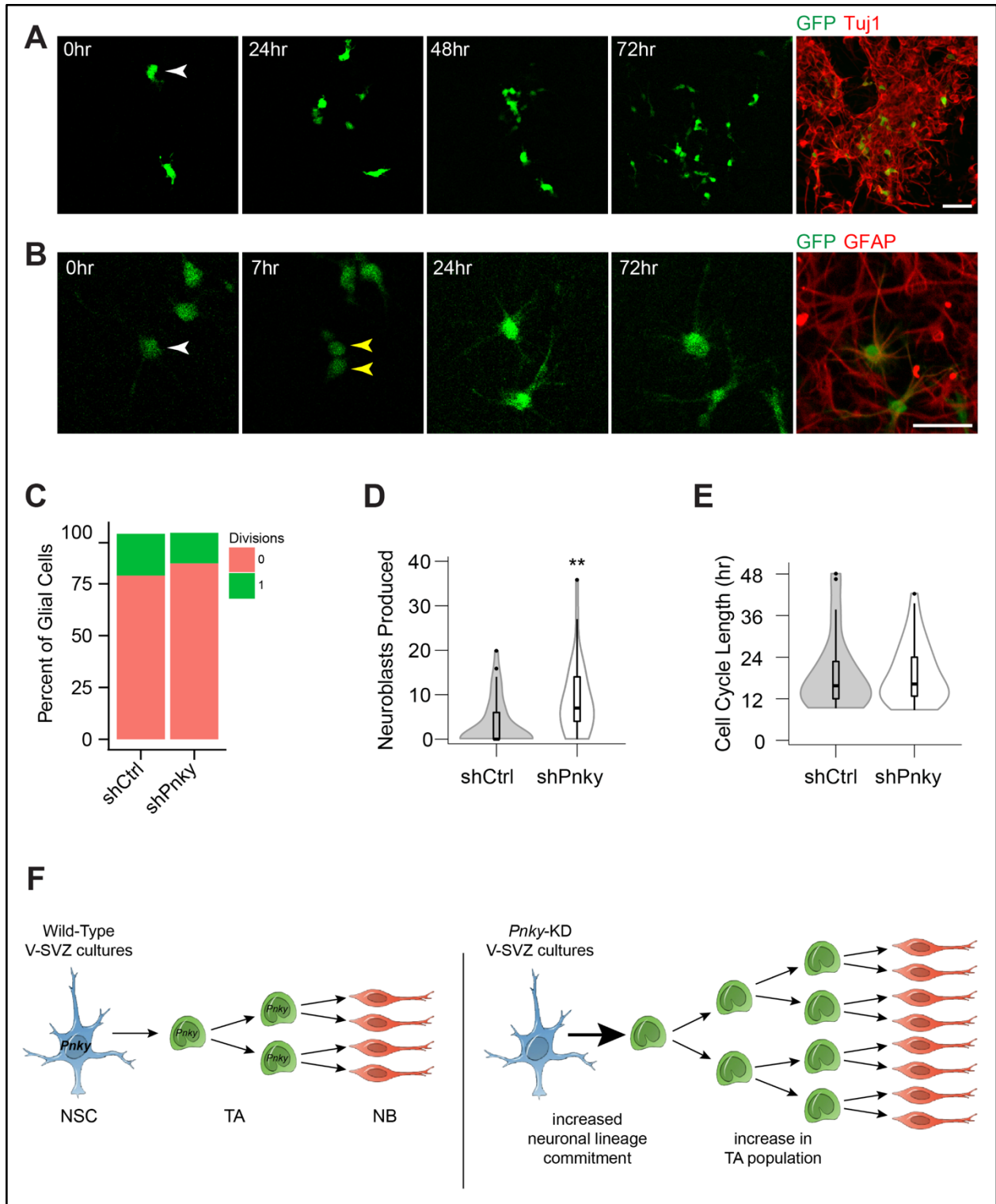


Figure 2.S2: Analysis of time-lapse imaging of V-SVZ cultures.

A, Frames from time-lapse movies, demonstrating a neurogenic clone. Immediately after imaging, plate was fixed and immunostained for GFP (green) and TuJ1 (red). White arrow indicates initial tracked NSC. Scale bar = 50 μ m. **B**, Frames from time-lapse movies, demonstrating a glial clone undergoing one division. White arrow indicates initial tracked NSC

and yellow arrows indicate daughter cells resulting from a division. Immediately after imaging, plate was fixed and immunostained for GFP (green) and GFAP (red). Scale bar = 50 μ m. **C**, Bar graph representing the number of glial cell divisions per clone as a proportion of all glial clones. N = 481 shCtrl cells and 272 sh*Pnky* cells. **D**, Violin plot overlaying box-and-whisker plot representing the total number of progeny produced per initial neurogenic NSC. N = 44 shCtrl and 33 sh*Pnky* progenitors. **E**, Violin plot overlaying box-and-whisker plot representing the cell cycle length from the first to second divisions of shCtrl and sh*Pnky* cells. N= 27 shCtrl divisions and 45 sh*Pnky* divisions. **F**, Schematic depicting the role of *Pnky* in postnatal V-SVZ NSCs. Left: Normal lineage progression of neuronal production from V-SVZ NSCs (blue) to DLX2+ transit amplifying cells (TA, green) to Tuj1+ young neurons (red). Bottom: *Pnky*-KD promotes neuronal production. With *Pnky*-KD, a greater proportion of NSCs commit to the neurogenic lineage, and TA cells undergo more cell divisions. **p <0.01, Student's t-test.

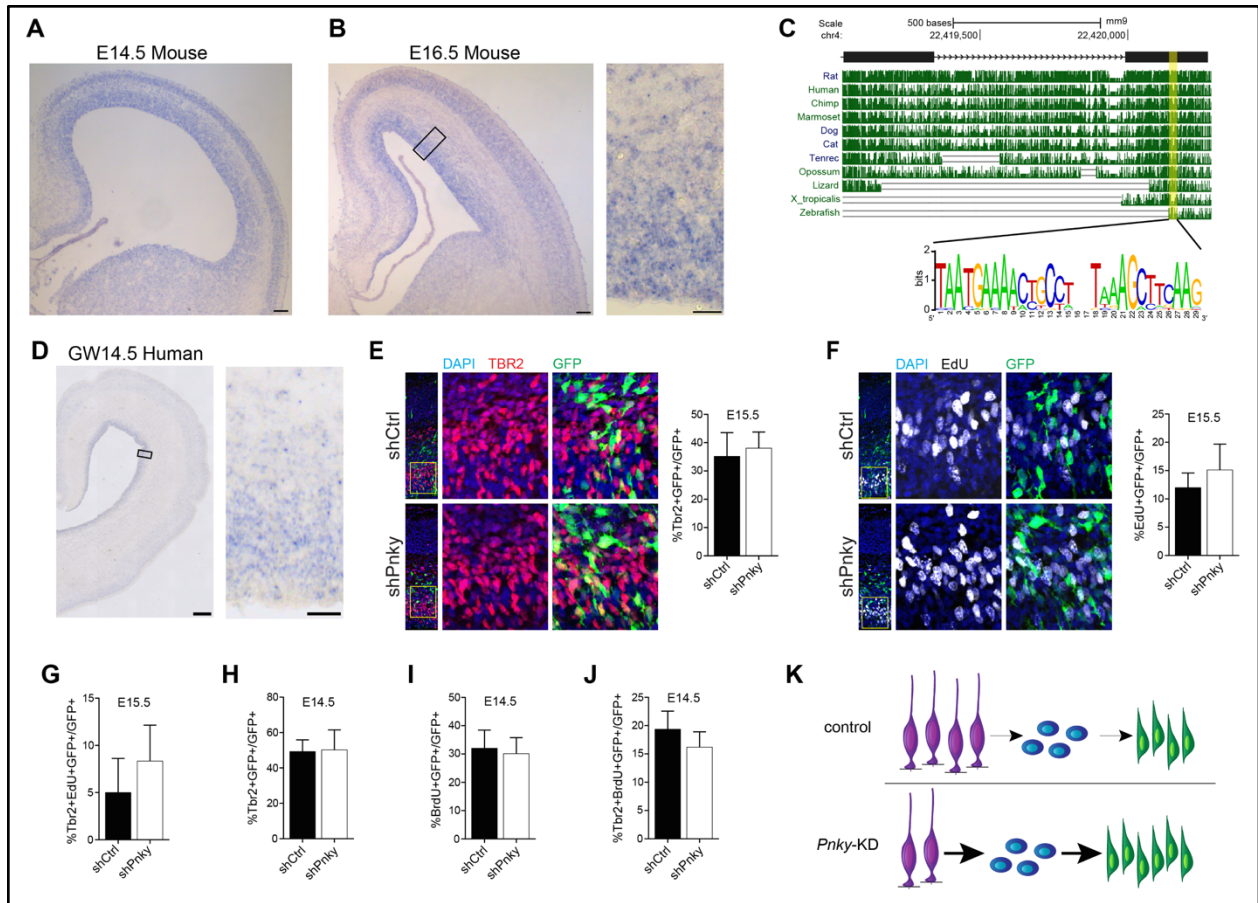


Figure 2.S3: *Pnky* is evolutionarily conserved and expressed in the developing mouse and human cortex.

A, *In situ* hybridization of *Pnky* in embryonic day 14.5 (E14.5) mouse brain. Scale bar = 100 μ m. **B**, *In situ* hybridization for *Pnky* in E16.5 mouse brain. Scale bar = 100 μ m. Black box indicates area of detail shown at right and in Figure 2.3A. Scale bar for high magnification image = 25 μ m. **C**, Genome browser view of exons 2 and 3 of mouse *Pnky* and PhastCons scores across indicated vertebrates. The blue box highlights a sequence conserved to zebrafish. In the sequence logo, a score of 2 bits indicates bases are perfectly conserved across all genomes shown. **D**, *In situ* hybridization of *PNKY* in human gestational week 14.5 (GW14.5) brain. Scale bar = 500 μ m. Black box indicates area of detail shown at right and in Figure 2.3C. Scale bar for high magnification image = 50 μ m. **E**, Left: Cortical sections at E15.5, 2d after electroporation with shCtrl or sh*Pnky*, stained for GFP (Green) and TBR2 (Red), with DAPI nuclear counterstain. Yellow box indicates region expanded in the subsequent panels. Right: quantification of TBR2+ GFP+ cells as a percentage of total GFP+ cells. Scale bar = 25 μ m. **F**, Left: Cortical sections at E15.5, 2d after electroporation with shCtrl or sh*Pnky*, stained for GFP (green) and EdU (white), with DAPI nuclear counterstain. Yellow box indicates region expanded in the subsequent panels. Right: quantification of EdU+ GFP+ cells as a percentage of total GFP+ cells. Scale bar = 25 μ m. **G**, Quantification of TBR2+EdU+GFP+ cells as a percentage of total GFP+ cells at E15.5, 2d after electroporation with shCtrl or sh*Pnky*. **H**, Quantification of TBR2+GFP+ cells as a percentage of total GFP+ cells at E14.5, 1d after electroporation with shCtrl or sh*Pnky*. **I**, Quantification of BrdU+GFP+ cells as a percentage of total GFP+ cells at E14.5, 1d after electroporation with shCtrl or sh*Pnky*. **J**, Quantification of TBR2+BrdU+GFP+ cells as a percentage of total GFP+ cells at E14.5, 1d after electroporation with shCtrl or

sh*Pnky*. **K**, Schematic depicting the role of *Pnky* in regulating embryonic corticogenesis. Top: Normal lineage progression of neuronal production from radial glial SOX2+ NSCs (purple) to TBR2+ intermediate neurogenic progenitors (blue) to SATB2+ young neurons (green). Bottom: *Pnky*-KD promotes progression through the neurogenic lineage, resulting in a depletion of NSCs and an increase in young neurons. The population of TBR2+ intermediate progenitors is not affected.

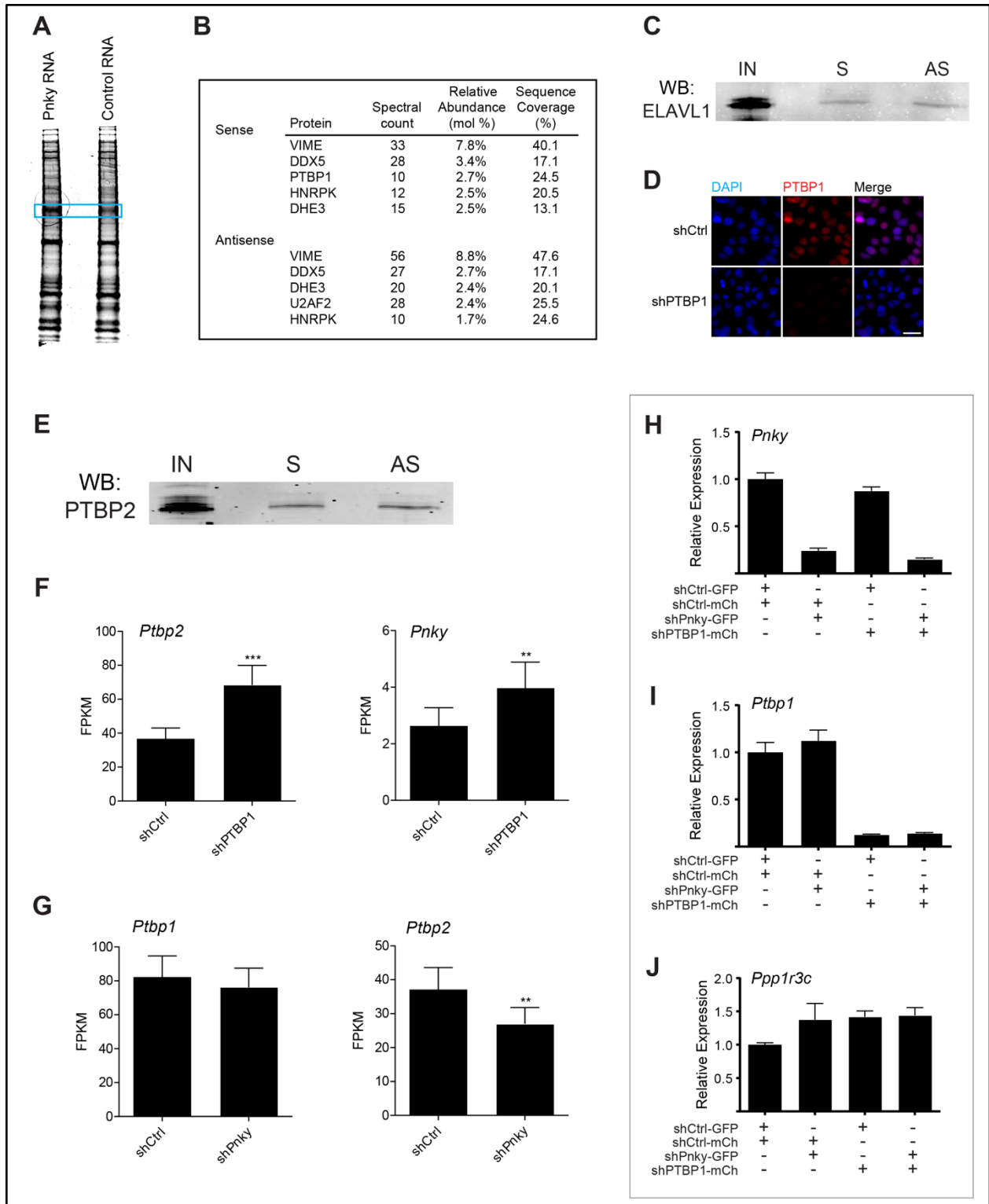


Figure 2.S4: Characterization of the interaction of *Pnky* and PTBP1.

A, Sypro Ruby-stained SDS-PAGE protein gel of proteins retrieved with biotinylated *Pnky* RNA or control RNA. Blue box indicates area excised and sent for mass spectrometry. **B**, Top proteins identified by mass spectrometry from excised bands, excluding keratin contaminant

peptides. **C**, Immunoblot for ELAVL1 from RNA-pulldown experiment with biotin-labeled sense (S) or anti-sense (AS) *Pnky* RNA incubated with N2A nuclear extract. **D**, Immunostaining for PTBP1 (red) in purified V-SVZ NSC cultures infected with control or shPTBP1. Nuclei are counterstained with DAPI. Scale bar = 25 μ m. **E**, FPKM values calculated by Cufflinks for *Ptbp1* or *Ptbp2* upon control or *Pnky* knockdown. Error bars represent 95% confidence intervals. **FDR<0.01. **F**, FPKM values calculated by Cufflinks for *Pnky* or *Ptbp2* upon control or *Ptbp1* knockdown. Error bars represent 95% confidence intervals. **FDR<0.01, ***FDR<0.001. **G**, Immunoblot for PTBP2 from RNA-pulldown experiment with biotin-labeled sense (S) or anti-sense (AS) *Pnky* RNA incubated with N2A nuclear extract. **H-J**, RT-qPCR detection of expression of indicated gene normalized to *Gapdh*. Expression in each condition is shown relative to control (shCtrl-GFP, shCtrl-mCherry). Error bars are 95% confidence intervals. Data are from 3 separate purified cultures.

Table 2.1: Differential expression of genes regulated by *Pnky* and PTBP1.

Genes that are differentially expressed (FDR<.05) in both sh*Pnky* and shPTBP1 cells. Log2 of average fold change over control from two biological replicates is shown.

Gene	sh <i>Pnky</i>	shPTBP1	Gene	sh <i>Pnky</i>	shPTBP1
Serpinf2	2.30059	3.10323	Nog	0.910957	1.76398
Ip6k3	2.38942	2.8193	Pdlim2	0.849767	1.80503
Rab11fip4	2.32631	2.61774	Traf1	0.556344	2.0955
Papss2	1.59071	3.30315	Chrn4	1.1419	1.49811
Paqr6	1.81384	3.04298	Necab3	1.07427	1.5591
Gpr50	1.77036	3.07164	Tfcp2l1	0.844945	1.76911
Thbs1	1.39774	3.43844	Gpc5	0.794615	1.81765
Fam107a	1.36752	3.19558	Phkg1	0.835399	1.77109
Pdgfrb	1.64163	2.61955	Fgf11	1.02041	1.58159
Afap1l2	1.16293	3.06282	Cdkl4	1.14149	1.44685
Hsd11b1	2.08792	2.03285	B3galt4	1.23903	1.34588
Adamts13	1.19762	2.73826	Syn2	1.06542	1.51499
Kcns3	2.20943	1.69586	Gpr155	1.22669	1.33492
Nxph4	1.63328	2.03415	Chst1	0.916777	1.64166
Kcne1l	1.34359	2.23993	AI848285	1.14364	1.39668
Stbd1	1.44447	2.01473	Fgl2	1.14218	1.39504
Rpe65	1.62675	1.82541	Zmynd10	0.878799	1.65255
Fam211b	1.92756	1.5164	2610034M16Rik	1.84508	0.670359
Tmem100	1.23795	2.19053	Pdk4	1.35961	1.15216
Cldn10	1.37751	2.00256	AI464131	1.38723	1.12357
Stpg1	1.32605	1.9838	Kcnj14	0.980144	1.52142
Bgn	1.64506	1.6591	Fndc5	1.03074	1.46212
Trim67	1.67737	1.5678	S100b	0.602441	1.8756
Trim43a	1.42133	1.79593	Plxdc1	1.19184	1.2857
Adora2b	1.42518	1.76504	Abhd3	0.927911	1.54781
Spns2	1.62792	1.56105	Ak4	1.07073	1.39396
Padi2	1.35945	1.82484	Igfbp5	1.10912	1.34999
Gucy1b2	1.87785	1.27978	Rnase4	1.29252	1.16531
Chd5	0.985959	2.0818	Map3k19	0.940244	1.50619
Lpcat2	0.99297	2.07188	Htr3a	1.54176	0.892346
Scd4	1.18149	1.86238	Ndr1	0.562612	1.83598
Hspa1a	1.07616	1.92115	Sertad4	1.32344	1.07454
Calb2	1.66689	1.32923	Ptgs1	0.89115	1.50219
Rassf4	1.1008	1.87142	4632428N05Rik	0.721087	1.66484
Lect1	0.87661	2.09321	Hr	1.07827	1.29219
Gng8	1.27979	1.68585	Nek5	0.938875	1.42271
Cdkn1c	1.17616	1.78618	Srcin1	1.08348	1.27315
Gm10635	0.735334	2.08352	G0s2	1.30704	1.04785
Cryab	0.840456	1.97388	Gria2	1.0299	1.31146
Siah3	1.9215	0.874546	Ephx2	1.0216	1.31067
Dpysl5	0.80098	1.99456	Gpr30	1.43892	0.887811
Ldlrad4	0.974843	1.8123	Med21	1.0966	1.20103
Wnt9a	0.785581	1.99001	Gjb2	1.20573	1.09083
Tgm2	0.904016	1.87046	Mfsd2a	0.522773	1.7572
Hcn2	1.53632	1.19646	Ccdc74a	0.690736	1.5738
Mettl20	0.805244	1.91015	Ifit3	1.0619	1.20076
Hapln1	0.804483	1.91034	Gad1	0.971514	1.28556
Pmepa1	0.796337	1.9175	Rhbdl3	1.52198	0.731892
Tspan17	0.894903	1.8156	Grin2c	0.832116	1.40886
Mpped1	1.7343	0.96083	Crybb1	1.11504	1.1233
Dhrs3	1.08368	1.59945	Ggt1	0.893934	1.33971
Tppp3	0.980402	1.70085	Bmf	1.56819	0.663505

Gene	shPnky	shPTBP1	Gene	shPnky	shPTBP1
Capn1	0.753011	1.47655	Slc6a15	0.572517	1.35288
Dusp28	0.839937	1.38893	P2ry6	0.696161	1.22134
Slc14a2	1.04187	1.18213	Pla2g5	0.625403	1.28851
Cd82	0.617826	1.60578	Paqr7	0.712042	1.20128
Nkain4	1.16575	1.056	Dok7	0.956926	0.956088
Scrg1	0.876592	1.33379	Ctsl	0.718427	1.18861
Fam198a	1.62601	0.583583	D030056L22Rik	0.932837	0.963847
Mal	0.888282	1.31959	1810043G02Rik	0.780346	1.10988
Galnt16	0.786054	1.41667	Rnd3	0.878588	0.995797
1500009C09Rik	0.873334	1.30783	6330403K07Rik	1.37802	0.496042
Cyp2d22	0.838094	1.33005	Macrof1	0.518072	1.35596
Cmb1	0.543347	1.62444	Serpinf1	0.918646	0.933933
Nmb	1.31994	0.838329	Hspa2	0.549559	1.2966
Tacr1	1.36311	0.794231	Optn	0.777479	1.06378
Epo	0.821142	1.33038	Kcna6	0.563461	1.27359
Pcgf2	0.920778	1.22906	Fam161a	0.874275	0.953428
H2-T23	1.29929	0.849674	Snapin	0.796726	1.03074
Churc1	0.833055	1.30542	A930017M01Rik	0.953049	0.872897
5430435G22Rik	0.797661	1.3403	4732415M23Rik	0.602189	1.21347
Slc24a4	1.30807	0.821584	B230217O12Rik	0.656718	1.15427
Usp18	0.847077	1.27837	Slc13a3	0.546034	1.26044
Hmgcs2	0.995312	1.12191	Irgm2	0.72814	1.07294
Sncb	0.996904	1.11855	Mdga1	0.807857	0.992435
Cst3	0.693639	1.40824	C1qtnf5	0.617096	1.17987
Slco1a4	0.787376	1.3127	Hspa1b	0.523147	1.25847
Ntsr2	0.912133	1.18027	Gulp1	0.727847	1.05298
Pth1r	0.856788	1.23178	Tmem167b	0.681846	1.09086
Irf7	0.9419	1.1411	Slc39a1	0.697153	1.07488
Htati2	0.581688	1.49735	Tnr	0.809248	0.946603
Slc7a2	0.706135	1.35612	Cmtm5	0.887367	0.867843
Sfrp5	1.27589	0.774777	Al414108	0.713927	1.03845
Ifit1	0.766603	1.28299	Miat	1.05852	0.684889
Cyp4f14	0.756275	1.29281	Tmem132b	0.607642	1.1315
Camkk1	0.719552	1.3263	Slc35b4	0.976828	0.758806
Snpc5	0.747749	1.28579	Smad6	0.615408	1.11633
Kcnd2	0.742653	1.28947	Pm20d2	0.642586	1.08009
Cacna2d2	1.13349	0.897368	Selenbp1	0.833268	0.888342
Stox1	0.655625	1.36621	Inpp5a	0.701438	1.00202
Fstl5	1.20197	0.815953	Pak6	0.817684	0.883816
Cxcr7	0.953465	1.05862	Cd99l2	0.628733	1.06983
Ccdc80	0.501816	1.50903	Igsf9b	0.745061	0.947917
Mob1a	1.0403	0.968691	Ppp1r3c	0.732782	0.958958
Kcnh2	1.02559	0.982532	1110015O18Rik	0.922927	0.768527
Ppp1r1b	1.25572	0.751198	Fam174b	0.581821	1.1033
Entpd2	0.684657	1.31553	Sesn1	0.876402	0.80188
A730020M07Rik	0.647387	1.34971	Psd2	0.707501	0.969223
D10Jhu81e	0.896141	1.10095	Fam114a1	0.601404	1.07065
Gem	0.838952	1.15378	Tppp	0.860026	0.803495
Ras12	0.948981	1.04206	Pcyt1b	0.677276	0.985644
Myrip	0.92793	1.05711	Atp1a2	0.621179	1.03844
Ampd3	0.748394	1.2329	Hmgcl	0.772967	0.884276
Diras1	1.19629	0.781692	Gpr37	0.839712	0.815229
Car4	1.17972	0.790403	Epm2a	0.556194	1.0932
Capn5	0.642573	1.32734	Furin	0.469644	1.17959
Jakmip1	0.755048	1.20743	Shpk	0.865939	0.782004
Gpr153	0.930684	1.0287	Daam2	0.556755	1.08999
Oasl2	1.06822	0.876013	Chgb	0.851711	0.793865

Gene	shPnky	shPTBP1	Gene	shPnky	shPTBP1
Cpne3	0.735603	0.905872	Klhdc8b	0.681325	0.784574
Ctnna2	0.712019	0.928771	Bsg	0.388273	1.06252
Rab6b	0.632101	1.00795	Scg5	0.972554	0.477527
Ppp1r3g	0.805178	0.83363	Abcd2	0.809262	0.639037
Gm16197	0.488605	1.14869	Chchd10	0.552723	0.895386
Klhdc7a	0.534541	1.09688	St8sia5	0.966053	0.476414
Pea15a	0.39126	1.23795	Nrbp2	0.51276	0.929075
Lynx1	0.845911	0.78038	Idi1	0.520889	0.920461
Loxl2	0.4742	1.14964	Abat	0.604691	0.836596
Stard10	0.607648	1.01352	3632451O06Rik	0.694869	0.744514
Cxxc4	0.743389	0.865933	Prelp	0.7405	0.698135
Armc2	0.543658	1.0626	Sema7a	0.413071	1.0249
Enho	0.679614	0.924974	Kcnk10	0.449766	0.987922
Gpr158	0.719723	0.881017	Stard8	0.646317	0.789074
Ccdc13	0.889851	0.707224	Fam5b	0.91805	0.516655
Socs2	0.89191	0.700865	2510009E07Rik	0.717101	0.714952
Endod1	0.566988	1.02447	Slco1c1	0.479807	0.951047
Apcdd1	1.16888	0.420012	Tspo	0.408099	1.01929
Nrarp	1.07274	0.515645	Syap1	0.714997	0.711183
Rd3	0.985576	0.601212	Car5b	0.639032	0.784938
Lipg	0.54055	1.0457	Gpt2	0.914118	0.509776
Plscr2	0.692834	0.889989	Gnao1	0.648613	0.773907
Gpr173	0.627916	0.954203	B3galt5	0.741134	0.677231
Fam5c	0.625994	0.952352	Zfp41	0.842378	0.571323
Fto	0.662545	0.913957	1830012O16Rik	0.952151	0.460627
BC064078	0.666646	0.89944	Eya2	0.714587	0.694635
Stac2	0.418004	1.14642	Rhob	0.543537	0.864193
Neto1	0.958095	0.605778	Rap1gap2	0.59722	0.808462
Pdzrn3	0.758215	0.792794	Scd1	0.550503	0.854772
Nupr1l	0.665017	0.881093	Ttyh1	0.515634	0.880976
Col26a1	0.709682	0.83514	Pdlim3	0.792015	0.603923
Tmem40	0.685243	0.855379	Serping1	0.613124	0.782578
Fam134b	0.707064	0.828588	Chi3l1	0.925676	0.467983
Naaa	0.581211	0.952148	Txndc5	0.733273	0.65688
Gpr179	1.03924	0.49329	Hapln4	0.533059	0.855876
Fbxl8	0.604912	0.920493	Pip4k2a	0.683049	0.703311
Lgi3	0.605148	0.919317	Spag1	0.540654	0.844328
Gm2115	0.645896	0.877055	4930451G09Rik	0.655234	0.726832
Mpp3	0.628194	0.893648	Grm4	0.820829	0.559552
Gpr146	0.670941	0.837005	Lamtor5	0.516829	0.863299
Sdc4	0.553749	0.953252	Klhl3	0.666394	0.699991
Insm1	0.841466	0.664221	Abi3	0.465051	0.901258
Vegfa	0.479271	1.02272	4930451C15Rik	0.73116	0.633891
Ppp1r3d	0.656397	0.844583	Pdk1	0.368445	0.99222
Cdk5r1	0.971679	0.527414	Aldoc	0.511088	0.836929
Mettl23	0.524798	0.964008	Rab3il1	0.827608	0.520185
Rasgrp1	0.508758	0.979051	Il6st	0.586513	0.74918
Nek9	0.650581	0.836002	Tns3	0.823057	0.512058
Dnase1l1	0.677679	0.804911	Gpam	0.670716	0.661959
C1r1	0.751552	0.729303	Zdhhc14	0.578539	0.752764
Pls1	0.493713	0.986167	Tns1	0.677783	0.652231
Map1b	0.661517	0.813081	Fmo5	0.456263	0.872311
Lbp	0.821922	0.651531	Scp2	0.464514	0.863896
Nedd9	0.623392	0.848451	Mpv17	0.469467	0.856435
Cetn4	0.690512	0.780678	Rcor2	0.972978	0.349369
Gpd1l	0.665979	0.804908	Wdr47	0.520743	0.799762
Sox2	0.839272	0.627919	Phactr1	0.791273	0.523987

Gene	shPnky	shPTBP1	Gene	shPnky	shPTBP1
Nat2	0.610278	0.703003	Emilin1	0.781335	0.382174
Arhgef19	0.682756	0.630277	Taf13	0.400227	0.763185
H2-D1	0.686615	0.62245	Rab30	0.526953	0.636289
Dok5	0.635958	0.672406	Phyhd1	0.493512	0.66851
Kazald1	0.50819	0.798313	Ldhd	0.4703	0.690877
Dab2	0.572853	0.731176	Adcy9	0.463191	0.693667
Cadm3	0.872909	0.429445	Slc14a1	0.472466	0.680226
Igtp	0.533476	0.765659	Ammecr1	0.600224	0.551833
Lrp4	0.817444	0.480448	Mmd2	0.473153	0.677471
Plscr1	0.647138	0.647396	Kcnn3	0.44139	0.706867
Cntfr	0.805303	0.488375	Syt17	0.529442	0.614268
Brsk2	0.655417	0.628185	Man1c1	0.387462	0.751215
Adcy8	0.684789	0.597294	Islr	0.553343	0.580212
Gm16515	0.644304	0.630088	Kif21a	0.582865	0.542569
Mfsd6	0.471841	0.801727	Akap5	0.445759	0.677892
Cmpk2	0.442746	0.824768	Prosapip1	0.552386	0.567383
Lingo1	0.612191	0.654308	Tyro3	0.746527	0.371927
Glcci1	0.77204	0.494072	Pdgfrl	0.498079	0.619416
Slc19a2	0.651351	0.614747	Inhbb	0.693053	0.422899
Lrrm1	0.896804	0.366831	Cdh11	0.521161	0.594051
4933431E20Rik	0.651782	0.611612	Rnd2	0.411886	0.700059
Snx10	0.496053	0.765691	Apba1	0.703463	0.40678
Chac1	0.528488	0.733144	Atxn1	0.426882	0.682019
Asap3	0.562858	0.698537	Unc5a	0.559766	0.546615
Slc48a1	0.488524	0.772675	Scd2	0.409204	0.696082
Celsr1	0.432969	0.826442	Pak1	0.387247	0.716792
Sh3bp4	0.695345	0.562834	Tmem180	0.400444	0.702912
Slc22a23	0.625112	0.629956	2610035D17Rik	0.663863	0.43901
Als2cl	0.816541	0.438413	Gamt	0.545347	0.550083
Morn5	0.690081	0.564827	Extl3	0.509253	0.586014
Usp53	0.405291	0.847337	Tmem255a	0.506589	0.586925
Cdc42ep4	0.717103	0.53131	Slc29a3	0.488137	0.60361
Cyth3	0.600778	0.642523	Sash1	0.442403	0.64463
Fam69c	0.712499	0.529115	Gpr137b	0.599521	0.487013
Tekt4	0.668436	0.565839	8-Sep	0.596231	0.489412
Myo10	0.516295	0.715762	Inca1	0.501776	0.580711
Hoga1	0.546605	0.680649	Psph	0.511851	0.570568
Luzp2	0.53474	0.689391	Arrb1	0.510328	0.567972
Syt7	0.731994	0.490473	Thra	0.409781	0.665164
Irgm1	0.586556	0.635282	Fam117a	0.681836	0.392781
Slc38a2	0.580464	0.63861	Slc38a1	0.503869	0.568215
Frmpd1	0.619026	0.597291	Wnk3	0.563483	0.506748
Fgfr2	0.396675	0.814782	Mtus1	0.644549	0.423494
Faim2	0.61689	0.591687	Fmn2	0.502418	0.565205
Muc1	0.621927	0.586574	Ipo7	0.409743	0.65759
Gng10	0.418336	0.780045	Gdpd5	0.435746	0.626294
Nod1	0.507388	0.679928	Akt3	0.492779	0.568129
Cdk16	0.55508	0.631386	Pdp2	0.450757	0.610104
Gpr137b-ps	0.57205	0.613093	Efna2	0.572844	0.485964
Scml4	0.552379	0.631237	AA986860	0.509646	0.547088
Naprt1	0.613272	0.570332	Rgs9	0.481537	0.57232
Txnip	0.700623	0.479887	Psmc9	0.432175	0.621531
Fancg	0.619722	0.56072	Ppap2b	0.472686	0.579783
Nr2e1	0.592389	0.58499	Ras11b	0.533582	0.516995
Vstm4	0.43753	0.73277	Maml1	0.561362	0.483114
Zkscan7	0.563745	0.604789	Fads1	0.563184	0.4787
Napepld	0.490884	0.674278	Dlgap1	0.558077	0.48285

Gene	shPnky	shPTBP1	Gene	shPnky	shPTBP1
Ypel3	0.450568	0.58766	Slc2a10	0.495	0.371115
Fam160b1	0.386944	0.651242	Tnrc6b	0.464779	0.399025
Acad12	0.436502	0.601494	Aldh5a1	0.375606	0.478651
Pygb	0.409374	0.626795	Dag1	0.384415	0.465319
Poldip2	0.445543	0.590233	Cpped1	0.403713	0.441474
Coasy	0.43184	0.594887	Srebf1	0.405512	0.43521
Cyp4f13	0.532569	0.493168	Gli2	0.466392	0.37122
Ankrd6	0.645152	0.371991	Rnf20	0.421041	0.405392
Enpp4	0.568464	0.445394	Ank	0.426497	0.386246
Rdm1	0.528879	0.484083	Itga2	0.442589	0.365908
Dhrs7	0.418839	0.589636	Ssc5d	0.38454	0.411609
Kcnab2	0.40742	0.595953	Mapt	0.413248	0.375535
Mrpl9	0.434474	0.568867	Trak1	0.431067	0.346507
Gcnt2	0.509581	0.487126	Bhlhe40	0.372618	0.404849
Med30	0.474712	0.521905	Cpt1a	0.426102	0.346971
Htra3	0.518587	0.471853	Tlr3	0.400687	0.359293
Slc46a1	0.39755	0.592294	Pice1	0.412807	0.346955
Gm973	0.50044	0.487873	Ddx21	-0.379583	-0.352167
8430427H17Rik	0.457264	0.528899	Ppid	-0.377404	-0.360666
Uhmk1	0.461784	0.522306	Tmem30a	-0.37588	-0.363209
Socs7	0.543737	0.433357	Nrcam	-0.368841	-0.374528
Phldb1	0.409567	0.566691	Lars	-0.411539	-0.33894
Acat2	0.483613	0.488448	Klc2	-0.394158	-0.360362
Adam17	0.503976	0.461726	Nucks1	-0.369869	-0.385708
Abcd1	0.421133	0.543636	Urb2	-0.438393	-0.354872
Maoa	0.438707	0.525785	Zfp704	-0.414209	-0.381033
Lgals8	0.388495	0.575243	Pwp2	-0.405821	-0.397167
Tapbp	0.371663	0.590462	Nol10	-0.456508	-0.346887
Lrp6	0.387767	0.569791	Cdc42bpg	-0.433773	-0.381022
Entpd5	0.38307	0.568353	Cwf19l2	-0.444541	-0.371641
Ugt1a6a	0.481613	0.464822	Bin1	-0.428728	-0.390435
Arxes1	0.44411	0.50036	Elf2b3	-0.437874	-0.381289
Rgl1	0.388539	0.552485	Pds5b	-0.429915	-0.394321
Adora2a	0.403204	0.537322	Chordc1	-0.406799	-0.42762
Ppp6r3	0.421008	0.516424	Fam179b	-0.466568	-0.372067
Tbcel	0.589091	0.347745	Ppan	-0.468453	-0.372628
Gstk1	0.424564	0.510077	Fam49a	-0.462347	-0.381497
Tlcd1	0.386775	0.546826	Cmtm6	-0.498365	-0.351418
Ston2	0.484572	0.446498	Plcl2	-0.425267	-0.425162
Bcl9l	0.456156	0.473338	Polr1b	-0.439696	-0.410982
Pik3ip1	0.465754	0.457373	Tbc1d1	-0.428519	-0.422431
Slc24a6	0.404716	0.517408	Smug1	-0.420093	-0.433989
Taz	0.412018	0.501741	Cnn2	-0.501665	-0.357299
Paqr4	0.530215	0.381361	Acsl4	-0.424318	-0.449957
Zfp37	0.483375	0.423157	Prkab1	-0.461913	-0.416162
Rdh13	0.483904	0.421749	Fam60a	-0.449971	-0.429449
Zfyve26	0.477991	0.42545	Mboat1	-0.393552	-0.489318
Mllt6	0.408301	0.492593	Pvr	-0.52013	-0.370568
Tle3	0.385485	0.507045	Grwd1	-0.435758	-0.457979
Fam168a	0.404185	0.480977	9430008C03Rik	-0.428109	-0.473026
Aif1l	0.543115	0.341578	Socs6	-0.443959	-0.458738
Slc16a3	0.389462	0.492011	Olig2	-0.528263	-0.376978
Pnmal2	0.494712	0.383794	Celf2	-0.490321	-0.418715
Ankrd10	0.535375	0.343066	Spred2	-0.444129	-0.469514
Fdxr	0.464714	0.411348	Zyx	-0.414414	-0.499764
Fbxo36	0.417968	0.457667	Rprm	-0.534995	-0.379629
Srgap3	0.408982	0.464147	Cpeb4	-0.460596	-0.464654

Gene	shPnky	shPTBP1	Gene	shPnky	shPTBP1
Dennd5a	-0.520624	-0.404771	Flt1	-0.751411	-0.387254
Pcbp3	-0.43694	-0.490754	Ano3	-0.416263	-0.726016
Nop2	-0.510794	-0.421599	Sox7	-0.715974	-0.427132
Fam110c	-0.552396	-0.382681	Phf15	-0.770455	-0.37541
Etv5	-0.553162	-0.384242	Osbp16	-0.691273	-0.454831
Thumpd3	-0.506987	-0.432079	Nid1	-0.406907	-0.747012
Plxna2	-0.380541	-0.563913	Arhgap26	-0.501876	-0.652513
Slain2	-0.444286	-0.501889	Irs1	-0.501259	-0.653262
Irf2bp1	-0.624113	-0.336281	Pmaip1	-0.654354	-0.500575
Lrp12	-0.492472	-0.47024	Olf287	-0.593878	-0.566741
Hprt	-0.481869	-0.484254	Arhgap18	-0.416943	-0.745274
Nhlrc3	-0.486745	-0.485426	Klf6	-0.768266	-0.395532
Purb	-0.452384	-0.522484	D10Wsu102e	-0.507244	-0.658671
Neat1	-0.404892	-0.57065	Adamts14	-0.689633	-0.476514
Vegfc	-0.541914	-0.443197	Rbm24	-0.6976	-0.473879
Ch11	-0.537757	-0.44876	Urb1	-0.715976	-0.456515
Fnip2	-0.531324	-0.457318	Hpcal1	-0.808504	-0.366482
Lrch2	-0.425561	-0.563416	Gm11974	-0.694908	-0.481688
Crem	-0.449741	-0.545846	Fblim1	-0.60816	-0.572212
Pde1c	-0.466639	-0.529541	Gm3002	-0.620164	-0.572215
Rai14	-0.614584	-0.38465	Ccdc106	-0.632812	-0.58299
B4galt6	-0.54714	-0.454229	Hs6st2	-0.596333	-0.620459
Cttnbp2nl	-0.645363	-0.361825	Prrg4	-0.820403	-0.400607
Adamts4	-0.582904	-0.428496	Spp1	-0.513355	-0.710445
Eva1c	-0.5582	-0.456307	Myc	-0.783321	-0.452098
Ccdc86	-0.555187	-0.466186	Cmtm3	-0.669107	-0.572739
Rap2c	-0.492877	-0.530635	Bbs12	-0.617133	-0.628536
Cited2	-0.484768	-0.545223	Il1rap	-0.548963	-0.699327
Fzd1	-0.576871	-0.464305	Cd93	-0.590929	-0.661858
1700003M07Rik	-0.436932	-0.612723	Pam	-0.436389	-0.817938
Rasa1	-0.526501	-0.52732	Synj2	-0.640222	-0.622595
Atp10a	-0.408299	-0.648741	Cml3	-0.574051	-0.689366
Ubald1	-0.531409	-0.533069	Enc1	-0.421315	-0.842572
Sf3b4	-0.378131	-0.688086	Myo1b	-0.562164	-0.711615
Lpar4	-0.588648	-0.485408	Stk32a	-0.488385	-0.787276
Ccnd1	-0.503435	-0.576236	Fam212b	-0.711408	-0.574227
Cacna2d1	-0.555198	-0.525584	Fndc3a	-0.42032	-0.869107
9530053A07Rik	-0.464201	-0.618075	Gpc3	-0.58054	-0.710089
Dio2	-0.635854	-0.448044	Syt13	-0.690273	-0.601903
Zbtb10	-0.447395	-0.641148	Pxdn	-0.444396	-0.849108
Npnt	-0.692028	-0.397382	Ccdc71l	-0.859553	-0.44263
Bcl2	-0.713221	-0.387857	Slc7a11	-0.563152	-0.747438
Zbtb7c	-0.706566	-0.394746	Frm4a	-0.801935	-0.511566
Foxn2	-0.673642	-0.433654	Nudt4	-0.704328	-0.609976
9930013L23Rik	-0.480464	-0.631478	Icam1	-0.615104	-0.700787
Efh2	-0.569572	-0.54453	Trf	-0.723178	-0.593486
Swap70	-0.49424	-0.620359	Zmat3	-0.862789	-0.45745
Hes1	-0.51574	-0.599448	Col5a1	-0.689285	-0.635923
Tbc1d10a	-0.628938	-0.488536	Cdk19	-0.738704	-0.595408
Gap43	-0.51628	-0.604095	Hapln3	-0.587256	-0.752111
Prr5l	-0.453844	-0.667018	Slc24a3	-0.737884	-0.615987
Ass1	-0.443222	-0.68311	Trim16	-0.819713	-0.540817
Hunk	-0.712529	-0.413972	Lypla2	-0.714384	-0.659399
Smurf1	-0.645168	-0.484233	Peg10	-0.621885	-0.756173
9330182L06Rik	-0.69277	-0.443664	Camk1d	-0.78308	-0.600461
Rybp	-0.694737	-0.442913	Tle2	-0.515783	-0.868167
Eil2	-0.666326	-0.472281	Vat1l	-0.544971	-0.841791

Gene	shPnky	shPTBP1	Gene	shPnky	shPTBP1
Ets2	-0.777257	-0.618923	Kcnj2	-0.89155	-0.898039
Kcnn4	-0.493637	-0.907876	Klk10	-1.06317	-0.757623
2310014L17Rik	-0.651678	-0.750881	Frzb	-0.678757	-1.1438
Slc4a7	-0.876963	-0.528544	Ptk2b	-0.655441	-1.1708
Col18a1	-0.723792	-0.683198	Tnc	-0.756506	-1.07491
Tmem173	-0.749231	-0.658614	Zfp711	-0.801249	-1.0606
Tgfb1	-0.870417	-0.540039	Heph	-0.7566	-1.12127
Fst	-0.610702	-0.801846	Spry4	-1.1986	-0.700883
Ust	-0.681012	-0.735362	Ptprj	-1.47406	-0.443934
Dusp4	-0.9546	-0.475193	Styk1	-0.967642	-0.965251
Pde2a	-0.680932	-0.759693	Egr1	-1.02955	-0.932774
Rgs17	-1.06679	-0.381573	Ras11a	-1.34918	-0.634787
4833427G06Rik	-0.807116	-0.641915	St14	-1.08511	-0.914283
Gja5	-0.830241	-0.621696	Hist1h1d	-1.00067	-1.00371
Sox3	-0.740708	-0.712438	Nkx6-2	-0.847716	-1.15874
Ube2ql1	-0.645712	-0.813347	S100a3	-1.30551	-0.701782
Tmc3	-0.475998	-0.984527	Col27a1	-1.21503	-0.80063
Cd38	-0.559373	-0.90284	Adamts1	-1.12722	-0.889559
Ly75	-0.762419	-0.711206	Tbc1d9	-0.79347	-1.23273
Amigo2	-0.842635	-0.639457	Trim47	-1.38519	-0.644473
Slc25a25	-0.967378	-0.519657	Mc3r	-1.19325	-0.841269
Polr1e	-0.710311	-0.790925	Casp1	-0.897687	-1.1768
Aldh1a7	-0.478422	-1.02796	Epha2	-1.46132	-0.620336
Ccnd2	-0.699429	-0.808642	Gria1	-1.02934	-1.135
Vav3	-0.674739	-0.835399	Cyp24a1	-1.43708	-0.760054
Marcks11	-0.574277	-0.939937	Chrm3	-1.18215	-1.01739
Mapre1	-1.12039	-0.403795	Fbln2	-0.393294	-1.84064
Elavl4	-0.577833	-0.951793	Jag1	-1.31432	-0.921421
Klk8	-0.835502	-0.716218	Sgms2	-1.77698	-0.468258
Sp8	-0.732421	-0.822348	Vstm2a	-0.982829	-1.28321
Ier3	-1.05356	-0.502037	Tinagl1	-0.91505	-1.36455
Ppip5k2	-0.54208	-1.02413	Unc5d	-1.18489	-1.09804
Phlda1	-0.699233	-0.869212	Mei4	-0.924214	-1.36864
Sphkap	-1.01334	-0.55524	Dgkk	-1.12279	-1.18492
Nkx2-2	-0.993971	-0.577516	Pcp4l1	-0.794389	-1.54577
Cdsn	-1.10071	-0.475284	Tlr2	-0.8927	-1.4617
Insr	-1.01407	-0.564107	Lalba	-1.17517	-1.18091
Lamb1	-0.950753	-0.628969	Lgr6	-1.77337	-0.595058
Rrad	-0.850299	-0.747402	Gimap8	-1.34554	-1.04283
Dact1	-0.890561	-0.707857	Vgf	-0.64195	-1.74825
Plk2	-0.828649	-0.770055	Car10	-1.24943	-1.14578
Vcan	-0.685734	-0.917602	Fbn2	-0.710466	-1.68663
Akap12	-0.942701	-0.666763	Slco1a6	-1.35923	-1.04105
D330050G23Rik	-1.01737	-0.593108	Phex	-1.01411	-1.40225
Gas7	-0.551006	-1.06347	Egr3	-1.12548	-1.29751
Fam96a	-1.22109	-0.405824	Tmod1	-1.24613	-1.17893
Myof	-1.24968	-0.410357	Sh3gl2	-1.26145	-1.16531
Slc5a3	-0.852283	-0.808608	Cd36	-0.986258	-1.4485
H19	-0.879319	-0.797706	Htr2a	-1.38293	-1.05663
Ptchd1	-0.869935	-0.808368	Shisa3	-1.32987	-1.11203
Cntn3	-0.88167	-0.851113	Liph	-1.34599	-1.09633
Ephb1	-0.522443	-1.21203	Nptx1	-1.56069	-0.905151
Pate2	-0.922112	-0.822022	Calcr1	-0.904031	-1.56556
Ankrd33b	-0.969605	-0.791879	Trp53i11	-0.759524	-1.71009
St6galnac2	-1.02479	-0.738283	Lanc13	-1.15093	-1.39701
Trim66	-0.904751	-0.861118	Ano1	-1.50615	-1.04589
Tes	-1.01791	-0.76607	F2rl1	-1.34216	-1.21353

Gene	shPnky	shPTBP1	Gene	shPnky	shPTBP1
Gm6634	-1.31492	-1.24635	Ifi204	-2.4435	-0.854482
Dcc	-0.852373	-1.73814	BC089491	-1.75852	-1.57988
A730090N16Rik	-1.05844	-1.57429	C030034L19Rik	-1.74539	-1.61767
AW551984	-1.33276	-1.30191	Hmga2	-1.80364	-1.56156
Ifi203	-1.61749	-1.08872	Plaur	-1.63126	-1.79582
Car13	-1.15643	-1.55463	Kcnma1	-2.07399	-1.3854
Perp	-1.23326	-1.53103	Pmp2	-2.29871	-1.52728
Clca2	-1.86282	-0.935391	Aldh1a3	-1.80587	-2.19694
Esm1	-1.83185	-1.00485	Ptx3	-2.1198	-1.93127
Fam19a1	-0.895592	-2.03852	Rit2	-1.58488	-2.54994
Nppc	-1.64723	-1.33004	Cxcl5	-2.40922	-2.05816
Dct	-1.32151	-1.65792	E330013P04Rik	-2.38383	-2.86701
Tnfsf18	-1.74904	-1.45646	Slitrk6	-2.33199	-4.01777
Mylk2	-1.46434	-1.76912			

Table 2.2: Gene ontology terms for *Pnky* and PTBP1 co-regulated genes.

Gene ontology terms with their DAVID p-value for set of genes that are differentially expressed by both *Pnky* and PTBP1 knockdown.

Term	Count	%	P Value
GO:0007267~cell-cell signaling	31	0.422	1.386E-06
GO:0019226~transmission of nerve impulse	26	0.354	3.195E-06
GO:0030155~regulation of cell adhesion	16	0.218	3.743E-06
GO:0045785~positive regulation of cell adhesion	11	0.150	4.964E-06
GO:0007268~synaptic transmission	22	0.299	7.177E-06
GO:0010810~regulation of cell-substrate adhesion	9	0.122	1.401E-04
GO:0007155~cell adhesion	41	0.558	2.155E-04
GO:0022610~biological adhesion	41	0.558	2.216E-04
GO:0040008~regulation of growth	23	0.313	5.199E-04
GO:0010811~positive regulation of cell-substrate adhesion	7	0.095	5.340E-04
GO:0030182~neuron differentiation	31	0.422	5.560E-04
GO:0043062~extracellular structure organization	16	0.218	8.044E-04
GO:0030511~positive regulation of transforming growth factor beta receptor signaling pathway	4	0.054	1.897E-03
GO:0050767~regulation of neurogenesis	14	0.190	2.141E-03
GO:0051960~regulation of nervous system development	15	0.204	2.152E-03
GO:0044057~regulation of system process	18	0.245	2.563E-03
GO:0007200~activation of phospholipase C activity by G-protein coupled receptor protein signaling pathway coupled to IP3 second messenger	6	0.082	2.585E-03
GO:0016044~membrane organization	22	0.299	2.626E-03
GO:0048666~neuron development	23	0.313	2.839E-03
GO:0007610~behavior	29	0.394	2.850E-03
GO:0007202~activation of phospholipase C activity	6	0.082	3.099E-03
GO:0010518~positive regulation of phospholipase activity	6	0.082	3.099E-03
GO:0010863~positive regulation of phospholipase C activity	6	0.082	3.099E-03
GO:0060193~positive regulation of lipase activity	6	0.082	3.682E-03
GO:0007169~transmembrane receptor protein tyrosine kinase signaling pathway	17	0.231	3.913E-03
GO:0048812~neuron projection morphogenesis	16	0.218	4.163E-03
GO:0010517~regulation of phospholipase activity	6	0.082	4.339E-03
GO:0008284~positive regulation of cell proliferation	22	0.299	4.373E-03
GO:0006813~potassium ion transport	15	0.204	4.386E-03
GO:0051240~positive regulation of multicellular organismal process	15	0.204	5.169E-03
GO:0031175~neuron projection development	18	0.245	5.836E-03
GO:0006811~ion transport	43	0.585	5.886E-03
GO:0042391~regulation of membrane potential	12	0.163	7.340E-03
GO:0060191~regulation of lipase activity	6	0.082	7.813E-03
GO:0021952~central nervous system projection neuron axonogenesis	4	0.054	7.946E-03
GO:0010647~positive regulation of cell communication	16	0.218	7.957E-03
GO:0045765~regulation of angiogenesis	7	0.095	8.073E-03
GO:0021954~central nervous system neuron development	6	0.082	8.916E-03
GO:0000904~cell morphogenesis involved in differentiation	17	0.231	9.927E-03
GO:0032990~cell part morphogenesis	17	0.231	9.927E-03
GO:0060284~regulation of cell development	14	0.190	1.027E-02
GO:0008219~cell death	32	0.435	1.042E-02
GO:0051094~positive regulation of developmental process	17	0.231	1.079E-02
GO:0007528~neuromuscular junction development	5	0.068	1.167E-02
GO:0007167~enzyme linked receptor protein signaling pathway	20	0.272	1.199E-02
GO:0048608~reproductive structure development	12	0.163	1.378E-02

Term	Count	%	P Value
GO:0007264~small GTPase mediated signal transduction	19	0.258	1.391E-02
GO:0048858~cell projection morphogenesis	16	0.218	1.411E-02
GO:0016265~death	32	0.435	1.427E-02
GO:0006112~energy reserve metabolic process	6	0.082	1.440E-02
GO:0010648~negative regulation of cell communication	15	0.204	1.560E-02
GO:0006940~regulation of smooth muscle contraction	5	0.068	1.567E-02
GO:0042063~gliogenesis	7	0.095	1.603E-02
GO:0048010~vascular endothelial growth factor receptor signaling pathway	4	0.054	1.605E-02
GO:0006897~endocytosis	15	0.204	1.697E-02
GO:0010324~membrane invagination	15	0.204	1.697E-02
GO:0015672~monovalent inorganic cation transport	21	0.286	1.718E-02
GO:0007242~intracellular signaling cascade	50	0.680	1.742E-02
GO:0008585~female gonad development	7	0.095	1.749E-02
GO:0030111~regulation of Wnt receptor signaling pathway	6	0.082	1.784E-02
GO:0043112~receptor metabolic process	5	0.068	1.796E-02
GO:0030178~negative regulation of Wnt receptor signaling pathway	5	0.068	1.796E-02
GO:0009968~negative regulation of signal transduction	14	0.190	1.797E-02
GO:0030198~extracellular matrix organization	10	0.136	1.818E-02
GO:0009967~positive regulation of signal transduction	14	0.190	1.877E-02
GO:0021955~central nervous system neuron axonogenesis	4	0.054	1.949E-02
GO:0007172~signal complex assembly	4	0.054	1.949E-02
GO:0032760~positive regulation of tumor necrosis factor production	4	0.054	1.949E-02
GO:0009611~response to wounding	23	0.313	1.959E-02
GO:0055082~cellular chemical homeostasis	19	0.258	1.971E-02
GO:0048015~phosphoinositide-mediated signaling	6	0.082	1.975E-02
GO:0000902~cell morphogenesis	21	0.286	2.077E-02
GO:0060601~lateral sprouting from an epithelium	3	0.041	2.096E-02
GO:0048570~notochord morphogenesis	3	0.041	2.096E-02
GO:0045137~development of primary sexual characteristics	10	0.136	2.159E-02
GO:0051272~positive regulation of cell motion	6	0.082	2.178E-02
GO:0032989~cellular component morphogenesis	23	0.313	2.201E-02
GO:0035270~endocrine system development	8	0.109	2.309E-02
GO:0051336~regulation of hydrolase activity	15	0.204	2.341E-02
GO:0021953~central nervous system neuron differentiation	6	0.082	2.395E-02
GO:0007611~learning or memory	9	0.122	2.405E-02
GO:0046545~development of primary female sexual characteristics	7	0.095	2.426E-02
GO:0048732~gland development	15	0.204	2.433E-02
GO:0060541~respiratory system development	11	0.150	2.478E-02
GO:0001822~kidney development	10	0.136	2.543E-02
GO:0051969~regulation of transmission of nerve impulse	10	0.136	2.543E-02
GO:0007613~memory	5	0.068	2.601E-02
GO:0051046~regulation of secretion	11	0.150	2.603E-02
GO:0030030~cell projection organization	21	0.286	2.794E-02
GO:0040014~regulation of multicellular organism growth	8	0.109	2.816E-02
GO:0048667~cell morphogenesis involved in neuron differentiation	14	0.190	2.828E-02
GO:0016477~cell migration	17	0.231	2.861E-02
GO:0043279~response to alkaloid	5	0.068	2.911E-02
GO:0006873~cellular ion homeostasis	18	0.245	2.979E-02
GO:0019725~cellular homeostasis	22	0.299	3.105E-02
GO:0006468~protein amino acid phosphorylation	36	0.490	3.172E-02
GO:0032755~positive regulation of interleukin-6 production	4	0.054	3.203E-02
GO:0003006~reproductive developmental process	18	0.245	3.271E-02

Term	Count	%	P Value
GO:0043434~response to peptide hormone stimulus	9	0.122	3.383E-02
GO:0006928~cell motion	23	0.313	3.429E-02
GO:0031644~regulation of neurological system process	10	0.136	3.453E-02
GO:0048741~skeletal muscle fiber development	5	0.068	3.592E-02
GO:0048663~neuron fate commitment	6	0.082	3.685E-02
GO:0010720~positive regulation of cell development	6	0.082	3.685E-02
GO:0022602~ovulation cycle process	6	0.082	3.685E-02
GO:0042417~dopamine metabolic process	4	0.054	3.696E-02
GO:0045666~positive regulation of neuron differentiation	4	0.054	3.696E-02
GO:0060572~morphogenesis of an epithelial bud	3	0.041	3.714E-02
GO:0008593~regulation of Notch signaling pathway	3	0.041	3.714E-02
GO:0044042~glucan metabolic process	5	0.068	3.965E-02
GO:0005977~glycogen metabolic process	5	0.068	3.965E-02
GO:0001541~ovarian follicle development	5	0.068	3.965E-02
GO:0006073~cellular glucan metabolic process	5	0.068	3.965E-02
GO:0042698~ovulation cycle	6	0.082	3.985E-02
GO:0010001~glial cell differentiation	6	0.082	3.985E-02
GO:0046660~female sex differentiation	7	0.095	3.991E-02
GO:0001666~response to hypoxia	7	0.095	3.991E-02
GO:0051345~positive regulation of hydrolase activity	8	0.109	4.045E-02
GO:0048709~oligodendrocyte differentiation	4	0.054	4.224E-02
GO:0070482~response to oxygen levels	7	0.095	4.257E-02
GO:0050808~synapse organization	6	0.082	4.300E-02
GO:0060348~bone development	10	0.136	4.366E-02
GO:0045597~positive regulation of cell differentiation	13	0.177	4.452E-02
GO:0030001~metal ion transport	26	0.354	4.527E-02
GO:0003018~vascular process in circulatory system	6	0.082	4.630E-02
GO:0045932~negative regulation of muscle contraction	3	0.041	4.652E-02
GO:0007271~synaptic transmission, cholinergic	3	0.041	4.652E-02
GO:0042135~neurotransmitter catabolic process	3	0.041	4.652E-02
GO:0045686~negative regulation of glial cell differentiation	3	0.041	4.652E-02
GO:0014014~negative regulation of gliogenesis	3	0.041	4.652E-02
GO:0006915~apoptosis	27	0.367	4.720E-02
GO:0007588~excretion	4	0.054	4.788E-02
GO:0045664~regulation of neuron differentiation	9	0.122	4.828E-02

Table 2.3: Differential exon usage for genes regulated by *Pnky* and PTBP1.
Differential exon usage upon *Pnky* knockdown or PTBP1 knockdown compared to control.

Gene	exon	sh <i>Pnky</i>	shPTBP1	Gene	exon	sh <i>Pnky</i>	shPTBP1
Sorbs3	18	0.553	0.731	Ccdc127	3	0.059	0.077
Camta1	15	0.382	0.552	Ensa	2	0.041	0.076
Slc44a1	16	0.113	0.394	Pnkd	11	0.039	0.042
ErbB2ip	5	0.176	0.328	Rpl22	3	0.019	0.059
Dclk1	12	0.255	0.207	Calm3	3	0.014	0.016
Lrrfip1	2	0.186	0.271	Ccnd1	1	-0.013	-0.010
Dclk1	11	0.254	0.198	Rpl22	2	-0.017	-0.009
Dclk1	8	0.268	0.178	Itm2b	1	-0.010	-0.021
Dclk1	9	0.277	0.159	Rpl5	8	-0.023	-0.036
Dclk1	15	0.231	0.204	Tmem30a	1	-0.027	-0.040
Dclk1	16	0.208	0.211	Ier3ip1	2	-0.028	-0.048
Mylk	31	0.199	0.210	Pcdh7	1	-0.045	-0.032
Dclk1	13	0.235	0.172	Calm3	1	-0.025	-0.062
Lrrfip1	23	0.167	0.238	Fam49a	12	-0.023	-0.065
Dclk1	17	0.194	0.207	Dnajc3	11	-0.065	-0.025
Lrrfip1	22	0.166	0.227	Ncaph2	19	-0.042	-0.051
Lcorl	1	0.192	0.189	Cadm1	1	-0.031	-0.079
Pcdh10	6	0.116	0.265	Syncrip	1	-0.059	-0.053
Dclk1	1	0.240	0.139	Whsc1l1	24	-0.054	-0.064
Dclk1	14	0.205	0.163	Ccdc127	2	-0.061	-0.064
Crif1	6	0.166	0.194	Rgs17	5	-0.058	-0.070
Kazn	1	0.109	0.233	Taf9	3	-0.054	-0.076
Lrrfip1	21	0.125	0.206	Rfxank	1	-0.097	-0.039
Taf9	5	0.135	0.187	Wnt9a	3	-0.084	-0.062
Dclk1	19	0.175	0.146	Arpp19	2	-0.094	-0.066
Taf9	4	0.147	0.169	Arpp19	1	-0.112	-0.048
Lrrfip1	24	0.124	0.191	Lamp2	1	-0.124	-0.069
Fis1	1	0.149	0.164	Dclk1	7	-0.096	-0.098
Taf9	6	0.128	0.166	Pcdhga11	1	-0.100	-0.095
Vmp1	7	0.168	0.097	Arpp19	1	-0.139	-0.063
Rabggta	11	0.141	0.121	Vmp1	1	-0.132	-0.082
Crif1	8	0.113	0.147	Pnkd	2	-0.116	-0.107
Ptprz1	15	0.085	0.163	Fopnl	3	-0.149	-0.118
Pcdh7	3	0.127	0.119	Vmp1	1	-0.171	-0.104
Vmp1	6	0.155	0.080	Kazn	7	-0.098	-0.211
Vmp1	4	0.140	0.094	Gm14326	1	-0.109	-0.201
Vmp1	2	0.130	0.100	Mpzl1	1	-0.164	-0.156
Vmp1	3	0.130	0.088	Ensa	3	-0.098	-0.226
Vmp1	5	0.134	0.082	Lrrfip1	19	-0.118	-0.218
Pigk	11	0.138	0.077	Kif1b	27	-0.158	-0.234
Zfp428	1	0.107	0.107	Pcdh7	1	-0.229	-0.192
Arpp19	3	0.066	0.144	Lcorl	1	-0.270	-0.206
Vmp1	1	0.134	0.075	Dclk1	1	-0.227	-0.253
Gls	1	0.068	0.137	Slc4a4	23	-0.188	-0.317
Fads3	11	0.104	0.098	Fbln1	16	-0.246	-0.267
Ubfd1	6	0.060	0.124	1500011B03Rik	1	-0.227	-0.320
PsmD9	5	0.096	0.077	Cox16	1	-0.259	-0.303
2610005L07Rik	4	0.034	0.123	Gpm6a	1	-0.231	-0.521
Lamp2	1	0.088	0.058	Crif1	2	-0.356	-0.460
Atp1a2	1	0.064	0.074	2610005L07Rik	1	-0.744	-0.790
Maoa	14	0.062	0.074				

Experimental Procedures

Accession Numbers

All data are deposited in NCBI GEO under accession number GSE65542.

ChIP-seq analysis

V-SVZ ChIP-seq library generation and analysis is described in ref. 13 and available in NCBI GEO under accession GSE45282. ESC, ESC-NSC, and MEF ChIP-seq data was originally described in (Mikkelsen et al., 2007), and analyzed in (Ramos et al., 2013).

RNA-seq analysis

Published RNA-seq datasets were downloaded from GSE29184 and GSE36026, and abundance estimation was performed using Cufflinks v2.1.1. Experiments were done in biological duplicates. RNA was extracted using TRIzol and loaded onto RNeasy columns (QIAGEN) for on-column DNase treatment. Strand-specific, poly(A) selected cDNA libraries were generated using TruSeq Stranded mRNA kit (illumina) according to the manufacturer's protocol. Library validation and normalization were performed using RT-PCR and Quant-iT PicoGreen (Invitrogen). Cluster generation and high-throughput sequencing were performed on a HiSeq 2500 (Illumina), using the paired-end 100 bp protocol. Reads were aligned to the mouse genome mm9, using Tophat v2.0.10 with the following arguments: -p 6 --library-type fr-firststrand. Differential expression was assessed using Cuffdiff v2.1.1 with the following arguments: -b genome.fa -u --library-type fr-firststrand. A transcriptome index that includes all UCSC genes and the *Pnky* sequence was used for Tophat and Cufflinks. Alternative splicing was analyzed using DEXSeq v1.8.0, using a FDR threshold of 0.01.

V-SVZ NSC cultures and differentiation assay

The brain of postnatal day 5-7 (P5-7) mice was removed from the skull and placed in ice-cold L15 media and a 0.5 mm thick coronal slab was obtained. V-SVZ was dissected from and dissociated with 0.25% trypsin with occasional agitation for 20 min at 37°C, and

resuspended in N5 medium (DMEM/F12 with Glutamax, 5% Fetal Bovine Serum, N2 supplement, 35 µg/mL bovine pituitary extract, 20 ng/mL EGF, 20 ng/mL FGF, antibiotic/antimycotic). For most experiments, C57/B6 mice were used. For GTVA experiments, the GFAP-TVA mouse (Holland and Varmus, 1998) was used.

Cells were split 1:2 to passage 6 or 7 before switching to differentiation medium (DMEM/F12 with Glutamax, 2% FBS, N2 supplement, 35 µg/mL bovine pituitary extract, antibiotic/antimycotic). For analysis of cell fate, cells were fixed with 4% PFA and stained with anti-Tuj1 (Covance, 1:1000), anti-GFAP (Dako, 1:500), or anti-DLX2 (1:500). For EdU incorporation assays, 10µM EdU was added to culture medium for 1 hour (**Figure 2.1H** and **2.1K**) or 3 hours (**Figure 2.1K**) before fixing.

Nuclear fractionation

~10 million V-SVZ NSCs were resuspended in 10 mL PBS, 2 mL nuclear isolation buffer (1.28 M sucrose, 40 mM Tris, pH 7.5, 20 mM MgCl₂, 4% Triton X-100), 6 mL of water, and incubated on ice for 20 mins with frequent mixing. Nuclei were then pelleted at 2500xg for 15 mins, resuspended in lysis buffer (150 mM KCl, 25 mM Tris pH 7.5, 5 mM EDTA, 0.5% Igepal, 0.5 mM DTT) and incubated on ice for 30 mins. For whole cell lysate, cell pellet was resuspended in lysis buffer and incubated on ice for 30 mins. RNA was extracted using Trizol LS according to manufacturer's instructions. 1 µg of RNA was used for first-strand synthesis with the Transcriptor First Strand cDNA Synthesis kit (Roche) using oligo-dT primers. cDNA was used for qPCR with Sybr Green master mix (Roche), run on a Light Cycler 480 (Roche).

Branched DNA *in situ* hybridization

Branched DNA *in situ* was performed on adult tissue according to manufacturer's instructions using the RNAScope 2.0 high definition BROWN kit (ACD). For V-SVZ cultures, cells were grown on laminin and poly-d-lysine coated Labtek 8-well chamber slides and fixed with 4% PFA. *In situ* was performed on cells according to manufacturer's instructions using the

RNAScope 2.0 high definition BROWN kit with the following modification: Pretreat solution 2 was added to cells and they were steam treated for 10 mins. No protease was used.

FACS-purified V-SVZ lineage and microarray

Purification of the V-SVZ lineage and subsequent custom lncRNA microarray hybridization has been described in (Ramos et al., 2013) and (Pastrana et al., 2009). Raw data is available at NCBI GEO under accession GSE45282. Processed data is available at <http://neurosurgery.ucsf.edu/danlimlab/lncRNA/>

Knockdown lentiviral constructs

All shRNA sequences were designed using the Dharmacon siDESIGN tool. shRNA oligos were ordered from ELIM Biosystems, annealed, and ligated into the PSICO-R vector (Ventura et al., 2004), which carries a GFP or mCherry marker. shRNA targeting luciferase was used as a control. To establish purified cultures, GFP+ cells or GFP+, mCherry+ double positive cells were sorted using a FACS Aria II.

Time-lapse imaging

Near-clonal density cultures were established by trypsinization and subsequent mixing of infected GFP+ cultures (shCtrl or sh*Pnky*) with wildtype, uninfected cultures at a ratio of 1:200 to give ~15 GFP+ cells/high powered field and cultured in proliferation media for 8 hours to allow cells to adhere to the plate. Cultures were switched to differentiation medium and imaged on a Leica SP5 inverted confocal microscope fitted with a Life Imaging Services microscope temperature control system. Cultures were maintained at 37°C and 5% CO₂, 21% O₂ and 8 optical sections were taken every 15 minutes for 3 days. Optical sections were summed and movies assembled with ImageJ. Cell fate was determined by morphology and representative fields were confirmed by fixing and staining for TUJ1 and GFAP. Cell cycle length was quantified as the amount of time between the first division of an NSC and the next division of each daughter that divided.

Human Fetal Tissue

Fetal cortical tissue was collected from elective pregnancy termination specimens at San Francisco General Hospital, usually within 2h of the procedure. Research protocols were approved by the Committee on Human Research (institutional review board) at University of California, San Francisco.

***In situ* hybridization**

In situs were performed as described (Jensen and Wallace, 1997). Briefly, DIG-labeled RNA probes were synthesized using the T7 high yield RNA synthesis kit (NEB) and a Digoxigenin RNA labeling mix (Roche), probes were hybridized overnight at 65 degrees. After washing, anti-digoxigenin Fab fragment (Roche) was added and incubated overnight at 4°C. Slides were washed and color reaction was carried out in 10% polyvinyl alcohol with NBT/BCIP (Roche) for 24-48 hours.

For mouse *Pnky*, the full-length transcript was cloned using SMARTer RACE cDNA amplification kit with RNA isolated from V-SVZ NSC cultures and cloned into the PGEM-Teasy vector (Promega). For human *Pnky*, a fragment corresponding to bp 367-1592 was cloned and used as an *in situ* probe.

***In utero* electroporation**

In utero electroporation was performed on E13.5 embryos from timed-pregnant wildtype Swiss-Webster mice (Simonsen labs) as described (Saito, 2006). Constructs used were PsicoR-shLuciferase (shCtrl), and PsicoR-sh*Pnky*-2 (sh*Pnky*). Embryos were harvested 24 or 48 hours later. One hour before harvesting, mice were given a single injection of either BrdU or EdU. Brains were fixed in 4% PFA, washed in PBS, and then equilibrated in 20% sucrose before embedding in 1:1 OCT:20% sucrose and sectioning on Cryostat.

1-3 non-adjacent coronal sections per brain were imaged for quantification. Optical sections through the dorso-lateral telencephalon containing GFP+ electroporated cells were

acquired at constant separation on a Leica SP5 Upright Confocal microscope. Three to four optical sections through the center were summed using ImageJ. Four animals from three separate surgeries were quantified for each experiment. For quantification of GFP+ cells in each zone, sections were costained with Nestin and Dcx. VZ was defined as NESTIN+DCX-, and CP was NESTIN-DCX+.

Antibodies

Goat anti-SOX2 (Santa Cruz Biotechnology), chicken anti-NESTIN (Aves), mouse anti-NESTIN (Millipore), rabbit anti-GFAP (DakoCytomation), chicken anti-GFP (Abcam), goat anti-GFP (Abcam), mouse anti-TUJ1 (Covance), mouse anti-PTBP1 (Invitrogen), guinea pig anti-DCX (Millipore), rabbit anti-SATB2 (Abcam), rabbit anti-TBR2 (Abcam), chicken anti-TBR2 (Millipore), rat anti-BrdU (Abcam). Guinea pig anti-DLX2 is described in (Kuwajima et al., 2006). For FACS-analysis of infected V-SVZ cultures, directly conjugated 555-Nestin and 647-GFAP (BD Pharmingen) were used.

RNA Immunoprecipitation Assay (RIP)

RIP assay was performed as described in (Rinn et al., 2007). $\sim 10^7$ V-SVZ cells or N2A cells were trypsinized and resuspended in 2 ml PBS, 6 ml water, 2 ml nuclear isolation buffer (1.28 M sucrose, 40 mM Tris pH 7.5, 20 mM MgCl₂, 4% Triton X-100) and incubated on ice for 20 mins. Nuclei were then pelleted at 2500 x g for 20 mins at 4°C. Nuclear pellets were resuspended in 1 mL RIP buffer (150 mM KCl, 25 mM Tris pH 7.4, 5 mM EDTA, 5 mM MgCl₂, 0.5% NP-40 0.5 mM DTT, PI tablet (Roche), and 100 u/ml RNase OUT (Invitrogen)), and sheared with 20 strokes in a dounce homogenizer. Nuclear debris was pelleted by centrifugation at max speed for 10 mins at 4°C. Nuclear lysate was split into two aliquots and 8 ug antibodies were added. Antibodies used were anti-PTBP1 (Invitrogen) and anti-FLAG (Sigma). IP was performed rotating at 4°C overnight. The next day, 50 ul washed Dynabeads Protein G were added and incubated for an additional 2 hours. Beads were washed on magnetic rack 3x with

RIP buffer, and resuspended in Trizol after final wash. Trizol extraction was carried out according to manufacturers' instructions, cDNA was made using the Transcriptor First Strand cDNA synthesis kit (Roche) with both oligo-dT and random hexamer primers. Transcripts were detected with qPCR as described above.

RNA-pulldown

Biotinylated RNA pulldown was performed as described in (Hacisuleyman et al., 2014). ~10⁷ V-SVZ-NSCs or N2A cells were pelleted and nuclei obtained as described for RIP protocol. To generate biotinylated RNA, *Pnky* sense and antisense were cloned into the PGEM-Teasy vector (Promega), which contains a T7 promoter. Biotinylated RNA was synthesized using the T7 High Yield Synthesis Kit (NEB) and biotinylated UTP (Roche). RNA probes were purified using the RNeasy mini kit (Qiagen). Immediately before use, 30 pmol RNA was resuspended in RNA structure buffer (10 mM HEPES pH 7, 10 mM MgCl₂), heated to 65°C, then slow-cooled to 4°C in a thermocycler. RNA was run on a 1% agarose gel to ensure integrity and correct size.

To generate lysate, nuclear pellet was resuspended in RIP buffer with 1% NP-40 and rotated for 30 mins at 4°C, and then debris was cleared by centrifugation at max speed for 30 mins. For preclear, 40 µL/pulldown MyOne T1 beads (Invitrogen) were washed/prepared according to manufacturer's instructions and added to the lysate. Mixture was rotated at 4°C for 1 hour, beads were removed with magnetic rack and discarded. Precleared lysate was diluted 1:2 in RIP buffer without NP-40 (Final concentration of NP-40 = 0.5%), and probes and yeast tRNA (final concentration = 0.1 µg/µL) (Invitrogen) were added. Binding reaction is carried out overnight at 4°C. The next day, 40 µL washed MyOne T1 beads are added for an additional 1 hour. Tubes are added to the magnetic rack and washed 3 x 10 mins at 4°C on the rack with wash buffer (RIP buffer with 1% NP-40 and 300 mM KCl). After final wash, 1X NuPage running buffer is added and beads are boiled for 10 mins to elute protein.

Mass spectrometry

Selected SDS PAGE-separated bands were excised and in-gel digested with trypsin according to the established protocols (Jiménez et al., 1998). LC MS analyses of tryptic peptides utilized LTQ Orbitrap Velos mass spectrometer (Thermo Scientific, San Jose, CA) equipped with a NanoLC Ultra System (Eksigent, Dublin, CA), as described (Roan et al., 2014). MS/MS data were interrogated with Mascot 2.2.04 search engine (Matrix Science) following their conversion to the .mgf format with an aid of Mascot Daemon (Matrix Science): Rodentia taxonomy of UniProt database (release 2014_01, 26206 entries) was searched. Dynamic modifications included sulfoxide oxidation at Met, deamidation at Asn or Gln, and Gln to pyro-Glu conversion at N-terminus. Carbamidomethyl at Cys was included as a static modification. One missed tryptic cleavage was allowed. Precursor and fragment ion mass tolerances were set to 5 ppm and 0.2 Da, respectively. A target-decoy strategy with a 0.045 target false discovery (FDR) rate was used for protein identification (Elias and Gygi, 2007). Relative abundances of proteins in the sense and antisense samples were estimated on the basis of two independent approaches: spectral counting (Liu et al., 2004; Lundgren et al., 2010) and the exponentially modified protein abundance indices (emPAI) . Spectral counting utilized peptides identified at or above identity. Protein molar content (mol %) was calculated as described by (Ishihama et al., 2005) using emPAI values generated by the Mascot algorithm: only peptides identified at or above homology threshold are included. (http://www.matrixscience.com/help/quant_empai_help.html).

RT-qPCR Analysis:

Sequences for some primers were found with PrimerBank (Wang et al., 2012). For averaging qPCR results over biological replicates in double KD experiments, the method suggested in (Willems et al., 2008) was used.

***Pnky* sequences:**

>Human *PINKY*

TAAGCAGTGGTATCAACGCAGAGTACATGGGGAGGCGCCAGGGGCCCGGTTGGCGCGAA
CGCCGGGTTCCGAGCACCTGGGCTTCCTTGTCTGCCTCCCAGCGCGGCACCTCTTCGG
GGCTCCCGAAACCTGAGCTCTCGCTGGTTTTAGGTCCAGACGGGGGCCTCTCCACCGGTT
CCTCCCCCGCCCCGGGCTCTGGGGCCATTCTTTGGGCTGACCCTGTCAGGGCAGAGTC
CGCGCGTCTGCCTGCCATTCTCCGCCCGCATAAAAGCACGTTGAAGGTGTCTCGGGCAGA
CACCTCCAGGTTTTGAATCAGTTTATTCCCTTTCCTGTTCAAAGCAGCTGTTCAAATACAC
AGGCTGCTTACGTTGACGTGGAGAGGATTTCAAACAACGCTAAAATGCTTTGAACTGACAA
GGTGTCTTGATATCTCCCTCACTCCATCCAGCACAGCTCCTCGAGATCACTCGCTAGGACA
ATGGCTGAGCAGGCGATTTCGTGCGGGCCTCGCCACCTCGGGGCGCGGACTGCGGGGTG
TCCTAAGCCCCTTCCGCAAGGACAGGATGGAGGCACCTGTAAGGAGATGCTGGCGCCAC
CCCAGCTTCTCCAGGTCCGGAGGAACCTCTACTCAGTCAATACCCTGAGCTGGACTTGT
CTGAAGAAACGGAGCCGACTCCCTCTTGCCGGGGTGCCTGAGTGGAGGGGAAACATCC
TCGAATAACAGAACTACACCAAAAAGACACCCATGTTATCTCTCACACTTTCACACTCCTCG
AGATAGTGAGCCGGACCTGGGTCTTAGTAGCACCCAGTACCTTGACACAAACCTCCCAAAT
TTCCACCTGAGTAACAGTTATGGGGTCAGTCCATGCACTGTAAGTGAAGTCTAATTTATTA
ACTATTTTCTATAGTAAACACACTCACACCATATATAAAATAGCATTATTTATTTCTATATAC
CAGGAGTTGGCAGAAAACCCACCGTGACCACTCCCATACATTGAGCTGGAGGCACACAAT
TACTAAAACAGAGGTGAGATGGTATTCATTTGATCTTAATTTTTTCTTATTTATGTAGTCCCA
GGATAATAGAAATCAGGAAACAAAAGAAAACAAAGAATTTTCTGAGGAGATGGCCATTGGG
GGAGTGGAGGTAGCAGCTGGTTTAAACCTAAGTAAACTAGAAAAAGAACTGCTGTTTCC
TTTTTCTTATATCCACCTTAGAGGATCATGTTTGAACGTCCCTACTCCTCCTCCTCTTTTTAA
AAAGCCTTGTCTCAGTCATTCATTCTGTGCTTCTGCTCTTCTGCTAGACCCAGCAGCT
GTTTGATTTGGTGAGGCCCCCTCCAACCTCTGAGTGGAAGTCTTTTTCTAAGGGCCTGCA
GAATGTCAAACCTGAGGCTCTGGCTTCGGAGCTAGAGCTTTGAACAGCCAATCCACACAAA

AAGGCAGCTGGCTGCTTTAATGAAAAGCTGCTATAAAGCTTCAAGAAGCTTTAGCCTTGGGGG
ATGCATTTATAAGGAACATGGAAAATGCATTTCCAAGTTGCTGGTTCTTGGGAGAGGCATA
ATAAACATTTACC

>Mouse *Pinky*

GGGAGAAGCAACTTCCTCTGGTCTTCTGGAGGTGTAACCTACGTGCCAGTAGGATATACT
GCCGGGTTGTGAAATGTCCACGCCTCTCCCAACTGTCTTCTTCCAGCCCTCCGGGCT
TGGCTTTCTTGCTTCCCAGGAGTTCAAATCTCCAACCTGCGGAAGAATTCAGCTGCTTGA
AAGGACTTAAGGCAGTGTGCGGAGGACATCTCCTTTCTCCGCCAGTAAAGAGAGCTGTTC
AAAGACCGAGGCTGCTTACGATGACGTGGAGAGGATTTCAAACAACCTTAACAGGCTTTGA
ACTGACAAGAAGCGGTGATATCTGCCTCACTCTGGCACAGCTCCTCCAGTGCACTTGCTAG
GACAATGGCTGAGAAAGCACTTGGTGCTGGCCTcTCTGCCGGGGGCGAGGACTGCCAAA
CCCCAGAGACCCTAAGGCAGGAGTTGCTGCACTaCAATGGAGAGGTCTTGTcTTAGGCTGC
ACCTCAGGTTCTcTCAGATcTTCTGGAAGGGCGTTATTCAGCGGTACTGTGGTTGCGCTGT
GCCAGCAGCTGCTTGATGGAGACCTCTTCTCCCCaCATCTGAATGGAACGTCTTTGCCAG
AGTcTACAGAATGTCAAAGCTGAGGCTCCGACCTCAGAGCTACAGCTTTAAGGACCACTCC
ACACAAAGAGGCAGCTGGTTGCTTTAATGAAAAGCTGCCTTTAAGCTTCAAGAAGCTGAGGCC
TTGGGGAATCCATTTATAAGGAGCCTAGAAAATGCATTTCCAAGTTGTATGTTcTTAGGAGA
TACAAAATAAAATTTACCTGAAAAAATTAATTGT

shRNA sequences:

Luciferase_F:

TGAGCTGTTTCTGAGGAGCCTTCAAGAGAGGCTCCTCAGAAACAGCTCTTTTTTC

Luciferase_R:

TCGAGAAAAAGAGCTGTTTCTGAGGAGCCTCTCTTGAAGGCTCCTCAGAAACAGCTC

Pnky_sh1_F:

TGGACAATGGCTGAGAAAGCTTCAAGAGAGCTTTCTCAGCCATTGTCTTTTTTC

Pnky_sh1_R:

TCGAGAAAAAAGGACAATGGCTGAGAAAGCTCTCTTGAAGCTTTCTCAGCCATTGTCC

Pnky_sh2_F:

TGATGACGTGGAGAGGATTTTTCAAGAGAAAATCCTCTCCACGTCATCTTTTTTC

Pnky_sh2_R:

TCGAGAAAAAAGATGACGTGGAGAGGATTTTCTCTTGAAAATCCTCTCCACGTCATC

shPTBP1_F:

TGGGTGAAGATCCTGTTCAATTCAAGAGATTGAACAGGATCTTCACCCTTTTTTC

shPTBP1_R:

TCGAGAAAAAAGGGTGAAGATCCTGTTCAATCTCTTGAATTGAACAGGATCTTCACCC

qPCR Primer Sequences:

Pnky_F1: TCTCCTTTCTCCGCCAGTAA

Pnky_R1: CACCGCTTCTTGTGAGTTCA

Pnky_F2: GCAGGAGTTGCTGCACTACA

Pnky_R2: GTACCGCTGAATAACGCCCT

GAPDH_F: GGGAAATTCAACGGCACAGT

GAPDH_R: AGATGGTGATGGGCTTCCC

U1_F: ACGAAGGTGGTTTTCCCAG

U1_R: GTCCCCCACTACCACAAA

B-Act_F: CTAAGGCCAACCGTGAAAAG

B-Act_R: ACCAGAGGCATACAGGGACA

PTBP1_F: AGTGCGCATTACACTGTCCA

PTBP1_R: CTTGAGGTCGTCCTCTGACA

Igfbp5_F: CCCTGCGACGAGAAAAGCTC

Igfbp5_R: GCTCTTTTCGTTGAGGCAAACC

Ppp1r3c_F: TGATCCATGTGCTAGATCCACG

Ppp1r3c_R: ACTCTGCGATTTGGCTTCCTG

Ntsr2_F: TTCACCGCGCTCTATTCGC

Ntsr2_R: AGGGGTAGTGGGACCACAC

Scrg1_F: CCTTGGGCTAACTTTGCTGTT

Scrg1_R: TGGACATTTGCATCTATCAGCTT

Chapter 3: The long noncoding RNA *Pnky* is a *trans*-acting regulator of cortical development *in vivo*

Summary

While it is now appreciated that certain long noncoding RNAs (lncRNAs) have important functions in cell biology, relatively few have been shown to regulate development *in vivo*, particularly with genetic strategies that establish *cis* versus *trans* mechanisms. *Pnky* is a nuclear-enriched lncRNA that is transcribed divergently from the neighboring proneural transcription factor *Pou3f2*. Here we show that conditional deletion of *Pnky* from the developing cortex regulates the production of projection neurons from neural stem cells (NSCs) in a cell-autonomous manner, altering postnatal cortical lamination. Surprisingly, *Pou3f2* expression is not disrupted by deletion of the entire *Pnky* gene. Moreover, expression of *Pnky* from a BAC transgene rescues the differential gene expression and increased neurogenesis of *Pnky*-knockout NSCs, as well as the developmental phenotypes of *Pnky*-deletion *in vivo*. Thus, despite being transcribed divergently from a key developmental transcription factor, the lncRNA *Pnky* regulates development in *trans*.

Introduction

The mammalian genome produces tens of thousands of distinct long noncoding RNAs (lncRNAs) – transcripts longer than 200 nucleotides (nt) that do not encode proteins (Djebali et al., 2012) – and a growing number of lncRNAs have been shown to play important biological roles in cultured cells. However, because genetic studies of lncRNA function *in vivo* are currently lacking, the biological significance of most lncRNAs for the development of tissues and organs *in vivo* is unclear (Nakagawa, 2016). Moreover, for most lncRNAs that have been discovered to have function, the mechanism(s) by which they regulate cell biology remain

enigmatic (Bassett et al., 2014; Kopp and Mendell, 2018). A fundamentally important question is whether the lncRNA locus functions in *cis* – regulating local gene transcription on the same chromosome – and/or in *trans* – producing a molecule that functions at cellular locations distant from where it is produced.

Pnky is an 825 nt, evolutionarily-conserved, nuclear-enriched, polyadenylated lncRNA that is expressed in neural stem cells (NSCs) both *in vitro* and *in vivo* (Ramos et al., 2015). We have previously shown that short-hairpin RNA (shRNA)-mediated *Pnky* knockdown (KD) increases neuronal production from NSCs in culture as well as in the developing cortex (Ramos et al., 2015). However, methods that directly target lncRNA transcripts for degradation, such as the use of shRNAs and antisense oligonucleotides (ASOs), do not clearly distinguish between *cis*- and *trans*-acting mechanisms, particularly for lncRNAs that localize to the nucleus (Kopp and Mendell, 2018; Wagschal et al., 2012). In addition to reducing potential *trans*-activities of a lncRNA, KD of the lncRNA can also modulate local gene expression (Luo et al., 2016; Ørom et al., 2010; Wang et al., 2011). Finally, in addition to potential off-target effects and issues related to partial KD, the use of shRNAs and ASOs for *in vivo* developmental studies can be technically challenging (Kaczmarek et al., 2017).

For a relatively small number of lncRNAs, genetic deletions have been used to reveal developmental phenotypes *in vivo* (Bassett et al., 2014). However, in addition to testing potential *trans* function, genetic deletions can also perturb *cis*-regulatory mechanisms (*e.g.*, through the removal of transcriptional enhancers). The insertion of poly-adenylation (poly-A) signals into lncRNAs can disrupt transcriptional elongation and reveal *in vivo* phenotypes (Anderson et al., 2016; Bond et al., 2009), but given that transcriptional activity local to the lncRNA transcriptional start site (TSS) can often regulate nearby genes, poly-A insertion may not inactivate all potential lncRNA functions. Despite these and other known shortcomings, genetic methods are powerful tools for studying phenotypes *in vivo* and understanding

molecular mechanism, particularly when different genetic strategies are combined in a complementary manner.

In this chapter, we integrated multiple genetic approaches to investigate the function and molecular mechanism of the lncRNA *Pnky* in brain development. The TSS of *Pnky* is located ~2.2kb from that of the neighboring gene *Pou3f2* (Dominguez et al., 2013), which is transcribed in the opposite direction. This “divergent” orientation has been described for approximately 20% of mammalian lncRNAs and has been found to predict a *cis* regulatory interaction with the coding gene neighbor (Luo et al., 2016). Surprisingly, *Pnky*-deletion did not disrupt the expression of *Pou3f2*. To test the alternative hypothesis – that *Pnky* regulates neural development in *trans* – we generated transgenic mice that express *Pnky* at physiological levels from an integrated bacterial artificial chromosome (BAC) construct. *Pnky* expressed from this BAC rescued the differential gene expression and cellular phenotype of *Pnky*-knockout NSCs, as well as the developmental phenotypes of *Pnky*-deletion *in vivo*. Thus, the integration of these complementary genetic strategies reveals that *Pnky* functions in *trans* to regulate brain development *in vivo*.

Results

Generation of a conditional *Pnky* deletion allele

To enable temporal and cell type-specific control over *Pnky* loss-of-function *in vivo*, we used a Cre-loxP strategy. In the design of this genetic approach, we remained agnostic about the specific mechanism(s) by which *Pnky* might function. We therefore generated a conditional *Pnky* allele that removes the broad range of potential lncRNA mechanisms (both *cis* and *trans*) by flanking the entire *Pnky* gene including its TSS with loxP sites (**Figures 3.1A-B**), and we produced mice with this “floxed” *Pnky* allele (*Pnky*^F).

The genetic removal of an entire lncRNA locus might not produce the same phenotype as degradation of the lncRNA transcript itself (Bassett et al., 2014; Nakagawa, 2016). In NSC

cultures from the postnatal mouse ventricular-subventricular zone (V-SVZ), shRNA-mediated *Pnky* KD increases neurogenesis by 3-4 fold (Ramos et al., 2015). We therefore investigated whether acute *Pnky* conditional knockout (*Pnky*-cKO) in V-SVZ NSC cultures would also increase neurogenesis. V-SVZ NSC cultures were established from postnatal *Pnky*^{F/F} or wild-type (*Pnky*^{+/+}) mice that carried the tamoxifen-inducible UBC-Cre-ERT2 transgene. To induce Cre-mediated recombination, cultures were treated with 4-hydroxytamoxifen (4-OHT) (**Figure 3.S1A**). In *Pnky*^{F/F};UBC-Cre-ERT2 cultures, 4-OHT treatment abolished *Pnky* expression (-95.6%) (**Figure 3.1C**), and these *Pnky*-cKO NSCs exhibited increased neurogenesis, producing nearly 6-fold more neurons than control cultures (**Figures 3.1D-E**). Thus, conditional deletion of the entire *Pnky* gene produces a phenotype similar to that of *Pnky* transcript KD in cultured NSCs.

Divergent lncRNAs are transcribed in the opposite direction of nearby genes in a “head-to-head” configuration (Luo et al., 2016), and *Pnky* is divergent to the proneural transcription factor *Pou3f2* (Dominguez et al., 2013). In a study of 12 different lncRNAs divergent to transcription factors, shRNA-mediated lncRNA KD consistently downregulates the coding gene neighbor (Luo et al., 2016). We re-analyzed RNA-sequencing (RNA-seq) data of shRNA-mediated *Pnky* KD in V-SVZ NSCs (Ramos et al., 2015) and did not observe differential expression of *Pou3f2* or any other gene +/- 2.5 MB from *Pnky* (**Figure 3.S1B**). However, it is unclear whether shRNA-mediated KD affects the processes of transcription and splicing of RNA transcripts (Wagschal et al., 2012; West et al., 2004). This mechanistic consideration is important as some lncRNAs – independent of the specific transcripts themselves – regulate their divergent gene neighbor through these processes (Engreitz et al., 2016). Surprisingly, *Pnky*-cKO did not affect the abundance of *Pou3f2* transcript in V-SVZ NSCs ($p = 0.40$) (**Figure 3.1C**). Thus, *Pou3f2* expression in cultured NSCs does not appear to require the *Pnky* transcript, processes related to its local transcription, splicing of the lncRNA, or potential regulatory elements contained within the deleted DNA sequence.

Pnky regulates development of the mouse neocortex

The mammalian neocortex is a dorsal brain structure comprised of six layers of projection neurons, and the proper development of these layers is critical to cognitive function (Lodato and Arlotta, 2015; Molyneaux et al., 2007; Rubenstein, 2011). In addition to projection neurons, the cortex contains many interneurons that are dispersed throughout. In the embryonic brain, cortical projection neurons are born locally from NSCs in the dorsal brain (pallium), whereas cortical interneurons arise from ventral regions (subpallium). During development, changes in the production of cortical interneurons can modulate the genesis of projection neurons (Silva et al., 2018), and vice versa (Lodato et al., 2011). *Pnky* is expressed in NSCs in both the pallium and subpallium of the embryonic brain (Ramos et al., 2015). Thus, to investigate whether *Pnky* directly regulates the production of cortical projection neurons, we focused our *in vivo* analysis on the cell lineages derived from pallial NSCs.

We targeted *Pnky*-cKO to pallial NSCs with *Emx1^{Cre}*, which expresses Cre in the pallium beginning at ~ embryonic day (E) 9.5 (Briata et al., 1996; Gorski et al., 2002; Simeone et al., 1992) (**Figure 3.S1C**). Embryonic brain NSCs reside in the ventricular zone (VZ), and *in situ* hybridization (ISH) revealed *Pnky* expression in the pallial VZ by E10.0 (**Figure 3.S1D**). In *Pnky^{F/F};Emx1^{Cre}* mice, *Pnky* expression in the pallium was ablated as assessed by ISH, with very few *Pnky* transcripts detected in the pallium at E10.0 (**Figure 3.S1D**), and none by E13.5 (**Figure 3.1F**) or postnatal day (P) 14 (**Figure 3.S1E**). As expected, in the subpallium of *Pnky^{F/F};Emx1^{Cre}* mice, *Pnky* expression was not decreased (**Figures 3.1F** and **3.S1D**). Thus, before the onset of cortical neurogenesis, *Pnky^{F/F};Emx1^{Cre}* mice have undergone *Pnky*-cKO selectively in the NSCs that give rise to cortical projection neurons.

Despite evidence of homozygous *Pnky* deletion, the expression of POU3F2 in the *Pnky^{F/F};Emx1^{Cre}* pallium was indistinguishable from that of littermate controls (**Figures 3.1G** and **3.S1F**). Consistent with these immunohistochemical (IHC) results, RNA-seq analysis of acutely-dissected E12.5 pallium showed that *Pnky*-cKO abolished *Pnky* expression (**Figure 3.S1G**)

without perturbing *Pou3f2* transcript levels (adjusted $p = 0.37$) (**Figure 3.S1H**). While *Pnky*-cKO resulted in differential expression of genes with roles in cortical development and neurogenesis, including *Lhx9* (Peukert et al., 2011) and *Fezf2* (Molyneaux et al., 2005; Zhang et al., 2014), differential expression was not observed within +/- 20 MB of *Pnky* (**Table 3.1**). Moreover, we did not find POU3F2 binding motifs within the promoter region of any of the differentially-expressed genes (data not shown). The E12.5 cortex of *Pnky*^{F/F};*Emx1*^{Cre} mice also exhibited changes in alternative splicing (**Figure 3.S1I** and **Table 3.2**), affecting transcripts with known neurodevelopmental roles such as *Ank3* (Durak et al., 2015) and *Tcf12* (Mesman and Smidt, 2017). Thus, in the early embryonic pallium, *Pnky*-cKO affects the abundance and splicing of transcripts related to neural development, but does not disrupt the expression of *Pou3f2* mRNA or protein.

The development of the laminar structure of the cortex progresses temporally in an “inside-out” manner: NSCs first give rise to projection neurons for the deep layers (5 and 6), while later-born neurons migrate past them to form the upper layers (2/3 and 4) (Lodato and Arlotta, 2015). In mice, the birth of deep layer neurons peaks around E13.5. As compared to littermate controls, the *Pnky*^{F/F};*Emx1*^{Cre} cortex of E13.5 mice had increased numbers of CTIP2+ neurons in the cortical plate (CP) (+24.3%) (**Figures 3.2A-B**). This increase in neurogenesis was accompanied by a decrease in proliferating VZ cells as determined by analysis of phosphorylated histone H3 (pH3) (-17.3%) (**Figures 3.2C-D**) and phosphorylated Vimentin (pVIM) (-11.8%) (**Figures 3.S2A-B**). Thus, consistent with prior results obtained with shRNA-mediated *Pnky* KD (Ramos et al., 2015), *Pnky*-cKO targeted to pallial NSCs increases neuronal production but decreases the pool of proliferative NSCs.

Given the increase in early-born CTIP2+ neurons at E13.5 (**Figures 3.2A-B**), we assessed for changes in the number of deep layer neurons at P14, when the laminar structure of the cortex is fully evident. As compared to littermate controls, *Pnky*^{F/F};*Emx1*^{Cre} mice exhibited an increased number of CTIP2+ neurons in layer (L) 6, the deepest cortical layer (+8.1%)

(**Figures 3.2E-F**). Since the number of proliferative VZ cells was reduced in *Pnky*^{F/F};*Emx1*^{Cre} mice at E13.5 (**Figures 3.2C-D** and **3.S2A-B**), and the peak of upper layer neurogenesis occurs later (~E15.5), we considered that upper layer neurogenesis might be affected in *Pnky*^{F/F};*Emx1*^{Cre} mice. As compared to littermate controls, the P14 cortex of *Pnky*^{F/F};*Emx1*^{Cre} mice exhibited fewer CUX1+ neurons in the upper cortical layers (-14.4%) (**Figures 3.2G-H**). Furthermore, we used 5-bromo-2'-deoxyuridine (BrdU) to label neurons born at E15.5, and the P14 cortex of *Pnky*^{F/F};*Emx1*^{Cre} mice also had reduced numbers of BrdU+;CUX1+ cells in the upper layers (-14.5%) (**Figure 3.S2C**). Essentially all BrdU+ cells in all mice were located in the upper layers, and there was no change in the proportion these cells that were also CUX1+ ($p = 0.25$) (**Figure 3.S2D**), indicating that *Pnky*-deletion does not simply cause a loss of CUX1 expression or mis-specification. Thus, *Pnky*-cKO in the early embryonic pallium causes malformation of the postnatal neocortex, increasing the number of deep layer neurons while decreasing the population of upper layer neurons.

To determine whether *Pnky* function is cell-autonomous, we targeted *Pnky*-cKO to a small cohort of NSCs by injecting a Cre-expressing adenovirus (Ad:Cre) (**Figures 3.S3A-B**) into the lateral ventricles of E13.5 *Pnky*^{F/F} mice or wild-type (*Pnky*^{+/+}) littermate controls *in utero* (**Figures 3.3A** and **3.S3C**). For fate-tracing analysis, these mice carried the Ai14 transgenic reporter that expresses tdTomato after Cre-mediated recombination (**Figure 3.3B**). Two days after Ad:Cre injection, *Pnky*^{F/F};Ai14 mice exhibited an increase in the proportion of tdTomato+ cells that were found in the CP (+82.7%) (**Figures 3.3C-D**), as well as in the proportion of CTIP2+ CP cells (+86.4%) (**Figure 3.3E**). To investigate whether this increase in early neurogenesis leads to changes in the postnatal cortex, we analyzed mice 20 days post-injection (at P14). Consistent with *Pnky*-cKO at E13.5 causing an overproduction of deep layer neurons at the expense of the later upper layer neurons, the postnatal cortex of *Pnky*^{F/F};Ai14 mice exhibited an increase in the ratio of CTIP2+ deep layer to CUX1+ upper layer cells within the

tdTomato+ population (+19.9%) (**Figures 3.3F-G** and **3.S3D**). These results indicate that *Pnky* regulates cortical neurogenesis in a cell-autonomous manner.

Pnky functions in *trans* to regulate cortical development

Given the lack of evidence for *Pnky* regulating *Pou3f2* or other genes in *cis*, we developed genetic methods to test whether *Pnky* functions in *trans*. We obtained a bacterial artificial chromosome (BAC) containing ~170kb of the genomic sequence surrounding *Pnky* and removed the coding sequence of *Pou3f2*, the only other complete gene in this BAC (**Figures 3.4A** and **3.S4A**). We then generated transgenic mice (BAC^{*Pnky*}) that express *Pnky* from this modified BAC construct and bred them with mice carrying the *Pnky*^F allele. We established cortical NSC (cNSC) cultures from *Pnky*^{+/+}, *Pnky*^{F/F}, and *Pnky*^{F/F};BAC^{*Pnky*} E12.5 embryos, and used Ad:Cre to induce recombination. Three days later, we performed RNA-seq from these cultures as well as paired untreated control cultures (**Figure 3.S4B**). While the addition of Ad:Cre to *Pnky*^{F/F} cultures abolished the expression of *Pnky*, the presence of BAC^{*Pnky*} maintained *Pnky* at approximately 20% of wildtype levels (**Figure 3.4B**).

In these undifferentiated cNSCs, *Pnky*-cKO resulted in the differential expression of 55 other genes (**Figure 3.4C** and **Table 3.3**), including genes known to have roles in neurodevelopment such as *Miat* (*Gomafu*) (Aprea et al., 2013; Barry et al., 2014; Spadaro et al., 2015) and *Erb4* (Perez-Garcia, 2015). None of the differentially-expressed genes contained POU3F2 binding motifs within their promoter regions (data not shown). Strikingly, the vast majority (47 of 55, 85.5%) of the genes that were differentially expressed with *Pnky*-cKO was significantly rescued by the presence of BAC^{*Pnky*}, such that these genes were no longer differentially expressed in *Pnky*^{F/F};BAC^{*Pnky*} cultures (**Figure 3.4D**). Of the 27 genes that were increased in *Pnky*-cKO cultures, 21 (77.8%) were decreased by the presence of BAC^{*Pnky*}. Similarly, 92.9% (26 of 28) of the genes downregulated by *Pnky*-cKO were increased by BAC^{*Pnky*}. Of note, the transcriptional changes related to BAC^{*Pnky*} were significantly restricted to

those genes differentially expressed in *Pnky*-cKO cells ($p = 1.33 \times 10^{-51}$, hypergeometric test). Thus, expression of *Pnky* from a BAC transgene specifically rescues the transcriptional changes that result from deletion of endogenous *Pnky*.

In postnatal V-SVZ NSCs, *Pnky* physically interacts with PTBP1 (Ramos et al., 2015) – an mRNA splicing factor that regulates neurogenesis in NSCs (Zhang et al., 2016). RNA immunoprecipitation (RIP) with PTBP1 antibodies also enriched the *Pnky* transcript from cNSC cultures (**Figure 3.4E**). In cNSCs, *Pnky*-cKO affected 220 splicing events as compared to *Pnky*^{+/+} controls (**Figure 3.4F** and **Table 3.4**), and 22 of these events were rescued (no longer significantly differentially spliced) by the presence of BAC^{*Pnky*} ($p = 1.99 \times 10^{-8}$, hypergeometric test) (**Figure 3.4G**). We also compared the splicing changes that occur upon loss of *Pnky* with two previously-generated datasets of PTBP1 KD in different neural cells (Raj et al., 2014; Ramos et al., 2015). Interestingly, 47 events were also differentially spliced upon PTBP1 KD in at least one dataset, and 13 of these were differentially spliced in both PTBP1 datasets ($\chi^2=7.7$; $p = 0.0006$) (**Figure 3.4C**). These data suggest that in addition to regulating the abundance of specific transcripts (**Figures 3.4C-D**), *Pnky* also influences mRNA splicing.

After removal of mitogenic growth factors, cNSCs produce neurons in culture (**Figure 3.4B**). Coherent with the increase in cortical neurogenesis observed with *Pnky*-cKO *in vivo* and the analysis of V-SVZ NSCs *in vitro*, cNSCs with *Pnky*-cKO produced ~3-fold more neurons as compared to the *Pnky*^{+/+} controls (+2.88 fold) (**Figures 3.4H-I**). The presence of BAC^{*Pnky*} in *Pnky*-cKO cNSCs reduced neurogenesis to levels observed in *Pnky*^{+/+} cultures ($p = 0.41$) (**Figures 3.4H-I**), indicating that the BAC^{*Pnky*} transgene can rescue the neurogenic phenotype of *Pnky*-cKO *in vitro*.

To investigate whether BAC^{*Pnky*} can rescue the phenotype of *Pnky*-deletion *in vivo*, we generated mice with germline *Pnky*-deletion (*Pnky*^{null/null}) and crossed these two mouse lines to produce *Pnky*^{null/null};BAC^{*Pnky*} mice (**Figure 3.4D**). While *Pnky*^{null/null} mice had no detectable *Pnky* transcripts, *Pnky*^{null/null};BAC^{*Pnky*} mice exhibited a similar pattern and level of *Pnky* expression as

Pnky^{+/+} animals (**Figures 3.4J** and **3.S4E**). Therefore, expression of *Pnky* from the BAC mimics that from the endogenous *Pnky* locus. In comparison to *Pnky*^{+/+} littermates, E13.5 *Pnky*^{null/null} embryos had fewer CTIP2+ neurons in the CP (-16.6%) (**Figures 3.4K-L**). This decrease in neurogenesis may relate to the constitutive absence of *Pnky* causing an earlier loss of proliferative NSCs. Consistent with this notion, we observed a decrease in proliferative pH3+ progenitor cells in the VZ of *Pnky*^{null/null} mice (-9.7%) (**Figures 3.4M-N**), and the overall thickness of the cortex was also reduced in these animals (**Figure 3.S4F**). Importantly, the presence of the BAC^{*Pnky*} transgene was sufficient to rescue all of these phenotypes in *Pnky*^{null/null};BAC^{*Pnky*} mice (**Figures 3.4K-N** and **3.S4F**). Thus, the expression of *Pnky* in *trans* from a BAC rescues the phenotype of *Pnky*-deletion in the developing cortex *in vivo*.

To determine whether loss of *Pnky* and the resulting alterations in early embryonic cortical development lead to persistent defects in the cortex, we analyzed *Pnky*^{null/null} mice and *Pnky*^{+/+} littermates at P14. Similar to the changes we had found in E13.5 embryos, we observed a decrease in CTIP2+ deep layer neurons (-11.9%) (**Figures 3.5A-B**). Since the layering of the cortex is evident by this age, we were also able to quantify the CTIP2+ cells by layer. While there was a decrease in L6 CTIP2+ cells, it did not reach statistical significance (-11.7%, $p = 0.056$) (**Figure 3.5C**). However, we did observe a significant decrease in the number of L5 CTIP2+ cells (-12.5%) (**Figure 3.5D**). Furthermore, there was also a decrease in the CUX1+ upper layer population (-9.1%) (**Figures 3.5E-F**). Thus, loss of *Pnky* persistently alters the abundance of multiple neuronal subpopulations in the cortex. As we have previously shown that *Pnky* is conserved in human (**Figure 2.3B**) and similarly expressed in the VZ of the developing cortex (**Figure 2.3C**), it will be important to determine whether human *PNKY* also regulates cortical neurogenesis. Interestingly, we find that human *PNKY* is expressed in human cerebral organoids, and seems to be enriched around the VZ-like regions of the organoid (**Figure 3.5G**). Cerebral organoids may therefore serve as a tractable model system for future studies to determine the function of human *PNKY*.

Discussion

There are currently few genetic studies of lncRNA function *in vivo*, and thus the biological significance of most lncRNAs during mammalian development is unclear (Bassett et al., 2014; Nakagawa, 2016). Using a combination of genetic methods in mice to systematically study the function and genetic mechanism of *Pnky*, we show that this lncRNA functions in *trans* to regulate the development of the neocortex. By targeting conditional *Pnky* deletion to specific cell types in the embryonic brain, we found that *Pnky* regulates the genesis of neocortical projection neurons in a cell-autonomous manner. Surprisingly, *Pnky*-deletion did not produce evidence that this lncRNA regulates gene expression in *cis*. Moreover, when expressed from a BAC transgene, *Pnky* rescued both the differential gene expression and cellular phenotype of cultured *Pnky*-cKO NSCs. BAC^{*Pnky*} was also sufficient to rescue the *in vivo* phenotypes of *Pnky*-deletion in the developing cortex, indicating that *Pnky* functions in *trans*.

The production of projection neurons for the different layers of the mammalian neocortex is a critical, highly regulated aspect of brain development (Lodato and Arlotta, 2015). For instance, deletion of the transcription factor *Eomes/Tbr2* in the embryonic brain decreases the CUX1+ upper layers by ~20% (Arnold et al., 2008). *Pnky*-cKO targeted to NSCs in the early embryonic pallium with *Emx1*^{Cre} altered postnatal cortical lamination such that there were ~10% more deep layer 6 neurons and ~15% fewer upper layer neurons. This postnatal phenotype corresponded to an increase in early neurogenesis (during deep layer production) *in vivo* at the expense of proliferating VZ cells, which later give rise to upper layer neurons. Coherent with these *in vivo* observations, acute *Pnky*-cKO in cultured NSCs also increased neurogenesis. This *in vitro* phenotype was previously observed with shRNA-mediated *Pnky* KD, indicating that deletion of the *Pnky* gene has similar effects to targeting the transcript. The cellular phenotypes of *Pnky*-cKO and *Pnky* KD were more dramatic in cultured NSCs as compared to those in the developing cortex, suggesting that there are mechanisms *in vivo* that can partially compensate for the loss of *Pnky* transcript.

Interestingly, constitutive deletion of the lncRNA locus for *linc-Brn1b* also results in more (~20%) deep layer neurons and fewer (~10%) upper layer cells in the postnatal cortex (Sauvageau et al., 2013). However, in contrast to *Pnky*-KO, deletion of *linc-Brn1b* reduces expression of its neighboring transcription factor, *Pou3f3* (Sauvageau et al., 2013), which is a paralog of the *Pnky* neighbor *Pou3f2*. Another lncRNA, *linc-Brn1a* (a.k.a. *Pou3f3os*) is divergent to *Pou3f3*, and shRNA-mediated KD of this lncRNA also reduces levels of *Pou3f3* (Luo et al., 2016). Thus, even closely related genes such as *Pou3f2* and *Pou3f3* appear to have very different functional relationships with nearby lncRNAs.

Divergent lncRNAs are strongly predicted to regulate the expression of transcription factor gene neighbors (Luo et al., 2016). Even the processes of lncRNA transcription and splicing, independent of the mature lncRNA transcript itself, can regulate expression of the divergent gene neighbor (Engreitz et al., 2016; Kopp and Mendell, 2018). For example, the lncRNA upperhand (*Uph*) is divergent to the transcription factor *Hand2*, and insertion of a poly-A cassette into *Uph* abolishes the expression of *Hand2* in *cis*, resulting in severe cardiac defects *in vivo* (Anderson et al., 2016). However, ASO-mediated KD of *Uph* does not affect *Hand2* levels. Importantly, *Uph* is transcribed through known enhancers of *Hand2*, and transcription of this lncRNA appears to establish a more permissive chromatin state for these enhancers. In contrast, *Pnky*-deletion did not affect expression of *Pou3f2*. Of note, the *Pnky* locus is not known to harbor transcriptional enhancers, and we have not observed strong enhancer-like activity of *Pnky* DNA sequences in cell culture reporter assays (unpublished observations). We therefore speculate that whether a divergent, functional lncRNA has *cis* and/or *trans* mechanisms relates in part to the local presence (or absence) of transcriptional enhancers.

Divergent lncRNAs can also regulate the function of the protein that arises from the coding gene neighbor. For instance, the lncRNA *Paupar* – which is transcribed through an enhancer of its neighbor *Pax6* – not only regulates *Pax6* expression but also physically interacts with the PAX6 transcription factor to affect its regulation of target genes (Pavlaki et al., 2018;

Vance et al., 2014). In the developing retina, the divergent lncRNA *Six3OS* appears to act as a molecular scaffold, regulating the activity of its transcription factor neighbor, SIX3 (Rapicavoli et al., 2011). While modulation of POU3F2 activity is a plausible mechanism of *Pnky* function, we have not observed interactions between *Pnky* transcript and POU3F2 protein (not shown), and *Pnky*-deletion did not affect the expression of potential POU3F2 target genes.

It remains possible that *Pnky* regulates *Pou3f2* in other cellular contexts, or alters transcriptional dynamics that might not change steady-state levels of mRNA (Imayoshi and Kageyama, 2014; Lenstra et al., 2016). Importantly, lncRNA mechanisms are not necessarily mutually exclusive, and there are examples of lncRNAs that carry out multiple distinct molecular roles through both *cis* and *trans* mechanisms (Cajigas et al., 2018; Pavlaki et al., 2018; Vance et al., 2014). However, the rescue of *Pnky*-deletion phenotypes by BAC^{Pnky} strongly suggests that *Pnky* primarily functions in *trans* in NSCs. While BAC^{Pnky} also contains the untranslated regions (UTRs) of *Pou3f2*, and it is conceivable that these sequences contribute to the rescue, it is remarkable that essentially all of the differential gene expression resulting from *Pnky*-deletion was significantly and specifically rescued by BAC^{Pnky} . *Pnky* RNA physically interacts with PTBP1, a factor that regulates both transcript abundance and splicing, and BAC^{Pnky} rescued ~10% of the differentially-spliced events in *Pnky*-cKO NSCs. While there was significant overlap between the differentially-spliced events upon *Pnky*-cKO and *Ptbp1*-KD, how *Pnky* might affect PTBP1-dependent splicing remains to be discovered. Furthermore, *Pnky* may have additional roles that are independent of PTBP1. Future work to more comprehensively identify proteins that interact with *Pnky* will be important to further determine the mechanism(s) by which this lncRNA regulates transcript abundance and splicing, and ultimately neural development.

The developing brain expresses many thousands of different lncRNAs, and there are emerging examples of lncRNAs with relevance to neurodevelopmental disorders (Briggs et al., 2015; Meng et al., 2015), underscoring the need to determine the functions of lncRNAs during brain development in animal models. While efforts have been made to predict lncRNA biology

from their underlying DNA sequence and genomic location (Engreitz et al., 2016; Liu et al., 2017; Luo et al., 2016), at this point in this emerging field of research, testing individual lncRNAs systematically will likely be required to decipher fundamental aspects of their developmental function and mechanism. Because the range of potential mechanisms of lncRNAs is fundamentally more broad (*cis* and *trans*) than protein coding genes or microRNAs, it is unlikely that any one experimental method will be sufficient to lay the groundwork for understanding molecular mechanism, and instead an integration of multiple approaches will often be required (Liu and Lim, 2018). Moving forward, *in vivo* studies of lncRNA function will serve as a crucial foundation for understanding how this class of noncoding transcripts can regulate normal brain development and contribute to neurological disorders.

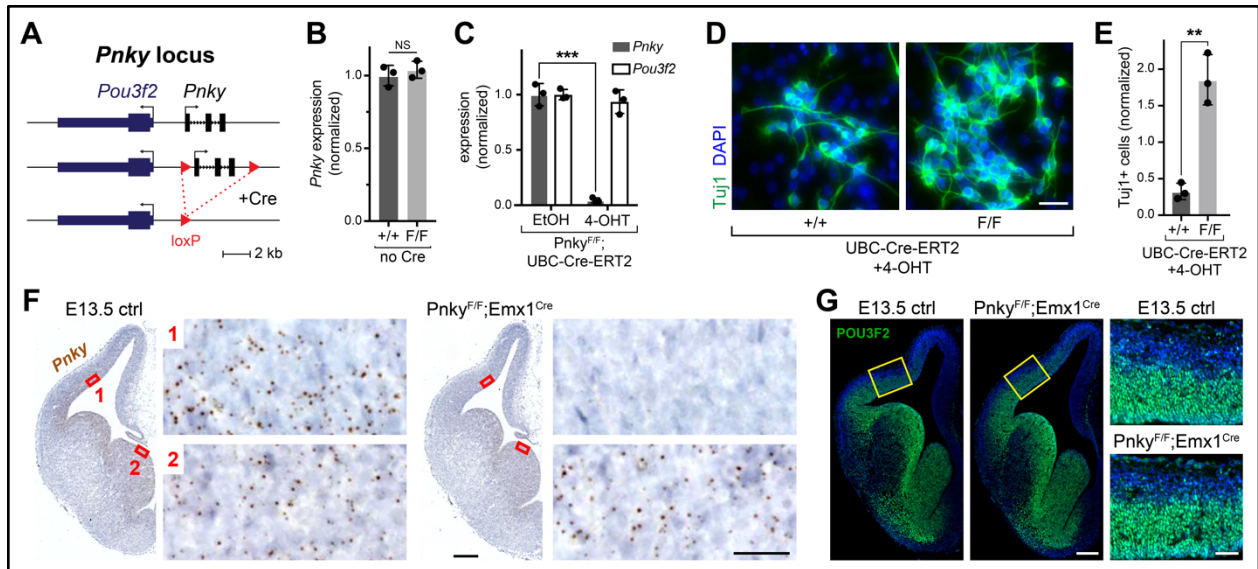


Figure 3.1: Generation of a conditional deletion allele for the lncRNA *Pnky*.

Quantifications: mean +/- SD. NS = not significant, ** = p < 0.01, *** = p < 0.001, unpaired two-tailed t test. **A**, Schematic of *Pnky* locus and loxP site insertions. **B**, *Pnky* levels in V-SVZ cultures by qRT-PCR. Biological replicate littermates, normalized to *Pnky*^{+/+} mean. **C**, *Pnky* and *Pou3f2* in ethanol (EtOH)- or 4-OHT-treated V-SVZ cultures by qRT-PCR. Technical replicates, normalized to EtOH-treated mean. **D**, Tuj1 ICC in d4 differentiated V-SVZ cultures. Scale bar = 25 μm. **E**, Quantification of (D). Technical replicates with independent EtOH or 4-OHT treatment, normalized to EtOH-treated cultures for each genotype. **F**, ISH of *Pnky* (brown puncta) in coronal brain sections, with hematoxylin nuclear counterstain (blue). Red boxes = regions of pallium (1) and subpallium (2) enlarged in adjacent panels. Scale bars = 250 μm (hemispheres) and 25 μm (insets). **G**, POU3F2 IHC with DAPI nuclear stain (blue). Yellow boxes = regions of pallium enlarged in adjacent panels. Scale bars = 200 μm (hemispheres) and 50 μm (insets). See also Figure 3.S1.

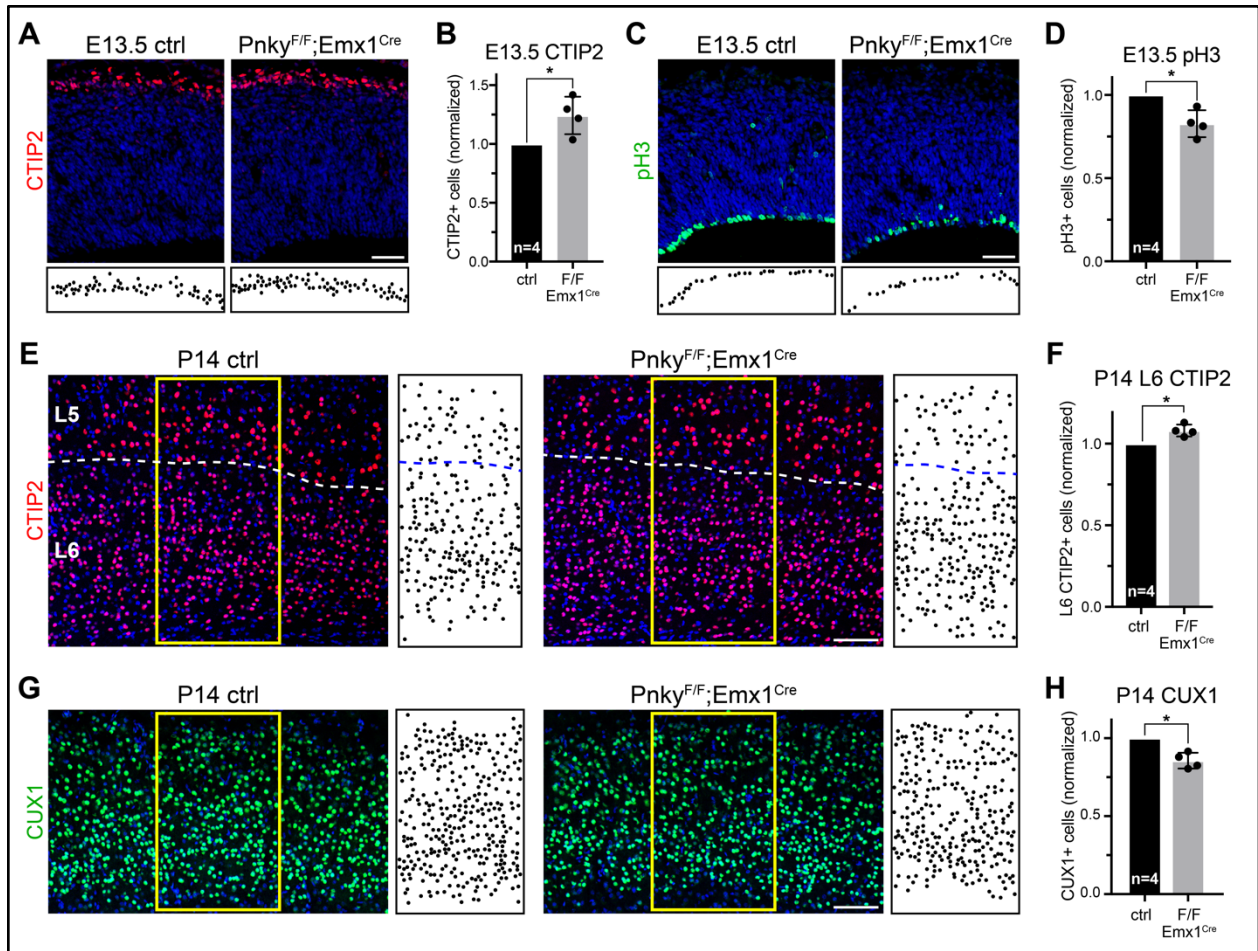


Figure 3.2: *Pnky* regulates cortical neurogenesis *in vivo*.

Quantifications: mean +/- SD of biological replicates, normalized to littermate controls. * = $p < 0.05$, two-tailed ratio paired t test. **A**, CTIP2 IHC with DAPI (blue). Locations of CTIP2+ cells in CP depicted below. Scale bar = 50µm. **B**, Quantification of (A). **C**, pH3 IHC with DAPI (blue). Locations of pH3+ cells in VZ depicted below. Scale bar = 50µm. **D**, Quantification of (C). **E**, CTIP2 IHC in the deep layers of P14 cortex, with DAPI (blue). Dotted line = border between L5 and L6. Locations of CTIP2+ cells within yellow boxes depicted to the right. Scale bar = 100µm. **F**, Quantification of (E). **G**, CUX1 IHC in the upper layers of P14 cortex, with DAPI (blue). Locations of CUX1+ cells within yellow boxes depicted to the right. Scale bar = 100µm. **H**, Quantification of (G). See also Figure 3.S2.

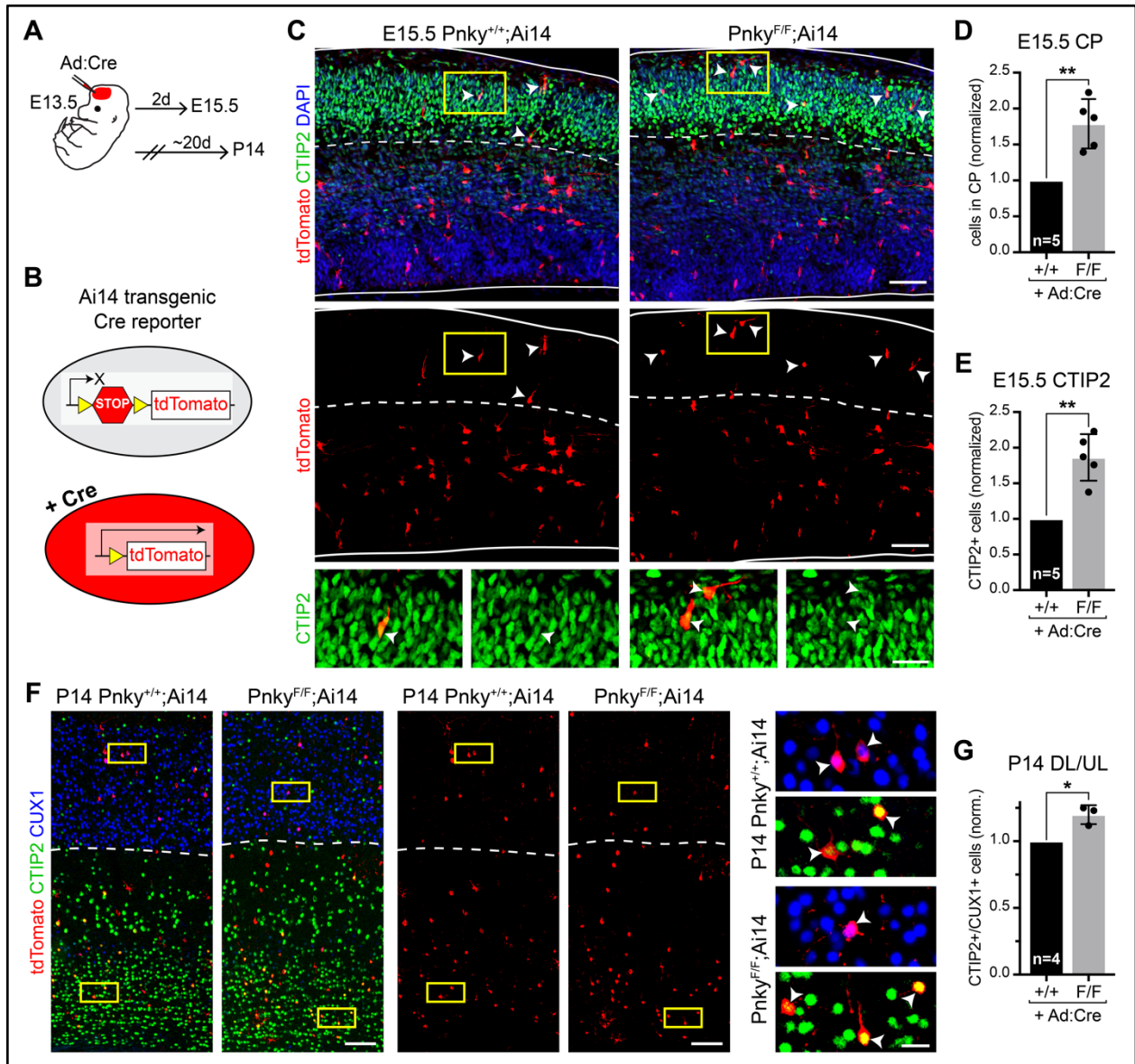


Figure 3.3: *Pnky* functions cell-autonomously in the developing cortex.

Quantifications: mean \pm SD of biological replicates, normalized to littermate controls. * = $p < 0.05$, ** = $p < 0.01$, two-tailed ratio paired t test. **A**, Schematic of *in utero* Ad:Cre viral injections.

B, Schematic of Ai14 transgenic Cre reporter. **C**, IHC of tdTomato and CTIP2 at E15.5.

Arrowheads = double-positive cells within CP, demarcated by dotted line. Yellow boxes = regions enlarged below. Scale bars = $50\mu\text{m}$ and $20\mu\text{m}$ (insets). **D**, Quantification of proportion of tdTomato+ cells in the CP. **E**, Quantification of proportion of tdTomato+ cells located in CP and CTIP2+. **F**, IHC for tdTomato, CTIP2, and CUX1 at P14. Dotted line = border between deep and upper cortical layers. Yellow boxes = regions enlarged in adjacent panels. Arrowheads = double-positive cells. Scale bars = $100\mu\text{m}$ and $20\mu\text{m}$ (insets). **G**, Quantification of ratio of CTIP2+ deep layer cells to CUX1+ upper layer cells within tdTomato+ population at P14. See also Figure 3.S3.

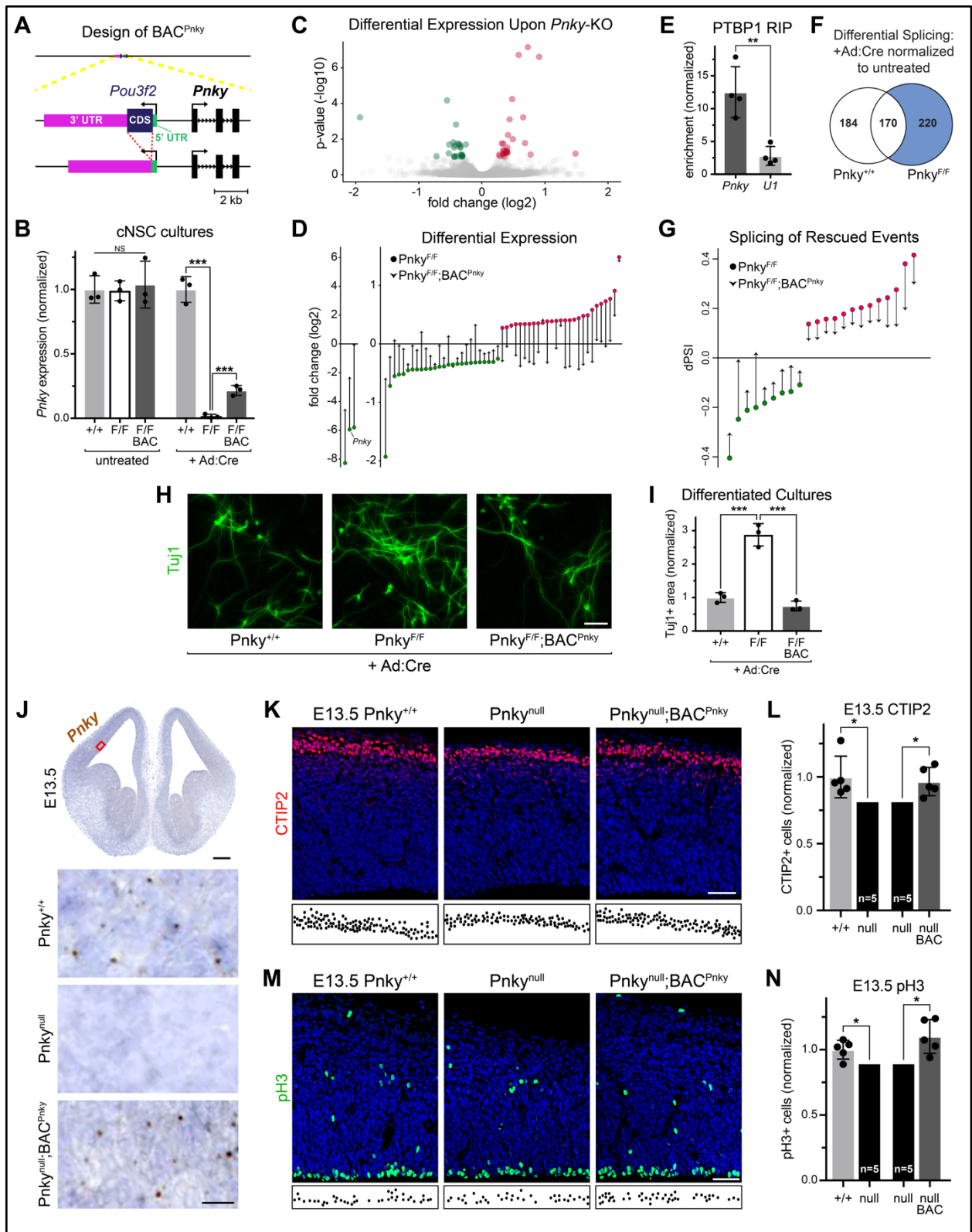


Figure 3.4: BAC transgenic expression of *Pnky* rescues loss of the endogenous gene. Quantifications: mean \pm SD of separate biological replicates, except as indicated in (I). NS = not significant, * = $p < 0.05$, *** = $p < .001$. **A**, Schematic of BAC^{Pnky} transgene. **B**, *Pnky*

expression in untreated or +Ad:Cre cNSC cultures by RNA-seq. Normalized to *Pnky*^{+/+} mean for each treatment group. **C**, Volcano plot of differentially-expressed genes upon *Pnky*-cKO. Three genes with fold changes outside this range are not displayed here (see D). **D**, Log2 fold changes of all significantly differentially-expressed genes in *Pnky*^{F/F} +Ad:Cre cultures (circles). Arrowheads = log2 fold changes for these genes in *Pnky*^{F/F};BAC^{*Pnky*} +Ad:Cre cultures. **E**, Enrichment following RIP with PTBP1 antibodies from cNSC cultures. Four technical replicates from 2 separate experiments, normalized to levels of *β-actin*. **F**, Alternatively-spliced events in cNSCs upon Ad:Cre treatment. Significant events in *Pnky*^{F/F} +Ad:Cre samples that did not overlap with events in *Pnky*^{+/+} +Ad:Cre samples were analyzed further. **G**, Log2 fold changes of rescued alternatively-spliced events. **H**, Tuj1 ICC in d7 differentiated cNSC cultures. Scale bar = 50μm. **I**, Quantification of Tuj1+ area from (H). Mean +/- SD from technical triplicates comprised of cells pooled from three biological replicates. Normalized to uninfected controls and to *Pnky*^{+/+} +Ad:Cre values. Statistical analysis = one-way ANOVA with Turkey's multiple comparisons test. **J**, ISH of *Pnky* (brown puncta) with hematoxylin counterstain (blue). Representative section with red box indicating approximate region of pallium enlarged below. Scale bars = 250μm and 25μm (insets). **K**, CTIP2 IHC with DAPI (blue). Locations of CTIP2+ cells in CP depicted below. Scale bar = 50μm. **L**, Quantification of (K), two-tailed ratio paired t test. **M**, pH3 IHC with DAPI (blue). Locations of pH3+ cells in VZ depicted below. Scale bar = 50μm. **N**, Quantification of (M), two-tailed ratio paired t test. See also Figure 3.S4 and Tables 3.3 and 3.4.

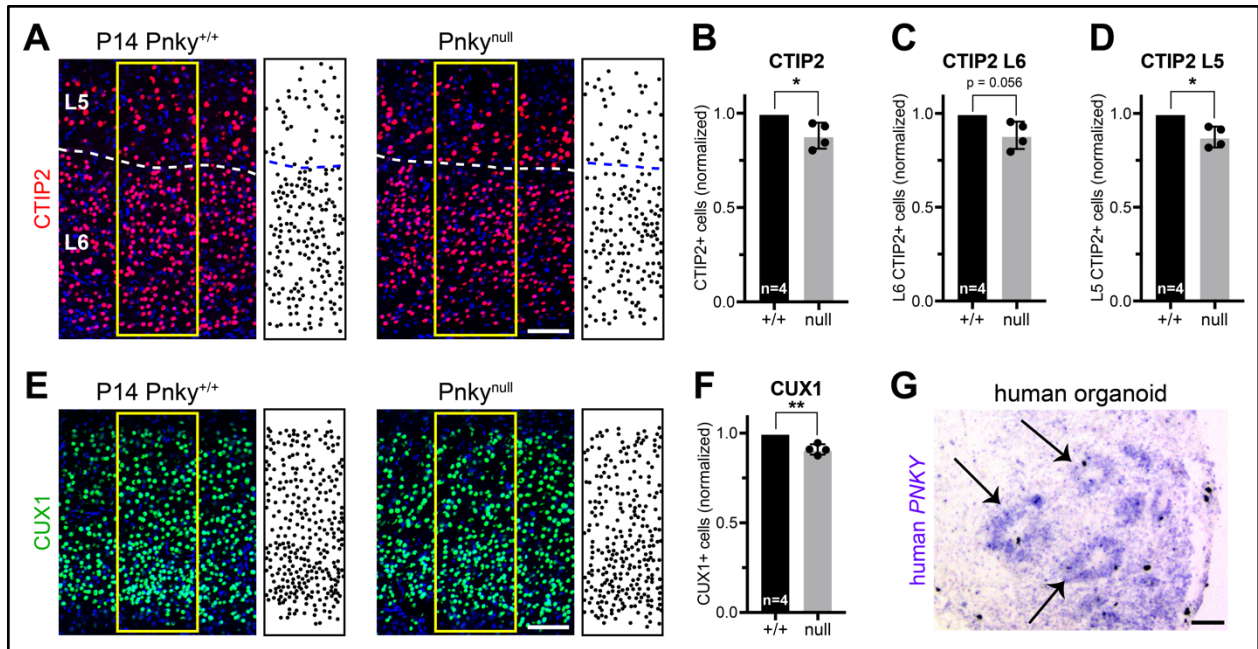


Figure 3.5: Loss of *Pnky* leads to persistent defects in the postnatal cortex.

Quantifications: mean +/- SD of biological replicates, normalized to littermate controls. * = $p < 0.05$, ** = $p < 0.01$, two-tailed ratio paired t test. Scale bars = 100 μ m. **A**, CTIP2 IHC in the deep layers of P14 cortex, with DAPI (blue). Dotted line = border between L5 and L6. Locations of CTIP2+ cells within yellow boxes depicted to the right. **B-D**, Quantifications of (A). **E**, CUX1 IHC in the upper layers of P14 cortex, with DAPI (blue). Locations of CUX1+ cells within yellow boxes depicted to the right. **F**, Quantification of (E). **G**, Human *PNKY* ISH in week 11 human cerebral organoid.

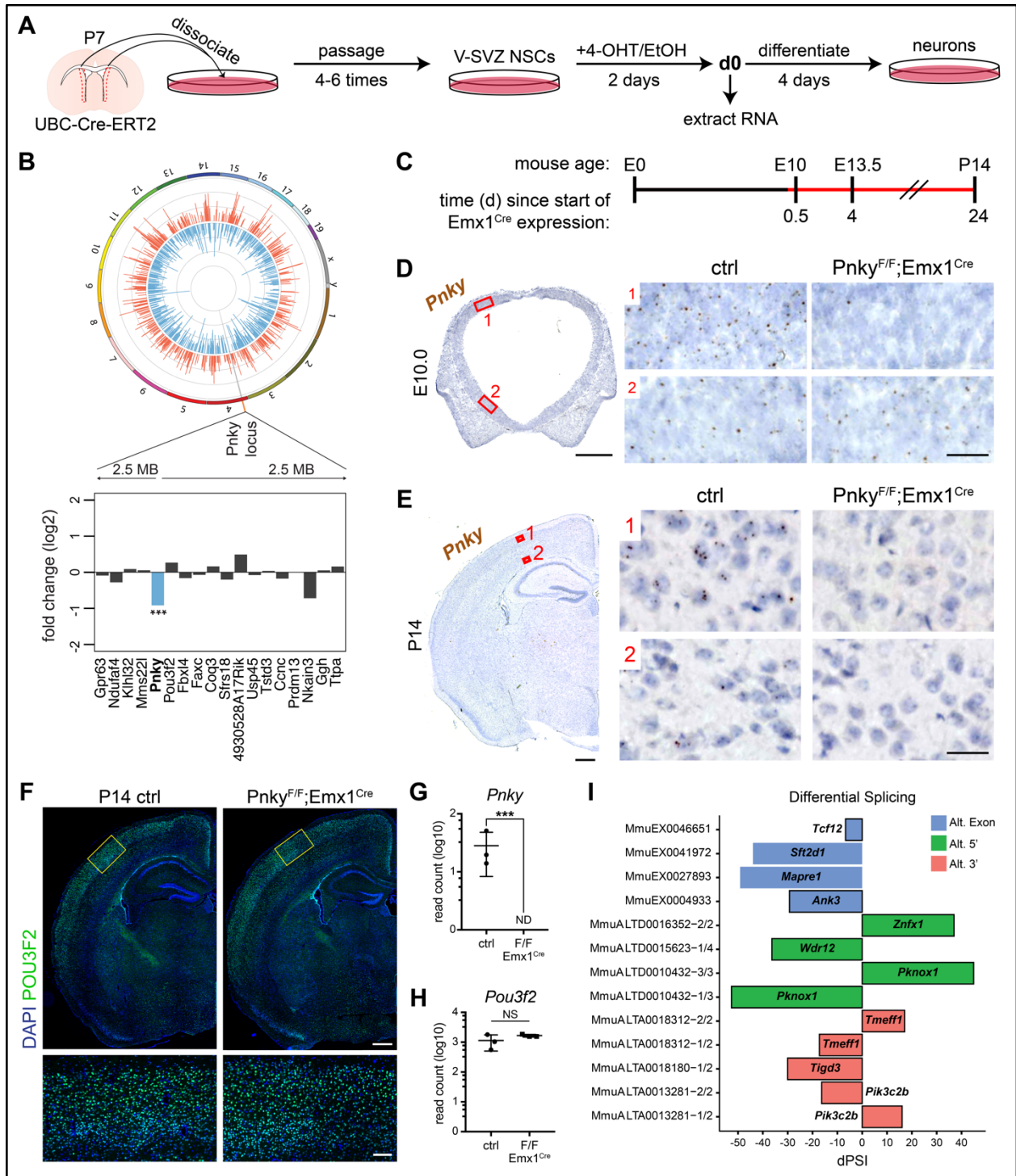


Figure 3.S1: Conditional deletion of *Pnky* in cultured cells and *in vivo*.

Quantifications displayed as mean \pm SD. NS = not significant, *** = $p < 0.001$. **A**, Schematic of V-SVZ cultures. **B**, Circos plot of genomic locations of differentially-expressed genes upon *Pnky*-KD in V-SVZ cultures (Ramos et al., 2015). Expanded region depicts genes within 2.5 MB of *Pnky*. **C**, Schematic of *Emx1*^{Cre} expression during mouse development. **D-E**, ISH of *Pnky* (brown puncta) with hematoxylin counterstain (blue). For E10.0 (D), representative coronal

section with red boxes to indicate approximate regions of pallium (1) and subpallium (2) enlarged in adjacent panels. Scale bars = 250 μ m and 25 μ m (insets). For P14 (E), representative coronal hemisphere with red boxes to indicate approximate regions of upper (1) and deep (2) cortical layers enlarged in adjacent panels. Scale bars = 500 μ m and 25 μ m (insets). **F**, IHC of POU3f2 with DAPI nuclear stain (blue). Scale bars = 500 μ m and 100 μ m (insets). **G-H**, Levels of *Pnky* (G) or *Pou3f2* (H) in E12.5 cortical tissue by RNA-seq. ND = not detected. **I**, Significant differentially-spliced events from biological triplicate samples. Gene names depicted within graph, with specific event names along y-axis. Events with black border = highly supported. Difference in percent spliced in (dPSI) calculated as $PSI(Pnky-cKO) - PSI(ctrl)$.

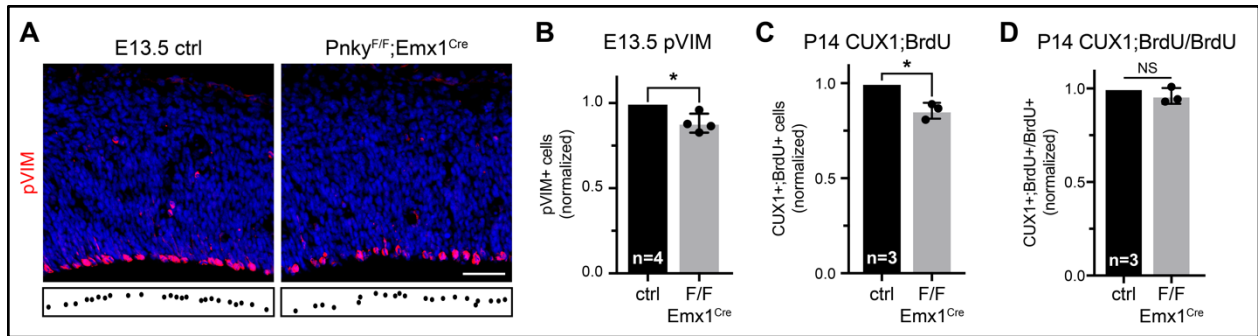


Figure 3.S2: Loss of *Pnky* disrupts cortical development.

Quantifications displayed as mean +/- SD from separate biological replicates, normalized to littermate controls. NS = not significant, * = $p < 0.05$, two-tailed ratio paired t test. **A**, pVIM IHC, with DAPI nuclear stain (blue). Locations of pVIM+ cells in VZ depicted below. Scale bar = 50 μ m. **B**, Quantification of (A). **C**, Quantification of BrdU+;CUX1+ cells in upper layers of P14 cortex. BrdU administered at E15.5. **D**, Quantification of the proportion of BrdU+ cells that also express CUX1 in the P14 cortex. BrdU administered at E15.5.

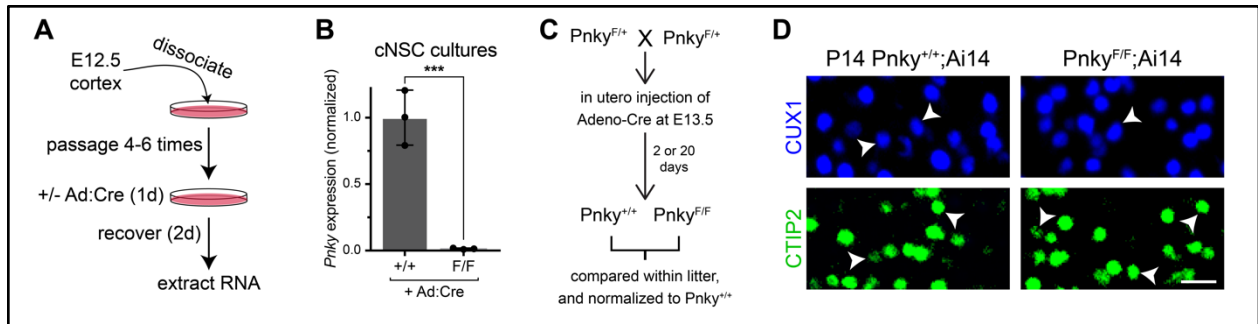


Figure 3.S3: *Pnky* deletion from a small cohort of cells in the developing cortex.

A, Schematic of cNSC culture derivation to test Ad:Cre-mediated deletion of *Pnky*. **B**, *Pnky* expression in Ad:Cre-treated cNSC cultures, quantified by qRT-PCR. Mean +/- SD from separate biological replicates, normalized to paired uninfected controls and to average *Pnky^{+/+}* +Ad:Cre value. *** = $p < 0.001$, two-tailed ratio paired t test. **C**, Schematic of genetic crosses used to produce littermates for in utero experiments. **D**, CTIP2 and CUX1 IHC at P14, following in utero injection of Ad:Cre at E13.5. Arrowheads = tdTomato+ cells, as shown in Figure 3.3F. Scale bar = 20 μ m.

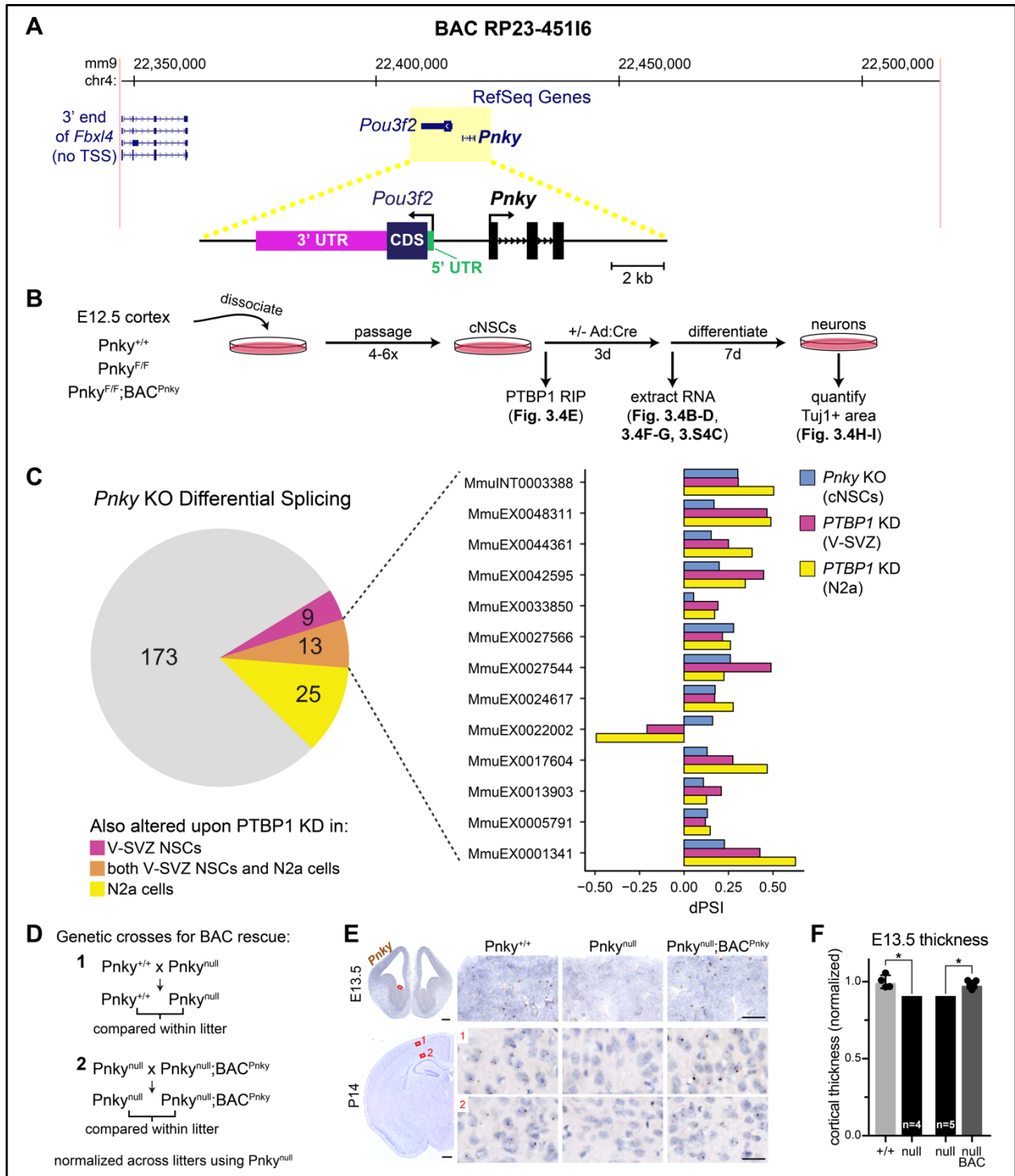


Figure 3.S4: Loss of *Pnky* is rescued by transgenic expression from a BAC.

Quantifications displayed as mean \pm SD. * = $p < 0.05$, ** = $p < 0.01$, two-tailed ratio paired t test. **A**, Diagram of the BAC used to generate BAC^{Pnky} transgenic mouse line. Coding sequence (CDS) of *Pou3f2* was removed, leaving untranslated regions (UTRs) intact. **B**, Schematic depicting cNSC culture experiments in the figures indicated. **C**, Overlap of differentially-spliced events upon *Pnky*-KO or PTBP1-KD (Raj et al., 2014; Ramos et al., 2015). Difference in percent

spliced in (dPSI) = PSI(experimental) – PSI(ctrl). **D**, Diagram of genetic crosses for BAC rescue experiments. **E**, ISH of *Pnky* (brown puncta) in E13.5 and P14 sections, with hematoxylin counterstain (blue). For E13.5, representative coronal section (also in Figure 3.4J) with red box to indicate approximate regions of subpallium enlarged in adjacent panels. Scale bars = 250 μ m and 25 μ m (insets). For P14, representative coronal hemisphere with red boxes to indicate the approximate regions of upper (1) and deep (2) cortical layers enlarged in adjacent panels. Scale bars = 500 μ m and 25 μ m (insets). **F**, Quantification of cortical thickness. Littermate biological replicates, normalized as indicated in (D).

Table 3.1: *Pnky* knockout *in vivo* alters transcript abundance.

Significant differentially-expressed genes in the E12.5 cortex upon loss of *Pnky* through *Emx1^{Cre}*, from biological triplicate samples. The threshold for statistical significance was set as an adjusted p value of 0.1 or lower. Sex-linked genes were excluded.

Gene name	Gene ID	Base mean	log2 fold	Adj p value
Gm30731 (<i>Pnky</i>)	ENSMUSG00000107859	14.105	-7.070	2.859E-09
Gm20305	ENSMUSG00000103979	22.574	-2.645	1.063E-02
Afp	ENSMUSG00000054932	30.918	-1.822	3.687E-02
Pax7	ENSMUSG00000028736	78.720	-1.811	1.257E-03
Prelp	ENSMUSG00000041577	87.114	-1.391	5.704E-04
Grhl3	ENSMUSG00000037188	133.830	-1.122	2.793E-04
Cas21	ENSMUSG00000028977	134.182	-0.885	3.666E-02
Gm10524	ENSMUSG00000097141	574.384	-0.842	3.611E-06
Gm42427	ENSMUSG00000105263	206.312	-0.748	1.677E-02
Gm32061	ENSMUSG00000108986	164.534	-0.710	2.102E-02
Cacna1e	ENSMUSG00000004110	573.191	-0.698	1.243E-05
Prmt8	ENSMUSG00000030350	1035.605	-0.597	1.225E-07
Lrrc4	ENSMUSG00000049939	603.380	-0.529	9.051E-02
Zic4	ENSMUSG00000036972	540.856	-0.525	1.228E-02
Chst8	ENSMUSG00000060402	342.681	-0.523	1.396E-02
Laptm4b	ENSMUSG00000022257	4680.463	-0.506	4.397E-05
Prox1	ENSMUSG00000010175	361.913	-0.497	1.211E-02
Trim9	ENSMUSG00000021071	355.924	-0.465	7.871E-02
Apcdd1	ENSMUSG00000071847	2111.707	-0.436	2.888E-05
Cacna1g	ENSMUSG00000020866	3304.459	-0.434	1.077E-03
Tenm2	ENSMUSG00000049336	2481.990	-0.406	7.472E-03
Igfbp5	ENSMUSG00000026185	16175.237	-0.394	1.470E-04
Scube1	ENSMUSG00000016763	1239.890	-0.371	2.541E-02
Igdcc3	ENSMUSG00000032394	2019.079	-0.366	8.595E-02
Sgsm1	ENSMUSG00000042216	815.305	-0.365	9.521E-03
Ptpro	ENSMUSG00000030223	1111.608	-0.363	6.140E-02
1700048O20Rik	ENSMUSG00000043773	562.773	-0.351	4.885E-02
Map3k13	ENSMUSG00000033618	635.452	-0.350	2.801E-02
Rfx2	ENSMUSG00000024206	1358.676	-0.330	6.727E-03
Gm37608	ENSMUSG00000103831	1783.562	-0.322	6.530E-02
Dpysl4	ENSMUSG00000025478	2687.373	-0.313	4.118E-04
Kdm4b	ENSMUSG00000024201	5334.415	-0.312	3.218E-02
Sez6l	ENSMUSG00000058153	2793.075	-0.301	1.063E-02
Cntn2	ENSMUSG00000053024	7212.608	-0.295	7.065E-04
Afap1	ENSMUSG00000029094	2184.820	-0.275	1.655E-03
Lhx9	ENSMUSG00000019230	2635.710	-0.272	8.397E-04
Peak1	ENSMUSG00000074305	1422.946	-0.267	8.224E-02
Hif3a	ENSMUSG00000004328	5718.068	-0.261	4.979E-02
Ddit4	ENSMUSG00000020108	4006.824	-0.261	1.054E-03
Clcn6	ENSMUSG00000029016	5413.591	-0.257	5.363E-04
Celf5	ENSMUSG00000034818	2323.746	-0.254	2.395E-02
Agrn	ENSMUSG00000041936	38779.967	-0.246	3.271E-02
Mdga1	ENSMUSG00000043557	2963.660	-0.246	5.882E-03

Gene name	Gene ID	Base mean	log2 fold	Adj p value
Nova2	ENSMUSG00000030411	3882.623	-0.246	2.663E-03
Gaa	ENSMUSG00000025579	2834.526	-0.239	2.541E-02
Tctn2	ENSMUSG00000029386	1663.336	-0.236	8.288E-02
Map1a	ENSMUSG00000027254	4742.149	-0.229	7.052E-02
Nav1	ENSMUSG00000009418	8672.378	-0.228	3.687E-02
Tstd2	ENSMUSG00000035495	4987.924	-0.225	1.228E-02
Cdh4	ENSMUSG00000000305	3804.511	-0.221	8.021E-02
Amotl2	ENSMUSG00000032531	5476.077	-0.218	2.804E-02
Fam214b	ENSMUSG00000036002	2413.626	-0.217	6.740E-02
Peg3	ENSMUSG00000002265	9573.935	-0.215	2.725E-02
Fezf2	ENSMUSG00000021743	8330.306	-0.205	2.320E-02
Nfatc4	ENSMUSG00000023411	4461.711	-0.201	3.687E-02
Atp13a2	ENSMUSG00000036622	5422.134	-0.196	2.333E-02
Scrt2	ENSMUSG00000060257	3696.498	-0.196	8.021E-02
Igfbpl1	ENSMUSG00000035551	12131.789	-0.181	4.218E-02
Kif1a	ENSMUSG00000014602	21562.101	-0.176	8.288E-02
Ctsb	ENSMUSG00000021939	10453.814	0.157	9.064E-02
Mpped2	ENSMUSG00000016386	18647.222	0.177	2.276E-02
Scrn1	ENSMUSG00000019124	25592.573	0.182	7.871E-02
Hba-a1	ENSMUSG00000069919	71770.272	0.209	8.213E-04
Hba-a2	ENSMUSG00000069917	52800.504	0.240	1.524E-05
Id4	ENSMUSG00000021379	26910.698	0.256	1.188E-02
Ctsd	ENSMUSG00000007891	8217.724	0.265	3.468E-05
Gria2	ENSMUSG00000033981	7760.445	0.294	8.021E-02
Dixdc1	ENSMUSG00000032064	2715.635	0.297	3.428E-03
mt-Rnr2	ENSMUSG00000064339	19296.535	0.367	3.611E-06
Ccng1	ENSMUSG00000020326	2229.070	0.376	1.077E-03
Apoe	ENSMUSG00000002985	1978.419	0.390	1.475E-05
Alad	ENSMUSG00000028393	4398.804	0.391	1.588E-08
Fam46c	ENSMUSG00000044468	1089.975	0.400	6.874E-02
Gsg1l	ENSMUSG00000046182	499.825	0.422	8.885E-02
Sparcl1	ENSMUSG00000029309	1764.208	0.424	5.260E-02
Hspb8	ENSMUSG00000041548	1286.734	0.470	2.804E-02
Polr2k	ENSMUSG00000045996	1226.543	0.477	9.521E-03
Hexb	ENSMUSG00000021665	574.815	0.484	2.581E-04
F13a1	ENSMUSG00000039109	438.686	0.489	2.609E-03
Csf1r	ENSMUSG00000024621	797.314	0.540	6.599E-05
Fcer1g	ENSMUSG00000058715	173.413	0.638	3.404E-02
Ighm	ENSMUSG00000076617	126.966	0.665	8.548E-02
Cfh	ENSMUSG00000026365	213.233	0.689	1.388E-03
Ctss	ENSMUSG00000038642	256.539	0.694	1.188E-02
Cx3cr1	ENSMUSG00000052336	483.858	0.695	2.625E-08
Slc4a11	ENSMUSG00000074796	200.275	0.698	1.932E-02
Hdhd3	ENSMUSG00000038422	344.462	0.702	4.606E-03
C1qa	ENSMUSG00000036887	308.343	0.711	7.928E-05
C3ar1	ENSMUSG00000040552	130.591	0.739	1.677E-02
C1qc	ENSMUSG00000036896	389.965	0.742	2.108E-06
C1qb	ENSMUSG00000036905	473.194	0.750	2.355E-07

Gene name	Gene ID	Base mean	log2 fold	Adj p value
Ly86	ENSMUSG00000021423	109.075	0.793	2.542E-02
Tyrobp	ENSMUSG00000030579	187.317	0.818	8.135E-04
Fcgr3	ENSMUSG00000059498	162.649	0.837	3.532E-04
Adgre1	ENSMUSG00000004730	211.310	0.853	7.377E-06
Lyz2	ENSMUSG00000069516	164.858	0.886	3.796E-04
P2ry13	ENSMUSG00000036362	72.125	0.942	3.666E-02
Cd300a	ENSMUSG00000034652	60.194	0.957	7.171E-02
Aif1	ENSMUSG00000024397	88.894	1.006	2.585E-03
Cd53	ENSMUSG00000040747	76.137	1.011	3.687E-02
Mpeg1	ENSMUSG00000046805	496.818	1.059	2.353E-12
Fcrls	ENSMUSG00000015852	302.335	1.094	1.150E-09
Gm3788	ENSMUSG00000094392	93.529	1.156	1.692E-03
Trpm3	ENSMUSG00000052387	76.375	1.198	7.580E-02
P2ry12	ENSMUSG00000036353	140.913	1.224	2.174E-04
Trem2	ENSMUSG00000023992	106.407	1.262	8.238E-07
Cryba4	ENSMUSG00000066975	30.067	1.665	2.653E-02
Moxd1	ENSMUSG00000020000	18.920	2.008	1.228E-02
Dnah6	ENSMUSG00000052861	23.923	3.090	2.018E-03

Table 3.2: *Pnky* knockout *in vivo* alters transcript splicing.

Significant differentially-spliced events in the E12.5 cortex upon loss of *Pnky* through *Emx1^{Cre}*, from biological triplicate samples. PSI = percent spliced in. Difference in PSI (dPSI) was calculated as $PSI(Pnky\text{-cKO}) - PSI(ctrl)$.

Gene	Event	Type	Ctrl PSI	<i>Pnky</i> -cKO PSI	dPSI
<i>Tcf12</i>	MmuEX0046651	Alt. exon	0.486448	0.419536	-0.066912
<i>Ank3</i>	MmuEX0004933	Alt. exon	0.521069	0.228324	-0.292745
<i>Sft2d1</i>	MmuEX0041972	Alt. exon	0.578115	0.138313	-0.439802
<i>Mapre1</i>	MmuEX0027893	Alt. exon	0.947902	0.456416	-0.491486
<i>Pik3c2b</i>	MmuALTA0013281-1/2	Alt. 3'	0.010564	0.171178	0.160613
<i>Pik3c2b</i>	MmuALTA0013281-2/2	Alt. 3'	0.989261	0.826046	-0.163215
<i>Tmeff1</i>	MmuALTA0018312-1/2	Alt. 3'	0.186722	0.014464	-0.172258
<i>Tmeff1</i>	MmuALTA0018312-2/2	Alt. 3'	0.813897	0.984829	0.170933
<i>Tigd3</i>	MmuALTA0018180-1/2	Alt. 3'	0.568521	0.26813	-0.300391
<i>Pknox1</i>	MmuALTD0010432-1/3	Alt. 5'	0.576768	0.050754	-0.526014
<i>Pknox1</i>	MmuALTD0010432-3/3	Alt. 5'	0.39978	0.848442	0.448662
<i>Wdr12</i>	MmuALTD0015623-1/4	Alt. 5'	0.713615	0.350129	-0.363487
<i>Znfx1</i>	MmuALTD0016352-2/2	Alt. 5'	0.430702	0.800535	0.369833

Table 3.3: BAC^{Pnky} rescues transcript abundance changes in Pnky-KO cNSCs.

Significant differentially-expressed genes in cNSC cultures upon loss of *Pnky* from *Pnky*^{F/F} +Ad:Cre samples relative to *Pnky*^{+/+} +Ad:Cre samples. Biological triplicate samples were used, and statistical analysis was performed incorporating pairing of each biological sample treated with Ad:Cre to its own untreated control. The threshold for statistical significance was set as an adjusted p value of 0.1 or lower.

Gene name	Base mean	log2 fold	Adj p	Chr	Rescue	Pnky(F/F);BAC vs Pnky(F/F)	
						log2 fold	Adj p value
Pakap	72.1605	-8.2753	9.097E-02	4	TRUE	3.790035	NS
Gm30731 (Pnky)	212.9631	-5.9516	3.405E-12	4	TRUE	3.690448	1.464E-05
Rdh16f1	73.5835	-5.8044	2.140E-03	10	TRUE	5.863822	4.208E-03
Gm28048	167.8959	-1.9319	6.027E-04	11	TRUE	1.357093	7.121E-02
Trim16	501.1538	-0.7199	9.097E-02	11	TRUE	0.522363	NS
Dusp4	2893.5979	-0.5524	6.765E-05	8	TRUE	0.638384	5.127E-06
Fzd5	1431.3498	-0.5244	6.275E-02	1	TRUE	0.520710	4.781E-02
Gpnmb	1594.0437	-0.5165	2.018E-02	6	TRUE	0.453949	5.605E-02
Prr14l	4899.3839	-0.4534	1.528E-02	5	TRUE	0.130605	NS
Rassf3	2172.9505	-0.4389	9.097E-02	10	TRUE	0.433017	7.534E-02
Fgfr2	4996.9537	-0.4379	2.964E-02	7	TRUE	0.357932	NS
Sik1	1635.6897	-0.4371	9.921E-02	17	TRUE	0.663603	3.554E-04
Itpr1	2468.0757	-0.4296	2.272E-02	6	TRUE	0.378461	6.438E-02
Klhdc8b	3346.9800	-0.4263	9.460E-02	9	TRUE	0.245373	NS
Aph1b	4707.0825	-0.4109	1.549E-03	9	F	0.091947	NS
Spry4	4321.5621	-0.3910	9.097E-02	18	TRUE	0.390154	6.832E-02
Cybrd1	6715.3517	-0.3854	1.735E-02	2	TRUE	0.171469	NS
Pdxk	8259.2391	-0.3576	2.018E-02	10	TRUE	0.511716	3.251E-05
Selenoi	4657.4214	-0.3520	2.018E-02	5	F	-0.064260	NS
Pou3f2	3740.5123	-0.3434	2.964E-02	4	TRUE	0.124324	NS
Rnft1	3886.8998	-0.3391	2.734E-02	11	TRUE	0.213439	NS
Ephb2	4468.1146	-0.3320	7.367E-02	4	TRUE	0.347450	3.751E-02
Hmox1	3505.7299	-0.3253	9.921E-02	8	TRUE	0.428644	3.990E-03
Angpt2	6319.5063	-0.3178	7.367E-02	8	TRUE	0.666246	4.002E-09
Anxa5	3418.8983	-0.3143	8.426E-02	3	TRUE	0.231670	NS
Tbc1d1	7681.4311	-0.3111	9.255E-02	5	TRUE	0.228851	NS
Epb4111	4274.4480	-0.3099	8.432E-02	2	TRUE	0.188056	NS
Slc35c2	5629.8848	-0.3096	9.255E-02	2	TRUE	0.224309	NS
Slc48a1	14156.6291	-0.2545	2.006E-02	15	TRUE	0.243985	2.634E-02
Sox10	8497.6741	0.2731	7.465E-02	15	TRUE	-0.591959	1.140E-09
Tnk2	15824.5831	0.2839	9.097E-02	16	TRUE	-0.357518	5.917E-03
Ppp1r7	4286.1507	0.3157	1.771E-02	1	F	-0.052014	NS
Tnr	47494.5257	0.3363	4.276E-02	1	TRUE	-0.559288	3.239E-06
3110035E14Rik	5513.6393	0.3365	8.426E-02	1	TRUE	-0.743845	5.849E-10
Nnat	31465.1338	0.3385	6.539E-02	2	TRUE	-0.611325	8.910E-07
Amotl2	4608.9040	0.3393	1.771E-02	9	TRUE	-0.675906	1.069E-10
Slc1a1	4964.3920	0.3491	6.275E-02	19	TRUE	-0.720722	3.271E-09
Tmem132b	8055.7886	0.3516	4.276E-02	5	TRUE	-0.522518	6.804E-05
Ece1	9422.1161	0.3597	9.921E-02	4	F	0.074534	NS
5730559C18Rik	2523.3077	0.3850	6.125E-02	1	TRUE	-0.731332	8.727E-08
Zfp423	2443.9575	0.3859	4.981E-02	8	F	0.000765	NS
Gm44645	2385.1453	0.3927	4.370E-02	7	TRUE	-0.497762	1.694E-03
Nrbp2	2551.6618	0.4011	5.369E-02	15	TRUE	-0.117353	NS
1810041L15Rik	2740.2447	0.4026	2.964E-02	15	TRUE	-0.835411	1.476E-10

Gene name	Base mean	log2 fold	Adj p	Chr	Rescue	<u>Pnky(F/F);BAC vs Pnky(F/F)</u>	
						log2 fold	Adj p value
Plxnb3	2487.6676	0.4047	5.838E-02	X	TRUE	-0.820751	4.151E-09
Unc79	2466.5036	0.4151	5.913E-03	12	F	-0.044978	NS
Prkcq	4839.8432	0.4393	7.836E-04	2	TRUE	-0.902493	8.099E-13
Sh3bp4	9318.1982	0.4785	5.686E-05	1	TRUE	-0.859595	8.099E-13
ErbB4	3109.8488	0.4904	1.010E-02	1	TRUE	-0.664238	3.251E-05
Miat	11769.7388	0.5821	1.901E-07	5	TRUE	-0.917292	8.099E-13
Myrf	4449.8380	0.6529	6.027E-04	19	TRUE	-0.613494	2.721E-03
Snx22	1171.7958	0.6836	1.667E-02	9	TRUE	-0.671267	1.575E-02
Bcas1	14026.7671	0.7284	6.977E-08	2	TRUE	-0.797640	2.537E-08
9630013A20Rik	453.2918	0.7719	7.317E-02	14	TRUE	-0.746261	6.759E-02
Gfap	5318.8898	0.9084	2.448E-07	11	F	-0.449695	NS
A330093E20Rik	89.1163	1.4833	6.539E-02	18	F	-0.091809	NS

Table 3.4: Altered splicing in *Pnky*-KO cNSCs overlaps PTBP1-regulated events.

Significant differentially-spliced events in cNSC cultures upon loss of *Pnky* from *Pnky*^{F/F} +Ad:Cre samples relative to untreated controls. Events that also occurred in *Pnky*^{+/+} +Ad:Cre samples relative to untreated controls were removed. PSI = percent spliced in. Difference in PSI (dPSI) was calculated as PSI(*Pnky*-cKO) – PSI(ctrl). dPSI values from re-analysis of previous PTBP1-KD experiments (Raj et al., 2014; Ramos et al., 2015) are also included.

Gene	Event	Type	PSI		dPSI	Rescue	dPSI PTBP1-KD	
			Ctrl	<i>Pnky</i> -cKO			SVZ (Ramos)	N2a (Raj)
4632411B12Rik	MmuINT0003388	IR	0.385166	0.687769	0.3026	TRUE	0.305042	0.504216
Magi3	MmuEX0027566	S	0.451254	0.730043	0.2788	F	0.215939	0.261016
Magi1	MmuEX0027544	S	0.050226	0.310762	0.2605	F	0.489215	0.224481
4632411B12Rik	MmuEX0001341	S	0.667823	0.894965	0.2271	F	0.426991	0.626542
Slc12a7	MmuEX0042595	MIC	0.105611	0.303352	0.1977	F	0.447714	0.34434
Itga6	MmuEX0024617	S	0.479366	0.65432	0.1750	F	0.172461	0.276208
Trnk2	MmuEX0048311	S	0.331623	0.500548	0.1689	F	0.466341	0.488407
Gse1	MmuEX0022002	S	0.712154	0.873152	0.1610	F	-0.208138	-0.493055
Sorbs1	MmuEX0044361	C2	0.166832	0.319521	0.1527	F	0.249938	0.38287
Arhgap12	MmuEX0005791	S	0.481946	0.613606	0.1317	F	0.119965	0.147308
Exoc7	MmuEX0017604	C1	0.07555	0.205484	0.1299	F	0.274541	0.467833
Dclk2	MmuEX0013903	S	0.269212	0.378386	0.1092	F	0.209555	0.126373
Pbx1	MmuEX0033850	S	0.27234	0.326462	0.0541	F	0.190801	0.171952
Arhgap39	MmuEX0005870	S	0.469588	0.768395	0.2988	F	-0.2221	NA
Nrxn1	MmuEX0032375	MIC	0.2402	0.43109	0.1909	F	0.180689	NA
Nav2	MmuEX0030958	C3	0.123677	0.269392	0.1457	F	0.233562	NA
Prrc2b	MmuEX0037403	S	0.514688	0.649359	0.1347	F	0.184	NA
Ptprz1	MmuINT0129632	IR	0.344003	0.462708	0.1187	F	-0.085943	NA
Acss2	MmuEX0003610	S	0.087117	0.131175	0.0441	F	0.297999	NA
Prepl	MmuEX0037022	S	0.490981	0.335391	-0.1556	F	-0.177151	NA
Slc9a5	MmuEX0043616	S	0.95531	0.761021	-0.1943	F	0.340132	NA
Braf	MmuEX0008162	S	0.753816	0.530338	-0.2235	F	0.358507	NA
Ddx26b	MmuINT0047668	IR	0.510914	0.848756	0.3378	F	NA	-0.217894
Magi1	MmuEX0027548	S	0.58168	0.882637	0.3010	F	NA	0.159087
Atp2b4	MmuEX0006835	S	0.390962	0.685637	0.2947	F	NA	-0.55525
Ddx26b	MmuEX0014076	S	0.419292	0.711335	0.2920	F	NA	-0.164908
Sun1	MmuEX0045737	C3	0.576065	0.829316	0.2533	TRUE	NA	-0.13526
Zfp692-ps	MmuINT0179730	IR	0.443346	0.693001	0.2497	F	NA	-0.161421
Gabbr1	MmuINT0066904	IR	0.356135	0.560321	0.2042	F	NA	-0.203036
Crtc1	MmuEX0012788	C1	0.625839	0.827396	0.2016	F	NA	-0.181283
Zcchc2	MmuEX0052809	S	0.256485	0.453192	0.1967	F	NA	-0.153172
Bcl9l	MmuEX0007868	C2	0.313227	0.500196	0.1870	F	NA	-0.292843
AU019823	MmuEX0002794	S	0.317464	0.494672	0.1772	F	NA	0.208715
Arhgef40	MmuALTA0001991-2/2	Alt3	0.081324	0.241718	0.1604	TRUE	NA	0.155785
D19Wsu162e	MmuEX0013522	S	0.18717	0.346409	0.1592	TRUE	NA	-0.171179
Camk2g	MmuEX0008985	C2	0.543464	0.69709	0.1536	F	NA	0.191518
Tbc1d9b	MmuEX0046525	C1	0.760261	0.905178	0.1449	F	NA	0.175872
Neb1	MmuEX0031352	C3	0.126538	0.257081	0.1305	F	NA	0.227905
E130112L23Rik	MmuINT0054563	IR	0.08895	0.21941	0.1305	F	NA	0.182164
Prrc2b	MmuEX0037404	S	0.583669	0.707205	0.1235	F	NA	0.131838
Bcas1	MmuEX0007795	C3	0.7533	0.861707	0.1084	F	NA	-0.181176
Tef	MmuINT0158813	IR	0.143929	0.239619	0.0957	F	NA	-0.126609
Bcas1	MmuEX0007792	C2	0.815517	0.890328	0.0748	F	NA	-0.176812
Tra2a	MmuEX0048668	S	0.330394	0.182946	-0.1474	F	NA	0.115329
Mfn1	MmuINT0098176	IR	0.309877	0.153013	-0.1569	F	NA	0.135366
Slc25a27	MmuEX0042882	S	0.910505	0.710975	-0.1995	TRUE	NA	-0.291824
Rbm15	MmuINT0132595	IR	0.816931	0.551683	-0.2652	F	NA	-0.14303
Ccl25	MmuALTD0002742-1/2	Alt5	0.394666	0.852694	0.4580	TRUE	NA	NA
Plec	MmuEX0035674	S	0.409832	0.828146	0.4183	F	NA	NA
Rhbdl3	MmuEX0039713	C1	0.322502	0.72256	0.4001	F	NA	NA
Gm16862	MmuEX0021009	C1	0.308026	0.707464	0.3994	TRUE	NA	NA
2210403K04Rik	MmuINT0002008	IR	0.318831	0.671328	0.3525	F	NA	NA
Mttnr1	MmuEX0030051	C2	0.466375	0.802214	0.3358	F	NA	NA

Gene	Event	Type	PSI		dPSI	Rescue	dPSI PTBP1-KD	
			Ctrl	<i>Pnky</i> -cKO			SVZ (Ramos)	N2a (Raj)
Atm	MmuEX0006713	S	0.581345	0.887676	0.3063	F	NA	NA
Triobp	MmuEX0048976	C1	0.342237	0.639831	0.2976	F	NA	NA
4932438A13Rik	MmuALTA0000546-2/2	Alt3	0.366196	0.645288	0.2791	F	NA	NA
Brca1	MmuEX0008173	C2	0.134532	0.412352	0.2778	F	NA	NA
Adamts9	MmuEX0003885	S	0.32475	0.595379	0.2706	TRUE	NA	NA
E2f6	MmuEX0016112	C1	0.214755	0.471539	0.2568	F	NA	NA
Snx11	MmuEX0044216	S	0.271734	0.521868	0.2501	F	NA	NA
Gpcpd1	MmuEX0021570	S	0.408843	0.658809	0.2500	F	NA	NA
Cenpp	MmuEX0010853	S	0.694477	0.943256	0.2488	F	NA	NA
Itpr2	MmuEX0024744	S	0.696097	0.941091	0.2450	F	NA	NA
Csmd2	MmuEX0012905	C2	0.52726	0.769193	0.2419	F	NA	NA
Nelf	MmuINT0107693	IR	0.290961	0.523604	0.2326	F	NA	NA
Polk	MmuEX0036247	S	0.694468	0.923109	0.2286	F	NA	NA
Tor1aip2	MmuEX0048534	C1	0.211896	0.434362	0.2225	F	NA	NA
Fam135a	MmuEX0017953	C2	0.597295	0.819665	0.2224	F	NA	NA
6030446N20Rik	MmuEX0002114	S	0.693155	0.911869	0.2187	F	NA	NA
Cd97	MmuEX0010283	C3	0.178527	0.396355	0.2178	F	NA	NA
Cdk5rap2	MmuEX0010608	C2	0.70475	0.921675	0.2169	F	NA	NA
Cyp4f15	MmuEX0013398	C3	0.482933	0.699454	0.2165	F	NA	NA
Lrrc40	MmuEX0026996	S	0.625858	0.842198	0.2163	F	NA	NA
Cdk5rap2	MmuEX0010609	C1	0.672805	0.887633	0.2148	F	NA	NA
Sept6	MmuALTD0012613-2/2	Alt5	0.546954	0.761718	0.2148	F	NA	NA
Prmt1	MmuALTD0011032-2/2	Alt5	0.100183	0.30957	0.2094	F	NA	NA
Cyp4f15	MmuINT0045386	IR	0.166983	0.37615	0.2092	TRUE	NA	NA
Slx4	MmuEX0043742	S	0.567372	0.775945	0.2086	F	NA	NA
Cyp4f15	MmuEX0013399	S	0.59203	0.800134	0.2081	F	NA	NA
Cnot1	MmuALTD0003348-3/3	Alt5	0.197471	0.405006	0.2075	TRUE	NA	NA
Tnc	MmuEX0048242	C2	0.569992	0.777131	0.2071	F	NA	NA
Csmd2	MmuEX0012909	C3	0.648334	0.85325	0.2049	TRUE	NA	NA
Sergef	MmuEX0041748	S	0.729231	0.931856	0.2026	F	NA	NA
Abca3	MmuEX0002974	S	0.642429	0.843656	0.2012	F	NA	NA
Flii	MmuALTA0007276-2/2	Alt3	0.565016	0.759842	0.1948	F	NA	NA
BC034090	MmuEX0007465	S	0.681819	0.876271	0.1945	F	NA	NA
Rufy2	MmuEX0040750	S	0.774552	0.968208	0.1937	TRUE	NA	NA
Tns1	MmuEX0048416	C3	0.553617	0.745611	0.1920	F	NA	NA
Elf2	MmuALTA0006312-1/2	Alt3	0.514305	0.70529	0.1910	F	NA	NA
Flywch1	MmuEX0019365	S	0.188717	0.379649	0.1909	F	NA	NA
Unk	MmuALTD0015291-2/3	Alt5	0.550776	0.740887	0.1901	F	NA	NA
Mbp	MmuEX0028128	C3	0.106565	0.292964	0.1864	F	NA	NA
G2e3	MmuEX0019838	S	0.685097	0.868176	0.1831	F	NA	NA
Fam45a	MmuEX0018317	S	0.561348	0.744362	0.1830	F	NA	NA
Tnc	MmuEX0048241	C1	0.388984	0.571834	0.1829	F	NA	NA
Clk4	MmuEX0011727	C1	0.127482	0.307656	0.1802	F	NA	NA
Dlgap4	MmuINT0050037	IR	0.081756	0.261829	0.1801	F	NA	NA
Ralgds	MmuALTA0014810-2/2	Alt3	0.411809	0.591241	0.1794	F	NA	NA
Apobec1	MmuEX0005576	C1	0.552429	0.72973	0.1773	F	NA	NA
Ep400	MmuEX0016972	S	0.610194	0.784102	0.1739	TRUE	NA	NA
Plp1	MmuALTD0010553-1/2	Alt5	0.378063	0.551899	0.1738	F	NA	NA
Mapk8ip3	MmuALTD0008197-2/2	Alt5	0.503531	0.674698	0.1712	F	NA	NA
D4Ertid22e	MmuEX0013584	S	0.372786	0.542442	0.1697	F	NA	NA
Trmt1	MmuINT0165615	IR	0.300458	0.469156	0.1687	F	NA	NA
Tns1	MmuEX0048418	C3	0.625307	0.792998	0.1677	F	NA	NA
Dst	MmuEX0015748	C2	0.295038	0.459628	0.1646	F	NA	NA
Cyp4f15	MmuEX0013400	C1	0.709812	0.874228	0.1644	F	NA	NA
Golga1	MmuEX0021409	S	0.790339	0.950597	0.1603	F	NA	NA
Phf21a	MmuEX0034760	S	0.547029	0.706705	0.1597	F	NA	NA
Pknox2	MmuEX0035447	S	0.66581	0.825438	0.1596	TRUE	NA	NA
Ubr3	MmuALTD0015182-2/2	Alt5	0.107032	0.262912	0.1559	F	NA	NA
Gbp1	MmuEX0021556	S	0.326007	0.481055	0.1550	F	NA	NA
Cep78	MmuEX0011029	S	0.706308	0.860217	0.1539	F	NA	NA
Acbd5	MmuALTA0001011-2/2	Alt3	0.431229	0.579808	0.1486	F	NA	NA
Fgfr3	MmuEX0019167	S	0.677273	0.825297	0.1480	F	NA	NA

Gene	Event	Type	PSI		dPSI	Rescue	dPSI PTBP1-KD	
			Ctrl	Pnky-cKO			SVZ (Ramos)	N2a (Raj)
Dlg4	MmuALTA0005545-3/3	Alt3	0.698296	0.84495	0.1467	F	NA	NA
Msl1	MmulNT0101257	IR	0.135295	0.280258	0.1450	F	NA	NA
Mxra7	MmuEX0030256	S	0.224846	0.369621	0.1448	F	NA	NA
Ndufb2	MmuALTD0009246-1/2	Alt5	0.590494	0.734159	0.1437	F	NA	NA
Fuz	MmuEX0019772	S	0.771361	0.914324	0.1430	F	NA	NA
Nlgn3	MmuEX0031825	C1	0.452579	0.594279	0.1417	F	NA	NA
Trip12	MmuEX0048991	S	0.113273	0.253728	0.1405	F	NA	NA
Zfp106	MmuEX0053021	C1	0.736306	0.87657	0.1403	F	NA	NA
Gsg1l	MmuEX0022005	S	0.532474	0.67259	0.1401	F	NA	NA
Gnb1	MmuEX0021329	S	0.495403	0.635035	0.1396	F	NA	NA
Atp6v0a1	MmuEX0006886	C2	0.790787	0.925992	0.1352	F	NA	NA
Sfswap	MmuALTD0012721-1/2	Alt5	0.079981	0.213014	0.1330	F	NA	NA
Nabl	MmuEX0031351	C3	0.121641	0.25429	0.1326	F	NA	NA
Tnc	MmuEX0048237	C2	0.627197	0.758078	0.1309	F	NA	NA
2310008H04Rik	MmuEX0000869	S	0.832988	0.96269	0.1297	F	NA	NA
Tnc	MmuEX0048238	C3	0.644297	0.773844	0.1295	F	NA	NA
Agfg1	MmuEX0004229	S	0.782742	0.911757	0.1290	F	NA	NA
Mbd3	MmuALTA0010624-1/2	Alt3	0.79111	0.91869	0.1276	F	NA	NA
Cnot1	MmulNT0038107	IR	0.109633	0.23628	0.1266	F	NA	NA
Ralgapa1	MmuEX0038609	S	0.03757	0.163493	0.1259	F	NA	NA
Bmpr2	MmuALTA0002803-2/2	Alt3	0.739772	0.862793	0.1230	F	NA	NA
Phf1	MmuEX0034916	S	0.832516	0.954869	0.1224	F	NA	NA
Ank2	MmuEX0004904	C2	0.633834	0.755222	0.1214	F	NA	NA
Kif1a	MmuEX0025487	C3	0.151075	0.271756	0.1207	F	NA	NA
Tusc3	MmuEX0049949	S	0.708206	0.825854	0.1176	F	NA	NA
Tnc	MmuEX0048239	C3	0.666541	0.783619	0.1171	F	NA	NA
Lsamp	MmuEX0027189	C1	0.075176	0.187087	0.1119	F	NA	NA
Bcas1	MmuEX0007794	C2	0.772479	0.88197	0.1095	F	NA	NA
Puf60	MmuEX0038025	S	0.134693	0.241048	0.1064	F	NA	NA
Carkd	MmuEX0009178	S	0.751775	0.857111	0.1053	F	NA	NA
Aldh1l1	MmuALTD0001193-2/2	Alt5	0.34713	0.447359	0.1002	F	NA	NA
Dnajc7	MmulNT0051651	IR	0.136362	0.231392	0.0950	F	NA	NA
Jmjd6	MmulNT0085017	IR	0.122452	0.212269	0.0898	F	NA	NA
Tcf4	MmuALTD0014098-1/2	Alt5	0.378026	0.463581	0.0856	F	NA	NA
Anapc5	MmuALTA0001553-2/4	Alt3	0.455057	0.537875	0.0828	F	NA	NA
Ncam1	MmuEX0031043	MIC	0.711448	0.794009	0.0826	F	NA	NA
Rbm39	MmuEX0039150	S	0.089391	0.171189	0.0818	F	NA	NA
Hif1a	MmuALTA0008598-1/3	Alt3	0.142147	0.210521	0.0684	F	NA	NA
Nrxn1	MmuALTD0009572-2/2	Alt5	0.455093	0.519973	0.0649	F	NA	NA
Lhx2	MmuALTA0010033-1/2	Alt3	0.859844	0.92227	0.0624	F	NA	NA
Ncam1	MmuEX0031041	S	0.093661	0.150055	0.0564	F	NA	NA
Aif1l	MmuEX0004409	C2	0.879507	0.933673	0.0542	F	NA	NA
Papss1	MmuEX0033619	S	0.24543	0.298201	0.0528	F	NA	NA
Pcbp2	MmuALTA0012810-1/2	Alt3	0.42439	0.475852	0.0515	F	NA	NA
Sf1	MmuEX0041897	S	0.945154	0.880569	-0.0646	F	NA	NA
Ppp6r3	MmuEX0036871	S	0.595275	0.526732	-0.0685	F	NA	NA
Slc25a3	MmulNT0145616	IR	0.224075	0.138974	-0.0851	F	NA	NA
Azin1	MmuEX0007181	S	0.221312	0.121864	-0.0994	F	NA	NA
Aldh1l1	MmuALTD0001193-1/2	Alt5	0.653357	0.553078	-0.1003	F	NA	NA
Bmpr2	MmuALTA0002803-1/2	Alt3	0.258524	0.139167	-0.1194	F	NA	NA
0610011L14Rik	MmuEX0000055	S	0.20017	0.072347	-0.1278	F	NA	NA
Rbm5	MmulNT0132891	IR	0.62253	0.49208	-0.1305	TRUE	NA	NA
Uhrf2	MmuEX0050520	S	0.949273	0.815976	-0.1333	F	NA	NA
Ap3d1	MmuEX0005451	S	0.197983	0.062268	-0.1357	F	NA	NA
Dlg4	MmuALTA0005545-1/3	Alt3	0.291272	0.151029	-0.1402	F	NA	NA
Ndufb2	MmuALTD0009246-2/2	Alt5	0.407905	0.261738	-0.1462	F	NA	NA
Tia1	MmulNT0160065	IR	0.48905	0.339171	-0.1499	TRUE	NA	NA
Acbd5	MmuALTA0001011-1/2	Alt3	0.567567	0.417537	-0.1500	F	NA	NA
Dmpk	MmulNT0050325	IR	0.273801	0.119949	-0.1539	F	NA	NA
Irf3	MmulNT0083308	IR	0.364673	0.206406	-0.1583	F	NA	NA
Pdzd11	MmuALTD0010148-2/3	Alt5	0.688864	0.528532	-0.1603	F	NA	NA
Arhgef40	MmuALTA0001991-1/2	Alt3	0.918542	0.754981	-0.1636	TRUE	NA	NA

Gene	Event	Type	PSI		dPSI	Rescue	dPSI PTBP1-KD	
			Ctrl	<i>Pnky</i> -cKO			SVZ (Ramos)	N2a (Raj)
Phf20l1	MmuINT0118816	IR	0.333998	0.167771	-0.1662	F	NA	NA
Ccdc97	MmuEX0010001	C1	0.290562	0.123723	-0.1668	F	NA	NA
Sema6a	MmuEX0041633	S	0.675069	0.505438	-0.1696	F	NA	NA
Gmn	MmuALTD0006077-3/4	Alt5	0.29762	0.126503	-0.1711	F	NA	NA
Zfp740	MmuEX0053595	S	0.447018	0.274663	-0.1724	F	NA	NA
Plpn11	MmuALTA0014494-1/2	Alt3	0.811927	0.639477	-0.1725	F	NA	NA
Ralgds	MmuALTA0014810-1/2	Alt3	0.586903	0.410327	-0.1766	F	NA	NA
Plp1	MmuALTD0010553-2/2	Alt5	0.629666	0.452985	-0.1767	F	NA	NA
Rpsud1	MmuEX0040553	S	0.952977	0.774952	-0.1780	F	NA	NA
Mapk8ip3	MmuALTD0008197-1/2	Alt5	0.500811	0.320902	-0.1799	F	NA	NA
Sept8	MmuALTA0016147-3/3	Alt3	0.574427	0.393713	-0.1807	F	NA	NA
Zfp369	MmuINT0179102	IR	0.494675	0.310852	-0.1838	TRUE	NA	NA
Unk	MmuALTD0015291-1/3	Alt5	0.435683	0.251706	-0.1840	F	NA	NA
Acbd4	MmuEX0003417	S	0.974693	0.790321	-0.1844	F	NA	NA
Epc2	MmuEX0017058	S	0.881081	0.694898	-0.1862	F	NA	NA
Thbs3	MmuINT0159733	IR	0.729132	0.542061	-0.1871	F	NA	NA
Prdm5	MmuEX0036988	C2	0.935072	0.746052	-0.1890	F	NA	NA
Flii	MmuALTA0007276-1/2	Alt3	0.434791	0.242905	-0.1919	F	NA	NA
Eif2	MmuALTA0006312-2/2	Alt3	0.489811	0.297747	-0.1921	F	NA	NA
Psip1	MmuALTA0014336-6/7	Alt3	0.448715	0.255654	-0.1931	F	NA	NA
Atf2	MmuEX0006584	C2	0.727928	0.519908	-0.2080	TRUE	NA	NA
3110082J24Rik	MmuEX0001318	C2	0.616249	0.405345	-0.2109	F	NA	NA
Bptf	MmuEX0008154	C2	0.513193	0.301784	-0.2114	F	NA	NA
Ppp1r12a	MmuEX0036680	C1	0.91743	0.706017	-0.2114	F	NA	NA
Ubp1	MmuEX0050295	S	0.735824	0.52359	-0.2122	F	NA	NA
Eps15	MmuINT0058416	IR	0.303191	0.088493	-0.2147	F	NA	NA
Cnot1	MmuALTD0003348-2/3	Alt5	0.799946	0.584331	-0.2156	TRUE	NA	NA
Sept6	MmuALTD0012613-1/2	Alt5	0.456038	0.239696	-0.2163	F	NA	NA
Mapre3	MmuALTD0008207-2/2	Alt5	0.62424	0.402733	-0.2215	F	NA	NA
Rsrc2	MmuINT0137658	IR	0.50335	0.281118	-0.2222	F	NA	NA
Pion	MmuINT0120077	IR	0.686996	0.457965	-0.2290	F	NA	NA
Vcan	MmuINT0172769	IR	0.470954	0.237299	-0.2337	F	NA	NA
3110039M20Rik	MmuINT0003230	IR	0.44656	0.2099	-0.2367	F	NA	NA
Ccl25	MmuEX0010020	C1	0.712955	0.460916	-0.2520	TRUE	NA	NA
2410004B18Rik	MmuEX0000998	S	0.548076	0.293821	-0.2543	F	NA	NA
Zdhhc4	MmuEX0052936	S	0.510341	0.240117	-0.2702	F	NA	NA
4932438A13Rik	MmuALTA0000546-1/2	Alt3	0.632839	0.362048	-0.2708	F	NA	NA
2310035C23Rik	MmuEX0000913	C1	0.470064	0.183335	-0.2867	F	NA	NA
6720401G13Rik	MmuINT0005770	IR	0.638107	0.333282	-0.3048	F	NA	NA
Ccdc85a	MmuEX0009949	C2	0.865326	0.557119	-0.3082	F	NA	NA
Dmpk	MmuINT0050316	IR	0.47811	0.155384	-0.3227	F	NA	NA
Mtf2	MmuEX0029976	C3	0.736313	0.30725	-0.4291	F	NA	NA
Ccl25	MmuALTD0002742-2/2	Alt5	0.608609	0.155552	-0.4531	TRUE	NA	NA

Experimental Procedures

Key Resources Table

REAGENT or RESOURCE	SOURCE	IDENTIFIER
Antibodies		
Anti-Tubulin β 3 (Tuj1)	Biologend	Cat. # 801201
Anti-POU3F2	Cell Signaling Technology	Cat. # 12137
Anti-CTIP2	Abcam	Cat. # ab18465
Anti-phospho-histone H3 (pH3)	Millipore Sigma	Cat. # 06570
Anti-phosphorylated vimentin (pVim)	MBL	Cat. # D076-3
Anti-CUX1	Santa Cruz	Cat. # sc-13024
Anti-BrdU	Abcam	Cat. # ab6326
Anti-tdTomato	Takara	Cat. # 632496
Anti-tdTomato	Sicgen	Cat. # AB8181-200
Anti-PTBP1	ThermoFisher	Cat. # 32-4800
Bacterial and Virus Strains		
Ad:Cre	Alvarez-Buylla Lab	Merkle et al., 2007
Chemicals, Peptides, and Recombinant Proteins		
4-Hydroxytamoxifen (4-OHT)	Millipore Sigma	Cat. # H7904
5-Bromo-2'-deoxyuridine (BrdU)	Millipore Sigma	Cat. # B5002
Critical Commercial Assays		
RNAscope 2.5 HD Assay — BROWN	Advanced Cell Diagnostics	Cat. # 322300
RNAscope Probe-Mm-Pnky	Advanced Cell Diagnostics	Cat. # 405551
Deposited Data		
RNA-seq: <i>Emx1</i> -Cre cortex and cNSC cultures	This work	GEO: GSE127987
Experimental Models: Organisms/Strains		
Mouse: wild-type: C57BL/6J	The Jackson Laboratory	MGI: 3028467
Mouse: UBC-Cre-ERT2: Ndor1 ^{Tg(UBC-cre/ERT2)1Ejb}	The Jackson Laboratory	Ruzankina et al., 2007
Mouse: <i>Emx1</i> ^{Cre} ; <i>Emx1</i> ^{tm1(cre)Kvj}	The Jackson Laboratory	Gorski et al., 2002
Mouse: Ai14: Gt(ROSA)26Sor ^{tm14(CAG-tdTomato)Hze}	The Jackson Laboratory	Madisen et al., 2010
Mouse: E2a-Cre: Tg(Ella-cre)C5379Lmgd	The Jackson Laboratory	Lakso et al., 1996
Mouse: <i>Pnky</i> ^F	This work	N/A
Mouse: <i>Pnky</i> ^{null}	This work	N/A
Mouse: BAC ^{<i>Pnky</i>}	This work	N/A
Oligonucleotides		
qPCR: <i>Rplp0</i> F: CCGATCTGCAGACACACT	Ramos et al., 2013	N/A
qPCR: <i>Rplp0</i> R: ACCCTGAAGTGCTCGACATC	Ramos et al., 2013	N/A
qPCR: <i>Pnky</i> F: TCTCCTTTCTCCGCCAGTAA	Ramos et al., 2015	N/A
qPCR: <i>Pnky</i> R: CACCGCTTCTTGTCAGTTCA	Ramos et al., 2015	N/A
qPCR: <i>Pou3f2</i> F: ATGTGCAAGCTGAAGCCTTT	Bonvin et al., 2012	N/A
qPCR: <i>Pou3f2</i> R: CTCACCACCTCCTTCTCCAG	Bonvin et al., 2012	N/A
qPCR: <i>U1</i> F: ACGAAGGTGGTTTTCCCAG	Ramos et al., 2015	N/A
qPCR: <i>U1</i> R: GTCCCCACTACCACAAA	Ramos et al., 2015	N/A
qPCR: β -actin F: CTAAGCCAACCGTGAAAAG	Ramos et al., 2015	N/A
qPCR: β -actin R: ACCAGAGGCATACAGGGACA	Ramos et al., 2015	N/A

Recombinant DNA		
BAC containing the mouse <i>Pnky</i> locus	BACPAC Resources Center	Clone RP23-45116
Software and Algorithms		
Hisat2 v2.1.0	Kim et al., 2015	https://ccb.jhu.edu/software/hisat2/index.shtml
DESeq2	Love et al., 2014	https://bioconductor.org/packages/release/bioc/html/DESeq2.html
fdrtool	Strimmer, 2008	https://CRAN.R-project.org/package=fdrtool
Homer findMotifs.pl	Heinz et al., 2010	http://homer.ucsd.edu/homer/motif/
VAST-TOOLS v.1.0; VAST-TOOLS diff module	Braunschweig et al., 2014; Irimia et al., 2014; Han et al., 2017	https://github.com/vastgroup/vast-tools
Kallisto v0.43.1	Bray et al., 2016	https://github.com/pachterlab/kallisto/releases
Fiji / ImageJ	Schindelin et al., 2012	https://fiji.sc
Prism 7	GraphPad Software	N/A
Adobe Photoshop	Adobe Systems Inc.	N/A
Adobe Illustrator	Adobe Systems Inc.	N/A

Mus musculus

All mice were group-housed and maintained in the University of California, San Francisco Laboratory Animal Resource Center under protocols approved by the Institutional Animal Care and Use Committee. All relevant ethical regulations were followed. Mice of both sexes were used for all experiments, and were analyzed at multiple ages between E10.0 and P14 as described in the text and figure legends for each experiment. All samples were analyzed relative to littermates. For *Emx1^{Cre}* experiments, control samples were *Pnky^{+/+};Emx1^{Cre}* or any combination of *Pnky* alleles in the absence of *Emx1^{Cre}*. Details regarding mouse strains are as follows (see also Key Resources Table):

UBC-Cre-ERT2: Tg(UBC-cre/ERT2)1Ejb, described in (Ruzankina et al., 2007).

Emx1^{Cre}: *Emx1^{tm1(cre)Kvj}*, described in (Gorski et al., 2002).

Ai14: Gt(ROSA)26Sor^{tm14(CAG-tdTomato)Hze}, described in (Madisen et al., 2010).

E2a-Cre: Tg(Ella-cre)C5379Lmgd, described in (Lakso et al., 1996).

Generation of the *Pnky* conditional (*Pnky*^F) mouse line

A conditional allele of *Pnky* was created by inGenious Targeting Laboratory through homologous recombination in C57BL/6 x 129/SvEv hybrid embryonic stem (ES) cells. The targeting construct contained a Neomycin resistance cassette to enable drug selection of recombined cells. Targeted ES cells were microinjected into C57BL/6 blastocysts. Resulting chimeras with a high percentage agouti coat color were mated to C57BL/6 FLP mice to remove the Neomycin resistance cassette. The resulting *Pnky*^F allele has the entire *Pnky* gene flanked by loxP sites, with one loxP site 727 bp upstream of the TSS and the other 938 bp downstream of the transcriptional end site (TES).

Generation of the *Pnky* constitutive deletion (*Pnky*^{null}) mouse line

Constitutive deletion of *Pnky* was obtained through mating the *Pnky*^F line to the germline-expressed E2a-Cre mouse line. Progeny with germline deletion of *Pnky* were then mated to wild-type mice to obtain *Pnky*^{null/+} founders that lacked the E2a-Cre transgene.

Generation of the BAC^{*Pnky*} mouse line

BAC clone RP23-45116 was obtained from the BACPAC Resources Center and modified as shown (**Figure 3.S4A**) to remove the coding sequence (CDS) from *Pou3f2*, leaving the UTRs intact. Modifications were made as described in (Warming et al., 2005), and using the detailed protocols found at <https://ncifrederick.cancer.gov/research/brb/protocol.aspx>. We primarily used “Recombineering Protocol #3” and referred to “Recombineering Protocol #1” for additional details. The modified BAC was microinjected into C57BL/6 zygotes by the Transgenic Gene Targeting Core (Gladstone Institutes, UCSF).

Polymerase chain reaction (PCR)-based genotyping of *Pnky* and BAC^{*Pnky*}

DNA from small tissue samples was prepared by boiling in 100μL of lysis buffer (0.2mM EDTA, 25mM NaOH) for 1 hr, followed by quenching in 100μL of neutralization buffer (40mM Tris HCl pH 7.5). Genotyping was performed using GoTaq (Promega, M3001) and the following

reaction components, for a final volume of 12 μ L per reaction: 7.76 μ L of H₂O, 2.4 μ L of 5x buffer, 0.36 μ L of 50mM MgCl₂, 0.24 μ L of 10mM DNTPs, 0.12 μ L of primer mix (with each primer at 10 μ M), 0.12 μ L of GoTaq, 1 μ L of sample DNA. Reactions were incubated on a thermocycler as follows: 94°C for 2 min; 35 cycles of 94°C for 30 seconds (s), 60°C for 30 s, and 72°C for 1 min; 72°C for 5 min; 4°C hold. Reaction products were separated on a 2% agarose gel with ethidium bromide. The following primers were used (all listed 5' to 3'):

Primers for *Pnky*^F, *Pnky*⁺, and *Pnky*^{null} alleles:

Pnky GT F: TAAGCTCAAACCTCCGGTCCCGGGA

Pnky GT R1: TCAGGGACAAAGAACCAAAACGAGC

Pnky GT R2: AATGCTCCCTCTGAGCCTCAATT

Reaction products: 120bp (*Pnky*^{null}), 221bp (*Pnky*⁺), and 348 (*Pnky*^F). Since BAC^{*Pnky*} contains unaltered *Pnky*, this will produce the 221bp product, even in the absence of endogenous *Pnky* (see next section: Quantitative PCR (qPCR)-based genotyping for BAC^{*Pnky*}).

Primers for BAC^{*Pnky*}:

BAC GT F: CACCTGCTACCTGATATAGGA

BAC GT R: CAGCAGTAATAGCAAGAGCA

Reaction product: 416bp (contains BAC^{*Pnky*}). No amplification in the absence of BAC^{*Pnky*}.

Quantitative PCR (qPCR)-based genotyping for BAC^{*Pnky*}

Because BAC^{*Pnky*} contains unmodified *Pnky*, it is indistinguishable from *Pnky*⁺ in standard PCR-based genotyping. Therefore, certain genetic crosses required the use of qPCR to determine the endogenous *Pnky* alleles. This was done using 25ng of sample DNA (prepared as described above), along with 4 μ L SYBR green (Roche) and 2 μ L of primer mix (with each primer at 5 μ M) per 8 μ L qPCR reaction. Reactions were amplified on a LightCycler 480 II (Roche) using standard conditions. To quantify the number of copies of particular endogenous *Pnky* alleles, the $\Delta\Delta C_t$ method was used: a control genomic region was used to normalize for

DNA content per reaction, and multiple samples with known endogenous *Pnky* alleles were used to compare to unknown samples.

Primers for control genomic region:

Ctrl qPCR GT F: TGGTCGTTCTACAGGCCTTC

Ctrl qPCR GT R: GGACCGGTGACAGAGAACTG

Primers for *Pnky*^{null} allele:

Pnky qPCR GT F: AGTTGGTCGTCCGCGTACGGTAC

Pnky^{null} qPCR GT R (same as *Pnky* GT R1): TCAGGGACAAAGAACCAAAACGAGC

Product: 97bp from *Pnky*^{null} allele. No amplification from other *Pnky* alleles or BAC^{*Pnky*}.

Primers for *Pnky*^F allele:

Pnky qPCR GT F: AGTTGGTCGTCCGCGTACGGTAC

Pnky^F qPCR GT R: CCGGATCTTTCCTTTACCCGCAATAAC

Product: 228bp from *Pnky*^F allele. No amplification from other *Pnky* alleles or BAC^{*Pnky*}.

BrdU administration

Mice were administered 5-bromo-2'-deoxyuridine (BrdU, Millipore Sigma) reconstituted in sterile PBS through intraperitoneal injection, at a dose of 50mg BrdU per kg of mouse weight.

Primary cell culture

All cells were grown in humidified incubators at 37°C in 5% CO₂.

V-SVZ cultures

The brains of P7 mice were dissected out of the skull, and then a coronal slab of approximately 0.5 mm in thickness was obtained manually or by using a vibratome. Dissections were performed in ice-cold L15 medium (ThermoFisher 11415064) to collect the V-SVZ region along the lateral walls of the lateral ventricles. The tissue was dissociated with 300 μL of 0.25% trypsin-EDTA (ThermoFisher 25200056) with occasional agitation for 20 min at 37°C, and then the trypsin was quenched with 600 μL of N5 growth medium (see below). Cells were dissociated

by trituration and then pelleted by centrifugation at 300 g for 5 min. Cells were resuspended in fresh N5 growth medium and plated in one well of a 12-well tissue culture plate per mouse.

Cells were grown in N5 growth medium: DMEM/F-12 with GlutaMAX (ThermoFisher 10565018) supplemented with 5% Fetal Bovine Serum (Fisher Scientific SH30070.03), N2 supplement (ThermoFisher 17502048, 1:100), 35 µg/mL bovine pituitary extract (ThermoFisher 13028014), Antibiotic-Antimycotic (ThermoFisher 15240062, 1:100), 20 ng/mL epidermal growth factor (EGF, PeproTech AF-100-15), and 20 ng/mL basic fibroblast growth factor (bFGF, PeproTech 100-18B).

For routine passaging, cells were grown to hyperconfluency and then dissociated using 0.25% trypsin-EDTA (ThermoFisher 25200056) for 3-5 minutes in the incubator. This was diluted with an equal volume of growth medium, and the cells were dissociated by trituration. Cells were pelleted as described above, then resuspended in fresh culture medium to plate in 2 times the original culture area. For recombination using the tamoxifen-inducible UBC-Cre-ERT2 transgene, cultures were treated with 10nM 4-hydroxytamoxifen (4-OHT) for 48 hours. 4-OHT was reconstituted in EtOH, and all experimental cultures were normalized to paired EtOH-treated control cultures. To differentiate the cells, cultures were grown to hyperconfluency and then the medium was replaced without EGF or FGF.

Cortical neural stem cell cultures

Tissue culture plates were prepared by coating with 1 mg/mL poly-D-lysine (Millipore A-003-E) for at least 4 hours in the incubator. This was rinsed twice with PBS or water and replaced with 5 µg/mL laminin (ThermoFisher 23017015) in the incubator O/N. As laminin is highly sensitive to drying, this was removed well-by-well and immediately replaced with enough culture medium to cover the surface of the well. Cells were then plated in the remaining volume.

Cultures of cNSCs were derived from E12.5 mice as described in (Currel et al., 2007), with modifications. The developing cortex was dissected from E12.5 embryos in ice-cold high-glucose DMEM (ThermoFisher 31053028) and then dissociated with 100 µL of 0.05% trypsin-

EDTA (ThermoFisher 25300054) for 20 min at 37°C. Trypsinization was halted using 200 µL of 0.25 mg/mL soybean trypsin inhibitor (ThermoFisher 17075029). Cells were mechanically dissociated by trituration and then pelleted by centrifugation at 1000 g for 3 min. Cells were resuspended in 1mL of PBS to rinse, and then re-pelleted. Cells were finally resuspended in growth medium (see below) and plated in one well of a pre-treated (see above) 12-well tissue culture plate per embryo.

Cells were grown in the following medium slightly modified from (Hudlebusch et al., 2011): 50% DMEM/F-12 medium (ThermoFisher 11330057) and 50% Neurobasal medium (ThermoFisher 21103049) supplemented with N2 (ThermoFisher 17502048, 1:100), B27 (ThermoFisher 17504044, 1:50), Antibiotic-Antimycotic (ThermoFisher 15240062, 1:100), HEPES (ThermoFisher 15630080, 1:200), 2 µg/ml Heparin sodium salt (Millipore Sigma H3149), Bovine Albumin Fraction V (ThermoFisher 15260037, 1:750), MEM non-essential amino acids (ThermoFisher 11140050, 1:100), GlutaMAX (ThermoFisher 35050061, 1:100), Sodium Pyruvate (ThermoFisher 11360070, 1:100), β-mercaptoethanol (Millipore ES-007-E, 1:5000), 10 ng/ml epidermal growth factor (EGF, PeproTech AF-100-15) and 20 ng/ml basic fibroblast growth factor (bFGF, PeproTech 100-18B).

For routine passaging, cells were grown to confluency and then dissociated using StemPro Accutase (ThermoFisher A1110501) for 5 minutes in the incubator. This was diluted with an equal volume of growth medium, and the cells were dissociated by trituration. Cells were pelleted as described above, then resuspended in fresh culture medium to plate in 3 times the original culture area. To differentiate the cells, cultures were grown to confluency and then the medium was replaced without EGF or FGF.

Tissue/cell preparation

Cultured cells and human cerebral organoids were fixed in 4% paraformaldehyde (PFA, Millipore Sigma 158127) for 30 min at RT. Embryonic specimens up to E13.5 were fixed in 4%

PFA as whole heads, up to overnight (O/N) at 4°C. For E15.5 samples, brains were dissected out of the skull prior to fixation in 4% PFA, up to O/N at 4°C. Transcardiac perfusion was performed on postnatal animals with phosphate buffered saline (PBS) followed by 4% PFA. The brains were then dissected out of the skull and additionally fixed in 4% PFA O/N at 4°C.

Cryosectioning

All specimens were rinsed in PBS and then cryoprotected with 30% sucrose in PBS. Cryoprotected samples were then equilibrated in a 1:1 mixture of 30% sucrose and Tissue-Tek Optimal Cutting Temperature (OCT) (Thermo Fisher Scientific) for 1 hour (hr) at 4°C, then frozen in a fresh batch of the same mixture using dry ice. Frozen blocks were equilibrated in the cryostat at -23°C for at least 3 hrs prior to sectioning. Sections (12-14µm thick) were collected on Superfrost Plus Microscope Slides (Thermo Fisher Scientific) and stored at -80°C. Prior to IHC, tissue slides were rinsed in PBS with rotation for 10 minutes (min) at room temperature (RT) to remove sucrose/OCT.

Immunohistochemistry (IHC) and immunocytochemistry (ICC)

IHC and ICC were performed using blocking buffer consisting of PBS with 1% BSA (Millipore Sigma), 0.3M glycine (Thermo Fisher Scientific), 0.3% TritonX100 (Millipore Sigma), and either 10% normal goat serum or 10% normal donkey serum (Jackson ImmunoResearch Laboratories) depending on the species of origin of the secondary antibodies to be used.

IHC was performed on tissue sections and ICC was performed on cells as follows:

Blocking: incubated in blocking buffer for 1-2 hrs (IHC) or 1 hr (ICC) at RT.

Primary antibodies: incubated in primary antibodies diluted in blocking buffer O/N at 4°C (IHC) or 2 hrs at RT (ICC).

Wash 1: washed 3 times in PBS at RT for 10 (IHC) or 5 min (ICC).

Secondary antibodies: incubated in secondary antibodies (Alexa Fluor antibodies from Thermo Fisher Scientific, 1:500) and DAPI (Thermo Fisher Scientific, 1:1000) diluted in blocking buffer for 30 min at RT (both IHC and ICC).

Wash 2: same as wash 1 above. This completed ICC.

Mounting coverslips: for IHC, slides were mounted with coverslips using Aqua Poly/Mount (Polysciences).

Antigen Retrieval

For certain antibodies (see below), antigen retrieval was performed using 10mM sodium citrate (pH 6.0) prior to IHC. Slides were incubated horizontally with 500 μ L of sodium citrate on top of the tissue for 2-3 min at RT. This was replaced with fresh sodium citrate, and the slides were moved to a pre-heated vegetable steamer. After 15 min, the slides were removed from the steamer and allowed to cool for 2-3 min at RT. The sodium citrate was then dumped off of the tissue and the slides were rinsed in PBS.

Primary antibodies for IHC/ICC

Please see Key Resources Table for antibody specifications. Antibodies were used as follows: **Tuj1**: diluted 1:1000 for ICC. **POU3F2**: diluted 1:250 for IHC (performed antigen retrieval for tissue of all ages). **CTIP2**: diluted 1:500 for IHC (performed antigen retrieval for postnatal tissue). **pH3**: diluted 1:400 for IHC. **pVim**: diluted 1:500 for IHC. **CUX1**: diluted 1:500 for IHC (performed antigen retrieval for postnatal tissue). **BrdU**: diluted 1:200 for IHC (performed antigen retrieval for tissue of all ages). **tdTomato** (Takara or Sicgen): diluted 1:500 for IHC or ICC (does not work after antigen retrieval, see below).

IHC for tdTomato in combination with antigen retrieval

IHC for tdTomato was performed as described above, then the tissue was re-fixed with 4% PFA for 45 minutes at RT. Slides were rinsed in PBS, then antigen retrieval was performed followed by IHC for the other antigens as described above.

***In Situ* Hybridization (ISH) – Mouse tissue**

ISH was performed on tissue sections (prepared as described above) using the RNAscope 2.5 HD Assay — BROWN. Probes targeting the mouse *Pnky* transcript were used (RNAscope Probe-Mm-Pnky).

Sample Preparation: Followed the Sample Preparation Technical Note for Fixed Frozen Tissue with the following modifications:

1. Before starting the protocol, let slides dry and then drew a barrier around tissue sections using ImmEdge Hydrophobic Barrier PAP Pen (Vector Laboratories). Let barrier dry, then rinsed tissue in PBS for 10 min at RT with rotation to remove sucrose/OCT. Post-fixed with 4% PFA for 20 min at RT, then rinsed in PBS for 5 min at RT. Started at Part 2: Tissue Pretreatment section of the Technical Note.
2. Instead of submerging slides in boiling Target Retrieval solution, added pre-heated Target Retrieval solution on top of horizontal slides and incubated in pre-heated vegetable steamer.
3. Used Protease III instead of Protease Plus. Incubated for 10 min at RT.

ISH: Followed the standard RNAscope 2.5 Assay protocol except for the following modifications:

1. Hybridized probes for 3 hrs.
2. Hybridized AMP 5 for 90 min.
3. Incubated in DAB for 1 hr.
4. For all wash steps, incubated for 2 min with gentle rotation instead of agitating (to preserve tissue integrity).

***In Situ* Hybridization (ISH) – Human cerebral organoids**

ISH was performed as previously described (see **Chapter 2**) (Jensen and Wallace, 1997).

Microscopy and image analysis

Samples were imaged using Leica TCS SP5 X confocal, Leica DMI8, Leica DMI4000 B, and Keyence BZ-X710 inverted microscopes. For tissue samples that had received *in utero*

injection of Ad:Cre, the contralateral hemisphere was analyzed whenever possible. For all other tissue samples, both hemispheres were analyzed from 2-4 non-adjacent regions. All image analysis and quantification was performed using Fiji (Schindelin et al., 2012). To quantify Tuj1+ area (**Figures 3.4H-I**), the “threshold” and “measure” functions of Fiji were used.

RNA isolation

Total RNA was isolated from tissue and cultured cells using TRIzol (Thermo Fisher Scientific) and purified using Direct-zol RNA Purification Kits (Zymo Research). DNase digestion was performed as suggested.

Quantitative reverse transcription PCR (qRT-PCR)

cDNA synthesis was performed using the Transcriptor First Strand cDNA synthesis kit (Roche). qRT-PCR was performed using SYBR green (Roche) on a LightCycler 480 II (Roche). Relative gene expression was calculated using the $\Delta\Delta C_t$ method, using *Rplp0* as a housekeeping gene for differential gene expression analyses. All qRT-PCR assays were performed using technical triplicate wells. See Key Resources Table for primer sequences.

RNA-seq library preparation

Prior to library preparation, RNA integrity was assessed using TapeStation 4200 (Agilent). Strand-specific poly(A) selected cDNA libraries were generated using TruSeq Stranded mRNA kit (Illumina). Paired-end, 150bp sequencing of libraries was performed on a HiSeq 4000 (Illumina) by Novogene.

RNA Immunoprecipitation (RIP)

RIP using an antibody against PTBP1 (ThermoFisher) was performed as described previously (Ramos et al., 2015; Rinn et al., 2007) from cNSC cultures in 4 technical replicates from 2 separate experiments. The immunoprecipitated RNA was quantified by qRT-PCR using the percent input method. For each replicate, data were normalized to *β -actin* levels. *U1* was used as a negative control.

Cre-expressing adenovirus (Ad:Cre)

Ad:Cre (Merkle et al., 2007) was produced using 293A cells (Thermo Fisher Scientific, catalog number R70507). Concentrated adenovirus was prepared using the Fast Trap Adenovirus Purification and Concentration Kit (Millipore Sigma, catalog number FTAV00003).

***In utero* injections**

Injections were performed on timed-pregnant mice as previously described (Wang and Mei, 2013), except as follows: manual pipettes were used instead of mouth pipettes, and protocol sections 3.7-3.8 (delivery of electric pulses for electroporation) were skipped. Ad:Cre virus was mixed 1:1 with Trypan Blue to enable visualization of the injected solution. ~ 1 μ L of this mixture was injected into one of the lateral ventricles of E13.5 embryos. All protocols and procedures followed the guidelines of the Laboratory Animal Resource Center at the University of California, San Francisco and were conducted with IACUC approval.

Figure preparation

Figures were prepared using Photoshop and Illustrator (Adobe) and Prism (GraphPad).

Quantification and Statistical Analysis

All *in vivo* quantifications were normalized to littermate controls. For *in vivo* BAC rescue experiments, there was a low probability of obtaining all of the relevant experimental genotypes ($Pnky^{+/+}$, $Pnky^{null/null}$, and $Pnky^{null/null};BAC^{Pnky}$) within the same litter. Therefore, we used one set of crosses to analyze $Pnky^{+/+}$ and $Pnky^{null/null}$ littermates as one group, and another set of crosses to analyze $Pnky^{null/null}$ and $Pnky^{null/null};BAC^{Pnky}$ littermates as a separate group. To compare phenotypes between these two groups, we normalized results to the genotype common to both ($Pnky^{null/null}$), as shown in **(Figure 3.S4D)**.

For ICC quantification, technical triplicate wells of each genotype and treatment combination were analyzed. All cultures were normalized to their own treatment control.

The statistical details of each experiment can be found in the relevant figure legends, with additional details for RNA-seq experiments described below.

RNA-seq analysis of *Emx1*^{Cre} experiments (Figure 3.S1, and Tables 3.1 and 3.2):

Reads were aligned to the mouse genome mm10 using Hisat2 v2.1.0 (Kim et al., 2015). At least 77 million mapped reads were obtained per sample. Differential gene expression was analyzed by DESeq2 (Love et al., 2014) and correction for multiple hypothesis testing was performed using the R package fdrtool (Strimmer, 2008). Transcription factor motif enrichment analysis was performed on differentially-expressed gene sets using the Homer findMotifs.pl command (Heinz et al., 2010) with default settings, using all genes detected by RNA-seq as the background list (data not shown).

Analysis of alternative splicing (including alternative exons, micro-exons, 3' and 5' splice sites, and retained introns) was performed using VAST-TOOLS v.1.0 (Braunschweig et al., 2014; Irimia et al., 2014). To determine if events were differentially spliced between the cortical tissues of *Pnky*-cKO and control mice, lowly-expressed transcripts (cRPKM < 3) and all events with low inclusion (PSI < 5%) were removed. The VAST-TOOLS diff module (Han et al., 2017) was used to both calculate the difference in percent spliced in (dPSI) between conditions and to identify statistically significant differences in splicing for all events with at least 10 reads support. All reported events were found to have significant dPSI: the probability of an event having |dPSI| of at least 5% is greater than 95%. Highly supported events have more than 10 reads mapping to the event in at least 50% of the profiled samples.

RNA-seq analysis of cNSC experiments (Figures 3.4 and 3.S4, and Tables 3.3 and 3.4):

Reads were pseudo-aligned to the Gencode M18 GRCm38.p6 transcriptome with Kallisto v0.43.1 (Bray et al., 2016). Differential expression analysis was performed using DESeq2 (Love et al., 2014), using the model (\sim grp + grp:ind.n + grp:cnd) where grp = genotype, ind.n = individual biological replicate, and cnd = condition (untreated or +Ad:Cre) to

identify genotype-specific effects of Ad:Cre. Correction for multiple hypothesis testing was performed using the R package *fdrtool* (Strimmer, 2008). As described above, transcription factor motif enrichment analysis was performed on differentially-expressed gene sets using the Homer *findMotifs.pl* command (Heinz et al., 2010) with default settings, using all genes detected by RNA-seq as the background list (data not shown).

For splicing analysis, the data were aligned to the mouse genome by *vast-tools* (Braunschweig et al., 2014; Irimia et al., 2014) with default options using *-mm10*. Analysis included all events that had at least 10 samples with 95% > PSI > 5% and for which *vast-tools* identified coverage as 'OK' or 'SOK' in at least 50% of samples. The VAST-TOOLS *diff* module (Han et al., 2017) was used to identify significantly differentially-spliced events, which required a minimum of 15 reads ($-e\ 15$) and called events significantly different between conditions only if $|dPSI| > 0.05$. A splicing event was deemed to be 'rescued' by BAC^{Pnky} if $|dPSI|$ between $Pnky^{F/F};BAC^{Pnky}$ untreated and +Ad:Cre samples was < 0.05 , $|dPSI|$ between in $Pnky^{F/F}$ untreated and +Ad:Cre samples was significant, and if the rescue caused a shift away from $Pnky$ -cKO conditions by at least $|dPSI| > 0.05$. For *Ptbp1*-KD comparison, we re-analyzed the data from previous studies in mouse N2a cells (Raj et al., 2014) and in V-SVZ NSCs (Ramos et al., 2015). From these two studies, we generated lists of events which were significantly affected by *Ptbp1*-KD at a $|dPSI| > 0.05$ cut-off. We compared these events (N=230 overlapping events in 227 genes) to those we found to be regulated by *Pnky* (N=220 events in 182 genes).

Data and Software Availability

The RNA-seq datasets generated during this study are available in the public repository GEO, available at <https://www.ncbi.nlm.nih.gov/geo/>. Data are listed with the accession number GSE127987.

Chapter 4: Loss of *Pnky* disrupts neurogenesis and long-term neural stem cell abundance in the ventricular-subventricular zone

Summary

Certain long noncoding RNAs (lncRNAs) are now known to carry out important biological roles, however there are few examples of lncRNAs that regulate neurogenesis *in vivo*. *Pnky* is a lncRNA that is enriched in the neural stem cells (NSCs) of the ventricular-subventricular zone (V-SVZ). Here we show that *Pnky* deletion leads to the aberrant formation of intraventricular neuroblast nodules. Loss of *Pnky* also disrupts normal progression through the V-SVZ neurogenic lineage, expanding the transit amplifying stage. Furthermore, long-term NSC abundance is reduced in *Pnky* knockout mice, possibly as a consequence of precocious neurogenic differentiation. To understand how *Pnky* carries out its functions at the molecular level, we also identified several putative *Pnky*-binding proteins, many of which are related to the process of RNA splicing. Thus, *Pnky* is an important mediator of V-SVZ neurogenesis *in vivo*, potentially through its interactions with splicing factors.

Introduction

Tens of thousands of distinct long noncoding RNAs (lncRNAs) – transcripts longer than 200 nucleotides (nt) that lack evident protein coding potential (Djebali et al., 2012) – are produced by the mammalian genome. There is a growing number of lncRNAs that have been shown to regulate important biological processes, including those that underlie human disease (Batista and Chang, 2013; Briggs et al., 2015; Lee, 2012; Mercer and Mattick, 2013; Rinn and Chang, 2012). A remarkable diversity of lncRNAs can be found in the developing and adult central nervous system, and many of these lncRNAs seem to be brain-specific (Derrien et al., 2012; Mercer et al., 2008). However, there have been few genetic studies of lncRNA function in

animal models, and therefore the biological significance of most lncRNAs *in vivo* remains unclear (Nakagawa, 2016). This is particularly true for the central nervous system: while several lncRNAs have now been found to perform important roles in different neural cell types, (Aprea and Calegari, 2015; Briggs et al., 2015; Clark and Blackshaw, 2014; Hart and Goff, 2016; Ramos et al., 2016), only a handful have been experimentally manipulated *in vivo* in mice (Andersen and Lim, 2018).

Neural stem cells (NSCs) are glial cells that can self-renew as well as differentiate into intermediate progenitors, which divide at least once before producing neuronal progeny (Kriegstein and Alvarez-Buylla, 2009). Such NSCs exist in the embryonic cortical ventricular zone, and we have previously shown that the lncRNA *Pnky* regulates neurogenesis in the developing neocortex (Andersen et al., 2019). In the mouse, there is also a population of long-term NSCs that exists within the walls of the lateral ventricles, in a niche known as the ventricular-subventricular zone (V-SVZ) (Lim and Alvarez-Buylla, 2014, 2016). The V-SVZ neurogenic lineage has been extensively described (Doetsch et al., 1999; Lois and Alvarez-Buylla, 1994; Luskin, 1998; Peretto et al., 1997): throughout the adult life of a mouse, V-SVZ NSCs generate transit amplifying cells, which give rise to multiple neuroblasts. These neuroblasts then travel anteriorly through the rostral migratory stream to the olfactory bulb, where they terminally differentiate into mature interneurons.

Pnky was originally identified as a lncRNA enriched in V-SVZ NSCs, and we previously found that knockdown or deletion of *Pnky* promotes neurogenic differentiation in V-SVZ NSC cultures (see **Chapter 2** and **Chapter 3**). However, many aspects of the V-SVZ neurogenic lineage *in vivo* cannot be recapitulated using *in vitro* cultures, and it was unknown whether *Pnky* regulates processes such as neuroblast migration to the olfactory bulbs or long-term NSC maintenance. Here we show that genetic deletion of *Pnky* results in aberrant progression through the V-SVZ neurogenic lineage and the formation of intraventricular neuroblast nodules. We also find that loss of *Pnky* leads to reduced long-term NSC abundance. Furthermore, we

identify a novel set of putative *Pnky* binding proteins, many of which are known to regulate RNA splicing. Together, these data demonstrate an important role for *Pnky* in a long-term NSC population *in vivo* and provide new insights into the potential molecular function of this lncRNA.

Results

We previously described the generation of a conditional *Pnky* knockout allele with loxP sites flanking the entire *Pnky* gene (see **Chapter 3**). This genetic tool enabled us to determine that deletion of *Pnky* from V-SVZ cultures results in substantially increased neurogenic output (**Figure 3.1D-E**), similar to the effect of knocking down *Pnky* transcript levels (**Figure 2.1I-J**). However, monolayer *in vitro* cultures cannot recapitulate certain important aspects of the V-SVZ neurogenic lineage. Therefore, to assess the function of *Pnky* in the V-SVZ *in vivo*, we targeted deletion of *Pnky* to the nervous system using *Nestin-Cre*, and also analyzed constitutive *Pnky*^{null} knockout mice (both hereafter referred to as *Pnky*-KO). In both cases, a subset of the *Pnky*-KO mice exhibited a striking phenotype: nodules of cells residing within the ventricles (**Figure 4.1A**). Further analysis revealed that these nodules were comprised of tightly-packed DCX+ neuroblasts (**Figure 4.1B**), consistent with increased neurogenesis upon loss of *Pnky*. Supporting an immature neuroblast identity, we did not detect expression of the mature neuronal marker NeuN (data not shown).

While these neuroblast nodules were not found in any of the littermate control mice, they were observed in approximately half of the *Pnky*-KO mice at a variety of postnatal ages (**Figure 4.1C** and **Table 4.1**). The average dimensions of the nodules were $67 \pm 16\mu\text{m}$ in the mediolateral axis and $174 \pm 30\mu\text{m}$ in the dorsoventral axis (**Figure 4.1D** and **Table 4.1**). While the cells within these nodules were not proliferative (**Figure 4.1E**), birth dating analysis using 5-bromo-2'-deoxyuridine (BrdU) in adult mice demonstrated that many of them had been recently produced (**Figure 4.1F**), suggesting an ongoing disruption of postnatal V-SVZ neurogenesis.

Some *Pnky*-KO animals also exhibited additional abnormalities, including neuroblast nodules along the walls of the ventricles (**Figure 4.1G**). Thus, genetic deletion of *Pnky* disrupts the proper architecture of the V-SVZ *in vivo*.

We next sought to determine how the intraventricular neuroblast nodules were formed. The neuroblasts produced in the V-SVZ normally migrate anteriorly through the rostral migratory stream to reach the olfactory bulbs (Lim and Alvarez-Buylla, 2014). However, certain genetic mutations, such as loss of the chromatin modifier *mixed-lineage leukemia 1 (Mll1)*, can impair neurogenic differentiation and disrupt this migration (Lim et al., 2009). Therefore, we first assessed whether deletion of *Pnky* blocked the migration of neuroblasts to the olfactory bulbs. We administered BrdU to control and *Pnky*-KO littermates at postnatal day (P) 60, and then waited two weeks in order to allow sufficient time for the newly-born BrdU+ neuroblasts to migrate to the olfactory bulbs. In both control and *Pnky*-KO mice, we observed many BrdU+ cells dispersed throughout the olfactory bulbs (**Figure 4.2A**). We also found BrdU-labeled cells within the core of the olfactory bulbs, which is where the migrating neuroblasts first arrive. Therefore, loss of *Pnky* does not grossly disrupt neuroblast migration from the V-SVZ.

In order to analyze progression through the V-SVZ neurogenic lineage, we performed additional BrdU labeling experiments. We administered BrdU to P30 mice, and then waited one week to allow differentiation into transit amplifying cells and neuroblasts. We found no statistically significant difference in the overall number of BrdU+ cells along the V-SVZ in control vs *Pnky*-KO littermates (control: 102.9 ± 24.4 ; *Pnky*-KO: 89.0 ± 26.1 ; ratio paired t test: $p = 0.27$). However, loss of *Pnky* resulted in altered progression through this lineage, leading to an increase in the proportion of BrdU+ cells that were DLX2+;DCX- transit amplifying cells and a corresponding decrease in the proportion of BrdU+ cells that were DCX+ neuroblasts (**Figure 4.2B**). These data are consistent with previous *in vitro* time lapse imaging results, which indicated that depletion of *Pnky* leads to an expansion of the transit amplifying phase (**Figures 2.2E** and **2.S2F**). Thus, *Pnky* regulates neurogenic differentiation in the V-SVZ *in vivo*.

We further sought to determine whether loss of *Pnky* and altered progression through the neurogenic lineage lead to long-term effects on the V-SVZ NSC population. We collected wholemount V-SVZ preparations, which enable the *en face* visualization of the V-SVZ NSC pinwheel structure (Mirzadeh et al., 2008) (**Figure 4.2C**). We quantified the number of apical NSC processes from pinwheels in the V-SVZ of 6-month old mice and found that *Pnky* deletion significantly reduced their abundance by 41.5% (**Figure 4.2D**). Taken together with our previous results, these data suggest that loss of *Pnky* promotes neurogenic differentiation and transit amplifying cell expansion at the expense of long-term NSC abundance, and that increased V-SVZ neurogenesis may underlie the formation of neuroblast nodules within the ventricles.

While we have now shown that *Pnky* carries out important roles in multiple neurogenic populations *in vivo*, the molecular mechanisms through which *Pnky* functions are largely unknown. We previously determined that *Pnky* does not regulate its neighbor *Pou3f2* in *cis* but rather acts in *trans* during cortical development (see **Chapter 3**). Furthermore, we found that *Pnky* physically interacts with the splicing regulator PTBP1 in NSCs of both the V-SVZ and developing cortex, and that depletion or loss of *Pnky* results in altered splicing in these populations (see **Chapter 2** and **Chapter 3**). However, whether *Pnky* interacts with additional proteins to carry out its *trans* functions remained unclear.

In order to identify novel *Pnky* binding partners through an unbiased approach, we used human proteome microarrays (Siprashvili et al., 2012). We first *in vitro* transcribed both mouse and human *Pnky*, as well as a scrambled version of mouse *Pnky* as a negative control. We then covalently labeled the transcripts with fluorescent Cy5 dye at an average labeling density of approximately 1 Cy5 molecule per 784 nt of RNA. By incubating the proteome arrays with the fluorescent RNA transcripts, we were able to identify a set of proteins that physically interact with mouse and/or human *Pnky* (**Table 4.2**). A subset of these proteins showed strong enrichment of both mouse and human *Pnky*, suggesting a potentially conserved interaction. Interestingly, the proteins found to enrich mouse and/or human *Pnky* were associated with

Gene Ontology terms (Mi et al., 2010; Thomas et al., 2003) related to RNA splicing and posttranscriptional regulation of gene expression (**Table 4.3**). Moving forward, determining whether these interactions with *Pnky* occur *in vivo* may provide key insights into how this lncRNA regulates neurogenesis and long-term neural stem cell abundance.

Discussion

In this chapter, we have demonstrated that genetic deletion of the lncRNA *Pnky*, which is enriched in V-SVZ NSCs, results in aberrant neurogenic differentiation and reduced long-term NSC abundance in the V-SVZ *in vivo*. Surprisingly, loss of *Pnky* led to the formation of intraventricular neuroblast nodules, which could be found at a variety of postnatal ages. These nodules do not seem to result from grossly impaired neuroblast migration, as neuroblasts were able to successfully reach the olfactory bulbs in adult *Pnky*-KO mice. Rather, the nodules may arise as a consequence of increased neurogenesis, as previously found with *Pnky* knockdown and knockout in V-SVZ cultures as well as *Pnky* deletion in the developing cortex. Preliminary observations (not shown) indicate that the establishment of V-SVZ NSCs is not affected in *Pnky*-KO mice, suggesting that the decrease in their long-term abundance is due to impaired NSC maintenance. Taken together, the data are consistent with a model in which loss of *Pnky* promotes neurogenic differentiation at the expense of the NSC population, and expands the transit amplifying phase to further increases neuroblast production.

We also identified additional putative *Pnky* binding proteins through human proteome microarrays. While we have previously found that *Pnky* interacts with PTBP1 in mouse NSCs from both the V-SVZ and the embryonic cortex, we did not detect an interaction between the Cy5-labeled *Pnky* transcripts and PTBP1 on the arrays. This may be due to a variety of technical issues stemming from how the proteins are produced in yeast and then purified and affixed to the arrays. Alternatively, this could reflect a biologically meaningful result; for instance, it is conceivable that *Pnky* may only be able to interact with PTBP1 as part of a larger complex.

Therefore, while these proteome arrays cannot provide a comprehensive set of *Pnky* interacting proteins, they can be very useful for identifying highly robust interactions.

Interestingly, the putative *Pnky*-interacting proteins that were identified are enriched for Gene Ontology terms related to splicing and posttranscriptional regulation of gene expression. As PTBP1 is also a splicing regulator, we have previously analyzed the splicing changes that occur upon depletion or loss of *Pnky* and found that they significantly overlap with PTBP1-regulated splicing events. It will be important to further analyze the *Pnky*-dependent splicing changes to determine if they also overlap with events regulated by any of the newly-identified putative *Pnky*-interacting proteins.

Of particular interest, quaking (QKI) was found to strongly interact with both mouse and human *Pnky* transcripts. While a statistically significant interaction was also found with the scrambled negative control, the intensity of this interaction was far weaker. QKI has been shown to influence neurogenic differentiation (Hayakawa-Yano et al., 2017; Shu et al., 2017), and also to regulate splicing networks that overlap with PTBP1-dependent splicing events (Gazzara et al., 2014; Hall et al., 2013; Wu et al., 2002). Therefore, unraveling how *Pnky* affects the interplay between these two splicing regulators may prove crucial to understanding the role of *Pnky* in neural stem cells.

QKI has also been found to physically interact with another lncRNA called *Gomafu* (Barry et al., 2014) (see **Chapter 1**). *Gomafu* orthologs in several species all contain multiple QKI consensus recognition sequences (Rapicavoli et al., 2010), however this was not the case for mouse or human *Pnky*. Interestingly, *Gomafu* also interacts with another splicing regulator serine/arginine-rich splicing factor 1 (SRSF1) (Barry et al., 2014), which we found to interact with *Pnky* as well. The related proteins SRSF9 and SRSF10 were also found to weakly interact with human *PNKY* but not mouse *Pnky*. Since *Gomafu* has been implicated in regulating neurogenic differentiation in the developing cortex (Aprea et al., 2013), it will be important to determine whether *Pnky* and *Gomafu* functionally influence one another.

As it is now clear that *Pnky* plays significant roles during neurogenic differentiation *in vivo*, moving forward it will be important to shift focus toward understanding how *Pnky* functions at the molecular level. The list of putative *Pnky*-binding proteins identified here will serve as a useful resource, providing new directions to explore. Further analyses to determine how *Pnky* regulates splicing, and whether its interaction with PTBP1 or other splicing factors is essential for this function, will also be revealing. Given that the molecular mechanisms of most lncRNAs with *in vivo* roles are poorly understood, gaining deeper insights into how *Pnky* functions will have broad implications for the field of lncRNA biology.

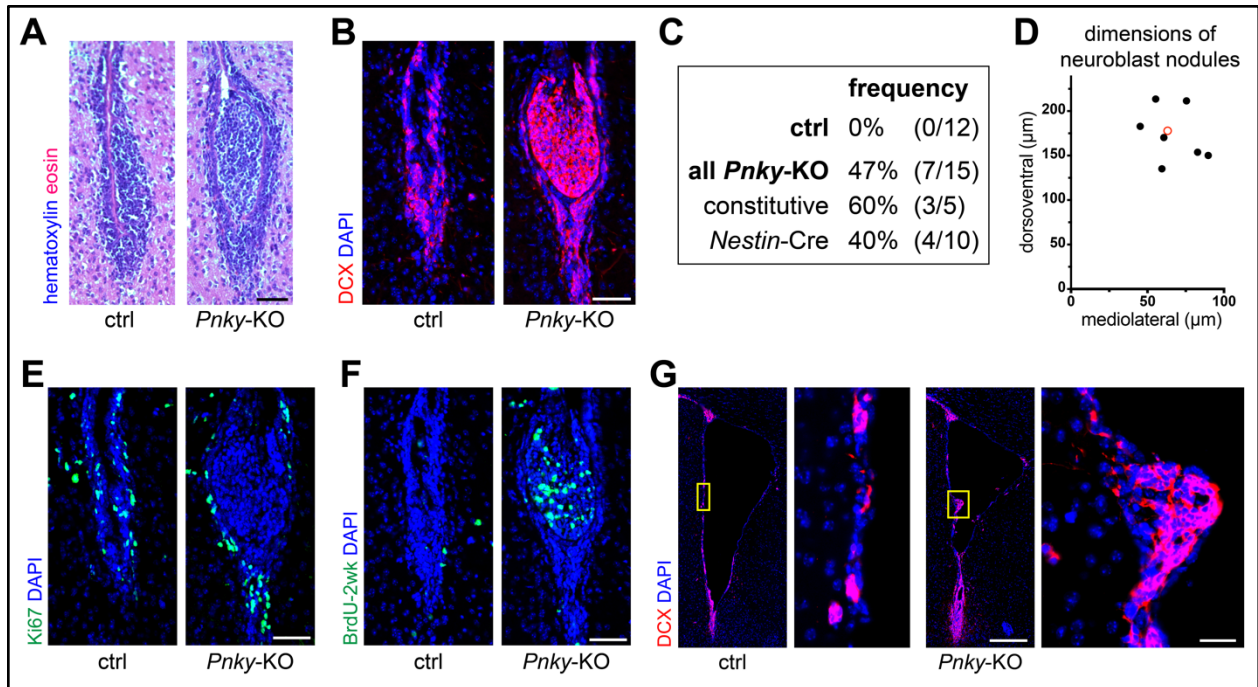


Figure 4.1: Loss of *Pnky* results in the aberrant formation of neuroblast nodules.

A, Eosin (pink) with hematoxylin nuclear counterstain (blue), showing the ventral tip of the lateral ventricle in coronal sections from P21 mice. Scale bar = $50\mu\text{m}$. **B**, DCX IHC, with DAPI nuclear counterstain, showing the ventral tip of the lateral ventricle in coronal sections from P74 mice. Scale bar = $50\mu\text{m}$. **C**, Frequencies of intraventricular neuroblast nodules within control or *Pnky*-KO mice of various postnatal ages. See also Table 4.1. **D**, Dimensions of the neuroblast nodules, with the average dimensions depicted by a hollow red circle. **E**, Ki67 IHC, with DAPI nuclear counterstain, showing the V-SVZ as in (B). Scale bar = $50\mu\text{m}$. **F**, BrdU IHC, with DAPI nuclear counterstain, showing the V-SVZ from the same coronal sections as in (B). BrdU was administered 2 weeks prior at P60. Scale bar = $50\mu\text{m}$. **G**, DCX IHC, with DAPI nuclear counterstain, showing the lateral ventricle and expanded insets from P37 mice. Scale bars = $250\mu\text{m}$ and $25\mu\text{m}$ (insets).

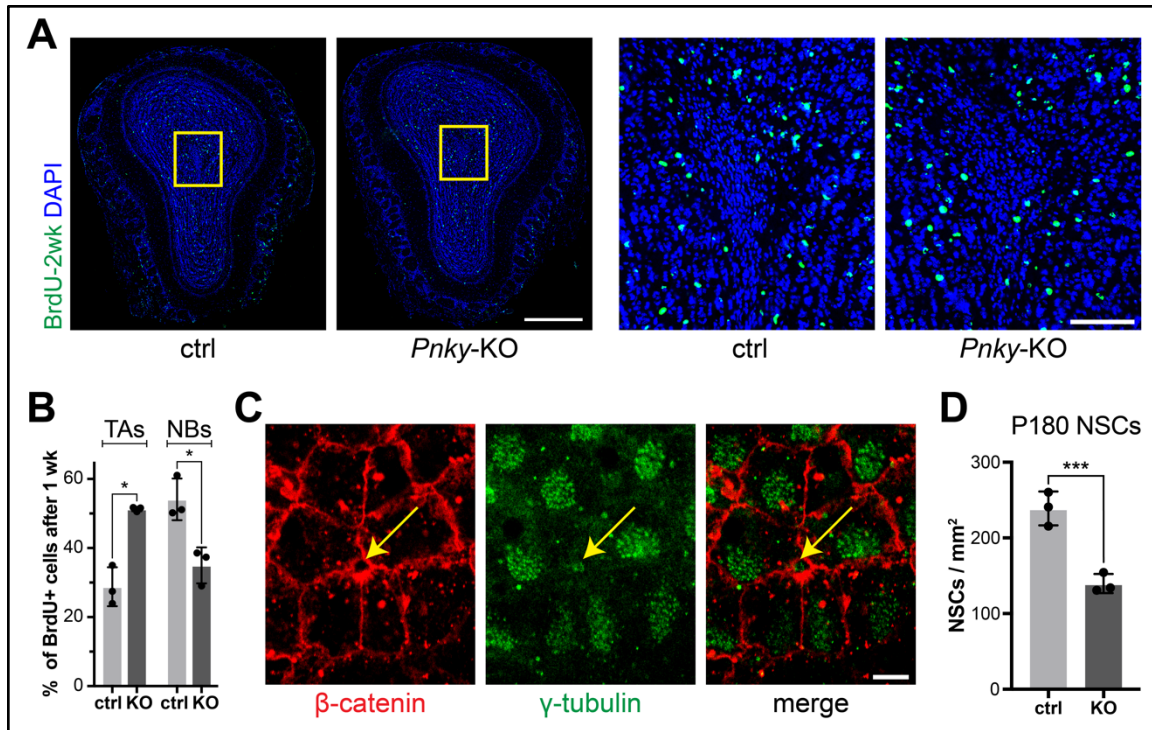


Figure 4.2: *Pnky* regulates progression through the V-SVZ neurogenic lineage.

A, BrdU IHC, with DAPI nuclear counterstain, showing the olfactory bulb in coronal sections and expanded insets from P74 mice. BrdU was administered 2 weeks prior, at P60. Scale bars = 500 μ m and 100 μ m (insets). **B**, Quantification of the percentage of BrdU-labeled cells in the V-SVZ that were transit amplifying cells (TAs, DLX2+;DCX-) or neuroblasts (NBs, DCX+). BrdU was administered at P30, and analysis performed 1 week later. * = $p < 0.05$, paired t test. **C**, IHC for β -catenin and γ -tubulin, showing representative V-SVZ pinwheel from *en face* wholemount dissections. Scale bar = 10 μ m. **D**, Quantification of NSCs from P180 mice, using pinwheel analysis as shown in (C). *** = $p < 0.001$, ratio paired t test.

Table 4.1: Deletion of *Pnky* results in intraventricular neuroblast nodules.

Descriptions of the mice in which intraventricular neuroblast nodules were observed, as well as the dimensions of the nodules themselves. Mediolateral (M-L) and dorsoventral (D-V) dimensions were measured directly in coronal sections. Anteroposterior (A-P) dimensions were approximated based on how the cryosectioning was performed.

Mouse	Genotype	Age	Sex	M-L (μm)	D-V (μm)	A-P (μm)
1	<i>Pnky</i> ^{F/F} ;Nestin-Cre	P30	M	55.3	213.5	360-720
2	<i>Pnky</i> ^{F/F} ;Nestin-Cre	P60	M	82.8	153.7	<360
3	<i>Pnky</i> ^{F/F} ;Nestin-Cre	P74	F	59.4	135.1	<360
4	<i>Pnky</i> ^{F/F} ;Nestin-Cre	P74	M	89.7	150.1	<360
5	<i>Pnky</i> ^{null}	P21	F	45.2	182.8	<360
6	<i>Pnky</i> ^{null}	P21	F	75.5	211.5	<360
7	<i>Pnky</i> ^{null}	P37	F	60.7	170.2	180-540

Table 4.2: Mouse and human *Pnky* RNA physically interact with multiple proteins.
Interactions between Cy5-RNA and proteins. Z-scores above 3 are considered significant.

ID	Gene	Z-Score		
		Neg. Control	Mouse <i>Pnky</i>	Human <i>PNKY</i>
JHU15165.B10C25R56	QKI	3.874	17.178	37.849
JHU19422.B20C1R14	PRB1	3.281	11.408	26.867
JHU08508.B6C3R48	QKI	3.735	10.123	28.067
JHU19422.B16C12R26	PRB1	3.926	7.844	13.916
JHU11870.B11C30R4	QKI	3.844	7.318	21.451
JHU21628.B19C1R18	ALDOA	3.792	6.241	11.874
JHU10401.B5C3R74	KCNJ1	0.34	5.387	0.228
JHU15238.B9C13R60	KHDRBS1	2.178	5.006	9.163
JHU15450.B11C27R64	MEX3B	2.411	4.906	18.188
JHU03020.B13C17R10	IFIT5	1.751	4.865	4.435
JHU02903.B13C14R12	DNAJA3	2.829	4.101	0.391
JHU15238.B9C18R60	KHDRBS1	1.913	4.008	6.713
JHU02852.B16C3R78	SERPINF1	1.234	3.841	4.53
JHU03804.B2C21R60	NHLH1	2.23	3.772	1.447
JHU05650.B2C19R88	TRUB1	1.727	3.76	0.479
JHU02880.B4C17R44	ZNF346	1.248	3.613	4.894
JHU05180.B3C22R82	ZNF385A	1.962	3.477	7.04
JHU04939.B1C10R78	ISG20	0.217	3.398	2.003
JHU05618.B3C4R88	MAGEB4	2.673	3.348	0.832
JHU14803.B14C2R80	WARS	0.906	3.336	-0.074
JHU02652.B3C10R38	PECR	2.906	3.306	0.131
JHU06552.B5C3R16	FTL	0.436	3.27	0.32
JHU03700.B4C4R58	LARP1_frag	2.725	3.236	0.957
JHU01296.B15C11R72	HEXIM1	2.681	3.232	0.517
JHU03058.B1C13R48	SRSF1	0.671	3.225	5.168
JHU18315.B15C22R48	SH3BP1	0.247	3.208	4.795
JHU02905.B1C19R46	EBI3	0.009	3.172	2.383
JHU19679.B13C14R2	PURA	0.107	3.041	3.367
JHU14619.B11C32R54	AK2	0.83	3.034	6.131
JHU15001.B12C29R60	A1CF	0.657	3.013	0.808
JHU16024.B11C7R68	PRB3_frag	1.585	2.672	4.039
JHU12670.B15C7R10	HNRNPUL1	2.627	2.534	3.298
JHU15111.B11C1R56	CPT1A	2.164	2.498	3.149
JHU12670.B11C3R24	HNRNPUL1	2.378	2.475	3.096
JHU19586.B15C15R6	Lin28a	2.063	1.729	6.971
JHU29900.B19C26R42	TGM3	2.189	1.601	13.163
JHU07314.B10C9R88	CRYZ	0.586	1.577	6.076
JHU09928.B5C10R64	KHDRBS3	0.176	1.567	4.324
JHU08280.B7C11R40	YBX3	0.788	1.56	3.597
JHU11244.B15C6R80	CAT	0.695	1.298	3.54
JHU11878.B9C30R6	SRSF9	-0.079	1.227	3.002
JHU04650.B3C12R74	SRSF10	0.808	1.01	3.731
JHU19394.B15C9R80	KHSRP	0.22	0.427	3.473

Table 4.3: *Pnky*-interacting proteins are associated with RNA processing.

Gene Ontology (GO) terms significantly enriched by the proteins found to interact with *Pnky*. “Hits” refers to the number of *Pnky*-interacting proteins associated with each GO term. FDR correction was performed to produce adjusted p values (Adj p).

GO Term (set: Biological Process Complete)	Hits	fold enriched	Adj p
regulation of alternative mRNA splicing, via spliceosome	4	25.46	0.0270
regulation of mRNA splicing, via spliceosome	5	21.57	0.0073
regulation of RNA splicing	5	16.18	0.0229
regulation of mRNA processing	5	15.78	0.0235
regulation of mRNA metabolic process	8	10.75	0.0038
regulation of cytoplasmic translation	3	50.64	0.0358
regulation of translation	8	10.25	0.0032
regulation of cellular amide metabolic process	8	9.00	0.0052
mRNA localization resulting in posttranscriptional regulation of gene expression	2	> 100	0.0373
posttranscriptional regulation of gene expression	9	7.61	0.0050
RNA localization	7	15.80	0.0025
negative regulation of mRNA metabolic process	4	21.27	0.0381
RNA transport	5	12.69	0.0409
establishment of RNA localization	5	12.52	0.0393
nucleic acid transport	5	12.69	0.0388
mRNA splice site selection	3	41.59	0.0453
mRNA processing	9	8.65	0.0031
RNA processing	12	6.31	0.0037
RNA metabolic process	13	3.56	0.0384
nucleobase-containing compound metabolic process	17	2.82	0.0346
organic cyclic compound metabolic process	18	2.56	0.0430
cellular nitrogen compound metabolic process	20	2.67	0.0134
heterocycle metabolic process	17	2.64	0.0459
gene expression	14	3.13	0.0449
mRNA metabolic process	10	6.56	0.0054
mRNA cis splicing, via spliceosome	3	38.82	0.0484

Experimental Procedures

Mus musculus

Mice were cared for as described in (**Chapter 3**). Mice of both sexes were used for all experiments, and were analyzed at multiple ages between P14 and P180 as described in the text and figure legends for each experiment. All samples were analyzed relative to littermates. For *Nestin-Cre* experiments, control samples were *Pnky*^{+/+}; *Nestin-Cre* or any combination of *Pnky* alleles in the absence of *Nestin-Cre*. Details regarding mouse strains are as follows: *Nestin-Cre*: Tg(Nes-cre)1Kln, described in (Tronche et al., 1999). *Pnky*^F and *Pnky*^{null}: described in (**Chapter 3**).

BrdU administration

Mice were administered 5-bromo-2'-deoxyuridine (BrdU, Millipore Sigma) reconstituted in sterile PBS through intraperitoneal injection, at a dose of 50mg BrdU per kg of mouse weight.

Tissue preparation

For samples to be cryosectioned, transcardiac perfusion was performed using phosphate buffered saline (PBS) followed by 4% paraformaldehyde (PFA, Millipore Sigma 158127). The brains were then dissected out of the skull and additionally fixed in 4% PFA overnight at 4°C. Fixed specimens were rinsed in PBS and stored at 4°C in PBS with sodium azide. Cryosectioning was performed as described in (**Chapter 3**).

Wholemount dissections were performed as described in (Mirzadeh et al., 2010).

Hematoxylin and eosin staining

Cryosection slides were incubated serially in the following solutions: 95% EtOH (2 min), 70% EtOH (2 min), running tap water (5 min), Gill's hematoxylin (3 min), running tap water (5 min), Scott's solution (3 min), running tap water (5 min), eosin (20 sec), 70% EtOH (30 sec), 95% EtOH (30 sec), 100% EtOH (30 sec), Xylene (5 min). The slides were then allowed to dry

completely (at least 5 min) before they were mounted with coverslips using Permount (Fisher).
Scott's solution: 2g sodium bicarbonate, 20g MgSO₄, 1 liter water.

Immunohistochemistry (IHC)

IHC on cryosections was performed as described in (**Chapter 3**). IHC on wholemount dissections was performed as follows:

Blocking: incubated in blocking buffer for 1 hr at RT. Blocking buffer: PBS with 1% BSA (Millipore Sigma), 0.3M glycine (Thermo Fisher Scientific), 0.5% TritonX100 (Millipore Sigma), and 10% normal goat serum (Jackson ImmunoResearch Laboratories).

Primary antibodies: incubated in primary antibodies diluted in blocking buffer for 24 hrs at 4°C.

Wash 1: rinsed twice in PBS, then washed 3 times in PBS with rotation for 20 min at RT.

Secondary antibodies: incubated in secondary antibodies (Alexa Fluor antibodies from Thermo Fisher Scientific, 1:500) and DAPI (Thermo Fisher Scientific, 1:1000) diluted in blocking buffer for 24 hrs at 4°C.

Wash 2: same as wash 1 above.

After IHC, the wholemount dissection was completed as described in (Mirzadeh et al., 2010).

The tissue was then mounted on Superfrost Plus Microscope Slides (Thermo Fisher Scientific) with coverslips using Aqua Poly/Mount (Polysciences).

Primary antibodies for IHC

Cryosections:

DCX: Abcam (ab18723) diluted 1:500.

NeuN: Millipore (MAB377) diluted 1:500.

Ki67: BD Biosciences (556003) diluted 1:200. Performed citrate antigen retrieval prior to IHC (see below).

BrdU: Abcam (ab6326) diluted 1:200. Performed HCl antigen retrieval prior to IHC (see below).

Wholemount dissections

β -catenin: Sigma (C2206) diluted 1:1000.

γ -tubulin: Abcam (ab11316) diluted 1:1000.

Citrate antigen retrieval for Ki67 IHC

For Ki67 IHC, antigen retrieval was performed using 10mM sodium citrate (pH 6.0) prior to IHC. Slides were incubated horizontally with 500 μ L of sodium citrate on top of the tissue for 2-3 min at RT. This was replaced with fresh sodium citrate, and the slides were moved to a pre-heated vegetable steamer. After 15 min, the slides were removed from the steamer and allowed to cool for 2-3 min at RT. The sodium citrate was then dumped off of the tissue and the slides were rinsed in PBS.

HCl antigen retrieval for BrdU IHC

For BrdU IHC, antigen retrieval was performed using HCl and boric acid prior to IHC. Slides were first rinsed in PBS with rotation for 10 min at RT. The slides were then incubated in fresh 2N HCl at 37°C for 30 min. Boric acid (100mM, pH 8.5) was used to rinse the slides to remove all HCl. The slides were then incubated in fresh boric acid with rotation for 10 min at RT. After rinsing the slides with PBS, IHC was performed as described above.

If BrdU IHC was to be performed in combination with IHC for other antigens, IHC for these antigens was completed first. The tissue was re-fixed in 4% PFA for 30 min at RT and rinsed in PBS. HCl antigen retrieval was then performed, followed by BrdU IHC.

Microscopy and image analysis

Microscopy and image analysis performed as described in (**Chapter 3**).

Human proteome microarrays

Mouse and human *Pnky* RNA transcripts, along with a scrambled mouse *Pnky* control, were produced using the HiScribe T7 High Yield RNA Synthesis Kit (New England Biosciences).

RNA was purified using Trizol (Invitrogen). *Label IT*® Nucleic Acid Labeling Reagents Cy5 Kit (Mirus) was used to label RNA with Cy5. Labeled 25µg of RNA per 62.5µL reaction, and performed 8 reactions per transcript in order to obtain enough RNA for subsequent proteome microarray analysis. In order to achieve a labeling density of approximately 1-3 Cy5 dye molecules per transcript (Siprashvili et al., 2012) used Cy5 Label IT Reagent at a ratio of 1:20 and incubated at 37°C for 3 hours. Extracted labeled RNA using EtOH precipitation. Quantified labeling density as described in the *Label IT*® Nucleic Acid Labeling manual.

CDI Laboratories, Inc. performed human proteome microarray analysis using the Cy5-labeled transcripts described above and the HuProt v4.0 arrays. Interactions with Z-scores above 3.0 were statistically significant.

Scrambled mouse *Pnky* sequence

GTGGGTGCTACGCCCCATTATATCCGGGCGACGACAAGCACCGTTCAGCGTAATTA
ACACCTCGTTTCGGAACTTCTGACCACGAAGTTTTGAATGAATGCAGATTAGAGCACCGAT
CCAAATACTCGGTCGGTTGAGAGTGTAGCCGGCGGAACTGTCGTACCGTGTGACGCTTGA
ATCAGTTTACCTAATGTTGAGTAAAACCTCACAGAGAGCGCTACTTGTAACGTGTGCCCG
ATGCGGGAAACCTATGCATTGTTTCTACCTAGTCAGATTGGGAAACACCCCCGACCGCTTT
GAGTAGCTGTGCGAGGCATCGTGCGACCAGGCCTGCACTTAGACCGAAACGTAAACTGTG
ATAGCCCATCAACCGACAGCGTTGTAGTTAGTTCGCTCTCTGAAACACATTATGGCCCGAC
ACATAACTCACCATGCGCCGAGGGATACGACTCTCGAGTGTTGTCTGGTGCGTCACCCTG
TTTCTTCCACACGGTTGTTAATCGGTGGACCCCTCTTTAGCGGTTCAAAGATGTCTTTAGAT
CCCGCGCCAAGGGTAGCGGCCTACCTATATAGCATCGAGGGCAACCCGTCCGGTGATGC
CCAGGTGTTTGAGCCCCGTTTGTGAAATACATGCGCATACTCGCAGGAGCTATGGGTGTAA
AGATTCTCAGCAGAATAGATTCTAAATCTCCTGTTCCGAATGGATGTAGCCGTACATAACG
GAGTAAAGGGACGGTCGTACATCCTGGCCAGTTCGATCGTCATGTCATACGTTTAAGTACT
CCCACATACTAGCACTGAATAAGACGGTGAAATCAATATGT

Gene ontology analysis

Gene ontology analysis was performed using the Panther Classification System (Mi et al., 2010; Thomas et al., 2003), with the *Pnky*-interacting proteins listed in (**Table 4.2**) as the experimental set and all proteins present on the HuProt v4.0 microarrays as the background set. Performed “GO Biological Process Complete” analysis with FDR correction.

Figure preparation

Figures were prepared using Photoshop and Illustrator (Adobe) and Prism (GraphPad).

Quantification and Statistical Analysis

All *in vivo* quantifications were normalized to littermate controls. The statistical details of each experiment can be found in the relevant figure legends.

Chapter 5: Conclusions and Future Directions

Long noncoding RNAs (lncRNAs) comprise a class of noncoding transcripts that is extremely diverse in terms of biological function and molecular mechanism. While this diversity is quite intriguing, it introduces additional complications when attempting to determine what role a particular lncRNA might play. Whether a lncRNA has an important cellular function in a given tissue, and how the lncRNA might carry out that function at the molecular level, currently remain very difficult to predict. Moreover, certain lncRNAs — despite being expressed by multiple cell types — seem to have exquisitely cell type-specific biological functions (Liu et al., 2017). Because of this, experimental manipulations of lncRNA expression can produce complex phenotypes that vary based on the timing of the lncRNA perturbation and the cell type under investigation. Combining multiple complimentary approaches may therefore prove particularly useful for revealing the functions of lncRNAs.

This dissertation illustrates how we have now integrated a variety of experimental techniques to determine the role of the lncRNA *Pnky* in two distinct neural stem cell populations *in vivo*. **Chapter 2** describes how we began investigating the function of *Pnky* by using short hairpin RNAs (shRNAs) to deplete *Pnky* transcripts. These initial experiments predominantly relied on cultured neural stem cells (NSCs) from the mouse ventricular-subventricular zone (V-SVZ), and revealed that *Pnky* knockdown promotes neurogenic differentiation and expansion of the transit amplifying population. We also identified the splicing regulator PTBP1 as a protein interacting partner of *Pnky*. **Chapter 3** describes the generation of multiple novel genetic mouse lines to analyze the function of *Pnky* in the developing neocortex. Through conditional *Pnky* deletion in a small cohort of cortical NSCs, we demonstrate that loss of *Pnky* leads to precocious neurogenic differentiation in a cell-autonomous manner. By combining constitutive *Pnky* knockout with BAC transgenic expression of *Pnky*, we further determine that *Pnky*

regulates transcript abundance and splicing in *trans*, potentially through its physical interaction with PTBP1. **Chapter 4** focuses on the role of *Pnky* in the V-SVZ *in vivo*, and demonstrates that loss of *Pnky* results in the formation of intraventricular neuroblast nodules. Furthermore, *Pnky*-deletion alters progression through the V-SVZ neurogenic lineage by expanding the transit amplifying phase, and also leads to reduced long-term NSC abundance. In order to begin understanding the molecular function of *Pnky*, we identified a novel set of putative *Pnky*-interacting proteins, which were enriched for roles relating to RNA splicing. Taken together, these analyses demonstrate that *Pnky* is a lncRNA with important functions in neurogenesis *in vivo*, potentially through its physical interactions with splicing regulators.

As the lncRNA field moves forward, understanding the precise details of their intricate molecular mechanisms will be crucial for revealing how particular lncRNAs can play important roles in neurogenesis and neurological disorders. Toward this end, we combined multiple genetic mouse lines to determine that *Pnky* does not regulate its neighboring gene *Pou3f2* in *cis*, and instead functions in *trans* (see **Chapter 3**). Furthermore, we identified the RNA splicing regulator PTBP1 as an interacting partner of *Pnky* (see **Chapter 2**). PTBP1 is an important regulator of neural development (Keppetipola et al., 2012; Shibasaki et al., 2013), direct neuronal reprogramming (Xue et al., 2013), and brain tumor growth (Ferrarese et al., 2014), making this physical interaction of particular interest.

Importantly, we determined that depletion or loss of *Pnky* leads to altered splicing (see **Chapter 2** and **Chapter 3**). These splicing changes were found to significantly overlap with known PTBP1-regulated splicing events, further suggesting a relationship between *Pnky* and PTBP1. However, the molecular details of how *Pnky* might affect PTBP1-dependent splicing remain unclear. To address this, analyses such as PTBP1 CLIP-seq (Van Nostrand et al., 2016; Xue et al., 2009) in wild type and *Pnky*-deleted NSCs might provide crucial mechanistic insight into *Pnky* function. Such experiments could reveal specific downstream targets that are altered upon loss of *Pnky* and may underlie the phenotypes we have observed.

While PTBP1 might be an important contributor to the molecular function of *Pnky*, it is possible that *Pnky* also carries out PTBP1-independent roles. Therefore, determining whether *Pnky* interacts with additional proteins to carry out its *trans* functions will be another significant focus of future work. We have now identified a new list of putative *Pnky*-interacting proteins using human proteome arrays (see **Chapter 4**). While these arrays will not provide an exhaustive list of all potential protein binding partners, they can identify robust interactions. We found that many of the putative *Pnky*-interacting proteins were related to RNA splicing, further implicating *Pnky* in this process. In particular, the protein QKI was found to interact with both mouse and human *Pnky*. Given the role of QKI in neurogenic differentiation (Hayakawa-Yano et al., 2017; Shu et al., 2017), as well as its regulation of splicing networks that overlap with those of PTBP1 (Gazzara et al., 2014; Hall et al., 2013; Wu et al., 2002), QKI may be an especially important putative binding partner for further analysis.

Loss of *Pnky* results in aberrant cortical neurogenesis during embryonic development, leading to postnatal alterations in neuronal subtype abundance (see **Chapter 3**). This raises the intriguing possibility that these developmental defects may result in behavioral abnormalities in *Pnky*-KO mice. Interestingly, knockout of the lncRNA *Gomafu* has been found to produce a mild hyperactivity phenotype in mice, which is exacerbated by the psychostimulant methamphetamine (Ip et al., 2016). *Gomafu* binds to the splicing regulators QKI and SRSF1 (Barry et al., 2014), which we also identified as putative interacting partners of both mouse and human *Pnky* (see **Chapter 4**). Manipulation of *Gomafu* levels can also disrupt neurogenic differentiation in the developing cortex (Aprea et al., 2013); therefore, it will be useful to explore whether *Gomafu* and *Pnky* functionally affect one another.

Assessing whether loss of *Pnky* leads to behavioral defects will be especially interesting given that *Pnky* is conserved in human. We have previously shown that human *PNKY* is expressed in the developing cortex in a very similar pattern to mouse *Pnky*, with enrichment in the ventricular zone (VZ) where the NSCs reside (see **Chapter 2**). Many of the putative *Pnky*

binding proteins were also detected to interact with both mouse and human *Pnky*, consistent with a conserved functional role. Interestingly, we also found proteins that seemed to uniquely interact with either mouse or human *Pnky*, suggesting that there may be species-specific differences in *Pnky*-binding partners. We have observed that human *PNKY* is expressed in cerebral organoids and seems to be enriched in the VZ-like regions of the organoids (**Figure 3.5G**). Thus, cerebral organoids may serve as a tractable model system that can facilitate future studies regarding the function of human *PNKY*.

The mammalian central nervous system expresses a large diversity of lncRNAs, but only a small set of these lncRNAs have been experimentally manipulated. There are emerging examples of lncRNAs that are relevant to neurodevelopmental disorders (Briggs et al., 2015; Meng et al., 2015), which highlights the need to functionally characterize the roles of lncRNAs during brain development using animal models. There have been attempts to predict the functions of lncRNAs based on their underlying DNA sequence or genomic configuration (Engreitz et al., 2016; Liu et al., 2017; Luo et al., 2016); however, this currently remains a difficult challenge. Therefore, experimentally manipulating individual lncRNAs with a combination of approaches will likely be required to uncover important features of their biological function and molecular mechanism. *In vivo* lncRNA studies will provide a critical foundation for understanding how this diverse class of noncoding molecules can influence brain development and neurological disorders. As we have now shown that *Pnky* has significant roles during neurogenesis *in vivo*, moving forward it will be valuable to turn our focus toward unraveling the molecular mechanism through which *Pnky* functions. Given that most lncRNAs with *in vivo* roles are poorly understood at the molecular level, gaining deeper insights into how *Pnky* functions will have broad implications for the field of lncRNA biology, and will ultimately pave the way toward understanding how this unique class of molecules regulates processes from normal development to disease.

References

- Aberg, K., Saetre, P., Lindholm, E., Ekholm, B., Pettersson, U., Adolfsson, R., and Jazin, E. (2006b). Human QKI, a new candidate gene for schizophrenia involved in myelination. *Am. J. Med. Genet. Part B Neuropsychiatr. Genet.* *141B*, 84–90.
- Aberg, K., Saetre, P., Jareborg, N., and Jazin, E. (2006a). Human QKI, a potential regulator of mRNA expression of human oligodendrocyte-related genes involved in schizophrenia. *Proc. Natl. Acad. Sci.* *103*, 7482–7487.
- Albrecht, U., Sutcliffe, J.S., Cattanach, B.M., Beechey, C. V, Armstrong, D., Eichele, G., and Beaudet, A.L. (1997). Imprinted expression of the murine Angelman syndrome gene, *Ube3a*, in hippocampal and Purkinje neurons. *Nat. Genet.* *17*, 75–78.
- Alfano, G., Vitiello, C., Caccioppoli, C., Caramico, T., Carola, A., Szego, M.J., McInnes, R.R., Auricchio, A., and Banfi, S. (2005). Natural antisense transcripts associated with genes involved in eye development. *Hum. Mol. Genet.* *14*, 913–923.
- Anders, S., Reyes, A., and Huber, W. (2012). Detecting differential usage of exons from RNA-seq data. *Genome Res.* *22*, 2008–2017.
- Andersen, R.E., and Lim, D.A. (2018). Forging our understanding of lncRNAs in the brain. *Cell Tissue Res.* *371*, 55–71.
- Andersen, R.E., Hong, S.J., Lim, J.J., Cui, M., Harpur, B.A., Hwang, E., Delgado, R.N., Ramos, A.D., Liu, S.J., Blencowe, B.J., et al. (2019). The Long Noncoding RNA *Pnky* Is a Trans-acting Regulator of Cortical Development In Vivo. *Dev. Cell* *49*, 632–642.e7.
- Anderson, D.M., Anderson, K.M., Chang, C.-L., Makarewich, C.A., Nelson, B.R., McAnally, J.R., Kasaragod, P., Shelton, J.M., Liou, J., Bassel-Duby, R., et al. (2015). A micropeptide encoded by a putative long noncoding RNA regulates muscle performance. *Cell* *160*, 595–606.
- Anderson, K.M., Anderson, D.M., McAnally, J.R., Shelton, J.M., Bassel-Duby, R., and Olson, E.N. (2016). Transcription of the non-coding RNA *upperhand* controls *Hand2* expression and heart development. *Nature* *539*, 433–436.
- Anderson, S.A., Eisenstat, D.D., Shi, L., and Rubenstein, J.L. (1997a). Interneuron migration from

- basal forebrain to neocortex: dependence on Dlx genes. *Science* 278, 474–476.
- Anderson, S.A., Qiu, M., Bulfone, A., Eisenstat, D.D., Meneses, J., Pedersen, R., and Rubenstein, J.L. (1997b). Mutations of the homeobox genes Dlx-1 and Dlx-2 disrupt the striatal subventricular zone and differentiation of late born striatal neurons. *Neuron* 19, 27–37.
- Andrews, S.J., and Rothnagel, J.A. (2014). Emerging evidence for functional peptides encoded by short open reading frames. *Nat. Rev. Genet.* 15, 193–204.
- Aprea, J., and Calegari, F. (2015). Long non-coding RNAs in corticogenesis: deciphering the non-coding code of the brain. *EMBO J.* 34, 2865–2884.
- Aprea, J., Prenninger, S., Dori, M., Ghosh, T., Monasor, L.S., Wessendorf, E., Zocher, S., Massalini, S., Alexopoulou, D., Lesche, M., et al. (2013). Transcriptome sequencing during mouse brain development identifies long non-coding RNAs functionally involved in neurogenic commitment. *EMBO J.* 32, 3145–3160.
- Aranda, S., Mas, G., and Di Croce, L. (2015). Regulation of gene transcription by Polycomb proteins. *Sci. Adv.* 1, e1500737–e1500737.
- Arnold, S.J., Huang, G.-J., Cheung, A.F.P., Era, T., Nishikawa, S.-I., Bikoff, E.K., Molnár, Z., Robertson, E.J., and Groszer, M. (2008). The T-box transcription factor Eomes/Tbr2 regulates neurogenesis in the cortical subventricular zone. *Genes Dev.* 22, 2479–2484.
- Bambah-Mukku, D., Travaglia, A., Chen, D.Y., Pollonini, G., and Alberini, C.M. (2014). A positive autoregulatory BDNF feedback loop via C/EBP β mediates hippocampal memory consolidation. *J. Neurosci.* 34, 12547–12559.
- Barry, G., Briggs, J.A., Vanichkina, D.P., Poth, E.M., Beveridge, N.J., Ratnu, V.S., Nayler, S.P., Nones, K., Hu, J., Bredy, T.W., et al. (2014). The long non-coding RNA Gomafu is acutely regulated in response to neuronal activation and involved in schizophrenia-associated alternative splicing. *Mol. Psychiatry* 19, 486–494.
- Bartolomei, M.S., and Ferguson-Smith, A.C. (2011). Mammalian Genomic Imprinting. *Cold Spring Harb. Perspect. Biol.* 3, a002592–a002592.
- Bassett, A.R., Akhtar, A., Barlow, D.P., Bird, A.P., Brockdorff, N., Duboule, D., Ephrussi, A.,

- Ferguson-Smith, A.C., Gingeras, T.R., Haerty, W., et al. (2014). Considerations when investigating lncRNA function in vivo. *Elife* 3, e03058.
- Batista, P.J., and Chang, H.Y. (2013). Long noncoding RNAs: cellular address codes in development and disease. *Cell* 152, 1298–1307.
- Berghoff, E.G., Clark, M.F., Chen, S., Cajigas, I., Leib, D.E., and Kohtz, J.D. (2013). Evf2 (*Dlx6as*) lncRNA regulates ultraconserved enhancer methylation and the differential transcriptional control of adjacent genes. *Development* 140, 4407–4416.
- Binder, D.K., and Scharfman, H.E. (2004). Brain-derived neurotrophic factor. *Growth Factors* 22, 123–131.
- Blackshaw, S., Harpavat, S., Trimarchi, J., Cai, L., Huang, H., Kuo, W.P., Weber, G., Lee, K., Fraioli, R.E., Cho, S.-H., et al. (2004). Genomic analysis of mouse retinal development. *PLoS Biol.* 2, e247.
- Bond, A.M., Vangompel, M.J.W., Sametsky, E. a, Clark, M.F., Savage, J.C., Disterhoft, J.F., and Kohtz, J.D. (2009). Balanced gene regulation by an embryonic brain ncRNA is critical for adult hippocampal GABA circuitry. *Nat. Neurosci.* 12, 1020–1027.
- Bonini, N.M., Leiserson, W.M., and Benzer, S. (1993). The eyes absent gene: genetic control of cell survival and differentiation in the developing *Drosophila* eye. *Cell* 72, 379–395.
- Boutz, P.L., Stoilov, P., Li, Q., Lin, C.-H., Chawla, G., Ostrow, K., Shiue, L., Ares, M., and Black, D.L. (2007). A post-transcriptional regulatory switch in polypyrimidine tract-binding proteins reprograms alternative splicing in developing neurons. *Genes Dev.* 21, 1636–1652.
- Braunschweig, U., Barbosa-Morais, N.L., Pan, Q., Nachman, E.N., Alipanahi, B., Gonatopoulos-Pournatzis, T., Frey, B., Irimia, M., and Blencowe, B.J. (2014). Widespread intron retention in mammals functionally tunes transcriptomes. *Genome Res.* 24, 1774–1786.
- Bray, N.L., Pimentel, H., Melsted, P., and Pachter, L. (2016). Near-optimal probabilistic RNA-seq quantification. *Nat. Biotechnol.* 34, 525–527.
- Briata, P., Di Blas, E., Gulisano, M., Mallamaci, A., Iannone, R., Boncinelli, E., and Corte, G. (1996). EMX1 homeoprotein is expressed in cell nuclei of the developing cerebral cortex and in the

- axons of the olfactory sensory neurons. *Mech. Dev.* 57, 169–180.
- Briggs, J.A., Wolvetang, E.J., Mattick, J.S., Rinn, J.L., and Barry, G. (2015). Mechanisms of Long Non-coding RNAs in Mammalian Nervous System Development, Plasticity, Disease, and Evolution. *Neuron* 88, 861–877.
- Brown, C.J., Hendrich, B.D., Rupert, J.L., Lafrenière, R.G., Xing, Y., Lawrence, J., and Willard, H.F. (1992). The human XIST gene: analysis of a 17 kb inactive X-specific RNA that contains conserved repeats and is highly localized within the nucleus. *Cell* 71, 527–542.
- Cabili, M.N., Trapnell, C., Goff, L., Koziol, M., Tazon-Vega, B., Regev, A., and Rinn, J.L. (2011). Integrative annotation of human large intergenic noncoding RNAs reveals global properties and specific subclasses. *Genes Dev.* 25, 1915–1927.
- Cajigas, I., Leib, D.E., Cochrane, J., Luo, H., Swyter, K.R., Chen, S., Clark, B.S., Thompson, J., Yates, J.R., Kingston, R.E., et al. (2015). *Evf2* lncRNA/BRG1/DLX1 interactions reveal RNA-dependent inhibition of chromatin remodeling. *Development* 142, 2641–2652.
- Cajigas, I., Chakraborty, A., Swyter, K.R., Luo, H., Bastidas, M., Nigro, M., Morris, E.R., Chen, S., VanGompel, M.J.W., Leib, D., et al. (2018). The *Evf2* Ultraconserved Enhancer lncRNA Functionally and Spatially Organizes Megabase Distant Genes in the Developing Forebrain. *Mol. Cell* 71, 956–972.e9.
- Campbell, J.N., and Meyer, R.A. (2006). Mechanisms of neuropathic pain. *Neuron* 52, 77–92.
- Cech, T.R., and Steitz, J.A. (2014). The noncoding RNA revolution — trashing old rules to forge new ones. *Cell* 157, 77–94.
- Cepko, C. (2014). Intrinsically different retinal progenitor cells produce specific types of progeny. *Nat. Rev. Neurosci.* 15, 615–627.
- Chalei, V., Sansom, S.N., Kong, L., Lee, S., Montiel, J.F., Vance, K.W., and Ponting, C.P. (2014). The long non-coding RNA *Dali* is an epigenetic regulator of neural differentiation. *Elife* 3, e04530.
- Chapleau, C.A., Larimore, J.L., Theibert, A., and Pozzo-Miller, L. (2009). Modulation of dendritic spine development and plasticity by BDNF and vesicular trafficking: fundamental roles in

- neurodevelopmental disorders associated with mental retardation and autism. *J. Neurodev. Disord.* *1*, 185–196.
- Clark, B.S., and Blackshaw, S. (2014). Long non-coding RNA-dependent transcriptional regulation in neuronal development and disease. *Front. Genet.* *5*, 164.
- Cobos, I., Calcagnotto, M.E., Vilaythong, A.J., Thwin, M.T., Noebels, J.L., Baraban, S.C., and Rubenstein, J.L.R. (2005). Mice lacking *Dlx1* show subtype-specific loss of interneurons, reduced inhibition and epilepsy. *Nat. Neurosci.* *8*, 1059–1068.
- Currle, D.S., Hu, J.S., Kolski-Andreaco, A., and Monuki, E.S. (2007). Culture of Mouse Neural Stem Cell Precursors. *J. Vis. Exp.* e152–e152.
- Derrien, T., Johnson, R., Bussotti, G., Tanzer, A., Djebali, S., Tilgner, H., Guernec, G., Martin, D., Merkel, A., Knowles, D.G., et al. (2012). The GENCODE v7 catalog of human long noncoding RNAs: analysis of their gene structure, evolution, and expression. *Genome Res.* *22*, 1775–1789.
- Dimitrova, N., Zamudio, J.R., Jong, R.M., Soukup, D., Resnick, R., Sarma, K., Ward, A.J., Raj, A., Lee, J.T., Sharp, P.A., et al. (2014). LincRNA-p21 activates p21 in cis to promote Polycomb target gene expression and to enforce the G1/S checkpoint. *Mol. Cell* *54*, 777–790.
- Dinger, M.E., Amaral, P.P., Mercer, T.R., Pang, K.C., Bruce, S.J., Gardiner, B.B., Askarian-Amiri, M.E., Ru, K., Solda, G., Simons, C., et al. (2008). Long noncoding RNAs in mouse embryonic stem cell pluripotency and differentiation. *Genome Res.* *18*, 1433–1445.
- Djebali, S., Davis, C.A., Merkel, A., Dobin, A., Lassmann, T., Mortazavi, A., Tanzer, A., Lagarde, J., Lin, W., Schlesinger, F., et al. (2012). Landscape of transcription in human cells. *Nature* *489*, 101–108.
- Doetsch, F., Caillé, I., Lim, D.A., García-Verdugo, J.M., and Alvarez-Buylla, A. (1999). Subventricular zone astrocytes are neural stem cells in the adult mammalian brain. *Cell* *97*, 703–716.
- Doetsch, F., Petreanu, L., Caille, I., and Alvarez-buylla, A. (2002). EGF Converts Transit-Amplifying Neurogenic Precursors in the Adult Brain into Multipotent Stem Cells. *Neuron* *36*, 1021–1034.
- Dominguez, M.H., Ayoub, A.E., and Rakic, P. (2013). POU-III transcription factors (*Brn1*, *Brn2*, and

- Oct6) influence neurogenesis, molecular identity, and migratory destination of upper-layer cells of the cerebral cortex. *Cereb. Cortex* 23, 2632–2643.
- Durak, O., de Anda, F.C., Singh, K.K., Leussis, M.P., Petryshen, T.L., Sklar, P., and Tsai, L.-H. (2015). Ankyrin-G regulates neurogenesis and Wnt signaling by altering the subcellular localization of β -catenin. *Mol. Psychiatry* 20, 388–397.
- Elias, J.E., and Gygi, S.P. (2007). Target-decoy search strategy for increased confidence in large-scale protein identifications by mass spectrometry. *Nat. Methods* 4, 207–214.
- Engreitz, J.M., Pandya-Jones, A., McDonel, P., Shishkin, A., Sirokman, K., Surka, C., Kadri, S., Xing, J., Goren, A., Lander, E.S., et al. (2013). The Xist lncRNA exploits three-dimensional genome architecture to spread across the X chromosome. *Science* 341, 1237973.
- Engreitz, J.M., Haines, J.E., Perez, E.M., Munson, G., Chen, J., Kane, M., McDonel, P.E., Guttman, M., and Lander, E.S. (2016). Local regulation of gene expression by lncRNA promoters, transcription and splicing. *Nature* 539, 452–455.
- Faghihi, M.A., Modarresi, F., Khalil, A.M., Wood, D.E., Sahagan, B.G., Morgan, T.E., Finch, C.E., St. Laurent III, G., Kenny, P.J., and Wahlestedt, C. (2008). Expression of a noncoding RNA is elevated in Alzheimer's disease and drives rapid feed-forward regulation of β -secretase. *Nat. Med.* 14, 723–730.
- Feng, J., Bi, C., Clark, B.S., Mady, R., Shah, P., and Kohtz, J.D. (2006). The Evf-2 noncoding RNA is transcribed from the Dlx-5/6 ultraconserved region and functions as a Dlx-2 transcriptional coactivator. *Genes Dev.* 20, 1470–1484.
- Ferrarese, R., Harsh, G.R., Yadav, A.K., Bug, E., Maticzka, D., Reichardt, W., Dombrowski, S.M., Miller, T.E., Masilamani, A.P., Dai, F., et al. (2014). Lineage-specific splicing of a brain-enriched alternative exon promotes glioblastoma progression. *J. Clin. Invest.* 124, 2861–2876.
- Fulco, C.P., Munschauer, M., Anyoha, R., Munson, G., Grossman, S.R., Perez, E.M., Kane, M., Cleary, B., Lander, E.S., and Engreitz, J.M. (2016). Systematic mapping of functional enhancer-promoter connections with CRISPR interference. *Science* 354, 769–773.
- Gazzara, M.R., Vaquero-Garcia, J., Lynch, K.W., and Barash, Y. (2014). In silico to in vivo splicing

- analysis using splicing code models. *Methods* 67, 3–12.
- Geng, X., Lavado, A., Lagutin, O. V., Liu, W., and Oliver, G. (2007). Expression of Six3 Opposite Strand (Six3OS) during mouse embryonic development. *Gene Expr. Patterns* 7, 252–257.
- Gill, M., Vallada, H., Collier, D., Sham, P., Holmans, P., Murray, R., McGuffin, P., Nanko, S., Owen, M., Antonarakis, S., et al. (1996). A combined analysis of D22S278 marker alleles in affected sib-pairs: Support for a susceptibility locus for schizophrenia at chromosome 22q12. *Am. J. Med. Genet.* 67, 40–45.
- Gonçalves, J.T., Schafer, S.T., and Gage, F.H. (2016). Adult neurogenesis in the hippocampus: from stem cells to behavior. *Cell* 167, 897–914.
- Gorski, J. a, Talley, T., Qiu, M., Puelles, L., Rubenstein, J.L.R., and Jones, K.R. (2002). Cortical excitatory neurons and glia, but not GABAergic neurons, are produced in the Emx1-expressing lineage. *J. Neurosci.* 22, 6309–6314.
- Groff, A.F., Sanchez-Gomez, D.B., Soruco, M.M.L., Gerhardinger, C., Barutcu, A.R., Li, E., Elcavage, L., Plana, O., Sanchez, L. V, Lee, J.C., et al. (2016). In vivo characterization of Linc-p21 reveals functional cis-regulatory DNA elements. *Cell Rep.* 16, 2178–2186.
- Guil, S., and Esteller, M. (2012). Cis-acting noncoding RNAs: friends and foes. *Nat. Struct. Mol. Biol.* 19, 1068–1075.
- Guttman, M., Donaghey, J., Carey, B.W., Garber, M., Grenier, J.K., Munson, G., Young, G., Lucas, A.B., Ach, R., Bruhn, L., et al. (2011). lincRNAs act in the circuitry controlling pluripotency and differentiation. *Nature* 477, 295–300.
- Hacisuleyman, E., Goff, L.A., Trapnell, C., Williams, A., Henao-Mejia, J., Sun, L., McClanahan, P., Hendrickson, D.G., Sauvageau, M., Kelley, D.R., et al. (2014). Topological organization of multichromosomal regions by the long intergenic noncoding RNA Firre. *Nat. Struct. Mol. Biol.* 21, 198–206.
- Hall, M.P., Nagel, R.J., Fagg, W.S., Shiue, L., Cline, M.S., Perriman, R.J., Donohue, J.P., and Ares, M. (2013). Quaking and PTB control overlapping splicing regulatory networks during muscle cell differentiation. *RNA* 19, 627–638.

Han, H., Braunschweig, U., Gonatopoulos-Pournatzis, T., Weatheritt, R.J., Hirsch, C.L., Ha, K.C.H., Radovani, E., Nabeel-Shah, S., Sterne-Weiler, T., Wang, J., et al. (2017). Multilayered Control of Alternative Splicing Regulatory Networks by Transcription Factors. *Mol. Cell* 65, 539–553.e7.

Hart, R.P., and Goff, L.A. (2016). Long noncoding RNAs: central to nervous system development. *Int. J. Dev. Neurosci.* 55, 109–116.

Hasbi, A., Fan, T., Alijaniam, M., Nguyen, T., Perreault, M.L., O'Dowd, B.F., and George, S.R. (2009). Calcium signaling cascade links dopamine D1-D2 receptor heteromer to striatal BDNF production and neuronal growth. *Proc. Natl. Acad. Sci.* 106, 21377–21382.

Haupt, Y., Alexander, W.S., Barri, G., Klinken, S.P., and Adams, J.M. (1991). Novel zinc finger gene implicated as myc collaborator by retrovirally accelerated lymphomagenesis in E mu-myc transgenic mice. *Cell* 65, 753–763.

Hayakawa-Yano, Y., Suyama, S., Nogami, M., Yugami, M., Koya, I., Furukawa, T., Zhou, L., Abe, M., Sakimura, K., Takebayashi, H., et al. (2017). An RNA-binding protein, Qki5, regulates embryonic neural stem cells through pre-mRNA processing in cell adhesion signaling. *Genes Dev.* 31, 1910–1925.

He, D., Wang, J., Lu, Y., Deng, Y., Zhao, C., Xu, L., Chen, Y., Hu, Y.-C., Zhou, W., and Lu, Q.R. (2017). lncRNA functional networks in oligodendrocytes reveal stage-specific myelination control by an lncOL1/Suz12 complex in the CNS. *Neuron* 93, 362–378.

Heinz, S., Benner, C., Spann, N., Bertolino, E., Lin, Y.C., Laslo, P., Cheng, J.X., Murre, C., Singh, H., and Glass, C.K. (2010). Simple combinations of lineage-determining transcription factors prime cis-regulatory elements required for macrophage and B cell identities. *Mol. Cell* 38, 576–589.

Hitoshi, N., Ken-ichi, Y., and Jun-ichi, M. (1991). Efficient selection for high-expression transfectants with a novel eukaryotic vector. *Gene* 108, 193–199.

Holland, E.C., and Varmus, H.E. (1998). Basic fibroblast growth factor induces cell migration and proliferation after glia-specific gene transfer in mice. *Proc. Natl. Acad. Sci. U. S. A.* 95, 1218–1223.

- Horike, S., Cai, S., Miyano, M., Cheng, J.-F., and Kohwi-Shigematsu, T. (2004). Loss of silent-chromatin looping and impaired imprinting of DLX5 in Rett syndrome. *Nat. Genet.* 37, 31–40.
- Huang, D.W., Sherman, B.T., and Lempicki, R.A. (2009). Systematic and integrative analysis of large gene lists using DAVID bioinformatics resources. *Nat. Protoc.* 4, 44–57.
- Hudlebusch, H.R., Skotte, J., Santoni-Rugiu, E., Zimling, Z.G., Lees, M.J., Simon, R., Sauter, G., Rota, R., De Ioris, M.A., Quarto, M., et al. (2011). MMSET Is Highly Expressed and Associated with Aggressiveness in Neuroblastoma. *Cancer Res.* 71, 4226–4235.
- Ihrie, R.A., and Álvarez-Buylla, A. (2011). Lake-Front Property: A Unique Germinal Niche by the Lateral Ventricles of the Adult Brain. *Neuron* 70, 674–686.
- Imayoshi, I., and Kageyama, R. (2014). Oscillatory control of bHLH factors in neural progenitors. *Trends Neurosci.* 37, 531–538.
- Ip, J.Y., Sone, M., Nashiki, C., Pan, Q., Kitaichi, K., Yanaka, K., Abe, T., Takao, K., Miyakawa, T., Blencowe, B.J., et al. (2016). Gomafu lncRNA knockout mice exhibit mild hyperactivity with enhanced responsiveness to the psychostimulant methamphetamine. *Sci. Rep.* 6, 27204.
- Irimia, M., Weatheritt, R.J., Ellis, J.D., Parikhshak, N.N., Gonatopoulos-Pournatzis, T., Babor, M., Quesnel-Vallières, M., Tapial, J., Raj, B., O’Hanlon, D., et al. (2014). A Highly Conserved Program of Neuronal Microexons Is Misregulated in Autistic Brains. *Cell* 159, 1511–1523.
- Ishihama, Y., Oda, Y., Tabata, T., Sato, T., Nagasu, T., Rappsilber, J., and Mann, M. (2005). Exponentially modified protein abundance index (emPAI) for estimation of absolute protein amount in proteomics by the number of sequenced peptides per protein. *Mol. Cell. Proteomics* 4, 1265–1272.
- Ishikawa, K., Tanaka, M., Black, J.A., and Waxman, S.G. (1999). Changes in expression of voltage-gated potassium channels in dorsal root ganglion neurons following axotomy. *Muscle Nerve* 22, 502–507.
- Jemc, J., and Rebay, I. (2007). The eyes absent family of phosphotyrosine phosphatases: properties and roles in developmental regulation of transcription. *Annu. Rev. Biochem.* 76, 513–538.
- Jensen, A.M., and Wallace, V.A. (1997). Expression of Sonic hedgehog and its putative role as a

- precursor cell mitogen in the developing mouse retina. *Development* 124, 363–371.
- Jeong, J., Li, X., McEvilly, R.J., Rosenfeld, M.G., Lufkin, T., and Rubenstein, J.L.R. (2008). Dlx genes pattern mammalian jaw primordium by regulating both lower jaw-specific and upper jaw-specific genetic programs. *Development* 135, 2905–2916.
- Jiménez, C.R., Huang, L., Qiu, Y., and Burlingame, A.L. (1998). In-Gel Digestion of Proteins for MALDI-MS Fingerprint Mapping. In *Current Protocols in Protein Science*, (Hoboken, NJ, USA: John Wiley & Sons, Inc.), p. 16.4.1-16.4.5.
- Johnsson, P., Lipovich, L., Grandér, D., and Morris, K. V. (2014). Evolutionary conservation of long non-coding RNAs; sequence, structure, function. *Biochim. Biophys. Acta - Gen. Subj.* 1840, 1063–1071.
- Kaczmarek, J.C., Kowalski, P.S., and Anderson, D.G. (2017). Advances in the delivery of RNA therapeutics: from concept to clinical reality. *Genome Med.* 9, 60.
- Keppetipola, N., Sharma, S., Li, Q., and Black, D.L. (2012). Neuronal regulation of pre-mRNA splicing by polypyrimidine tract binding proteins, PTBP1 and PTBP2. *Crit. Rev. Biochem. Mol. Biol.* 47, 360–378.
- Khalil, A.M., Guttman, M., Huarte, M., Garber, M., Raj, A., Rivea Morales, D., Thomas, K., Presser, A., Bernstein, B.E., van Oudenaarden, A., et al. (2009). Many human large intergenic noncoding RNAs associate with chromatin-modifying complexes and affect gene expression. *Proc. Natl. Acad. Sci.* 106, 11667–11672.
- Kim, D., Langmead, B., and Salzberg, S.L. (2015). HISAT: a fast spliced aligner with low memory requirements. *Nat. Methods* 12, 357–360.
- Kim, D.S., Choi, J.O., Rim, H.D., and Cho, H.J. (2002). Downregulation of voltage-gated potassium channel alpha gene expression in dorsal root ganglia following chronic constriction injury of the rat sciatic nerve. *Brain Res. Mol. Brain Res.* 105, 146–152.
- Kishino, T., Lalande, M., and Wagstaff, J. (1997). UBE3A/E6-AP mutations cause Angelman syndrome. *Nat. Genet.* 15, 70–73.
- Kohtz, J.D., and Fishell, G. (2004). Developmental regulation of EVF-1, a novel non-coding RNA

- transcribed upstream of the mouse *Dlx6* gene. *Gene Expr. Patterns* 4, 407–412.
- Kong, L., Zhang, Y., Ye, Z.-Q., Liu, X.-Q., Zhao, S.-Q., Wei, L., and Gao, G. (2007). CPC: assess the protein-coding potential of transcripts using sequence features and support vector machine. *Nucleic Acids Res.* 35, W345-9.
- Kopp, F., and Mendell, J.T. (2018). Functional Classification and Experimental Dissection of Long Noncoding RNAs. *Cell* 172, 393–407.
- Kornienko, A.E., Guenzl, P.M., Barlow, D.P., and Pauler, F.M. (2013). Gene regulation by the act of long non-coding RNA transcription. *BMC Biol.* 11, 59.
- Kraus, P., Sivakamasundari, V., Lim, S.L., Xing, X., Lipovich, L., and Lufkin, T. (2013). Making sense of *Dlx1* antisense RNA. *Dev. Biol.* 376, 224–235.
- Kriegstein, A., and Alvarez-Buylla, A. (2009). The glial nature of embryonic and adult neural stem cells. *Annu. Rev. Neurosci.* 32, 149–184.
- Kuwajima, T., Nishimura, I., and Yoshikawa, K. (2006). *Necdin* promotes GABAergic neuron differentiation in cooperation with *Dlx* homeodomain proteins. *J. Neurosci.* 26, 5383–5392.
- Laird, F.M., Cai, H., Savonenko, A. V, Farah, M.H., He, K., Melnikova, T., Wen, H., Chiang, H.-C., Xu, G., Koliatsos, V.E., et al. (2005). *BACE1*, a major determinant of selective vulnerability of the brain to amyloid-beta amyloidogenesis, is essential for cognitive, emotional, and synaptic functions. *J. Neurosci.* 25, 11693–11709.
- Lakso, M., Pichel, J.G., Gorman, J.R., Sauer, B., Okamoto, Y., Lee, E., Alt, F.W., and Westphal, H. (1996). Efficient *in vivo* manipulation of mouse genomic sequences at the zygote stage. *Proc. Natl. Acad. Sci. U. S. A.* 93, 5860–5865.
- Lee, J.T. (2012). Epigenetic regulation by long noncoding RNAs. *Science* 338, 1435–1439.
- Lenstra, T.L., Rodriguez, J., Chen, H., and Larson, D.R. (2016). Transcription Dynamics in Living Cells. *Annu. Rev. Biophys.* 45, 25–47.
- Li, W., Notani, D., Ma, Q., Tanasa, B., Nunez, E., Chen, A.Y., Merkurjev, D., Zhang, J., Ohgi, K., Song, X., et al. (2013). Functional roles of enhancer RNAs for oestrogen-dependent transcriptional activation. *Nature* 498, 516–520.

- Licatalosi, D.D., Yano, M., Fak, J.J., Mele, A., Grabinski, S.E., Zhang, C., and Darnell, R.B. (2012). Ptbp2 represses adult-specific splicing to regulate the generation of neuronal precursors in the embryonic brain. *Genes Dev.* 26, 1626–1642.
- Lim, D.A., and Alvarez-Buylla, A. (2014). Adult neural stem cells stake their ground. *Trends Neurosci.* 37, 563–571.
- Lim, D.A., and Alvarez-Buylla, A. (2016). The Adult Ventricular-Subventricular Zone (V-SVZ) and Olfactory Bulb (OB) Neurogenesis. *Cold Spring Harb. Perspect. Biol.* 8, a018820-.
- Lim, D. a, Huang, Y.-C., Swigut, T., Mirick, A.L., Garcia-Verdugo, J.M., Wysocka, J., Ernst, P., and Alvarez-Buylla, A. (2009). Chromatin remodelling factor Mll1 is essential for neurogenesis from postnatal neural stem cells. *Nature* 458, 529–533.
- Lin, M.F., Jungreis, I., and Kellis, M. (2011). PhyloCSF: a comparative genomics method to distinguish protein coding and non-coding regions. *Bioinformatics* 27, i275-82.
- Lin, N., Chang, K.-Y., Li, Z., Gates, K., Rana, Z.A., Dang, J., Zhang, D., Han, T., Yang, C.-S., Cunningham, T.J., et al. (2014). An evolutionarily conserved long noncoding RNA TUNA controls pluripotency and neural lineage commitment. *Mol. Cell* 53, 1005–1019.
- Lipovich, L., Dachet, F., Cai, J., Bagla, S., Balan, K., Jia, H., and Loeb, J.A. (2012). Activity-dependent human brain coding/noncoding gene regulatory networks. *Genetics* 192, 1133–1148.
- Liu, S.J., and Lim, D.A. (2018). Modulating the expression of long non-coding RNAs for functional studies. *EMBO Rep.* 19, e46955.
- Liu, H., Sadygov, R.G., and Yates, J.R. (2004). A model for random sampling and estimation of relative protein abundance in shotgun proteomics. *Anal. Chem.* 76, 4193–4201.
- Liu, J.K., Ghattas, I., Liu, S., Chen, S., and Rubenstein, J.L.R. (1997). Dlx genes encode DNA-binding proteins that are expressed in an overlapping and sequential pattern during basal ganglia differentiation. *Dev. Dyn.* 210, 498–512.
- Liu, Q.-R., Walther, D., Drgon, T., Polesskaya, O., Lesnick, T.G., Strain, K.J., de Andrade, M., Bower, J.H., Maraganore, D.M., and Uhl, G.R. (2005). Human brain derived neurotrophic factor (BDNF) genes, splicing patterns, and assessments of associations with substance abuse and

- Parkinson's Disease. *Am. J. Med. Genet. B. Neuropsychiatr. Genet.* 134B, 93–103.
- Liu, S.J., Nowakowski, T.J., Pollen, A.A., Lui, J.H., Horlbeck, M.A., Attenello, F.J., He, D., Weissman, J.S., Kriegstein, A.R., Diaz, A.A., et al. (2016). Single-cell analysis of long non-coding RNAs in the developing human neocortex. *Genome Biol.* 17, 67.
- Liu, S.J., Horlbeck, M.A., Cho, S.W., Birk, H.S., Malatesta, M., He, D., Attenello, F.J., Villalta, J.E., Cho, M.Y., Chen, Y., et al. (2017). CRISPRi-based genome-scale identification of functional long noncoding RNA loci in human cells. *Science* 355, eaah7111.
- Lodato, S., and Arlotta, P. (2015). Generating Neuronal Diversity in the Mammalian Cerebral Cortex. *Annu. Rev. Cell Dev. Biol.* 31, 699–720.
- Lodato, S., Rouaux, C., Quast, K.B., Jantrachotechatchawan, C., Studer, M., Hensch, T.K., and Arlotta, P. (2011). Excitatory Projection Neuron Subtypes Control the Distribution of Local Inhibitory Interneurons in the Cerebral Cortex. *Neuron* 69, 763–779.
- Lois, C., and Alvarez-Buylla, A. (1994). Long-distance neuronal migration in the adult mammalian brain. *Science* 264, 1145–1148.
- Love, M.I., Huber, W., and Anders, S. (2014). Moderated estimation of fold change and dispersion for RNA-seq data with DESeq2. *Genome Biol.* 15, 550.
- Lui, J.H., Hansen, D. V, and Kriegstein, A.R. (2011). Development and evolution of the human neocortex. *Cell* 146, 18–36.
- Lundgren, D.H., Hwang, S.-I., Wu, L., and Han, D.K. (2010). Role of spectral counting in quantitative proteomics. *Expert Rev. Proteomics* 7, 39–53.
- Luo, S., Lu, J.Y., Liu, L., Yin, Y., Chen, C., Han, X., Wu, B., Xu, R., Liu, W., Yan, P., et al. (2016). Divergent lncRNAs Regulate Gene Expression and Lineage Differentiation in Pluripotent Cells. *Cell Stem Cell* 18, 637–652.
- Luo, X., Zhang, X., Shao, W., Yin, Y., and Zhou, J. (2009). Crucial roles of MZF-1 in the transcriptional regulation of apomorphine-induced modulation of FGF-2 expression in astrocytic cultures. *J. Neurochem.* 108, 952–961.
- Luskin, M.B. (1998). Neuroblasts of the postnatal mammalian forebrain: their phenotype and fate. *J.*

Neurobiol. 36, 221–233.

- Madisen, L., Zwingman, T.A., Sunkin, S.M., Oh, S.W., Zariwala, H.A., Gu, H., Ng, L.L., Palmiter, R.D., Hawrylycz, M.J., Jones, A.R., et al. (2010). A robust and high-throughput Cre reporting and characterization system for the whole mouse brain. *Nat. Neurosci.* 13, 133–140.
- Maenner, S., Blaud, M., Fouillen, L., Savoye, A., Marchand, V., Dubois, A., Sanglier-Cianfèrari, S., Van Dorsselaer, A., Clerc, P., Avner, P., et al. (2010). 2-D structure of the A region of Xist RNA and its implication for PRC2 association. *PLoS Biol.* 8, e1000276.
- Matsuura, T., Sutcliffe, J.S., Fang, P., Galjaard, R.-J., Jiang, Y., Benton, C.S., Rommens, J.M., and Beaudet, A.L. (1997). De novo truncating mutations in E6-AP ubiquitin-protein ligase gene (UBE3A) in Angelman syndrome. *Nat. Genet.* 15, 74–77.
- Mattick, J.S., and Rinn, J.L. (2015). Discovery and annotation of long noncoding RNAs. *Nat. Struct. Mol. Biol.* 22, 5–7.
- McGuinness, T., Porteus, M.H., Smiga, S., Bulfone, A., Kingsley, C., Qiu, M., Liu, J.K., Long, J.E., Xu, D., and Rubenstein, J.L. (1996). Sequence, organization, and transcription of the Dlx-1 and Dlx-2 locus. *Genomics* 35, 473–485.
- Meng, L., Person, R.E., and Beaudet, A.L. (2012). Ube3a-ATS is an atypical RNA polymerase II transcript that represses the paternal expression of Ube3a. *Hum. Mol. Genet.* 21, 3001–3012.
- Meng, L., Person, R.E., Huang, W., Zhu, P.J., Costa-Mattioli, M., and Beaudet, A.L. (2013). Truncation of Ube3a-ATS unsilences paternal Ube3a and ameliorates behavioral defects in the Angelman syndrome mouse model. *PLoS Genet.* 9, e1004039.
- Meng, L., Ward, A.J., Chun, S., Bennett, C.F., Beaudet, A.L., and Rigo, F. (2015). Towards a therapy for Angelman syndrome by targeting a long non-coding RNA. *Nature* 518, 409–412.
- Meng, S., Luo, M., Sun, H., Yu, X., Shen, M., Zhang, Q., Zhou, R., Ju, X., Tao, W., Liu, D., et al. (2010). Identification and characterization of Bmi-1-responding element within the human p16 promoter. *J. Biol. Chem.* 285, 33219–33229.
- Mercer, T.R., and Mattick, J.S. (2013). Structure and function of long noncoding RNAs in epigenetic regulation. *Nat. Struct. Mol. Biol.* 20, 300–307.

- Mercer, T.R., Dinger, M.E., Sunkin, S.M., Mehler, M.F., and Mattick, J.S. (2008). Specific expression of long noncoding RNAs in the mouse brain. *Proc. Natl. Acad. Sci.* *105*, 716–721.
- Mercer, T.R., Qureshi, I.A., Gokhan, S., Dinger, M.E., Li, G., Mattick, J.S., and Mehler, M.F. (2010). Long noncoding RNAs in neuronal-glia fate specification and oligodendrocyte lineage maturation. *BMC Neurosci.* *11*, 14.
- Merkle, F.T., Mirzadeh, Z., and Alvarez-Buylla, A. (2007). Mosaic organization of neural stem cells in the adult brain. *Science* *317*, 381–384.
- Mesman, S., and Smidt, M.P. (2017). Tcf12 Is Involved in Early Cell-Fate Determination and Subset Specification of Midbrain Dopamine Neurons. *Front. Mol. Neurosci.* *10*, 353.
- Mi, H., Dong, Q., Muruganujan, A., Gaudet, P., Lewis, S., and Thomas, P.D. (2010). PANTHER version 7: improved phylogenetic trees, orthologs and collaboration with the Gene Ontology Consortium. *Nucleic Acids Res.* *38*, D204–D210.
- Mikkelsen, T.S., Ku, M., Jaffe, D.B., Issac, B., Lieberman, E., Giannoukos, G., Alvarez, P., Brockman, W., Kim, T.-K., Koche, R.P., et al. (2007). Genome-wide maps of chromatin state in pluripotent and lineage-committed cells. *Nature* *448*, 553–560.
- Mirzadeh, Z., Merkle, F.T., Soriano-Navarro, M., Garcia-Verdugo, J.M., and Alvarez-Buylla, A. (2008). Neural Stem Cells Confer Unique Pinwheel Architecture to the Ventricular Surface in Neurogenic Regions of the Adult Brain. *Cell Stem Cell* *3*, 265–278.
- Mirzadeh, Z., Doetsch, F., Sawamoto, K., Wichterle, H., and Alvarez-Buylla, A. (2010). The subventricular zone en-face: wholemount staining and ependymal flow. *J. Vis. Exp.* e1938.
- Miyazaki, K., Wakabayashi, M., Chikahisa, S., Sei, H., and Ishida, N. (2007). PER2 controls circadian periods through nuclear localization in the suprachiasmatic nucleus. *Genes to Cells* *12*, 1225–1234.
- Modarresi, F., Faghihi, M.A., Lopez-Toledano, M.A., Fatemi, R.P., Magistri, M., Brothers, S.P., van der Brug, M.P., and Wahlestedt, C. (2012). Inhibition of natural antisense transcripts in vivo results in gene-specific transcriptional upregulation. *Nat. Biotechnol.* *30*, 453–459.
- Mohammad, F., Mondal, T., and Kanduri, C. (2009). Epigenetics of imprinted long non-coding RNAs.

Epigenetics 4, 277–286.

Molyneaux, B.J., Arlotta, P., Hirata, T., Hibi, M., and Macklis, J.D. (2005). Fez1 Is Required for the Birth and Specification of Corticospinal Motor Neurons. *Neuron* 47, 817–831.

Molyneaux, B.J., Arlotta, P., Menezes, J.R.L., and Macklis, J.D. (2007). Neuronal subtype specification in the cerebral cortex. *Nat. Rev. Neurosci.* 8, 427–437.

Morikawa, T., and Manabe, T. (2010). Aberrant regulation of alternative pre-mRNA splicing in schizophrenia. *Neurochem. Int.* 57, 691–704.

Nagano, T., Mitchell, J.A., Sanz, L.A., Pauler, F.M., Ferguson-Smith, A.C., Feil, R., and Fraser, P. (2008). The Air noncoding RNA epigenetically silences transcription by targeting G9a to chromatin. *Science* (80-.).

Nakagawa, S. (2016). Lessons from reverse-genetic studies of lncRNAs. *Biochim. Biophys. Acta - Gene Regul. Mech.* 1859, 177–183.

Nan, X., Ng, H.-H., Johnson, C.A., Laherty, C.D., Turner, B.M., Eisenman, R.N., Bird, A., Nan, X., Ng, H.-H., Johnson, C.A., et al. (1998). Transcriptional repression by the methyl-CpG-binding protein MeCP2 involves a histone deacetylase complex. *Nature* 393, 386–389.

Nelson, B.R., Makarewich, C.A., Anderson, D.M., Winders, B.R., Troupes, C.D., Wu, F., Reese, A.L., McAnally, J.R., Chen, X., Kavalali, E.T., et al. (2016). A peptide encoded by a transcript annotated as long noncoding RNA enhances SERCA activity in muscle. *Science* (80-.). 351, 271–275.

Ng, S.-Y., Johnson, R., and Stanton, L.W. (2012). Human long non-coding RNAs promote pluripotency and neuronal differentiation by association with chromatin modifiers and transcription factors. *EMBO J.* 31, 522–533.

Ng, S.-Y., Bogu, G.K., Soh, B.S., and Stanton, L.W. (2013). The long noncoding RNA RMST interacts with SOX2 to regulate neurogenesis. *Mol. Cell* 51, 349–359.

Van Nostrand, E.L., Pratt, G.A., Shishkin, A.A., Gelboin-Burkhart, C., Fang, M.Y., Sundararaman, B., Blue, S.M., Nguyen, T.B., Surka, C., Elkins, K., et al. (2016). Robust transcriptome-wide discovery of RNA-binding protein binding sites with enhanced CLIP (eCLIP). *Nat. Methods* 13,

508–514.

- Oltersdorf, T., Ward, P.J., Henriksson, T., Beattie, E.C., Neve, R., Lieberburg, I., and Fritz, L.C. (1990). The Alzheimer amyloid precursor protein. Identification of a stable intermediate in the biosynthetic/degradative pathway. *J. Biol. Chem.* 265, 4492–4497.
- Ørom, U.A., Derrien, T., Beringer, M., Gumireddy, K., Gardini, A., Bussotti, G., Lai, F., Zytnicki, M., Notredame, C., Huang, Q., et al. (2010). Long noncoding RNAs with enhancer-like function in human cells. *Cell* 143, 46–58.
- Pandey, R.R., Mondal, T., Mohammad, F., Enroth, S., Redrup, L., Komorowski, J., Nagano, T., Mancini-Dinardo, D., and Kanduri, C. (2008). Kcnq1ot1 antisense noncoding RNA mediates lineage-specific transcriptional silencing through chromatin-level regulation. *Mol. Cell* 32, 232–246.
- Paralkar, V.R., Taborda, C.C., Huang, P., Yao, Y., Kossenkov, A. V., Prasad, R., Luan, J., Davies, J.O.J., Hughes, J.R., Hardison, R.C., et al. (2016). Unlinking an lncRNA from its associated cis element. *Mol. Cell* 62, 104–110.
- Park, D.H., Hong, S.J., Salinas, R.D., Liu, S.J., Sun, S.W., Sgualdino, J., Testa, G., Matzuk, M.M., Iwamori, N., and Lim, D.A. (2014). Activation of neuronal gene expression by the JMJD3 demethylase is required for postnatal and adult brain neurogenesis. *Cell Rep.* 8, 1290–1299.
- Pastrana, E., Cheng, L.-C., and Doetsch, F. (2009). Simultaneous prospective purification of adult subventricular zone neural stem cells and their progeny. *Proc. Natl. Acad. Sci. U. S. A.* 106, 6387–6392.
- Pavlaki, I., Alammari, F., Sun, B., Clark, N., Sirey, T., Lee, S., Woodcock, D.J., Ponting, C.P., Szele, F.G., and Vance, K.W. (2018). The long non-coding RNA *Paupar* promotes KAP1-dependent chromatin changes and regulates olfactory bulb neurogenesis. *EMBO J.* 37, e98219.
- Penny, G.D., Kay, G.F., Sheardown, S.A., Rastan, S., and Brockdorff, N. (1996). Requirement for Xist in X chromosome inactivation. *Nature* 379, 131–137.
- Peretto, P., Merighi, A., Fasolo, A., and Bonfanti, L. (1997). Glial tubes in the rostral migratory stream of the adult rat. *Brain Res. Bull.* 42, 9–21.

- Perez-Garcia, C.G. (2015). ErbB4 in Laminated Brain Structures: A Neurodevelopmental Approach to Schizophrenia. *Front. Cell. Neurosci.* 9, 472.
- Peukert, D., Weber, S., Lumsden, A., and Scholpp, S. (2011). Lhx2 and Lhx9 Determine Neuronal Differentiation and Compartmentation in the Caudal Forebrain by Regulating Wnt Signaling. *PLoS Biol.* 9, e1001218.
- Pignoni, F., Hu, B., Zavitz, K.H., Xiao, J., Garrity, P.A., and Zipursky, S.L. (1997). The eye-specification proteins So and Eya form a complex and regulate multiple steps in Drosophila eye development. *Cell* 91, 881–891.
- Plath, K., Mlynarczyk-Evans, S., Nusinow, D.A., and Panning, B. (2002). Xist RNA and the mechanism of X chromosome inactivation. *Annu. Rev. Genet.* 36, 233–278.
- Pleasure, S.J., Anderson, S., Hevner, R., Bagri, A., Marin, O., Lowenstein, D.H., and Rubenstein, J.L. (2000). Cell migration from the ganglionic eminences is required for the development of hippocampal GABAergic interneurons. *Neuron* 28, 727–740.
- Polydorides, A.D., Okano, H.J., Yang, Y.Y., Stefani, G., and Darnell, R.B. (2000). A brain-enriched polypyrimidine tract-binding protein antagonizes the ability of Nova to regulate neuron-specific alternative splicing. *Proc. Natl. Acad. Sci. U. S. A.* 97, 6350–6355.
- Ponti, G., Obernier, K., Guinto, C., Jose, L., Bonfanti, L., and Alvarez-Buylla, A. (2013). Cell cycle and lineage progression of neural progenitors in the ventricular-subventricular zones of adult mice. *Proc. Natl. Acad. Sci. U. S. A.* 110, E1045-54.
- Porteus, M.H., Bulfone, A., Liu, J.K., Puellas, L., Lo, L.C., and Rubenstein, J.L. (1994). DLX-2, MASH-1, and MAP-2 expression and bromodeoxyuridine incorporation define molecularly distinct cell populations in the embryonic mouse forebrain. *J. Neurosci.* 14, 6370–6383.
- Quinn, J.J., and Chang, H.Y. (2015). Unique features of long non-coding RNA biogenesis and function. *Nat. Rev. Genet.* 17, 47–62.
- Raj, B., Irimia, M., Braunschweig, U., Sterne-Weiler, T., O’Hanlon, D., Lin, Z.-Y., Chen, G.I., Easton, L.E., Ule, J., Gingras, A.-C., et al. (2014). A Global Regulatory Mechanism for Activating an Exon Network Required for Neurogenesis. *Mol. Cell* 56, 90–103.

- Ramos, A.D., Diaz, A., Nellore, A., Delgado, R.N., Park, K.-Y., Gonzales-Roybal, G., Oldham, M.C., Song, J.S., and Lim, D.A. (2013). Integration of genome-wide approaches identifies lncRNAs of adult neural stem cells and their progeny in vivo. *Cell Stem Cell* 12, 616–628.
- Ramos, A.D., Andersen, R.E., Liu, S.J., Nowakowski, T.J., Hong, S.J., Gertz, C.C., Salinas, R.D., Zarabi, H., Kriegstein, A.R., and Lim, D.A. (2015). The long noncoding RNA Pnky regulates neuronal differentiation of embryonic and postnatal neural stem cells. *Cell Stem Cell* 16, 439–447.
- Ramos, A.D., Attenello, F.J., and Lim, D.A. (2016). Uncovering the roles of long noncoding RNAs in neural development and glioma progression. *Neurosci. Lett.* 625, 70–79.
- Rani, N., Nowakowski, T.J., Zhou, H., Godshalk, S.E., Lisi, V., Kriegstein, A.R., and Kosik, K.S. (2016). A primate lncRNA mediates notch signaling during neuronal development by sequestering miRNA. *Neuron* 90, 1174–1188.
- Rapicavoli, N.A., Poth, E.M., and Blackshaw, S. (2010). The long noncoding RNA RNCR2 directs mouse retinal cell specification. *BMC Dev. Biol.* 10, 49.
- Rapicavoli, N.A., Poth, E.M., Zhu, H., and Blackshaw, S. (2011). The long noncoding RNA Six3OS acts in trans to regulate retinal development by modulating Six3 activity. *Neural Dev.* 6, 32.
- Rinn, J.L., and Chang, H.Y. (2012). Genome regulation by long noncoding RNAs. *Annu. Rev. Biochem.* 81, 145–166.
- Rinn, J.L., Kertesz, M., Wang, J.K., Squazzo, S.L., Xu, X., Brugmann, S. a., Goodnough, L.H., Helms, J. a., Farnham, P.J., Segal, E., et al. (2007). Functional Demarcation of Active and Silent Chromatin Domains in Human HOX Loci by Noncoding RNAs. *Cell* 129, 1311–1323.
- Roan, N.R., Chu, S., Liu, H., Neidleman, J., Witkowska, H.E., and Greene, W.C. (2014). Interaction of fibronectin with semen amyloids synergistically enhances HIV infection. *J. Infect. Dis.* 210, 1062–1066.
- Rougeulle, C., Glatt, H., and Lalande, M. (1997). The Angelman syndrome candidate gene, UBE3A/MECP2-AP, is imprinted in brain. *Nat. Genet.* 17, 14–15.
- Rubenstein, J.L.R. (2011). Annual Research Review: Development of the cerebral cortex:

- implications for neurodevelopmental disorders. *J. Child Psychol. Psychiatry.* 52, 339–355.
- Ruzankina, Y., Pinzon-Guzman, C., Asare, A., Ong, T., Pontano, L., Cotsarelis, G., Zediak, V.P., Velez, M., Bhandoola, A., and Brown, E.J. (2007). Deletion of the Developmentally Essential Gene ATR in Adult Mice Leads to Age-Related Phenotypes and Stem Cell Loss. *Cell Stem Cell* 1, 113–126.
- Saito, T. (2006). In vivo electroporation in the embryonic mouse central nervous system. *Nat. Protoc.* 1, 1552–1558.
- Sauvageau, M., Goff, L.A., Lodato, S., Bonev, B., Groff, A.F., Gerhardinger, C., Sanchez-Gomez, D.B., Hacisuleyman, E., Li, E., Spence, M., et al. (2013). Multiple knockout mouse models reveal lincRNAs are required for life and brain development. *Elife* 2, e01749.
- Schindelin, J., Arganda-Carreras, I., Frise, E., Kaynig, V., Longair, M., Pietzsch, T., Preibisch, S., Rueden, C., Saalfeld, S., Schmid, B., et al. (2012). Fiji: an open-source platform for biological-image analysis. *Nat. Methods* 9, 676–682.
- Shearwin, K.E., Callen, B.P., and Egan, J.B. (2005). Transcriptional interference — a crash course. *Trends Genet.* 21, 339–345.
- Shibasaki, T., Tokunaga, A., Sakamoto, R., Sagara, H., Noguchi, S., Sasaoka, T., and Yoshida, N. (2013). PTB deficiency causes the loss of adherens junctions in the dorsal telencephalon and leads to lethal hydrocephalus. *Cereb. Cortex* 23, 1824–1835.
- Shu, P., Fu, H., Zhao, X., Wu, C., Ruan, X., Zeng, Y., Liu, W., Wang, M., Hou, L., Chen, P., et al. (2017). MicroRNA-214 modulates neural progenitor cell differentiation by targeting Quaking during cerebral cortex development. *Sci. Rep.* 7, 8014.
- Silva, C.G., Peyre, E., Adhikari, M.H., Tielens, S., Tanco, S., Van Damme, P., Magno, L., Krusy, N., Agirman, G., Magiera, M.M., et al. (2018). Cell-Intrinsic Control of Interneuron Migration Drives Cortical Morphogenesis. *Cell* 172, 1063–1078.e19.
- Simeone, A., Acampora, D., Gulisano, M., Stornaiuolo, A., and Boncinelli, E. (1992). Nested expression domains of four homeobox genes in developing rostral brain. *Nature* 358, 687–690.
- Siprashvili, Z., Webster, D.E., Kretz, M., Johnston, D., Rinn, J.L., Chang, H.Y., and Khavari, P.A.

- (2012). Identification of proteins binding coding and non-coding human RNAs using protein microarrays. *BMC Genomics* 13, 633.
- Sone, M., Hayashi, T., Tarui, H., Agata, K., Takeichi, M., and Nakagawa, S. (2007). The mRNA-like noncoding RNA Gomafu constitutes a novel nuclear domain in a subset of neurons. *J. Cell Sci.* 120, 2498–2506.
- Spadaro, P.A., Flavell, C.R., Widagdo, J., Ratnu, V.S., Troup, M., Ragan, C., Mattick, J.S., and Bredy, T.W. (2015). Long noncoding RNA-directed epigenetic regulation of gene expression is associated with anxiety-like behavior in mice. *Biol. Psychiatry* 78, 848–859.
- Strimmer, K. (2008). fdrtool: a versatile R package for estimating local and tail area-based false discovery rates. *Bioinformatics* 24, 1461–1462.
- Su, Y., Ryder, J., and Ni, B. (2003). Inhibition of Abeta production and APP maturation by a specific PKA inhibitor. *FEBS Lett.* 546, 407–410.
- Sugitani, Y., Nakai, S., Minowa, O., Nishi, M., Jishage, K.-I., Kawano, H., Mori, K., Ogawa, M., and Noda, T. (2002). Brn-1 and Brn-2 share crucial roles in the production and positioning of mouse neocortical neurons. *Genes Dev.* 16, 1760–1765.
- Takahashi, S., Ohtsuki, T., Yu, S.-Y., Tanabe, E., Yara, K., Kamioka, M., Matsushima, E., Matsuura, M., Ishikawa, K., Minowa, Y., et al. (2003). Significant linkage to chromosome 22q for exploratory eye movement dysfunction in schizophrenia. *Am. J. Med. Genet.* 123B, 27–32.
- Talkowski, M.E., Maussion, G., Crapper, L., Rosenfeld, J.A., Blumenthal, I., Hanscom, C., Chiang, C., Lindgren, A., Pereira, S., Ruderfer, D., et al. (2012). Disruption of a large intergenic noncoding RNA in subjects with neurodevelopmental disabilities. *Am. J. Hum. Genet.* 91, 1128–1134.
- Tamagno, E., Bardini, P., Guglielmotto, M., Danni, O., and Tabaton, M. (2006). The various aggregation states of beta-amyloid 1-42 mediate different effects on oxidative stress, neurodegeneration, and BACE-1 expression. *Free Radic. Biol. Med.* 41, 202–212.
- Terranova, R., Yokobayashi, S., Stadler, M.B., Otte, A.P., van Lohuizen, M., Orkin, S.H., Peters, A.H.F.M., Bickmore, W.A., Feil, R., Segal, E., et al. (2008). Polycomb group proteins Ezh2 and

- Rnf2 direct genomic contraction and imprinted repression in early mouse embryos. *Dev. Cell* *15*, 668–679.
- Thomas, P.D., Campbell, M.J., Kejariwal, A., Mi, H., Karlak, B., Daverman, R., Diemer, K., Muruganujan, A., and Narechania, A. (2003). PANTHER: a library of protein families and subfamilies indexed by function. *Genome Res.* *13*, 2129–2141.
- Tronche, F., Kellendonk, C., Kretz, O., Gass, P., Anlag, K., Orban, P.C., Bock, R., Klein, R., and Schütz, G. (1999). Disruption of the glucocorticoid receptor gene in the nervous system results in reduced anxiety. *Nat. Genet.* *23*, 99–103.
- Tsuiji, H., Yoshimoto, R., Hasegawa, Y., Furuno, M., Yoshida, M., and Nakagawa, S. (2011). Competition between a noncoding exon and introns: Gomafu contains tandem UACUAAC repeats and associates with splicing factor-1. *Genes to Cells* *16*, 479–490.
- Ulitsky, I. (2016). Evolution to the rescue: using comparative genomics to understand long non-coding RNAs. *Nat. Rev. Genet.* *17*, 601–614.
- Ulitsky, I., Shkumatava, A., Jan, C.H., Sive, H., and Bartel, D.P. (2011). Conserved function of lincRNAs in vertebrate embryonic development despite rapid sequence evolution. *Cell* *147*, 1537–1550.
- Vance, K.W., Sansom, S.N., Lee, S., Chalei, V., Kong, L., Cooper, S.E., Oliver, P.L., and Ponting, C.P. (2014). The long non-coding RNA Paupar regulates the expression of both local and distal genes. *EMBO J.* *33*, 296–311.
- Vassar, R. (2001). The beta-secretase, BACE: a prime drug target for Alzheimer's disease. *J. Mol. Neurosci.* *17*, 157–170.
- Vassar, R., Bennett, B.D., Babu-Khan, S., Kahn, S., Mendiaz, E.A., Denis, P., Teplow, D.B., Ross, S., Amarante, P., Loeloff, R., et al. (1999). Beta-secretase cleavage of Alzheimer's amyloid precursor protein by the transmembrane aspartic protease BACE. *Science* *286*, 735–741.
- Venkatesh, S., and Workman, J.L. (2015). Histone exchange, chromatin structure and the regulation of transcription. *Nat. Rev. Mol. Cell Biol.* *16*, 178–189.
- Ventura, A., Meissner, A., Dillon, C.P., McManus, M., Sharp, P.A., Van Parijs, L., Jaenisch, R., and

- Jacks, T. (2004). Cre-lox-regulated conditional RNA interference from transgenes. *Proc. Natl. Acad. Sci. U. S. A.* *101*, 10380–10385.
- Vierbuchen, T., Ostermeier, A., Pang, Z.P., Kokubu, Y., Südhof, T.C., and Wernig, M. (2010). Direct conversion of fibroblasts to functional neurons by defined factors. *Nature* *463*, 1035–1041.
- Viré, E., Brenner, C., Deplus, R., Blanchon, L., Fraga, M., Didelot, C., Morey, L., Van Eynde, A., Bernard, D., Vanderwinden, J.-M., et al. (2005). The Polycomb group protein EZH2 directly controls DNA methylation. *Nature* *439*, 871–874.
- Vu, T.H., and Hoffman, A.R. (1997). Imprinting of the Angelman syndrome gene, UBE3A, is restricted to brain. *Nat. Genet.* *17*, 12–13.
- Wagschal, A., Rousset, E., Basavarajiah, P., Contreras, X., Harwig, A., Laurent-Chabalier, S., Nakamura, M., Chen, X., Zhang, K., Meziane, O., et al. (2012). Microprocessor, Setx, Xrn2, and Rrp6 co-operate to induce premature termination of transcription by RNAPII. *Cell* *150*, 1147–1157.
- Wang, C., and Mei, L. (2013). In Utero Electroporation in Mice. (Humana Press, Totowa, NJ), pp. 151–163.
- Wang, K.C., Yang, Y.W., Liu, B., Sanyal, A., Corces-Zimmerman, R., Chen, Y., Lajoie, B.R., Protacio, A., Flynn, R.A., Gupta, R.A., et al. (2011). A long noncoding RNA maintains active chromatin to coordinate homeotic gene expression. *Nature* *472*, 120–124.
- Wang, L., Park, H.J., Dasari, S., Wang, S., Kocher, J.-P., and Li, W. (2013). CPAT: Coding-Potential Assessment Tool using an alignment-free logistic regression model. *Nucleic Acids Res.* *41*, e74.
- Wang, W., Côté, J., Xue, Y., Zhou, S., Khavari, P.A., Biggar, S.R., Muchardt, C., Kalpana, G. V., Goff, S.P., Yaniv, M., et al. (1996). Purification and biochemical heterogeneity of the mammalian SWI-SNF complex. *EMBO J.* *15*, 5370–5382.
- Wang, X., Spandidos, A., Wang, H., and Seed, B. (2012). PrimerBank: a PCR primer database for quantitative gene expression analysis, 2012 update. *Nucleic Acids Res.* *40*, D1144-9.
- Warming, S., Costantino, N., Court, D.L., Jenkins, N.A., and Copeland, N.G. (2005). Simple and highly efficient BAC recombineering using galK selection. *Nucleic Acids Res.* *33*, e36.

- West, S., Gromak, N., and Proudfoot, N.J. (2004). Human 5' → 3' exonuclease Xrn2 promotes transcription termination at co-transcriptional cleavage sites. *Nature* 432, 522–525.
- Willem, M., Garratt, A.N., Novak, B., Citron, M., Kaufmann, S., Rittger, A., DeStrooper, B., Saftig, P., Birchmeier, C., and Haass, C. (2006). Control of peripheral nerve myelination by the beta-secretase BACE1. *Science* (80-.). 314, 664–666.
- Willems, E., Leyns, L., and Vandesompele, J. (2008). Standardization of real-time PCR gene expression data from independent biological replicates. *Anal. Biochem.* 379, 127–129.
- Wu, J.I., Reed, R.B., Grabowski, P.J., and Artzt, K. (2002). Function of quaking in myelination: Regulation of alternative splicing. *Proc. Natl. Acad. Sci.* 99, 4233–4238.
- Xue, Y., Zhou, Y., Wu, T., Zhu, T., Ji, X., Kwon, Y.-S., Zhang, C., Yeo, G., Black, D.L., Sun, H., et al. (2009). Genome-wide Analysis of PTB-RNA Interactions Reveals a Strategy Used by the General Splicing Repressor to Modulate Exon Inclusion or Skipping. *Mol. Cell* 36, 996–1006.
- Xue, Y., Ouyang, K., Huang, J., Zhou, Y., Ouyang, H., Li, H., Wang, G., Wu, Q., Wei, C., Bi, Y., et al. (2013). Direct conversion of fibroblasts to neurons by reprogramming PTB-regulated microRNA circuits. *Cell* 152, 82–96.
- Yamasaki, K., Joh, K., Ohta, T., Masuzaki, H., Ishimaru, T., Mukai, T., Niikawa, N., Ogawa, M., Wagstaff, J., and Kishino, T. (2003). Neurons but not glial cells show reciprocal imprinting of sense and antisense transcripts of Ube3a. *Hum. Mol. Genet.* 12, 837–847.
- Yang, Y., Wen, L., and Zhu, H. (2015). Unveiling the hidden function of long non-coding RNA by identifying its major partner-protein. *Cell Biosci.* 5, 59.
- Yap, K., Lim, Z.Q., Khandelia, P., Friedman, B., and Makeyev, E. V (2012). Coordinated regulation of neuronal mRNA steady-state levels through developmentally controlled intron retention. *Genes Dev.* 26, 1209–1223.
- Yin, Y., Yan, P., Lu, J., Song, G., Zhu, Y., Li, Z., Zhao, Y., Shen, B., Huang, X., Zhu, H., et al. (2015). Opposing roles for the lncRNA Haunt and its genomic locus in regulating HOXA gene activation during embryonic stem cell differentiation. *Cell Stem Cell* 16, 504–516.
- Yoshimura, R., Ito, K., and Endo, Y. (2009). Differentiation/maturation of neuropeptide Y neurons in

- the corpus callosum is promoted by brain-derived neurotrophic factor in mouse brain slice cultures. *Neurosci. Lett.* *450*, 262–265.
- Young, T.L., Matsuda, T., and Cepko, C.L. (2005). The noncoding RNA Taurine Upregulated Gene 1 is required for differentiation of the murine retina. *Curr. Biol.* *15*, 501–512.
- Zerucha, T., Stühmer, T., Hatch, G., Park, B.K., Long, Q., Yu, G., Gambarotta, A., Schultz, J.R., Rubenstein, J.L., and Ekker, M. (2000). A highly conserved enhancer in the Dlx5/Dlx6 intergenic region is the site of cross-regulatory interactions between Dlx genes in the embryonic forebrain. *J. Neurosci.* *20*, 709–721.
- Zhang, J.-W., Tang, Q.-Q., Vinson, C., and Lane, M.D. (2004). Dominant-negative C/EBP disrupts mitotic clonal expansion and differentiation of 3T3-L1 preadipocytes. *Proc. Natl. Acad. Sci.* *101*, 43–47.
- Zhang, L., Yang, Z., Trottier, J., Barbier, O., and Wang, L. (2017). Long noncoding RNA MEG3 induces cholestatic liver injury by interaction with PTBP1 to facilitate shp mRNA decay. *Hepatology* *65*, 604–615.
- Zhang, S., Li, J., Lea, R., Vleminckx, K., and Amaya, E. (2014). Fezf2 promotes neuronal differentiation through localised activation of Wnt/ β -catenin signalling during forebrain development. *Development* *141*, 4794–4805.
- Zhang, X., Chen, M.H., Wu, X., Kodani, A., Fan, J., Doan, R., Ozawa, M., Ma, J., Yoshida, N., Reiter, J.F., et al. (2016). Cell-Type-Specific Alternative Splicing Governs Cell Fate in the Developing Cerebral Cortex. *Cell* *166*, 1147–1162.e15.
- Zhao, X., Tang, Z., Zhang, H., Atianjoh, F.E., Zhao, J.-Y., Liang, L., Wang, W., Guan, X., Kao, S.-C., Tiwari, V., et al. (2013). A long noncoding RNA contributes to neuropathic pain by silencing *Kcna2* in primary afferent neurons. *Nat. Neurosci.* *16*, 1024–1031.
- Zheng, S., Gray, E.E., Chawla, G., Porse, B.T., O'Dell, T.J., and Black, D.L. (2012). PSD-95 is post-transcriptionally repressed during early neural development by PTBP1 and PTBP2. *Nat. Neurosci.* *15*, 381–388, S1.
- Zhou, Q.-P., Le, T.N., Qiu, X., Spencer, V., de Melo, J., Du, G., Plews, M., Fonseca, M., Sun, J.M.,

- Davie, J.R., et al. (2004). Identification of a direct Dlx homeodomain target in the developing mouse forebrain and retina by optimization of chromatin immunoprecipitation. *Nucleic Acids Res.* 32, 884–892.
- Zhu, C.C., Dyer, M.A., Uchikawa, M., Kondoh, H., Lagutin, O. V, and Oliver, G. (2002). Six3-mediated auto repression and eye development requires its interaction with members of the Groucho-related family of co-repressors. *Development* 129, 2835–2849.
- Zhu, S., Li, W., Liu, J., Chen, C.-H., Liao, Q., Xu, P., Xu, H., Xiao, T., Cao, Z., Peng, J., et al. (2016). Genome-scale deletion screening of human long non-coding RNAs using a paired-guide RNA CRISPR–Cas9 library. *Nat. Biotechnol.* 34, 1279–1286.
- Ziats, M.N., and Rennert, O.M. (2013). Aberrant expression of long noncoding RNAs in autistic brain. *J. Mol. Neurosci.* 49, 589–593.

Publishing Agreement

It is the policy of the University to encourage the distribution of all theses, dissertations, and manuscripts. Copies of all UCSF theses, dissertations, and manuscripts will be routed to the library via the Graduate Division. The library will make all theses, dissertations, and manuscripts accessible to the public and will preserve these to the best of their abilities, in perpetuity.

Please sign the following statement:

I hereby grant permission to the Graduate Division of the University of California, San Francisco to release copies of my thesis, dissertation, or manuscript to the Campus Library to provide access and preservation, in whole or in part, in perpetuity.

Rebecca E Andersen
Author Signature

5/20/19
Date